



University of Kentucky  
UKnowledge

---

University of Kentucky Doctoral Dissertations

Graduate School

---

2003

## CONTROLS ON MIDDLE TO LATE ORDOVICIAN SYNOROGENIC DEPOSITION IN THE SOUTHEASTERN CORNER OF LAURENTIA

German Bayona  
*University of Kentucky*, [gbayo2@uky.edu](mailto:gbayo2@uky.edu)

[Right click to open a feedback form in a new tab to let us know how this document benefits you.](#)

---

### Recommended Citation

Bayona, German, "CONTROLS ON MIDDLE TO LATE ORDOVICIAN SYNOROGENIC DEPOSITION IN THE SOUTHEASTERN CORNER OF LAURENTIA" (2003). *University of Kentucky Doctoral Dissertations*. 364. [https://uknowledge.uky.edu/gradschool\\_diss/364](https://uknowledge.uky.edu/gradschool_diss/364)

This Dissertation is brought to you for free and open access by the Graduate School at UKnowledge. It has been accepted for inclusion in University of Kentucky Doctoral Dissertations by an authorized administrator of UKnowledge. For more information, please contact [UKnowledge@lsv.uky.edu](mailto:UKnowledge@lsv.uky.edu).

ABSTRACT OF DISSERTATION

Germán Bayona

The Graduate School  
University of Kentucky  
2003

CONTROLS ON MIDDLE TO LATE ORDOVICIAN SYNOROGENIC  
DEPOSITION IN THE SOUTHEASTERN CORNER  
OF LAURENTIA

---

ABSTRACT OF DISSERTATION

---

A dissertation submitted in partial fulfillment of the  
requirements for the degree of Doctor of Philosophy in the  
College of Arts and Sciences  
at the University of Kentucky

By  
Germán Bayona

Lexington, Kentucky

Director: Dr. William A. Thomas, Professor of Geological Sciences

Lexington, Kentucky

2003

Copyright © Germán Bayona 2003

## ABSTRACT OF DISSERTATION

### CONTROLS ON MIDDLE TO LATE ORDOVICIAN SYNOROGENIC DEPOSITION IN THE SOUTHEASTERN CORNER OF LAURENTIA

Middle and Upper Ordovician strata in the southernmost Appalachians document initial collision along the southeastern margin of Laurentia during the Blountian orogeny, an early phase of the Taconic orogeny. Coeval drowning and exposure of different parts of the former platform and variations in stratal architecture have been attributed to tectonic and depositional loading along the collisional margin. Stratigraphic correlations, using a bentonite-graptolite-conodont time framework, a palinspastic map, and a map of subsurface basement structures, suggest that basement-fault reactivation, flexural subsidence, and eustasy variously controlled uplift, subsidence, and deposition at different sites within the peripheral foreland basin.

This dissertation documents how pre-existing structures in the continental margin and interior affected subsidence, deposition, diagenesis, and composition of foreland strata, and deformation in tectonic loads. Stratigraphic correlations document an early episode of basement-fault inversion in the distal foreland, and heterogeneous subsidence and provenance patterns in the middle and proximal foreland. Abrupt variations in depth of erosion of passive-margin strata and in thickness of distal foreland deposits coincide with the boundaries of the intraplate Birmingham graben. Inversion of the former graben increased the magnitude of erosion on

inverted upthrown blocks; increased tectonic subsidence in adjacent blocks; supplied chert and quartz detritus to shallow-marine carbonate depocenters; and facilitated influx of meteoric water to aquifers in shallow-marine limestones. Tectonic subsidence of middle and proximal foreland deposits reflects local irregularities in the foreland subsidence and different rates of migration of the flexural wave along strike. Differential subsidence between embayments and promontories may have caused reactivation of transverse basement faults. Relief produced by reactivation of transverse basement faults and flexural normal reactivation of basement faults may provide sources for local conglomerates interbedded with deep-water shales. Differences in orogenic-belt deformation are reflected in provenance analyses that suggest exposure of dominantly feldspar-bearing basement rocks in the orogenic belt adjacent to the promontory and exposure of basement rocks and sedimentary cover in the orogenic belt adjacent to the embayment. Results of this study reveal the importance of considering the effects of pre-existing structures in the interpretation of along- and across-strike variations of foreland strata. Therefore, geodynamic modeling of the Blountian foreland basin needs to consider along-strike variations in the geometry of tectonic loads and reactivation of different basement structures.

**KEYWORDS:** Blountian orogeny, reactivation, Ordovician, peripheral foreland, inversion

Germán Bayona

January 2003

CONTROLS ON MIDDLE TO LATE ORDOVICIAN SYNOROGENIC  
DEPOSITION IN THE SOUTHEASTERN CORNER  
OF LAURENTIA

By

Germán Bayona

William A. Thomas  
Director of Dissertation

Alan E. Fryar  
Director of Graduate Studies

January 2003

## RULES FOR THE USE OF DISSERTATIONS

Unpublished dissertations submitted for the Doctor's degree and deposited in the University of Kentucky Library are as rule open for inspection, but are to be used only with due regard to the right of the authors. Bibliographical references may be noted, but quotations or summaries of parts may be published only with the permission of the author, and with the usual scholarly acknowledgments.

Extensive copying or publication of the dissertation in whole or in part also requires the consent of the Dean of the Graduate School of the University of Kentucky.

DISSERTATION

Germán Bayona

The Graduate School  
University of Kentucky

2003



CONTROLS ON MIDDLE TO LATE ORDOVICIAN SYNOROGENIC  
DEPOSITION IN THE SOUTHEASTERN CORNER  
OF LAURENTIA

---

DISSERTATION

---

A dissertation submitted in partial fulfillment of the  
requirements for the degree of Doctor of Philosophy in the  
College of Arts and Sciences  
at the University of Kentucky

By  
Germán Bayona

Lexington, Kentucky

Director: Dr. William A. Thomas, Professor of Geological Sciences

Lexington, Kentucky

2003

Copyright © Germán Bayona 2003

*To my parents*

## ACKNOWLEDGEMENTS

This dissertation would have neither at begin nor at end without the support from my advisor, Dr. William A. Thomas. Thanks to Dr. Thomas, I was able to realize a dream and succeed in a goal; but more important, what I have learnt from him is now the motivation to built new dreams and goals in Colombia. He and his wife, Mrs. Rachel Thomas, gave me encouragement and support in several stages of my doctoral studies, and there are not words to express my appreciation for their friendship and scientific guidance in these four years.

Committee members, Frank Etensohn, Kieran O'Hara, James Drahovzal, Paul Howell, and Mark Hanson were very open for discussion of ideas and concepts, and their feedback allowed me to address the trajectory of my research. Alan Fryar, Sue Rimmer, and Dave Moecher, faculty of the Department of Geological Sciences, helped me to understand basic concepts of hydrology, clay mineralogy, petrology when I needed. Comments of Peter DeCelles (University of Arizona), improved the content of this dissertation. Mary Sue Johnson and Pam K. Stephens (staff of the Department of Geological Sciences) helped me in the paperwork of everything; thanks to Mary and Pam, I was able to concentrate in science.

This research was supported by grants to W. A. Thomas from the U. S. National Science Foundation grant EAR-9706735 and Donors of the Petroleum Research Fund (33390), administered by the American Chemical Society. Financial support also comes from the Geological Society of America and a Dissertation Enhancement Award (University of Kentucky Graduate School). Funds from the Department of Geological Sciences, the Southeastern Section of the Geological Society of America, and the Graduate School of the University of Kentucky supported the travel expenses for presentation of the results obtained from this dissertation.

Several professors and colleagues contributed in different ways in this dissertation. Tim Lawton, my former advisor at New Mexico State University, introduced me to Dr. Thomas and encouraged me to continue with my Ph. D. Ed Osborne (Alabama Geological Survey) gave me some unpublished information, and I enjoyed the time in the field with Ed discussing the stratigraphy and structure of the Alabama thrust belt. Dorothy Raymond and other members of the Alabama Geological Survey also shared new field data of Ordovician outcrops in the Alabama Appalachians. Tim Chowns and Randal L. Kath (State University of West Georgia), and Carl W. Stock (University of Alabama) pointed out some type localities and new outcrops. Stanley C. Finney (California State University) identified and assigned an age of graptolites

collected in the Athens Shale. Discussions of Ordovician conodonts with John Repetski (USGS) contributed to clarify the construction of the time framework of this study. Warren Huff (University of Cincinnati) explained patiently how to identify and to deal with a K-bentonite. Rob Van der Voo (University of Michigan) gave me the opportunity to work and learn about the theory and applications of paleomagnetism. James Gleason (University of Michigan) carried out the analysis of Nd isotopes, and explained to me the relevance of this method for provenance analysis. Ricardo Astini (Universidad de Córdoba, Argentina) gracias por compartir sus conocimientos en campo, tanto en Argentina como en Alabama. Camilo Montes (University of Tennessee) and Sofia, and Mauricio Baquero (Bowling Green University) and Alba Lucy for their hospitality in my several trips to Alabama and Michigan. Bob Hatcher (University of Tennessee) and Seismic Exchange Inc. for access to some seismic lines in Georgia. Nestor Cardozo (Cornell University) let me use his MatLab programs for subsidence and flexural analyses. Charles W. King and supervisors in Rockmart, Glencoe and Calera quarries of Vulcan Material Company, as well as Darin Klewsaat and quarry engineers at the Blue Circle Cement for authorizing the access to the quarries.

Life at Lexington was not only dissertation, and my friends in the geology, international, latino, and colombian cartels taught me the diversity of our world. The geology cartel includes Mark, Steve, Walter, Stephan, Milos, Marion, Maggie, Brent, Bryan, Tom, Matt, and Ravi. The international cartel was lead by Ajlina, who with Adna, Ariel, and Mete gave me diverse perspectives of the world. The Latino cartel includes first-class dancers: Lucia, Rodolfo, Juliana, Lorena, Jessi, among others; and the Colombian cartel: Luz and Francisco, Carlos and Angela, Juan Villalba, Elsy, and a list of other 30 more that I apologize for not including here, but all together made me feel like home.

Finally, and as important as the first, to my parents, Jose and Elvira, my sisters, Mafe and Claudia, and my brother Alejo, for all the lovely support of a family that I most missed in this American land. Friendship of ARES's members, Carlos, Germán M., Germán O., Oscar, Mauro, Daniel, Camilo, and Martin helped me to find the strength to finish this goal. In the last three years, Adriana Castaño has been a friend, and now the source of inspiration and love. Gracias negra por compartir éste y los demás momentos por venir.

## TABLE OF CONTENTS

ACKNOWLEDGMENTS.....	iii
LIST OF TABLES.....	ix
LIST OF FIGURES.....	x
LIST OF PLATES.....	xii
LIST OF FILES.....	xiii
<b>CHAPTER ONE</b>	
GENERAL INTRODUCTION, PURPOSE, SIGNIFICANCE, AND ORGANIZATION OF THE DISSERTATION .....	1
<b>CHAPTER TWO</b>	
GEOMETRY, KINEMATICS, AND RESTORATION OF THE APPALACHIAN FOLD AND THRUST BELT OF ALABAMA AND GEORGIA: LINKING SUB-DECOLLEMENT BASEMENT STRUCTURES WITH THIN-SKIN STRUCTURES .....	4
2.1 INTRODUCTION.....	4
2.2 REGIONAL SETTING.....	6
2.3 METHODS.....	8
2.4 THE ALABAMA AND GEORGIA FORELAND THRUST BELT .....	9
2.4.1 Area 1: Sequatchie, Wills Valey, and Murphrees Valley anticlines, and composite Chickamauga fault system .....	9
2.4.2 Area 2: Kingston and Chattooga thrust faults.....	10
2.4.3 Area 3: Peavine anticline.....	11
2.4.4 Area 4: Gadsden and Palmerdale mushwads and bounding thrust sheets.....	11
2.4.5 Area 5: composite Clinchport and composite Dalton fault systems, Rocky Mountain and Horseleg blind thrust systems; subsurface trailing imbricates of the Chattooga, Peavine, and Dunaway Mountain thrust faults.....	12
2.4.6 Area 6: Rome thrust sheet.....	14
2.4.7 Area 7: Western Coosa and Helena thrust sheets, and the Coosa deformed belt and Yellowleaf fault.....	15
2.4.8 Area 8: trailing trust sheets: eastern Coosa, Pell City, Jacksonville, Indian Mountain, Choccolocco Mountain, and Sleeping Giants thrust complexes.....	17
2.4.9 Area 9: Metamorphic belt.....	19
2.5 STRUCTURAL STYLES .....	20
2.5.1 Structural style one: fault-related folds .....	20
2.5.2 Structural style two: duplexes.....	21
2.5.3 Structural style three: imbricate fans.....	22
2.5.4 Structural style four: Rome thrust sheet and its palinspastic restoration.....	23
2.6 STRUCTURAL CONFIGURATION OF THE TOP OF BASEMENT.....	24
2.7 PRE-DEFORMATIONAL THICKNESS OF UNIT 1 AND LITHOFACIES OF THE CONASAUGA FORMATION.....	26
2.8 DISCUSSION.....	29
2.9 CONCLUSIONS.....	33

### **CHAPTER THREE**

#### **ROLE OF BASEMENT FAULT REACTIVATION IN THE EVOLUTION OF THE DISTAL BLOUNTIAN FORELAND BASIN .....51**

3.1 INTRODUCTION.....	51
3.2 GEOLOGIC AND STRATIGRAPHIC SETTING .....	53
3.2.1 Structures from the previous extensional tectonic setting.....	53
3.2.2 Taconic (Blountian) orogeny and foreland deposits .....	54
3.2.3 Flexural subsidence/uplift in southeastern Laurentia.....	55
3.3 METHODS .....	56
3.4 POST-KNOX UNCONFORMITY .....	57
3.5 MIDDLE AND UPPER ORDOVICIAN STRATIGRAPHY .....	58
3.5.1 Sections northwest of the northwestern fault system of the Birmingham graben .....	58
3.5.2 Sections inside the graben.....	60
3.5.3 Equant calcite cements in carbonate rocks of the Chickamauga Limestone and Sequatchie Formation.....	63
3.5.4 Sections southeast of the southeastern fault system of the Birmingham graben .....	64
3.6 STRATIGRAPHIC CORRELATION, DEPOSITIONAL ENVIRONMENTS, AND STACKING PATTERNS .....	68
3.6.1 Definition of stratigraphic surfaces of correlation .....	68
3.6.2 Strata and depositional systems of Interval I (upper Middle to lower Upper Ordovician) ..	70
3.6.3 Strata and depositional systems of Interval II (lower Upper Ordovician).....	72
3.6.4 Strata and depositional systems of Interval III (lower Upper Ordovician) .....	74
3.6.5 Strata and depositional systems of Interval IV (lower-middle Upper Ordovician) .....	75
3.6.6 Strata and depositional systems of Interval V (middle-upper Upper Ordovician).....	77
3.7 TECTONIC SUBSIDENCE OF THE DISTAL FORELAND.....	78
3.8 DISCUSSION .....	79
3.8.1 Lacuna geometry and stratigraphic patterns associated to early forebulge migration .....	80
3.8.2 Geometry of the post-Knox unconformity and intraforeland uplifts .....	81
3.8.3 Architecture of the Middle Ordovician carbonate platform .....	82
3.8.4 Upper Ordovician carbonate platform, progradation of the synorogenic clastic wedge, and eustasy.....	83
3.9 CONCLUSIONS.....	86

### **CHAPTER FOUR**

#### **INFLUENCE OF PRE-EXISTING STRUCTURES ON FOREDEEP STRATIGRAPHY, SUBSIDENCE, AND PROVENANCE OF THE BLOUNTIAN FORELAND BASIN ..... 111**

4.1 INTRODUCTION.....	111
4.2 GEOLOGIC AND STRATIGRAPHIC SETTING .....	113
4.2.1 Structures from the previous extensional tectonic setting.....	113
4.2.2 Taconic (Blountian) orogeny and foreland deposits .....	114
4.2.3 Previous subsidence studies in the central-southern Taconic foreland .....	116
4.2.4 Provenance in the central-southern Taconic foreland .....	116
4.2.5 Blountian allochthonous terranes in the southern Appalachians .....	118

4.3 METHODS .....	119
4.4 MIDDLE FORELAND STRATIGRAPHY AND COMPOSITION OF SILICICLASTIC DEPOSITS .....	121
4.4.1 Units, thickness, and age .....	121
4.4.2 Lithology.....	122
4.4.3 Composition of conglomerates and sandstones. ....	125
4.5 PROXIMAL FORELAND STRATIGRAPHY AND COMPOSITION OF SILICICLASTIC DEPOSITS .....	126
4.5.1 Units, thickness, and age .....	126
4.5.2 Lithology.....	127
4.5.3 Composition of conglomerates and sandstones .....	130
4.6 MIDDLE AND PROXIMAL FORELAND STRATIGRAPHIC CORRELATION, AND INTERPRETATION OF DEPOSITIONAL ENVIRONMENTS .....	132
4.6.1 Strata and depositional systems of Interval I (upper Middle to lower Upper Ordovician).....	132
4.6.2 Strata and depositional systems of Interval II (lower Upper Ordovician).....	134
4.6.3 Strata and depositional systems of Interval III (lower Upper Ordovician) .....	136
4.6.4 Strata and depositional systems of Interval IV (lower-middle Upper Ordovician). ....	138
4.6.5 Strata and depositional systems of Interval V (strata between correlation surfaces 9 and the post-Ordovician unconformity, lower-middle Upper Ordovician). ....	139
4.7 PROVENANCE OF SANDSTONES AND CONGLOMERATES AND ISOTOPIC NEODYMIUM ANALYSIS.....	140
4.7.1 Conglomerates.....	140
4.7.2 Sandstones.....	141
4.7.3 Shales and siltstones (Nd-isotopic analysis).....	143
4.8 TECTONIC SUBSIDENCE .....	144
4.9 DISCUSSION .....	145
4.9.1 Relationship between Blountian foreland basin evolution and the inherited the plate configuration of margin .....	145
4.9.2 Reactivation of pre-existing intraplate structures.....	148
4.9.3 Identification and trace of the foredeep side of the forebulge .....	148
4.9.4 Migration of the flexural wave.....	150
4.9.5 Interaction between Blountian hinterland and the inherited configuration of the plate margin .....	152
4.10 CONCLUSIONS.....	153
<b>CHAPTER FIVE</b>	
SUMMARY OF CONCLUSIONS .....	194
5.1 CONSTRUCTION OF THE PALINSPASTIC MAP AND A MAP OF SUBSURFACE BASEMENT FAULTS: INSIGHTS TO THE REGIONAL GEOMETRY AND KINEMATICS OF THE APPALACHIAN THRUST BELT IN ALABAMA AND GEORGIA.....	194
5.2 INTERACTION OF BIRMINGHAM GRABEN INVERSION AND FLEXURAL DEFORMATION AT DISTAL TO MIDDLE FORELAND SETTINGS.....	195

5.3 ROLE OF THE RIFTED-MARGIN CONFIGURATION OF LAURENTIA IN THE ARCHITECTURE AND COMPOSITION OF MIDDLE TO PROXIMAL FORELAND STRATA .....	198
5.4 MIGRATION OF THE BLOUNTIAN FLEXURAL WAVE .....	199
APPENDIX A IDENTIFICATION OF K-BENTONITES .....	203
APPENDIX B IDENTIFICATION OF GRAPTOLITES.....	208
APPENDIX C TECTONIC SUBSIDENCE DATA.....	210
APPENDIX D DESCRIPTION OF THIN SECTIONS AND HAND SAMPLES.....	236
REFERENCES .....	245
VITA .....	263



## LIST OF TABLES

<b>Table 3.1</b> Explanation of lithofacies codes and lithofacies interpretations for carbonate and mixed carbonate and siliciclastic deposits .....	88
<b>Table 3.2</b> Explanation of lithofacies codes and lithofacies interpretations for siliciclastic deposits .....	90
<b>Table 3.3</b> Explanation of key stratigraphic surfaces .....	92
<b>Table 4.1</b> Explanation of lithofacies codes and lithofacies interpretations for carbonate and mixed carbonate and siliciclastic deposits .....	155
<b>Table 4.2</b> Explanation of lithofacies codes and lithofacies interpretations for siliciclastic deposits .....	157
<b>Table 4.3</b> Explanation of key stratigraphic surfaces .....	159
<b>Table 4.4</b> Parameters for sandstone point counts.....	160
<b>Table 4.5</b> Raw point-count data and recalculated modal point-count data for sandstones of the Blountian clastic wedge .....	161
<b>Table 4.6</b> Sm-Nd isotopic data for Middle and Upper Ordovician strata from the Blountian clastic wedge .....	163

## LIST OF FIGURES

<b>Figure 2.1</b>	A) Salient-recess geometry of the southern Appalachians .....	35
<b>Figure 2.2</b>	Segments of a seismic reflection profile and interpreted cross section showing geometry of cover deformation and of sub-décollement basement structures .....	38
<b>Figure 2.3</b>	Selected parts of the 17 structural cross sections displayed in Plate 2.1 showing representative structures of the Appalachian thrust belt in Alabama and Georgia.....	39
<b>Figure 2.4</b>	Map showing traces of subsurface basement faults interpreted from seismic reflection profiles, depth to top of basement, and outcrop traces of representative thrust-belt structures.....	41
<b>Figure 2.5</b>	Palinspastic map of the Appalachian thrust belt of Georgia and Alabama at the top of the Conasauga Formation.....	42
<b>Figure 2.6</b>	Isopach map of compacted thickness of unit 1 in areas with seismic control .....	43
<b>Figure 2.7</b>	Map of lithofacies distribution of the Conasauga Formation at present locations in the southern Appalachians .....	44
<b>Figure 2.8</b>	Relationship between the palinspastic distribution of the Conasauga Formation lithofacies and the configuration of the Birmingham graben.....	45
<b>Figure 2.9</b>	Deformed and restored structural cross sections across part of the thrusts belt and on both sides of the Anniston transverse zone .....	46
<b>Figure 2.10</b>	A) Palinspastic restoration of folds and faults in the thrust belt, showing strike deviations and the relationship to the basement faults.....	47
<b>Figure 2.11</b>	Along-strike variation of shortening at leading, intermediate, and trailing structures of the Appalachian thrust belt in Alabama and Georgia .....	49
<b>Figure 3.1</b>	Illustration of the flexural geometry and distribution of depositional settings through time for three different configurations of the distal foreland lithosphere .....	93
<b>Figure 3.2</b>	Location of study sections and distribution of lithofacies belts of the Middle and Upper Ordovician strata in the Appalachian thrust belt of Georgia and Alabama.....	94
<b>Figure 3.3</b>	Palinspastic location of study sections, lines of stratigraphic correlation, and distribution of study sections and lithofacies belts in relation to mapped subsurface basement faults and the Birmingham basement graben.....	96
<b>Figure 3.4</b>	(A) Ordovician series (from Webby, 1998) and correlation of conodont zones, graptolite zones, and K-bentonite beds .....	97
<b>Figure 3.5</b>	Key to facies for stratigraphic columns in Figures 3.7, 3.8, and 3.9.....	99
<b>Figure 3.6</b>	Geometry of the truncation of Knox strata in the distal Blountian foreland basin ..	100
<b>Figure 3.7</b>	Line of stratigraphic correlation A (including section HL, which is southwest of line A) showing stratigraphic units, biostratigraphic data, lithofacies, stratigraphic correlation surfaces (numbers 1 to 10), and stratigraphic intervals (numbers I to V).....	101
<b>Figure 3.8</b>	Line of stratigraphic correlation B showing stratigraphic units, biostratigraphic data, lithofacies, stratigraphic correlation surfaces (numbers 1 to 10), and stratigraphic intervals (numbers I to V).....	103
<b>Figure 3.9</b>	Line of stratigraphic correlation C showing stratigraphic units, biostratigraphic data, lithofacies, stratigraphic correlation surfaces (numbers 1 to 10), and stratigraphic intervals (numbers I to V).....	104
<b>Figure 3.10</b>	Paleogeographic maps showing evolution of depositional environments in the distal foreland basin through the Middle and Late Ordovician .....	105

<b>Figure 3.11</b>	(A) Total and tectonic subsidence curves (lower and upper curves, respectively) for representative sections restoring along the northwestern shoulder of the graben (composite section CH-RI) and inside the graben (sections BI and DG) .....	107
<b>Figure 3.12</b>	Effects of tectonic loads in an intraplate setting, assuming that the load consists of the inverted Birmingham graben at early phases of deposition of Interval I (late Middle Ordovician).....	109
<b>Figure 4.1</b>	(A) Three-dimensional block diagram illustrates the marginal and intraplate basement structural configuration of southern Laurentia after Cambrian rifting .....	164
<b>Figure 4.2</b>	Location of study sections and distribution of lithofacies belts of the Middle and Upper Ordovician strata in the Appalachian thrust belt of Georgia and Alabama.....	165
<b>Figure 4.3</b>	Palinspastic map showing location of study sections, lines of stratigraphic correlation, and lithofacies belts .....	167
<b>Figure 4.4</b>	(A) Ordovician series (from Webby, 1998) and correlation of conodont zones, graptolite zones, and K-bentonite beds .....	169
<b>Figure 4.5</b>	Key to facies for stratigraphic columns in Figures 4.6 to 4.10 .....	171
<b>Figure 4.6</b>	(A) Along-strike stratigraphic correlation of the middle Blountian foreland showing stratigraphic units, biostratigraphic data, lithofacies, stratigraphic correlation surfaces (numbered 1 to 11), and stratigraphic intervals (numbers I to V) .....	172
<b>Figure 4.7</b>	Along-strike stratigraphic correlation of middle to distal foreland strata between stratigraphic surfaces of correlation 7 and 11 .....	174
<b>Figure 4.8</b>	(A) regional structural cross section across stratigraphic sections DG and HM and at the southern end of the north-plunging syncline that includes stratigraphic section CI .....	175
<b>Figure 4.9</b>	(A) and (B) are regional and local structural cross sections, respectively, near stratigraphic section RK .....	177
<b>Figure 4.10</b>	(A) and (B) are regional structural cross sections across sections GS, LM, FC (on Figure 10.A), and HV, which contain proximal foreland stratigraphy and restore on the Alabama promontory .....	179
<b>Figure 4.11</b>	Paleogeographic maps showing the evolution of the underfilled stage of the Blountian foreland basin through the Middle Ordovician to early Late Ordovician.....	181
<b>Figure 4.12</b>	Paleogeographic maps showing the evolution of the Blountian foreland basin through the Late Ordovician.....	183
<b>Figure 4.13</b>	Temporal and lateral variation of Nd-isotopic compositions of the Blountian clastic wedge .....	185
<b>Figure 4.14</b>	Total and tectonic subsidence curves (lower and upper curves, respectively) for representative sections in the middle (A) and proximal (B) foreland,.....	186
<b>Figure 4.15</b>	(A) Estimated position of the foredeep side of the forebulge at stratigraphic surface of correlation 3.....	188
<b>Figure 4.16</b>	(A) Estimated position of the foredeep side of the forebulge at stratigraphic surface of correlation 8.....	190
<b>Figure 4.17</b>	Two-dimensional tectonic evolution of the Laurentia margin during the Blountian orogeny.....	192
<b>Figure 5.1</b>	This diagram illustrates the role of different rift-related structures on the early geometry of the Blountian foredeep.....	202

## LIST OF PLATES

- Plate 2.1** Structural cross sections 1 to 17 perpendicular to structural strike along the Appalachians thrust belt in Alabama and Georgia
- Plate 3.1** Structural cross sections and description of the stratigraphic section in Dug gap (DG)
- Plate 3.2** Description of the stratigraphic section in Hamilton Mountain (HM).
- Plate 3.3** Description of the stratigraphic section in Horseleg Mountain (HL)
- Plate 3.4** Description of the stratigraphic section in Big Ridge (BR, Interstate 59)
- Plate 3.5** Description of the stratigraphic section in Dunaway Mountain (DM)
- Plate 3.6** Construction of the composite stratigraphic section in Greensport gap (GS)
- Plate 3.7** Construction of the composite stratigraphic section in Alabaster (AB)
- Plate 3.8** Construction of the composite stratigraphic section in Calera (CL)
- Plate 3.9** Description of stratigraphic section in Pratt Ferry (PF)
- Plate 3.10** Stratigraphic column of the Atalla Chert Conglomerate Member of the Chickamauga Limestone northeast of the Birmingham section
- Plate 4.1** Strike-perpendicular stratigraphic correlations of Middle and Upper Ordovician strata in palinspastic position
- Plate 4.2** Description of stratigraphic section in Cisco (CI)
- Plate 4.3** Construction of the composite stratigraphic section in Rockmart (RK)
- Plate 4.4** Outcrop photos and photomicrographs of sandstones of the Athens Shale in Hapersville area

## LIST OF FILES

**GbayonaDissert.pdf**

Abobe pdf file

202 MB

## CHAPTER ONE

### GENERAL INTRODUCTION, PURPOSE, SIGNIFICANCE, AND ORGANIZATION OF THE DISSERTATION

Middle and Upper Ordovician strata in the Appalachian thrust belt in Alabama and Georgia contain the record of the Blountian phase of the Taconic orogeny (Rodgers, 1953; Drake et al., 1989) (hereinafter referred to as the Blountian orogeny), that also marks the onset of several events of collision along the margin of Laurentia during the Paleozoic (Hatcher, 1989). This event of collision has been interpreted from deposition of Middle Ordovician basinal shales toward the pre-existing rifted margin of Laurentia and exposure of the platform toward the craton. The inherited structural zig-zag configuration of the southeastern Laurentian margin consisted of the Alabama promontory and Tennessee embayment along the margin and the intraplate Birmingham graben (Thomas, 1977, 1991). Irregularities of colliding crustal blocks and pre-existing internal structures within the blocks have not been given enough attention in the analysis of sedimentary basins associated with mountain-building processes. This dissertation focuses on the role of basement structures in the distribution and evolution of source areas and sedimentation at different settings within a peripheral foreland basin. The results of this dissertation document how intraplate basement faults may be reactivated as inverted faults, flexural normal faults, or transverse faults. Basement-fault reactivation may predate or be coeval with the migration of a flexural wave. Basement-fault reactivation distorts the pattern of lithospheric flexure predicted from geodynamic models and allows the accommodation of differential rates of subsidence and migration along strike of the foreland basin.

The significance of this research is that it uses a well-constrained palinspastic map and chronostratigraphic framework to relate changes in composition and architecture of synorogenic sedimentary successions to subsurface basement structures. This approach permits the distinction among (1) local effects of a fixed structure on composition and architecture of foreland deposits; (2) the plate-margin-scale pattern of foreland deposition controlled by migration of the flexural wave; and (3) cratonwide fluctuations of sea level. Synconvergence reactivation of rift-related basement faults and irregularities of the foreland plate margin adequately explain many otherwise unclear stratigraphic and compositional relationships in the

southern Blountian foreland basin. Consequently, integration of pre-existing structures into the comprehensive analysis of foreland or other synorogenic basins will contribute to a better understanding of causes of abrupt changes in the stratigraphy, structure, and composition of foreland basins.

This dissertation is divided into an introductory chapter (this chapter), three chapters that address specific goals (Chapters 2 to 4), and a final chapter with a summary of the conclusions (Chapter 5). For dissertation purposes, the major goal in Chapter 2 is the construction of a palinspastic map and a map of basement structures. An overlay of these two maps generates the base map for stratigraphic analysis of Blountian strata in Chapters 3 and 4. Another goal of Chapter 2 is to determine whether sub-décollement basement faults and variations of synrift deposits contributed to the regional kinematic and geometric partitioning of the Alabama and Georgia thrust belt. Chapter 2 examines the causes of small-scale curvatures of the thrust belt, and the relationship between structural styles of the thrust belt and the sub-décollement structural configuration of the basement.

How did the intraplate Birmingham graben and lithosphere flexure interact at distal foreland settings during the Middle and Late Ordovician Blountian orogeny? In order to answer this question, Chapter 3 documents distal and middle foreland variations of (1) stratal architecture, (2) composition of carbonate and siliciclastic deposits, and (3) tectonic subsidence using stratigraphic sections that restore palinspastically northwest (toward the craton), inside, and southeast (toward the plate margin) of the Birmingham graben. The palinspastic distribution of sections, which also covers different configurations of the Birmingham graben along strike, allows the determination of whether faults of the Birmingham graben system were reactivated as inverted faults. Chapter 3 presents an integrated analysis of basement-fault reactivation, flexural deformation, and sea-level fluctuations in order to estimate the control of erosion of passive-margin strata and subsequent distal to middle foreland deposition.

Chapter 4 describes the effects of the zig-zag configuration of the southeastern Laurentian margin and intraplate structures near the plate margin in the architecture and composition of middle to proximal foreland strata, as well as in deformation of the Blountian orogenic belt. The main goal of Chapter 4 is to document along-strike changes in the stratigraphy and composition of the Blountian foredeep, dispersal patterns of synorogenic sediments, and migration of the flexural wave; and to determine if the stratal architecture of the

Blountian foreland basin is somehow influenced by the pre-existing plate-margin configuration of the southern Laurentian margin. Provenance analysis presented in this chapter intends to examine along-strike variations in composition of synorogenic siliciclastic strata in order to predict a possible gradient of deformation of the Blountian orogenic belt. Integration of results of Chapters 3 and 4 allows (1) the identification of flexural deformation in the proximal to middle foreland, (2) the establishment of the extent of sea-level fluctuations in controlling foreland deposition, and (3) calculation of flexural wave migration in the Blountian foreland basin.

Chapter 5 brings together the results of Chapters 2 to 4. This chapter gives some insights into the geometry and kinematics of the Appalachian thrust belt in Alabama and Georgia, and summarizes the effects of pre-existing structural configuration of the foreland plate, flexural deformation, and sea-level fluctuations in deposition of the Blountian carbonates and synorogenic clastic wedge on the southeastern margin of Laurentia.



## CHAPTER TWO

# GEOMETRY, KINEMATICS, AND RESTORATION OF THE APPALACHIAN FOLD AND THRUST BELT OF ALABAMA AND GEORGIA: LINKING SUB-DÉCOLLEMENT BASEMENT STRUCTURES WITH THIN-SKINNED STRUCTURES

### 2.1 INTRODUCTION

Field and laboratory investigations have explored the causes of the curvature (salient and recess) geometry of fold-thrust belts (e.g., Thomas, 1977; Marshak et al., 1992; Macedo and Marshak, 1999; Paulsen and Marshak, 1999). The Pennsylvania salient (convex-to-the-foreland curve) of the central Appalachian thrust belt has been interpreted as a curvature inherited from the rifted continental margin of Laurentia (Rankin, 1976; Thomas, 1977; Kent, 1988; Stamatakos and Hirt, 1994). In the southern Appalachian thrust belt, the Tennessee salient and the Virginia recess (concave-to-the-foreland curve, Figure 2.1A) have been interpreted as a curvature related to the shape of an embayment-promontory pair of the rifted continental margin (e.g., Thomas, 1977, 1991; Spraggins and Dunne, 2002). Alternatively, this curvature has been modeled by pushing an indenter (i.e., island arc) into the continental margin (Macedo and Marshak, 1999). The abrupt Uinta recess in the Sevier thrust belt of Utah has been related to differential propagation of the thrust belt caused by along-strike variations in pre-deformational basin geometry (Paulsen and Marshak, 1999). Studies in the Wyoming-Idaho thrust belt have documented curvature in response to the buttressing effects of uplifted basement-cored blocks within the foreland (Grubbs and Van der Voo, 1976; Eldredge and Van der Voo, 1988). All these studies indicate that knowledge of the pre-existing intraplate configuration of basement and rifted continental margins is essential for the understanding of the geometry of the thrust belt. Furthermore, indenter geometry, convergence direction, lateral variations of orogenic taper, strength of detachment host rocks, and stratal architecture are other factors that may control the geometry of curved thrust belts (e.g., Marshak et al., 1992; Macedo and Marshak, 1999). Most mechanical models of mountain chains consider a low-angle, hinterlandward-dipping basal slope of the critical wedge as following the geometry of the top of basement (e.g., Chapple, 1978; Davis et al., 1983). This assumption eliminates consideration of the effects of an irregularly shaped basal detachment surface (e.g., Thomas, 1985, 2001) in the evolution of thrust belts. This

chapter illustrates how sub-detachment basement grabens and stratal architecture exert a primary control in the irregular surface trace of the basal detachment and in the geometry and kinematics of a thin-skinned thrust belt.

In the Appalachian thrust belt of Georgia and Alabama (southern part of the Tennessee salient and Alabama recess, Figure 2.1B), folds and faults in intermediate imbricates have local strike deviations which are not transmitted to either leading or trailing thrust sheets. An across-strike alignment of structures with strike deviations constitutes a transverse zone in the thrust belt (Thomas, 1990), such as the Anniston transverse zone (Figures 2.1B and 2.1C). Differences in style of deformation and kinematic evolution of the thrust belt across the Anniston transverse zone have been associated with differences in elevation of the top of basement and in synrift stratal architecture across a basement transverse fault (Thomas, 2001; Thomas and Bayona, 2002; Bayona et al., in press). Therefore, abrupt strike-parallel and strike-perpendicular internal changes in thrust-belt geometry might be related to variations in basement structural configuration and stratal architecture across intraplate structures, such as basement grabens. The question is whether sub-décollement basement faults and variations of synrift deposits contributed to the regional kinematic and geometric partitioning of the Alabama and Georgia thrust belt.

Examination of individual thrust surfaces, fault-related folds, and associated synorogenic deposits allows the identification of the timing, kinematics, and mechanical processes associated with thrust faulting (e.g., Boyer and Elliot, 1982; Mitra, 1997). Previous studies of thrust belts have considered the effects of pre-existing sub-thrust extensional basement faults and pre-deformational stratal architecture on ramp location, out-of-sequence thrusts, and arcuate thrust traces (e.g., Wiltschko and Eastman, 1983; Hayward and Graham, 1989; Mitra, 1997; Paulsen and Marshak, 1999). However, the moderate to poor resolution of gravity (e.g., Hutchinson et al., 1983) and seismic reflection profiles in several mountain belts to depths of crystalline basement does not allow determining a clear and direct link between basement and cover deformation in several mountain belts. Consequently, configuration of the top of basement is commonly constrained by the restored geometry of the sedimentary wedge. Seismic reflection profiles across the thrust belt of Georgia and Alabama used in this study distinctly depict the contact between sedimentary cover and crystalline basement, and allow deciphering the geometry of the top of basement (Figure 2.2).

## **2.2 REGIONAL STRUCTURAL SETTING AND DEFINITION OF LITHOTECTONIC UNITS**

The southern Appalachian thrust belt is the result of the Alleghanian orogeny, which affected the eastern margin of Laurentia in late Paleozoic time (Hatcher, 1989). The foreland thrust belt in Alabama and Georgia consists of large-scale, northeast-striking thrust faults and associated folds bounded by undeformed foreland strata on the northwest and by metamorphic rocks of the Talladega slate belt and western Blue Ridge on the southeast (Figure 2.1) (Pickering et al., 1976; Osborne et al., 1988). Paleozoic strata in the thrust belt have been tectonically transported to the northwest by thin-skinned thrust faults (Thomas, 1985).

Transverse zones, which are cross-strike alignments of lateral ramps, transverse faults, and displacement-transfer zones, cross much or all of a thrust belt (Wheeler, 1980; Thomas, 1990) and break the dominant northeasterly strike of the thrust belt. Straight long lineations perpendicular to the strike of the thrust belt were initially identified by multispectral photographs (e.g., Powell et al., 1970), and are parallel to transverse zones (e.g., Drahovzal, 1975).

Transverse structures link two frontal ramps across strike, and in map view they are marked by abrupt along-strike changes in thrust-belt structure, including plunging ends of ramp anticlines, bends of longitudinal thrust faults and associated folds, transverse faults, changes in stratigraphic level of detachment, displacement transfer between frontal ramps, and boundaries between structural styles (Wheeler, 1980; Thomas, 1990). In the Alabama and Georgia Appalachian thrust belt, the Bessemer, Harpersville, Anniston, and Rising Fawn transverse zones cut completely across the unmetamorphosed thrust belt (Figure 2.1C) (Thomas, 1990). In addition to these four transverse zones, this chapter describes two transverse zones of more local extent. The Clinchport and Rome transverse zones cut across intermediate to trailing structures of the Appalachian thrust belt in Georgia.

The dominant northeasterly strike of the thrust belt is better observed in leading structures than in intermediate and trailing structures. Several northeast-striking faults and folds in the leading thrust belt either terminate or deviate in strike within transverse zones (e.g., anticlines SQ and MV in Figure 2.1). In contrast, the strike in intermediate and trailing faults and folds shifts abruptly from northeast in Alabama to north-northeast in Georgia across the Anniston, Rome, Rising Fawn, and Clinchport transverse zones (Figure 2.1C). Additionally,

folds in intermediate thrust sheets and between the Rome and Clinchport transverse zones show interference patterns (points 10 and 11 in Figure 2.1C) (Bayona et al., in press).

Geometric analysis of structural trend-line patterns in thrust belts has contributed to the understanding of the generation of curved thrust belts (Macedo and Marshak, 1999). In map view, the shift in strike of faults and folds corresponds to a divergence of trend lines of faults in the southern part of the Tennessee salient, in opposition to convergence of faults in the apex of the Tennessee salient (figure 17 of Macedo and Marshak, 1999). A similar geometry of trend lines was obtained in sandbox models where the salient was the product of pushing an indenter into the foreland. Macedo and Marshak (1999) suggested that an Ordovician volcanic arc, caught during Laurentian-Gondwana collision, acted as the indenter in the Alleghanian orogeny. In this chapter, we argue that the shift of trend lines of faults is related to southwestward deepening of the top of basement and thickening of synrift strata across the Rising Fawn and Rome transverse zones.

The Paleozoic succession in the Appalachian thrust belt of Alabama and Georgia consists of upper Precambrian to Lower Ordovician synrift and passive-margin deposits (Thomas, 1991) overlain by Middle Ordovician to Carboniferous deposits associated with three contractional events: the Taconic, Acadian, and Alleghanian orogenies (Hatcher, 1989). On the basis of palinspastic restoration and stratigraphic analyses of synrift and passive-margin deposits in the Appalachian and Ouachita orogenic belts, Thomas (1977, 1991) proposed an orthogonal zig-zag geometry of the eastern Laurentian (North American) rift margin. The zig-zag configuration of the margin resulted from the Blue Ridge and Ouachita rifting episodes during late Precambrian and Early Cambrian times, respectively. Extension in Cambrian time reached intracratonic areas forming the Birmingham and Mississippi Valley grabens (Thomas, 1991), structures documented by reflection seismic profiles. The fault systems bounding the Birmingham graben are defined in greater detail in this chapter.

For cross-section construction, Paleozoic strata are divided into four lithotectonic units with distinct mechanical behavior, as described in Thomas (2001) (Figure 2.2). Lower to Middle Cambrian clastic and carbonate passive-margin strata and intraplate synrift strata are grouped in unit 1. The basal unit hosts the regional décollement and has a dominantly weak mechanical behavior during deformation (e.g., Thomas, 1985; Thomas and Bayona, 2001). Unit 2 consists of Upper Cambrian to Lower Ordovician passive-margin carbonate deposits of the Knox Group.

This unit 2 is 600 to 1250 m thick and is the regional stiff layer of the southern Appalachians thrust belt (Figure 2.2). Unit 3 consists of a heterogeneous carbonate-siliciclastic succession that includes Middle and Upper Ordovician synorogenic strata (the focus of Chapters 3 and 4), as well as Silurian to Lower Mississippian strata. The thickness of unit 3 ranges from 0 to 490 m. Upper levels of detachment are hosted in unit 3. Unit 4 includes Upper Mississippian-Pennsylvanian synorogenic foreland deposits and is passively transported above the stiff layer and upper levels of detachment.

### **2.3 METHODS**

Seventeen balanced cross sections were constructed using conventional methods (e.g., Dahlstrom, 1969; Marshak and Mitra, 1988), along lines perpendicular to thrust-belt strike (Figure 2.2 and Plate 2.1). The cross-section lines are distributed along strike to cover the complete thrust belt and the different transverse zones. The cross sections are based on outcrop geology (e.g., Pickering et al., 1976; Osborne et al., 1988; Szabo et al., 1988), stratigraphic thicknesses, bedding attitudes, seismic reflection profiles, and deep wells. Down-plunge projection provides geometric constraints on plunging folds that overlie both hanging-wall and footwall lateral ramps.

Mapping of subsurface basement faults relies on calculation of depth to the top of basement along 18 seismic reflection profiles. Breaks in the trace of the top of basement were identified in each line, and the probable range of position of basement fault(s) was located in a map. Vertical separation of the top of basement was calculated from the difference in depth to basement on opposite sides of the fault. Criteria for map connection and tracing of basement faults include: same sense of separation, similar or gradual change in the magnitude of vertical separation, and position within a regional graben (shoulder, margin, or floor). We used geometry of modern intraplate rifts (e.g., East Africa rift, Rosendahl, 1987) and accommodation (or transfer) zones of continental rifts (Moustafa, 2002) as a model to consider alternatives in the geometry of splays and along-strike changes in structural configuration of intraplate graben(s).

Restoration of the strike-perpendicular cross sections was accomplished by a combination of bed-length and area balance, as explained in Thomas (2001) and Thomas and Bayona (2002). A palinspastic map was constructed for the stratigraphic level of top of unit 1 in order to establish the distribution of dominant lithologies of the Conasauga Formation (dominant horizon

of detachment) and variations in thicknesses of the weak unit 1 (Rome and Conasauga Formations) across and along the Birmingham graben. The palinspastic map is also the base map to locate palinspastically the stratigraphic sections of Blountian strata described in Chapters 3 and 4. Restored cross sections and palinspastic maps are essential for the analysis of the pre-deformational geometry of the regional décollement and for establishing the mechanism that controls the position of ramps. In addition to the successful balance of cross sections, the validity of the palinspastic map is confirmed by comparison of the distribution of synrift (this Chapter) and synorogenic (Chapter 3) deposits with the structural map of the top of basement (Thomas et al., 2000; Bayona et al., 2001).

## **2.4 THE ALABAMA AND GEORGIA FORELAND THRUST BELT**

Structures with more than 15 km of lateral continuity are grouped into 9 areas on the basis of geographic position (Figure 2.1D), and the boundaries between areas are the surficial traces of regional structures. Description of the geometry of major thrust faults and folds in each area is from leading (northwest) to trailing structures (southeast), and from northeast to southwest along strike. All these structures are identified in cross sections 1 (northernmost section) to 17 (southernmost section) in Plate 2.1 (see Figure 1B for location of structural cross sections).

In the next section, the structures are grouped into four structural styles, which are identified on the basis of the geometry of faults and folds both in map and cross-section views. This section discusses the relation between fault and fold geometries, as well as the geometry and palinspastic restoration of the problematic Rome thrust sheet. Cross-section geometry of each structural style, as well as representative structures for areas 1 to 8, is shown in Figure 2.3.

### **2.4.1 Area 1: Sequatchie, Wills Valley, and Murphrees Valley anticlines, and composite Chickamauga fault system**

The northwestern (frontal) part of the thrust belt is dominated by three, large-scale, northeast-striking, shallow asymmetric anticlines (Figure 2.3A), which are the northwest-verging Sequatchie and Wills Valley anticlines and the southeast-verging Murphrees Valley anticline. These anticlines bound broad and flat-bottomed synclines, which are from north to south the Sand Mountain, Lookout, and Blount Mountain synclines (Figure 2.1B, Plate 2.1). The en

echelon arrangement and oppositely directed plunging of the Murphrees Valley and Wills Valley anticlines (point 1 in Figure 2.1C) together with a curve of the fold axis of the Sequatchie anticline define the northwestern segment of the Anniston transverse zone (ATZ). The northeastern plunging end of the Wills Valley anticline defines the northwestern segment of the Rising Fawn transverse zone (RFTZ) (Figures 2.1B and C). Anticlines southwest of the RFTZ are associated with thrust ramps that rise from the regional décollement (unit 1) to the present land surface. Structures northeast of the RFTZ within the composite Chickamauga fault system consist of four fault-bend folds. The trailing fold is associated with a thrust ramp that rises from the regional décollement, whereas the other three folds are associated with thrust faults with at least two levels of detachment in units 1 and 3 (cross section 1, Plate 2.1).

#### **2.4.2 Area 2: Kingston and Chattooga thrust faults**

The northeast-striking and northwest-verging Kingston and Chattooga faults have leading imbricates that strike parallel to the main fault and are detached from the regional décollement. Tight asymmetrical anticlines are in the leading imbricate slices between the Kingston fault and the leading imbricate (Figure 2.3B), and between the Chattooga fault and the leading imbricate. The linear traces of the Kingston and associated imbricate faults extend northeast straight across the RFTZ. Toward the southwest, the Kingston fault terminates in east-plunging folds defining the northwest segment of the RTZ (Figure 2.1C). The east-plunging folds mark the separation between two structurally distinct anticlines that in map view appear as a laterally continuous structure. Northeast of the east-plunging folds is the ramp anticline associated with the Kingston fault (Figure 2.3B), whereas southwest of the east-plunging folds is the detachment Peavine anticline (Figure 2.3C). The Chattooga fault and structures associated within the composite thrusts sheet terminate northward at lateral ramps within the RFTZ (Bayona et al., in press), whereas the same structures to the south are truncated by the Rome thrust sheet along the Rome transverse zone (RTZ).

Eroded hanging-wall cut offs of the Kingston and Chattooga thrust faults make balancing difficult. However, in the northeastern part of the trace, the thickness of unit 1 increases abruptly from the leading imbricate thrust sheet to the Kingston thrust sheet. Previous studies (e.g., Ferrill, 1989; Thomas, 1990) have related the abrupt increase in thickness of unit 1 to synsedimentary extensional basement faults. Additionally, basement faults are considered to be

as a stress concentration mechanisms leading to thrust ramps (Wiltschko and Eastman, 1983; Rowan and Linares, 2000). These general relationships suggest that the leading edge of the Kingston thrust sheet restores to the southeast of a down-to-southeast basement fault. Interactive comparison of location of sub-detachment basement faults and the palinspastic map at the top of unit 1 gives an estimate of the minimum bed length of erosion of the top of unit 1 at the leading edge of the Kingston fault.

### **2.4.3 Area 3: Peavine anticline**

Northeast of the ATZ, the Peavine anticline borders the southeast limb of the flat-bottomed Lookout Mountain syncline. Although the Rome thrust sheet truncates the southeastern flank of the Peavine anticline (Figure 2.3C), seismic reflection profiles image a long backlimb (Peavine thrust sheet) that dips southeast parallel to the average level of the top of basement rocks within a wide system of down-to-southeast basement faults. At the ATZ, the nearly symmetrical Peavine anticline and adjacent flat-bottomed Lookout Mountain syncline are truncated by a northwesterly curved fault at the northeast end of the Gadsden mushwad (point 2 in Figure 2.1C) which has unit 1 in the hanging wall.

Southeast- and northwest-dipping strata of the Knox Group (unit 2) define the Peavine anticline as a nearly symmetrical fold cored by strata of unit 1. Seismic reflection profiles image the continuation of the basal detachment across the down-to-southeast basement faults and the position of the Peavine anticline on the upthrown (northwest) basement block of the Birmingham graben. The Peavine anticline is interpreted as a detachment fold because of the large volume of unit 1 in the core and the continuation of the basal detachment beneath the Peavine anticline (Figure 2.3C). Tips of thrust ramps are within the core, and the thrust ramp breaks to the surface at the northeastern end of the Peavine anticline (cross section 6, Plate 2.1). As will be discussed later, the extra volume of unit 1 in the core of the Peavine anticline is restored in the downthrown block of the basement fault system.

### **2.4.4 Area 4: Gadsden and Palmerdale mushwads and bounding thrust sheets**

A mushwad comprises the core of a deformed detachment fold, in which the stiff layer is broken and uplifted by the tectonically thickened ductile core (Thomas, 2001). Two mushwads, the Gadsden and Palmerdale, have been identified in Alabama where the tectonically thickened,



ductilely deformed core consists of the shale-dominated unit 1. In the next paragraphs, I make reference to a structural link between mushwads and adjacent major structures; details in the description and kinematics of structures surrounded and/or affected by the two mushwads are in Thomas (2001).

The wide area of deformed strata of unit 1 at the present surface of the Gadsden mushwad is the product of erosion of the stiff-layer cover (Figure 2.3F). The northwest, leading edge of the upper part of the Gadsden mushwad is thrust over the northwest-facing forelimb in the footwall of the Big Canoe Valley fault, marking the exposed leading edge of the mushwad where the stiff-layer cover has been thrust upward and eroded. The Gadsden mushwad is bounded on the southeast by the broken Dunaway Mountain thrust sheet. The Gadsden mushwad is the structural unit that borders the southwest end of the Peavine anticline and adjacent flat-bottomed Lookout Mountain syncline at the ATZ (point 2 in Figure 2.1C). The southwest end of the Gadsden mushwad consists of a lower wedge of the mushwad that is inserted beneath the northeast end of the Cahaba synclinorium.

In contrast to the Gadsden mushwad, the stiff-layer cover of the Palmerdale mushwad is preserved as a wide exposure of the Knox Group (unit 2) in the Birmingham anticlinorium (Thomas, 2001). The northeastern end of the Palmerdale mushwad is marked by the northeastward plunge of units 2 to 4 into the flat-bottomed Blount Mountain syncline. From north to south, the Palmerdale mushwad is bounded on the northwest by the southern termination of the Muphrees Valley anticline, northwest-dipping strata in the footwall of the Opossum Valley fault, and a folded structure in the footwall of the Jones Valley fault. The southeastern boundary of the Palmerdale mushwad is depicted in structural cross sections by the long southeast-dipping forelimb of the Cahaba synclinorium in the hanging-wall of the Jones Valley fault (cross sections 13 to 16 in Plate 2.1).

#### **2.4.5 Area 5: composite Clinchport and composite Dalton fault systems, Rocky Mountain and Horseleg blind thrust systems; subsurface trailing imbricates of the Chattooga, Peavine, and Dunaway Mountain thrust faults**

Surficial structures of area 5 are bounded by structures of areas 1 to 3 on the northwest and by the eastern Coosa, western Coosa, and Helena thrust faults on the southeast. Structures

shown in geologic maps are bounded and truncated by the Rome thrust sheet; however the Rome thrust sheet covers structures that are imaged by seismic reflection profiles.

The northern parts of the composite Clinchport fault system and the composite Dalton fault system have two structural levels of deformation. Antiformal duplexes in the lower structural level duplicate the thickness of unit 1 (Figure 2.3E). The roof fault of the lower structural level is the detachment of an imbricate fan system involving units 2 and 3. Duplexes of the northern composite Clinchport thrust sheet change southward along strike to ramp anticlines as a response to the stratigraphic rise of detachment level from the middle to the top of unit 1 at a lateral ramp in the Clinchport transverse zone (CTZ). The change in rheology between lower and upper detachment levels has been suggested as the cause of strike deviation of southeast-plunging folds in the Clinchport thrust sheet (point 11 in Figure 2.1C) (Bayona et al., in press). In map view and from north to south, the Clinchport fault cuts up section from a thick unit 1 to a thin unit 1 and, farther south, to the stiff unit 2, forming two south-plunging hanging-wall lateral ramp anticlines. A rise of detachment to strata of unit 4 and a south-plunging fold mark the southern end of the Clinchport fault at the RFTZ. The surface trace of the Dalton fault ends southward at a north-plunging syncline that is near the north end of the Rome fault and within the CTZ.

South of the RFTZ, northeast-east-plunging asymmetrical anticlines and flat-bottomed synclines diverge from the northeast-striking Chattooga fault (point 10 in Figure 2.1C)(Coleman, 1988). Folds in this area have a wavelength shorter than folds in northwestern areas 1 and 2. Rocky Mountain and Horseleg folds are the surface expression of a blind thrust system (Figure 2.3D). These faults are detached within unit 1, and the faults cut up section along strike, in a short distance from south to north, to upper detachment levels within units 2 and 3. The strike deviation of Rocky Mountain and Horseleg folds has been associated with the change in rheology of units along the lateral ramp (Bayona et al., in press).

In the subsurface, two types of ramp anticlines are identified in seismic reflection profiles beneath the Rome thrust sheet and south of the Rocky Mountain-Horseleg folds. One type corresponds to high-amplitude (elevation of the lower detachment from near top of basement to surface) ramp anticlines in the trailing segments of the Chattooga and Peavine thrust sheets (cross sections 5 and 6, Plate 2.1). The other type is low-amplitude ramp anticlines with short separation identified in the intermediate segment of the Peavine thrust sheet (cross sections 6 and

7, Plate 2.1), and in the trailing segment of the composite Dunaway Mountain thrust sheet (Figure 2.3F). Low-amplitude ramp anticlines in the intermediate segment of the Peavine thrust sheet fold the high-amplitude ramp anticline in the trailing segment of the Peavine thrust sheet.

#### **2.4.6 Area 6: Rome thrust sheet**

Southeast of the Clinchport and Chattooga faults in Georgia and the Peavine anticline and Dunaway Mountain thrust sheet in Alabama is the Rome thrust sheet (Osborne et al., 1988). The Rome thrust sheet consists of deformed shale and thin-bedded limestone of unit 1 (Conasauga Formation), and the stiff-layer unit 2 cover has been eroded, except in a few very small areas. The present eroded trace of the leading edge of the Rome fault is sinuous and irregular, and in general, the dip of the Rome thrust sheet is very shallow, as discussed below.

The sinuosity and strike of the leading edge of the Rome thrust sheet changes across transverse zones. Between the CTZ and RTZ in Georgia, geologic map patterns (Cressler, 1970) show that the irregular trace of the Rome fault mimics the trace of the topographic contour lines (Figure 2.1B). Within the RTZ, the trace of the Rome fault curves westward widening the thrust sheet on the surface (point 5 in Figure 2.1C), as well as truncates and diagonally crosses strike of the Rocky Mountain-Horseleg folds, Chattooga and Kingston thrust systems. Between the RTZ and the ATZ, the Rome fault strikes southwestward and truncates beds in small folds on the southeast limb of the Peavine anticline (Figure 2.3C). Within the ATZ, the trace of the Rome fault curves southward and then southwestward along the Dunaway Mountain thrust sheet. Southwest of the ATZ, the Rome fault truncates southeast-dipping strata and local cross structures within the Dunaway Mountain thrust sheet (Figure 2.3F) (Garry, 1999).

The shallow dip of the Rome thrust sheet is evident from the irregular map trace, presence of windows, hanging-wall cut offs, and lack of seismic imaging of the near-surface fault (Figure 2.2). Within the ATZ and CTZ, the Ballplay and Lamasgus windows, respectively, expose rocks of unit 4 as a result of folding of the fault surface (Figure 2.1D). In Georgia, the Rome fault surface is folded coaxially but less steeply than footwall beds by the Rocky Mountain-Horseleg folds (Figure 2.3D). In the subsurface, the trailing imbricates of the Peavine and Chattooga thrust sheet are truncated by the Rome fault and also fold the shallow-dipping Rome fault. The northwest (leading) edge of the Rome thrust sheet is in upper Conasauga strata, whereas the southeast (trailing) edge is in lower Conasauga strata (e.g., Cressler, 1970), further

indicating shallow dip of the Rome fault. The lack of seismic imaging is consistent with a very thin, shallow thrust sheet that is lost in surface noise (Figure 2.2). Thus, the seismic profiles do not image a frontal ramp of the Rome thrust sheet rising from the décollement; in contrast, seismic reflectors clearly image strata of units 1 and 2 in frontal ramps of the Jones Valley and Helena thrust sheets.

The Rome thrust sheet narrows abruptly at its northern and southern ends. North of the CTZ, however, Cressler (1974) and Kesler (1975) mapped the Rome fault as a straight, north-striking fault that extends farther north beyond the Georgia-Tennessee state boundary. The structural equivalent along strike to the Rome thrust sheet and across the CTZ is an antiformal duplex of the Dalton thrust system (Figure 2.3E). As described above, the Rome fault is characterized by an irregular and sinuous trace rather than by a straight trace, and the thrust sheet dips nearly horizontal (Figure 2.3D) rather than with  $\sim 45^\circ$  to the southeast (Dalton fault in Figure 2.3E). Therefore, I consider that the shallow-dipping Rome thrust sheet ends within the CTZ and that the antiformal duplex of the Dalton fault in the north is a different structure that also terminates southward within the CTZ. The southwestern end of the Rome fault is truncated beneath the Helena thrust sheet.

#### **2.4.7 Area 7: Western Coosa and Helena thrust sheets, the Coosa deformed belt, and Yellowleaf fault**

The presently eroded leading trace of the western Coosa thrust sheet includes two small-scale salients separated by a small-scale recess within the ATZ. Northeast of the ATZ and within the ATZ, the level of detachment cuts irregularly up- and down-section in stratigraphic position within unit 1. Stratigraphic units hosting the lower detachment level in the northeastern salient are, in stratigraphic order, upper units of the Chilhowee Group, the Shady Dolomite, and the Rome and Conasauga Formations;  $\sim 800$  m separates the uppermost beds of the Chilhowee Group from the upper beds of the Conasauga Formation (Ferrill, 1989). At the northeast side of the ATZ, the western Coosa thrust sheet dips southeastward beneath the Pell City and Jacksonville thrust sheets, and the trailing edge is cut by leading (Talladega) fault of the metamorphic thrust belt deep in the subsurface (cross sections 7 and 8, Plate 2.1). The narrowest exposed segment of the western Coosa thrust sheet coincides with the small-scale recess geometry of the leading trace of the fault, and an east-striking segment and termination of the

Helena thrust sheet (Graham, 1999). At the southwest side of the ATZ, the western Coosa fault and a diverging splay bound the Angel block, which constitutes the southwestern small-scale salient. In both faults, the level of detachment rises southwestward from unit 1 to the lower beds of the Knox Group (unit 2). Farther southwest and along the southwest side of the Angel block, southwest-plunging, hanging-wall lateral-ramp folds mark the along-strike transition from the western Coosa thrust sheet to the Coosa deformed belt (Thomas and Bayona, 2002).

The eroded trace of the Helena thrust fault is characterized by two small-scale curves at the ATZ and Bessemer transverse zone (BTZ). A transverse fault within the ATZ divides the Helena thrust sheet into northeastern and southwestern segments. The Helena fault in the northeastern segment bends gradually to an eastward strike (point 3 in Figure 2.1C), the basal detachment cuts up section along strike from unit 1 into the basal part of unit 2, and the fault is truncated on the east by the western Coosa fault (Graham, 1999). Along the east-striking fault, beds in the Helena hanging wall dip southward following the southwestward dip of a footwall lateral ramp in unit 4 (Bayona et al., in press) and forming the shallower of two down-to-southwest plunging steps that account for ~4000 m of relief in the deep Coosa synclinorium in the Helena thrust sheet (Thomas, 1990). In cross section, the geometry of the Helena fault northeast of the ATZ follows the geometry of the footwall block (Peavine thrust sheet) with a very gentle southeastward dip. The Helena fault in the southwestern segment has an irregular southwesterly strike for more than 110 km. The Helena fault is detached from the regional décollement, which follows the geometry of the southeastern margin and floor of the Birmingham graben (BG) (Figure 2.3G). At the BTZ, the Helena fault curves gradually southward and then curves abruptly west-southwestward (point 4 in Figure 2.1C). The southern part of the Helena fault has a diverging splay (cross section 17, Plate 2.1), and farther south Cretaceous coastal plain deposits cover the traces of both faults. The detachment horizon (unit 1) in the southern part of the fault trace includes clastic deposits of the Rome Formation and a dominantly thick carbonate succession of the Conasauga Formation (Thomas et al., 2000).

The intermediate part of the Helena thrust sheet has two structural levels of deformation southwest of the ATZ. The lower level consists of a duplex system involving a very thin unit 1 and a thick unit 2 (Figure 2.3G) now located within the southeastern part of the Birmingham graben (cross sections 9 to 14, Plate 2.1). The trailing part of the Helena thrust sheet includes a ramp anticline that slightly folds overlying structures and a trailing flat segment. The upper level

of deformation is an emergent imbricate fan system, called the Coosa deformed belt (Figure 2.3G) (Thomas and Drahovzal, 1974). The stratigraphic position of the detachment level changes irregularly and northwesterly up section from the uppermost beds of unit 2 to lower beds of unit 3. All imbricates involve strata of the lower part of unit 4. The Coosa deformed belt ends northeastward along strike at the ATZ, where southwest-plunging folds mark the connection with the lower detachment level in the western Coosa thrust sheet along lateral ramps (Thomas and Bayona, 2002).

The southern end of the Coosa deformed belt merges with the Yellowleaf thrust sheet. The detachment level in the latter thrust sheet changes southward along strike from beds in unit 4 to beds in unit 1. On the surface, the Yellowleaf fault juxtaposes unit 4 strata against unit 4 strata. In the subsurface, however, the Yellowleaf thrust sheet includes a ramp anticline at different positions across the HTZ. Northeast of the HTZ, the ramp anticline is near the trailing segment of the thrust sheet, whereas the leading segment brings to surface strata of units 3 and 4 along the upper detachment level (cross section 14, Plate 2.1). Southwest of the HTZ, the ramp anticline is in the leading segment, but the ramp is completely in the subsurface (cross section 15, Plate 2.1). Therefore, the stratigraphic level of detachment of the Yellowleaf thrust sheet changes along strike along a southwest-dipping lateral ramp.

#### **2.4.8 Area 8: trailing trust sheets: eastern Coosa, Pell City, Jacksonville, Indian Mountain, Choccolocco Mountain, and Sleeping Giants thrust complexes**

Deformation in trailing thrust sheets involves at least two horizons of detachment that control deformation at two structural levels. In addition to detachment levels within unit 1, other levels of detachment are in beds near top of unit 2, along the contact between units 2 and 3, and within unit 3.

At least two structural levels of deformation are identified in the eastern Coosa thrust sheet. In northwestern Georgia, the eastern Coosa thrust sheet broadly exposes Conasauga and Knox strata (units 1 and 2) and Rome strata along the leading trace of the fault and in trailing structures. Strata of unit 3 are also exposed in trailing synclines north and south of the Clinchport and Rome transverse zones. The eastern Coosa thrust sheet overlies subsurface duplexes involving unit 1. Identification of subsurface duplexes is supported by the recognition in seismic reflection profiles of southeast-dipping reflectors characteristic of unit 1 and by the

calculation of depth to the top of basement at ~3 km. An east-west structural high aligned with the end of the Rome thrust sheet and within the CTZ (Figure 2.1C) separates tighter folds and thicker horses on the north (cross section 1, Plate 2.1) from wider folds and thinner horses on the south (cross section 2, Plate 2.1). The eastern Coosa thrust sheet between the CTZ and RTZ includes several leading imbricates with a northeasterly strike, and tight anticlines with broad synclines in the middle and trailing parts. This configuration, similar to structures in areas 1, 2 and 5, suggests a shallow detachment that may correspond to the roof of underlying duplexes. At the RTZ, the leading thrust fault at the eastern Coosa system bends abruptly (point 6 in Figure 2.1C) and trailing splays diverge with a more northerly strike forming horsetail structures. In Alabama, the eastern Coosa thrust sheet dips southeast, flattens above the trailing segment of the Peavine thrust sheet, is overlain by structures forming the Talladega fault salient (point 8 in Figure 2.1C), and is truncated on the southwest by the Pell City and Jacksonville thrust sheets.

Two down-to-southwest plunging steps of the structural level of the fault and corresponding southwestward rise in stratigraphic level of detachment characterize the geometry of the Pell City thrust sheet across the ATZ (Thomas, 1990). Northeast of the ATZ, the thrust sheet is a narrow belt that consists mostly of deformed unit 1 strata. Across the ATZ, the thrust sheet significantly widens and plunges southwestward, the trace of the leading edge has an abrupt dextral offset, and the detachment level cuts up section through the middle to upper beds of unit 1 to the base of unit 2 forming southwest-plunging, hanging-wall lateral-ramp anticlines. Farther southwest, the thrust sheet widens and the leading trace of the Pell City fault bends abruptly southeastward at the Harpersville transverse zone (HTZ, point 7 in Figure 2.1C). The southwestern end of the Pell City thrust sheet is marked by a rise of the level of detachment to the middle part of unit 2 (cross section 14, Plate 2.1), and by northwest-striking, upright isoclinal folds, involving beds of units 2 and 3, paralleling the northwest-striking trace of the Pell City fault (Thomas and Drahovzal, 1974; Cook, 2001). The surface of the Pell City fault is folded by ramp anticlines in the trailing part of the Helena thrust sheet (Figure 2.3G), producing the structural relief to expose deformed strata of units 3 and 4 in the Fort McClellan windows (Figure 2.1D). Also, the surface of the Pell City fault follows southwestward and northeastward dips of footwall lateral ramps in the Coosa deformed belt at the ATZ and HTZ, respectively.

Duplexes with floor and roof faults in strata of unit 1 are identified in the Jacksonville thrust sheet, as well as in the Indian Mountain, Choccolocco Mountain, and Sleeping Giants thrust

complexes. The Jacksonville thrust sheet changes from a duplex geometry in areas with exposures of lowermost beds of unit 1 into splays at both northern and southern ends, where strata of unit 2 are preserved. The preserved geometry of the floor detachment in the Indian Mountain, Choccolocco Mountain, and Sleeping Giants thrust complexes indicates a nearly flat surface forming klippe of lowermost beds of unit 1 (Bearce, 1978).

#### **2.4.9 Area 9: Metamorphic belt**

The Cartersville and Talladega faults separate rocks with no to very low-grade metamorphism and low topographic relief on the northwest from rocks with a higher grade of metamorphism and a pronounced topographic break on the southeast. The higher grade metamorphic rocks are grouped into the Talladega slate belt in Alabama and western Blue Ridge in Georgia, and they consist of polydeformed and variably metamorphosed metasedimentary cover rocks. Grenvillian basement rocks are exposed in the Blue Ridge in Georgia (Li and Tull, 1998). Affinity of the sedimentary cover and basement rocks with those inboard of the Laurentian margin suggests that these allochthons represent the outboard part of the Laurentian craton (Li and Tull, 1998; Tull, 1998). Surface mapping suggests that the minimum horizontal net slip of 23 km and a stratigraphic throw of 5 to 7 km in southernmost exposures in Alabama (Tull, 1998).

A small-scale salient curvature of the Cartersville and Talladega faults and the most hinterland unmetamorphosed thrust sheets (points 6 and 8 in Figure 2.1C) differs from the almost straight northeasterly strike of leading structures in areas 1 and 2 (Figure 2.1). The north-striking eastern Coosa and Cartersville faults bend abruptly southwestward at the RFTZ. This bend is south of the southernmost external basement massif in the Blue Ridge (Li and Tull, 1998). Between the RFTZ and RTZ, the trace of the Cartersville fault has a small-scale salient-recess geometry (point 9 in Figure 2.1C), and the Cartersville fault bends abruptly westward south of the RTZ. The leading trace of the eastern Coosa fault also bends westward at the RTZ. On the southwestern side of a prominent salient of the metamorphic belt at the ATZ (point 8 in Figure 2.1C), northeast-striking Jacksonville and Talladega faults bend abruptly northward at the ATZ. The traces of both the Cartersville and Talladega faults end in opposite directions in this prominent small-scale salient.



## 2.5 STRUCTURAL STYLES

### 2.5.1 Structural style one: fault-related folds

The first structural style is defined by a fault and associated fold. Structures of areas 1, 2, 3, and 5 include broad asymmetrical anticlines, flat-bottomed synclines, detachment folds, and tight asymmetrical folds (Figures 2.3A to D). The stratigraphic position of the detachment level is dominantly within upper beds of unit 1 (Conasauga Formation); therefore, these structures include a thickness of the weak layer (unit 1) that is less than half as thick as the thickness of the regional stiff layer (unit 2). In northwestern Georgia, geometry of fault-related folds is affected by the rise of the detachment level to strata of units 2 and 3 (Bayona et al., in press). All these folds are primarily associated with the three-dimensional ramp-flat geometry of the Appalachian thrust belt (e.g., Jamison, 1987). Footwall deformation includes moderate-dipping to overturned beds in the limb of the adjacent flat-bottomed syncline (Figure 2.3A) or a leading imbricate fault with an associated tight fold (Figure 2.3B). In northwest Georgia, the width of folds decreases southeastward from areas 1 to 2, and 5. The low amplitude of folds and relative short separation of thin-skinned faults in areas 1 to 3 are dominantly related to the shallow position of the top of basement. However, low-amplitude ramp anticlines are also imaged by seismic reflection profiles in the trailing segments of the Chattooga, Peavine, and Dunaway Mountain thrust sheets.

Southeast-dipping thrust sheets of the Helena (leading segment), western Coosa, and Pell City thrust sheets may also be included in structural style one. In general, the level of detachment of these structures is in upper beds of unit 1 (Rome and Conasauga Formations), but the stratigraphic position of detachment changes laterally either to upper levels or lower levels (e.g., western Coosa thrust sheet). The cross-section geometry of the Helena, western Coosa, and Pell City faults varies from a ramp-flat-ramp geometry to curved (concave) trajectory with more than 3 km relief. Plunging folds in the western Coosa and Pell City thrust sheets suggest that western Coosa, Helena, and Pell City thrusts include hanging-wall lateral ramp folds (Thomas and Bayona, 2002); however, frontal-ramp anticlines for the Coosa, Helena, and Pell City faults are not observed on the surface because of the present level of erosion. Thomas (2001) interpreted the Helena thrust sheet as an out-of-sequence ramp thrust with large amount of horizontal separation and with a fault-bend fold geometry at the leading (now eroded) segment of the fault. Near the southwest end of the Pell City thrust sheet, the subsurface structure of the hanging-wall cut off is interpreted as a wide ramp anticline (cross section 13, Plate 2.1).

The major difference in the structural geometry between structures in areas 1 to 3 and the Helena, western Coosa, and Pell City faults is that the latter structures have more curved and irregular trace of the fault in map view, larger amount of separation along the fault, and the Helena has evidence of out-of-sequence deformation. Therefore, leading structures of the Helena, western Coosa, and Pell City thrust sheets necessarily would not restore palinspastically in the same order. The Helena, western Coosa, and Pell City thrust are not affected by mushwad deformation.

### **2.5.2 Structural style two: duplexes**

The second structural style corresponds to duplex systems, which are differentiated on the basis of stratigraphic position of floor and roof detachment levels. The Gadsden and Palmedale mushwads are ductile duplex complexes with floor and roof levels within unit 1. Tectonic thickening of mushwad structures elevates and distorts the geometry of the overlying stiff layer (unit 2) (Thomas, 2001). Kinematic models of deformation of the mushwad Gadsden include fault-bend folds and detachment anticlines in the now eroded roof of the mushwad (Thomas, 2001). In contrast, small-amplitude anticlines are associated with a conjugate of frontal and back thrust in the roof of the Palmerville mushwad, that is the crest area of the Birmingham anticlinorium (Thomas, 2001).

Trailing structures (eastern Coosa, Jacksonville, and Sleeping Giants thrust complexes) have duplexes with floor and roof levels within unit 1 and the number of horses varies from 1 to 4. Horses are wider in the eastern Coosa thrust sheet than in the Jacksonville and Sleeping Giants thrust complexes. The roof of each duplex consists dominantly of a thrust sheet with an uncomplete stratigraphy of unit 1 and to variable record of the stratigraphy of the stiff layer, like in the eastern Coosa thrusts sheet. In Georgia and south of the CTZ, the duplex consists of only one wide horse, and in the area where the top of basement is shallow no duplex is interpreted in the subsurface. An important difference from mushwad structures is that these thrust sheets are in the trailing part of the thrust belt. It is inferred that Indian Mountain and Choccolocco Mountain thrust complexes also include duplex systems similar to the Jacksonville thrust sheet. However, present level of erosion does not allow the definition of the structural style of these structures.

Duplex structures are also interpreted in the Clinchport and Dalton thrust sheets, trailing segments of the eastern Coosa thrust sheet, and subsurface duplexes in the Helena thrust sheet. Antiformal duplexes of the Clinchport and Dalton thrust sheets include only one horse and have the floor detachment in the regional décollement and the roof at upper beds of unit 1 or at the contact between units 1 and 2 (Figure 2.3E). At the trailing segment of the eastern Coosa thrust sheet and south of the RTZ, a narrow duplex system includes beds of units 1 and 2 (cross sections 4 and 5, Plate 2.1). The duplex system in the intermediate segment of the Helena thrust sheet has the floor detachment within upper beds of unit 1 and the roof detachment within upper beds of unit 2 and lower beds of unit 3 (Figure 2.3G). The number of horses varies along strike from two to four.

### **2.5.3 Structural style three: imbricate fans**

The third structural style consists of emergent imbricate fan systems that are detached from beds within the uppermost unit 2 and unit 3 and overlie duplexes described in the previous paragraph. This structural style includes deformation of the Coosa deformed belt, and the roof of duplexes in Clinchport, Dalton, and trailing eastern Coosa thrusts sheet. The fan imbricate in Clinchport and Dalton involves a very thin unit 2 and beds of unit 3. In the Coosa deformed belt, the stratigraphic level of detachment rises irregularly from upper beds of unit 2 to lower beds of unit 3, and all the imbricates involve lower strata of unit 4.

In the trailing eastern Coosa, the imbricate fan system is very local and involves upper beds of unit 2 and lower beds of unit 3. Deformation in lower fine-grained deposits of unit 3 (Middle Ordovician Rockmart Slate and Athens shale) includes clay minerals and a structural fabric typical of low-grade metamorphic rocks, whereas clay minerals and structural fabric in upper beds of unit 3 (Devonian Frog Mountain Sandstone and Mississippian Fort Payne Chert) indicate a lower degree of deformation (Sibley, 1983; Renner, 1989). This change in degree of deformation within unit 3 has been used as evidence of a pre-Devonian deformation event (Sibley, 1983; Higgins et al., 1988; Renner, 1989).

#### **2.5.4 Structural style four: Rome thrust sheet and its palinspastic restoration**

The shallow Rome thrust sheet is characterized by its irregular and sinuous trace and by its nearly horizontal dip. No other regional thrust sheet in the Appalachian thrust belt of Tennessee, Georgia, and Alabama (Woodward, 1985) shares the same characteristics.

Because of its structural position in the footwall of the Helena, western Coosa, and eastern Coosa faults, the Rome fault has been considered as a splay from the regional décollement in the footwall of these faults (Thomas, 1985, 1990; Ferrill, 1989). If the Rome thrust sheet is palinspastically restored on the foreland side of the Helena thrust sheet, a large transverse offset in the leading frontal ramp is required to accommodate the abrupt southern termination of the Rome thrust sheet (Figure 2.1B). The present outcrop trace of the Helena fault indicates no offset at that location. The Helena fault generally places older hanging-wall rocks on younger footwall strata (both within unit 1) in a conventional break-forward pattern at the trailing cutoff of the Rome thrust sheet. The Helena fault, however, cuts up and down section (from unit 1 to unit 2) along strike in the hanging wall, placing younger rocks (unit 2) over older rocks (unit 1) along parts of the trailing cutoff of the Rome thrust sheet (Osborne et al., 1988). The along-strike variations in stratigraphic separation indicate out-of-sequence thrusting, similar to folding in the footwall of the Rome thrust sheet as documented by the Ballplay and Lamasgus windows, in the Rocky Mountain-Horseleg folds, and trailing imbricates of the Peavine and Chattooga thrust sheets.

An alternative interpretation is that the Rome thrust sheet restores in the foreland of the eastern Coosa thrust sheet and in the hinterland of the Helena and western Coosa thrust sheets. This interpretation allows a clearer explanation of the flat-dipping nature of the Rome thrust sheet, truncation of footwall folds, and out-of-sequence thrusting of the Helena thrust sheet and other footwall folds. In addition, the abrupt widening and narrowing of its preserved length, as described above, and the abrupt southern termination of the Rome fault would not affect the palinspastic restoration of the Helena thrust sheet. However, restoration of the Rome thrust sheet affects the restored geometry of southeastern trailing structures, such as the eastern Coosa and Pell City thrust sheets. Because of small-scale deformation, bed-length balance of unit 1 is not possible, and the lack of preserved stiff-layer cover precludes both bed-length balance of unit 2 and area balance of unit 1. The shape of the restored Rome thrust sheet is constrained by calculation of the minimum preserved length, by minimum estimate of the eroded cover, and by

matching the restored geometry of foreland thrust sheets and the most likely geometry of the leading trace of the Rome thrust sheet.

This alternative interpretation of the palinspastic restoration of the Rome thrust sheet raises a new question about the lateral continuity of the presently continuous eastern Coosa and western Coosa thrust sheets in their palinspastic position. Stratigraphic level of the basal detachment in the eastern Coosa fault is mainly in beds of the Rome Formation, whereas the detachment in the western Coosa fault cuts irregularly up and down and in short distances within the Conasauga and Rome Formations, the Shady Dolomite, and upper units of the Chilhowee Group. Beside the differences in geometry of detachment levels, a large offset is indicated between the eastern and western Coosa thrust sheets because apparently abrupt along-strike changes in stratigraphy of synrift strata of unit 1 (see below), synorogenic Middle and Upper Ordovician strata (Chapters 3 and 4), as well as Devonian and lower Mississippian strata of unit 3 (Ferrill, 1989). The substantial differences in stratigraphy further suggest large separation between the eastern and western Coosa thrust sheets, permitting the possibility that the eastern Coosa thrust sheet is part of the Pell City-Jacksonville thrust system, whereas the western Coosa thrust sheet and the Helena thrust sheet comprise another thrust system, interconnected with lateral ramps (Thomas and Bayona, 2002).

## **2.6 STRUCTURAL CONFIGURATION OF THE TOP OF BASEMENT**

The structure of the top of the Precambrian crystalline basement rocks beneath the thin-skinned Appalachian thrust belt is depicted by onlap and breaks of lowermost laterally continuous reflectors of unit 1 (e.g., Figure 2.2). The southeastern extent of seismic reflection profiles is limited near the Cartersville-Talladega faults, and one seismic line of the Consortium for Continental Reflection Profiling (COCORP) extends into the metamorphic thrust belt of Alabama and Georgia (Nelson et al., 1985; McBride, 2001). Therefore, documentation of possible basement faults farther southeast depends on interpretation of abrupt variations of lithofacies and thicknesses of syntectonic rocks, such as the synrift strata grouped in unit 1 or synorogenic strata in units 3 (Chapter 3) and 4. The dominant geometry the top of basement is of horst and half-graben structures (Ferrill, 1989), and a regional southwestward deepening of the top of basement across transverse basement faults (Figure 2.4).

Locations of northwest-striking transverse basement faults are less constrained because seismic reflection profiles are generally oriented northwest-southeast. Only two strike-parallel seismic lines document a southwestward drop in the top of basement rocks across the Anniston transverse zone (figure 3 in Coleman, 1988) and across the Rome transverse zone.

Consequently, the following criteria were used for identification of a transverse basement fault: abrupt along-strike change in offset of northeast-striking basement faults, differences in map-view and cross-section profiles of basement fault systems, and variations in thickness and lithology in late synrift strata of the Conasauga Formation (unit 1). Transverse basement faults make the boundaries of the three structural configurations of the top of basement (Figure 2.4), which are described below.

The northern configuration corresponds to the top of basement beneath the thrust belt in northwestern Georgia. Depth to top of basement is less than 3 km, and the basement is closely broken by an array of northeast-striking, down-to-southeast faults with small (< 500 m) vertical offsets. On the north side of the northernmost transverse basement fault, which coincides with the position of the Clinchport transverse zone in the thin-skinned thrust belt, northeasterly striking basement faults define two narrow half-grabens (Figure 2.4). Northward deepening of the top of basement across the northernmost transverse basement fault has been confirmed by a local gravity survey (Guinn and Long, 1978). The top of basement on the south side of the northernmost transverse basement fault has a nearly flat configuration with a graben structure with less than 500 m of relief.

The wider and deeper Birmingham graben (BG) beneath the thrust belt in Alabama defines the southern configuration. The northwestern shoulder of the BG is bounded by down-to-southeast faults with large (> 1000 m) vertical offsets. The graben is more than 37 km wide, and the graben floor is nearly flat in cross sections. Both the northwest shoulder and the bottom of the graben deepen southwestward (Figure 2.4). A narrow down-to-northwest fault system marks the southeastern margin of the BG, and has a dextral offset across a local transverse basement fault in the southern part of the southern configuration. This transverse fault also offsets a down-to-southeast basement fault system, that is the southernmost basement fault documented by seismic reflection profiles.

The central configuration corresponds to a transition from the northern shallow configuration of the top of basement to the wide and deep basement graben on the southwest.

The boundaries of the central configuration are a transverse basement fault on the southwest that coincides with the position of the ATZ in the thin-skinned thrust belt and two parallel transverse basement faults on the northeast that coincides with the boundaries of the RTZ in the thin-skinned thrust belt. The BG in the central configuration is less than 21 km wide and has a dextral offset across a transverse fault (Figure 2.4). The northwest boundary of the BG has a wide system of down-to-southeast basement faults, which have a dextral offset with respect to the down-to-southeast basement faults in the southern configuration. The down-to-northwest fault system has a sinistral offset across the southern transverse basement fault and a dextral offset across the northern transverse faults.

Southwestward deepening of the top of basement in the northwest shoulder and graben floor of the BG in southern and central configurations parallels southwestward deepening of the top of basement documented for the Black Warrior basin (Figure 2.4) (Thomas, 1988; Whiting and Thomas, 1994). The southeastern BG shoulder is deeper than the northwestern BG shoulder, but it does not follow the same southwestward pattern of deepening of the northwest shoulder. The deepest zone on the southeastern shoulder is in the central configuration and coincides with a small-scale salient in the Talladega fault (point 8 in Figure 2.1C, Figure 2.4). This difference in the regional deepening of the top of basement coincides with interference patterns of Black Warrior and Appalachian foreland subsidence documented by Whiting and Thomas (1994). Flexural subsidence in the Black Warrior basin increased southwestward and the clastic wedge thickens toward the Ouachita Mountains. Flexural subsidence in the Appalachian basin deepened the top of basement southeastward. Therefore, Appalachian and Ouachita tectonic loads affected the configuration of the top of basement (Figure 2.4).

## **2.7 PRE-DEFORMATIONAL THICKNESS OF UNIT 1 AND LITHOFACIES OF THE CONASAUGA FORMATION**

Because late Paleozoic tectonic loading influenced the present structural configuration of the top of basement, the early post-rift geometry of the top of basement was determined using a palinspastic map of the top of unit 1 (Figure 2.5) and the mapped basement structures (Figure 2.4) as the base on which an isopach map of the compacted thicknesses of unit 1 was constructed (Figure 2.6). The isopach map of unit 1 follows the regional trend defined by the present configuration of the top of basement: narrow and shallow half grabens beneath the thrust belt in

northwestern Georgia, and wider and deeper half grabens beneath the thrust belt in Alabama (Figure 2.6). However, details of the isopach map indicate a uniform thickness of unit 1 northwest of the graben, northwestward thickening across the half-graben, and a slightly greater thickness of unit 1 southeast of the graben than northwest of the graben. The isopach map of unit 1 also confirms that the BG is a complex system of half-graben structures with dextral offsets of half-graben depocenters across transverse basement faults.

The southernmost down-to-southeast basement fault beneath the leading edge of the metamorphic belt (Figures 2.4 and 2.6) may be the border of another graben on the southeast of the BG. However, there is no direct identification of basement faults southeast of the southeastern margin of the BG to delineate another basement structure. Consequently, basement faults southeast of the BG can only be inferred from the identification of abrupt variations in lithofacies and stratigraphic thickness of the Rome and Conasauga Formations (beds of unit 1 above the basal detachment).

The Rome Formation in outcrops is an irregular succession of mudstones, siltstones, and sandstones with some interbeds of limestone and dolostone (Raymond et al., 1988). In the subsurface and southeast of the Helena fault, the Rome Formation contains anhydrite in intervals near the thrust fault (Thomas et al., 2001). Outcrops of the Rome Formation restore southeast of the BG; however, Rome stratigraphy is documented in deep wells northwest of the BG (Thomas et al., 2001). Association of fauna, lithofacies, and sedimentary structures of the Rome Formation indicate deposition in fault-bounded horst and graben blocks of a continental rift setting during Early Cambrian time (Thomas et al., 2000).

The Conasauga Formation overlies the Rome Formation and includes a wide range of carbonate and siliciclastic deposits in the present deformed locations (Figure 2.7) (Osborne et al., 2000). Palinspastic restoration of major lithofacies of the Conasauga Formation supports an interpretation of the influence of mapped basement faults in the distribution of lithofacies (Figure 2.8) (Thomas et al., 2000). Carbonate lithofacies dominate on structurally high blocks, such as the northwestern shoulder of the BG, suggesting deposition in shallow-water environments. Stratigraphic sections and local outcrop data from the Gadsden mudstone (lithologic data from AMOCO No. 1 Young, Raymond, 1991) that restore within the BG (Thomas, 2001), and lithologic data from wells that have drilled into autochthonous Conasauga Formation within the BG (ARCO-Anschutz No. 1, Alabama Properties Co., Raymond, 1991) indicate that the



Conasauga Formation within the BG consists of a very thick succession (> 500 m) of thin interbeds of limestones and dark-colored shales.

The lithofacies assemblage of the Conasauga Formation within the BG is similar to the lithofacies assemblage of the Conasauga Formation in the leading and middle parts of the Rome thrust sheet. The palinspastic position of the Rome thrust sheet behind the Helena thrust sheet (Figure 2.5) places a thick succession of shale and thin-bedded limestone deposits southeast of carbonates and thin shale deposits (now in the Helena thrust sheet) that accumulated along the southeastern shoulder of the BG (Figure 2.8). The latter deposits constrain the location of another graben depocenter, named here as the Randolph-Heard graben (RHG, Figure 2.8).

Comparison of faunal assemblages from shales in the BG and in the Rome thrust sheet supports the interpretation of accumulation in two different graben systems. The assemblage of trilobites (*Glyptagnostus*) collected in the leading edge of the Rome thrust sheet indicates outer shelf oceanic conditions in the RHG, whereas limestones on the northwest shoulder of the BG are somewhat closer to the carbonate platform (A. R. Palmer written communication to W. A. Thomas, 2002).

Conasauga strata restoring southeast of the RHG have variable composition. In the trailing part of the Rome thrust sheet and eastern Coosa thrust sheet, interbeds of siltstone and sandstones in the Conasauga Formation (Cressler, 1970; Pickering et al., 1976) suggest proximity to uplifted areas on the eastern shoulder of the RHG in its northern part (Figure 2.8). The dominance of carbonate beds in the Conasauga Formation in the Pell City and Jacksonville thrust sheets, which restore southeast of the Rome thrust sheet, might indicate shallow-water clastic-free marine deposition on the southeastern shoulder of the RHG in its southern segment (Figure 2.8).

The geographic coincidence of thickness and lithofacies variations of the Conasauga Formation with contrasting relief of basement structures of the BG suggests accumulation on fault blocks and synsedimentary fault movement (Thomas et al., 2000). Lithologic similarity of autochthonous strata within the BG to strata in the Rome thrust sheet and palinspastic restoration of the Rome thrust sheet southeast of the Helena thrust sheet support the interpretation of deposition in a continental rift setting, including several fault-bounded horst and graben blocks, during Early and Middle Cambrian time.

## 2.8 DISCUSSION

Relationships between cover deformation and sub-detachment basement configuration may be established directly in areas with seismic information. This relationship is complemented with palinspastic maps showing variations in compacted thickness of the weak-layer unit 1 and lithofacies distribution of detachment-host units. Boundaries of structural styles and curvature of structures of the thin-skinned thrust belt are here related to abrupt differences of elevation of top of basement across basement faults. Lithofacies variations in the stratigraphic framework may control the stratigraphic position of upper detachment levels and the kinematics of thrust sheets.

Fault-related low-amplitude asymmetric anticlines of structural style one are formed dominantly in areas of shallow (< 3.5 km depth) basement affected by northeast-striking basement faults with small (< 350 m) vertical separation (Figures 2.3A and D). Palinspastic positions of ramp anticlines with footwall imbricates and detachment folds (Figures 2.3B and C) are related to isolated down-to-southeast basement faults with moderate vertical offsets (350-1000 m). This second group of structures reflects the resistance to foreland propagation of deformation because of the moderate shallowing of the top of basement and thinning of the weak-layer unit (e.g., Wiltschko and Eastman, 1983). Strike of all of these low-amplitude structures mimics the northeasterly trend of basement faults, suggesting that pre-existing extensional faults trigger frontal ramp generation as observed in other thrust belts (e.g., Hayward and Graham, 1989).

Tectonic growth of the Gadsden and Palmerdale mushwads of the structural style two is related to the large volume of unit 1 within the wide BG southwest of the ATZ and the large vertical offset of the top of basement (> 1000 m) along the northwestern margin of the BG (Figure 2.3F) (Thomas, 2001). Although the Peavine detachment fold (structural style one) and the Gadsden mushwad (structural style two) are adjacent to each other both in deformed and restored stages, the former restores above the central basement configuration and the latter restores above the southern basement configuration. The volume of unit 1 in the Gadsden mushwad restores within the broad BG, whereas the volume of unit 1 in the detachment fold restores in the downthrown block of a basement fault with moderate vertical separation (Figure 2.9).

Along-strike changes of structural styles in the thrust belt in northwestern Georgia are associated with variations in pre-deformational thickness of the weak unit 1. Interfering plunging folds (Rocky Mountain-Horseleg folds and folds in the Clinchport thrust sheet) restore in areas of shallow basement, but in places of abrupt thickening of unit 1 across transverse basement faults (Bayona et al., in press). In the Clinchport thrust sheet, the along-strike change from a duplex (Figure 2.3E) to a shallow, ramp anticline (similar to Figure 2.3D; cross section 2, Plate 2.1) is related to the northeastward deepening of the top of basement and associated thickening of the weak unit 1 across the Clinchport transverse zone. Similar to the mechanism for generation of frontal ramps, transverse basement faults also trigger lateral ramp generation. In addition to the lateral ramp geometry, the along-strike rise of detachment level from a thick unit 1 to a thin unit 1, and then to beds of units 2 and 3 caused vertical-axis thrust sheet rotations and the along-strike termination of these folds (Bayona et al., in press).

Assuming no scale dependency of structures, factors that control regional curvatures (e.g., Macedo and Marshak, 1999; Paulsen and Marshak, 1999) may also control small-scale curvatures. Abrupt curvatures of the northern Helena fault and the northern end of the Gadsden mushwad may be directly related to changes in elevation of the top of basement across transverse basement faults (points 2 and 3 in Figure 2.10A). The abrupt convex-to-the-foreland curve of the northeastern segment of the Helena fault reflects both the southwestward deepening of the top of basement across a transverse basement fault beneath the ATZ and the geometry of a southwest-dipping lateral ramp in the footwall (Bayona et al., in press). Southwestward deepening of the top of basement and thickening of the weak unit 1 across a transverse basement fault beneath the ATZ also correspond to the northeastern termination of the Gadsden mushwad (Thomas and Bayona, 2002).

Small-scale recesses are identified in the southern part of the Helena fault, at the southern end of the Pell City fault, and at the southern end of the Cartersville fault (points 4, 7, and 9 in Figures 2.10A and B). The southern curve of the Helena fault is gradual, probably reflecting a gradual northeastward deepening of the top of basement. At the position where the Helena fault broke upward (Thomas, 2001), the elevation of the top of basement changes southwestward from the floor to a shoulder configuration of the BG across a down-to-northeast basement transverse fault (point 4 in Figure 2.10A). This transverse fault is aligned with the Bessemer transverse zone in the thrust belt. The southward curvature of the Pell City fault and adjacent northwest-

striking structures in the hanging wall have been related to a northeast-dipping oblique ramp in the footwall (Cook, 2001). This lateral ramp in the footwall is aligned with the palinspastic position of a large, stepwise northeast-dipping lateral ramp of the Pell City thrust sheet along the Harpersville transverse zone (Figure 2.10B).

Along-strike variations in the strength of the detachment horizon is another mechanism that generates salients and recesses in thrust belts (e.g., Macedo and Marshak, 1999; Marret and Aranda-Garcia, 1999). Hence, along-strike variations in lithofacies of the Conasauga Formation in a palinspastic map (Figure 2.8) might have contributed to the generation of the small-scale salient in the Rome thrust sheet southwest of the RTZ (point 5 in Figure 2.10A). The apex of the Rome fault salient is dominated by shale and thin-bedded limestone lithologies. The Rome thrust sheet narrows abruptly northeast of the RTZ and includes coarser clastic deposits. In palinspastic maps, restoration of the Rome thrust sheet constrains the position of the RHG; therefore, the graben narrows and includes coarser lithologies northeastward from the RTZ. This configuration indicates that beds hosting the regional décollement had finer and shaly lithologies southwest of the RTZ, and favored an easier cratonward advance of that segment of the thrust sheet.

Basin geometry plays a primary control in along-strike variation in thrust-belt shortening (Figure 2.11) (Macedo and Marshak, 1999), in addition to strength of the detachment horizon. The slightly greater shortening in structures between the ATZ and RTZ (Figure 2.11) and small-scale salients of the eastern Coosa and Talladega thrust sheets (points 6 and 8 in Figure 2.10B) may be explained by deepening of the top of basement and associated thickening of weak strata in the RHG.

Small-scale curvatures of Rome, eastern Coosa, and Talladega-Cartersville faults between the Anniston and Rome transverse zones are similar to the convex-to-the-foreland curve of the northeastern segment of the Helena fault. However, no direct evidence links the curvature of the Rome, eastern Coosa, and Talladega-Cartersville faults to a change in elevation of the top of basement (points 5, 6, 8, and 9 in Figures 2.10A and B). On the basis of the relationship between syntectonic thickening across transverse basement faults and curvature of the Helena fault and Gadsden mushroom, several down-to-southwest transverse basement faults in the central configuration and southeast of the BG may be inferred (Figure 2.10B).

The present eroded trace of the Rome fault may also reflect the complex history of emplacement and rupture of the Rome thrust sheet. Truncation of footwall folds indicates that the Rome thrust fault has a component of out-of-sequence break-back movement. Folding of the Rome thrust sheet by footwall structures indicates a later break-forward movement on a deeper detachment. These relationships permit the suggestion of an early translation of the Rome thrust sheet that truncated fault-related folds developed as far as the northwest boundary of the BG. In this early event, strata in the Helena and western Coosa thrust sheets were translated with no deformation on a flat segment of the regional décollement. In a later event, the Helena and western Coosa faults broke upward displacing and breaking the Rome thrust sheet. Out-of-sequence faulting caused the erosion of the branch line and trailing segments of the Rome thrust sheet (Thomas and Bayona, 2002).

The zig-zag configuration of the shallow basement on the northwest shoulder of the Birmingham graben may represent structural highs or local promontories that controlled the kinematics of the thrust belt in intermediate and leading thrust sheets (e.g., Thomas and Bayona, 2002). These foreland obstacles act as stress concentrators that favored strain partitioning within the advancing thrust belt. For example, differences in the magnitude of shortening between the detachment fold and mushroom affect foreland structures. As the basal décollement propagated northwestward, minor differences in thrust-sheet translation were absorbed in a displacement transfer zone defined by the en echelon arrangement and along-strike terminations of the Wills Valley and Murphrees Valley anticlines (point 1 in Figure 2.10A; Thomas and Bayona, 2002). Similarly, differences in the magnitude of shortening along the Clinchport, Chattooga, and Kingston faults were absorbed in another displacement-transfer zone at the RFTZ defined by the along-strike terminations of the Wills Valley anticline and anticlines associated with the Chickamauga thrust system.

The differences in thrust-sheet translation on opposite sides of transverse basement faults formed displacement transfer zones, lateral ramps, and transverse faults. The alignment of these transverse structures in the thrust belt delineates the four transverse zones that cut across the entire Alabama and Georgia thrust belt (Figures 2.1C and 2.10B) (Thomas, 1990), and two local transverse zones, Rome and Clinchport, at the intermediate and trailing parts of the thrust belt. The coincidence in position of these transverse zones with transverse basement faults

corroborates the assumption of a genetic relation between transverse basement faults and transverse structures in the thrust belt (e.g., Thomas, 1990).

For intraplate rift configuration, the central configuration represents an accommodation (or transfer) zone between graben systems, according to the models of accommodation zones in the Suez rift (Moustafa, 2002). The southern transverse basement fault (parallel to the ATZ in the thrust belt) links northeast-striking basement faults with the same sense of throw. The transverse basement fault juxtaposes a deep and wide BG on the southwest with a narrower BG on the northeast. Northern transverse basement faults (parallel to the RTZ in the thrust belt) place the down-to-southeast fault system of the BG against shallow, tilted fault blocks of the northern configuration (Figure 2.4). Southeast of the tilted fault blocks, the depocenter of the RHG widens southwestward of the northern transverse basement faults (Figure 2.10A).

Vertical gradients of deformation within thrust sheets are interrupted by upper detachment horizons. Low-amplitude anticlines and associated faults that are detached from the regional décollement are an example of vertical attenuation of deformation (Figures 2.3A, B, and D). Positions of upper detachment levels encompass a wide range from strata in unit 2 to strata in unit 3. An upper detachment level separates the style of deformation in at least two structural levels with two different gradients of vertical attenuation of deformation. Duplexes dominate the lower structural level, whereas fan imbricates, such as the Coosa deformed belt, dominate the upper structural level. In trailing structures of the eastern Coosa thrust sheet, vertical attenuation of deformation in an upper structural level might have contributed to the up section decrease of structural fabrics and distinct clay mineral assemblage in beds of unit 3 (Sibley, 1983; Renner, 1989).

## **2.9 CONCLUSIONS**

Geometry and kinematics of structural styles in the thin-skinned and unmetamorphosed thrust belt of Alabama and Georgia may be directly and indirectly related to sub-décollement basement structures and the pre-deformational stratal architecture of the unit that hosts the regional décollement. In the leading and intermediate imbricates of Georgia and the leading imbricates in Alabama, low-amplitude fault-related anticlines form where depth to basement is shallow. In the intermediate imbricates in Alabama, high-amplitude fault-related anticlines form where the regional décollement is deep within the Birmingham graben; detachment folds

nucleate above down-to-southeast basement faults with moderate vertical separation; and a mushwad evolves above a broad graben bounded by basement faults with large vertical separation and containing a large volume of weak strata (i.e., shale).

Small-scale curvatures of the thrust belt are also related to differences in basement elevation across basement transverse faults. Small-scale salients or convex-to-the-foreland curvatures of the Helena fault and Gadsden mushwad are very abrupt, and they are related to a transverse basement fault that separates a narrow Birmingham graben on the northeast from a wider and deeper graben on the southwest. We use this direct observation to suggest that a transverse basement fault primarily controlled the salient geometry of the Rome, eastern Coosa, and Talladega faults. Abrupt curvatures are confined in transverse zones suggesting that distribution of northwest-striking basement faults and related differences in elevation of the top of basement played a primary role in the location of transverse structures in the thrust belt.

Vertical and horizontal gradients of deformation were partially controlled both by variation in elevation of the top of basement and pre-deformational basin architecture. Shallow basement promontories bounded by intersections of northeast-striking and northwest-striking transverse basement faults acted as stress concentrators that favored strain partitioning and differences in the style of deformation within the advancing thin-skinned thrust belt. These promontories contribute to the nucleation of thin-skinned transverse structures and the different transverse zones recognized in the thrust belt in Alabama and Georgia. The regional décollement is dominantly within weak layers of the Rome and Conasauga Formations, but thick shale beds in intermediate levels of the sedimentary wedge contributed to the generation of upper levels of detachment and the vertical differentiation of deformation into duplexes and imbricate-fan systems.

**Figure 2.1**

**ANTICLINES**

- BH - Birmingham
- CH - Clinchport
- MV - Murphrees Valley
- PV - Peavine
- RH - Rocky Mountain-Horseleg
- SQ - Sequatchie
- WV - Wills Valley

**SYNCLINES**

- BTM - Blount Mountain
- CAH - Cahaba
- CLB - Coalburg
- COO - Coosa
- FLD - Floyd
- LKT - Lookout Mountain
- SDM - Sand Mountain

**THRUST FAULTS**

- A - Chickamauga
- B - Big Canoe Valley
- C - western Coosa
- D - Dunaway Mountain
- E - eastern Coosa
- F - Kingston
- G - Jacksonville
- H - Helena
- I - Indian Mountain
- J - Jones Valley
- K - Sleeping Giants
- L - Dalton
- M - Choccolocco Mountain
- N - Chattooga
- O - Opossum Valley
- P - Pell City
- R - Rome
- S - Clinchport
- T - Talladega
- U - Coosa deformed belt, upper-level detachment
- V - Cartersville
- X - Straight Mountain
- Y - Yellowleaf

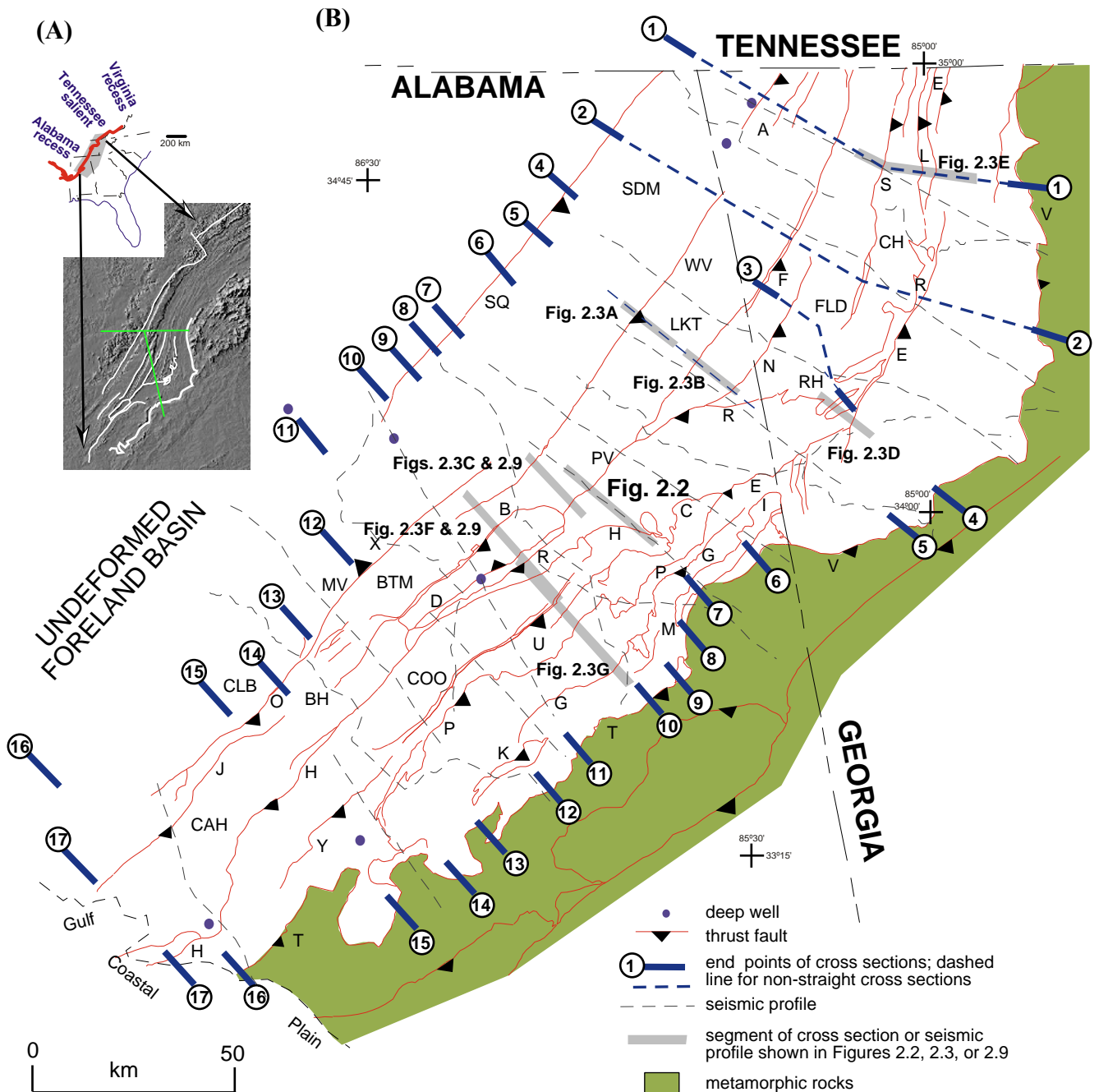
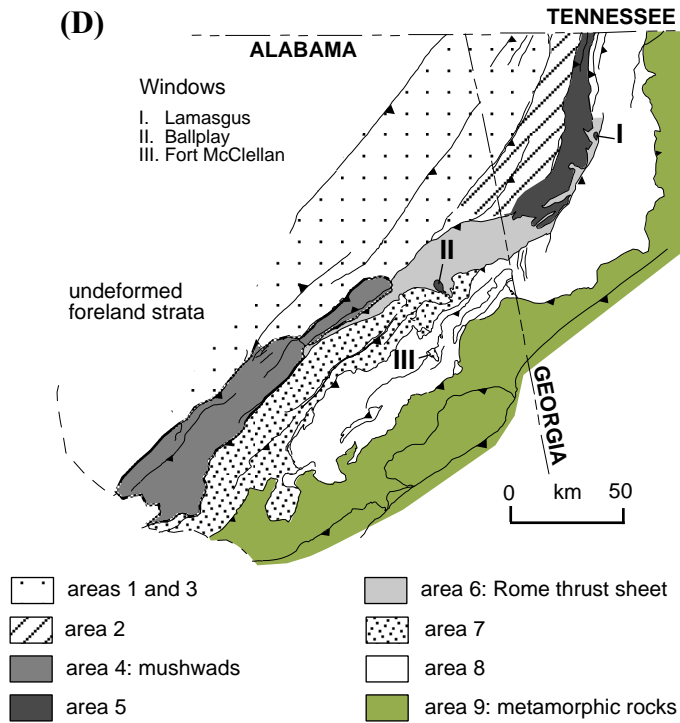
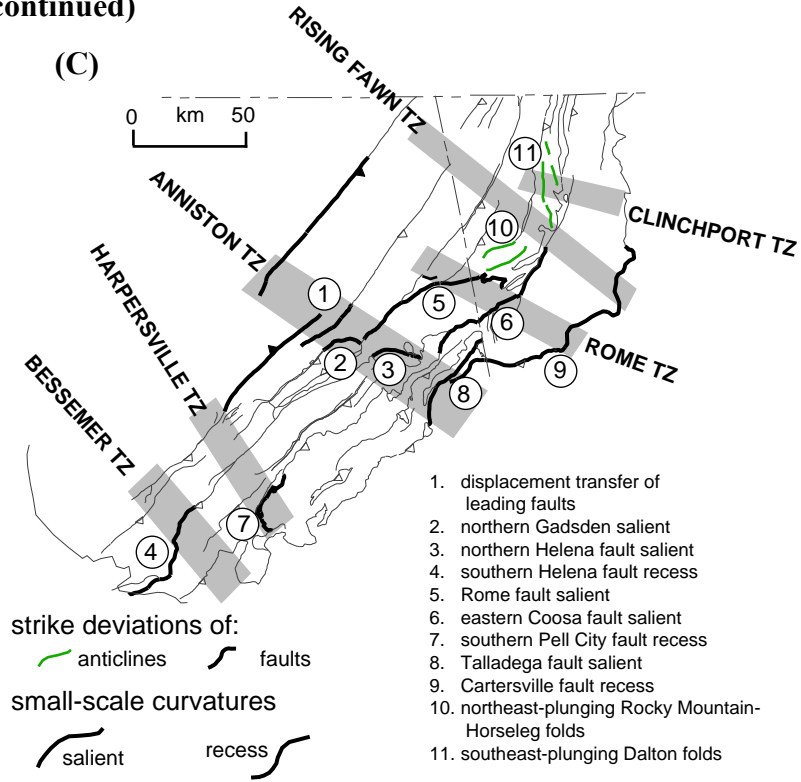


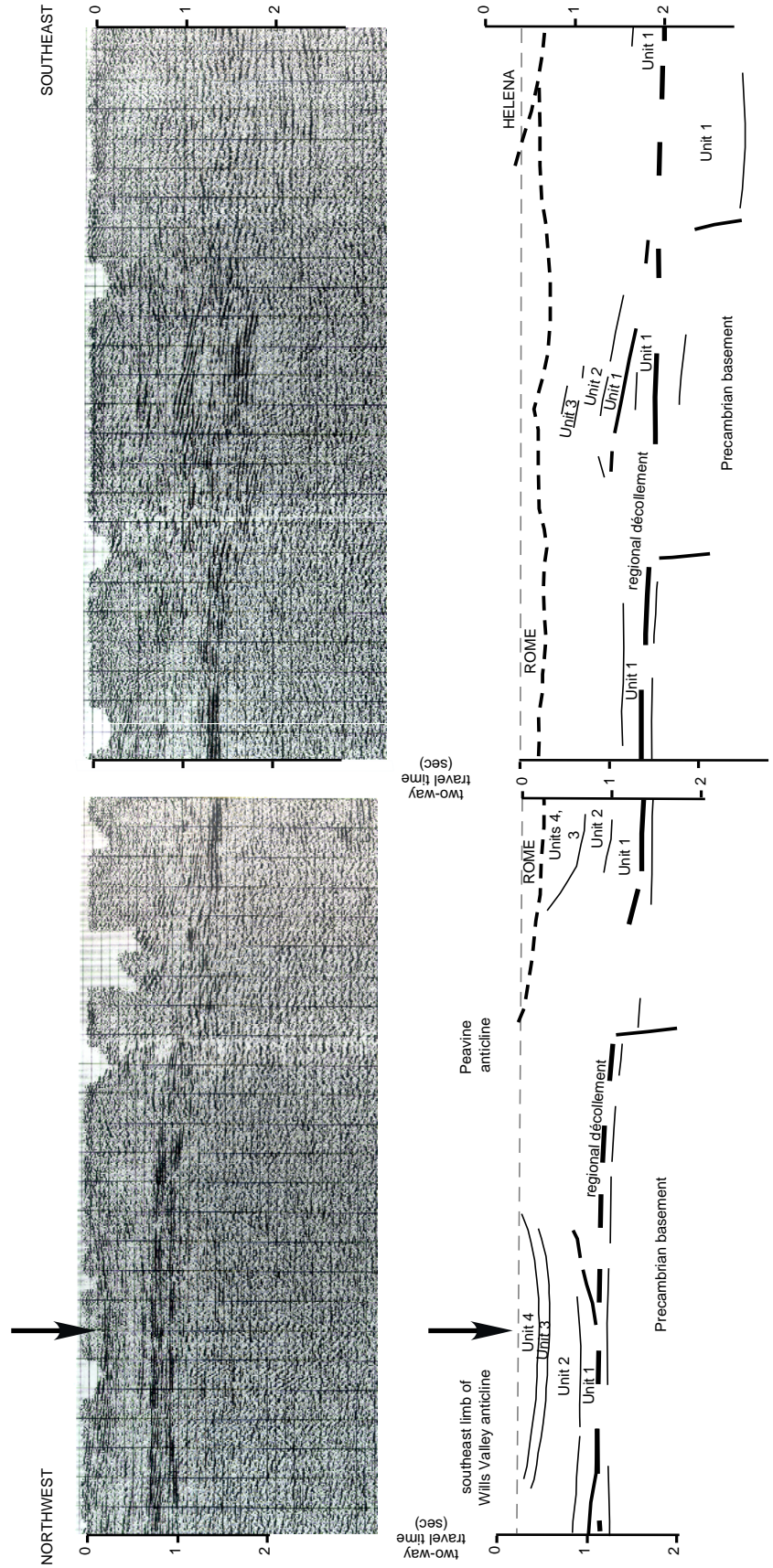


Figure 2.1 (continued)



**Figure 2.1** (previous two pages) A) Regional salient and recess geometry of the southern Appalachians (modified from Thomas, 1977). Digital shaded map shows the location of the Appalachian thrust belt in Alabama and Georgia (modified from Thelin and Pike, 1991). B) Structural outline map of Appalachian thrust belt in Alabama and Georgia, showing location of structural cross sections, deep wells, and seismic profiles (modified from Pickering et. al., 1976; Osborne et al., 1988; Szabo et al., 1988). See Coleman (1988) and Raymond (1991) for detailed information about deep wells. C) Location of abrupt small-scale curves of folds and faults in relation to the four transverse zones that cut across the entire thrust belt (from Thomas, 1990), and the more local Rome and Clinchport transverse zones documented in this study. Abbreviation: TZ = transverse zone. D) Map showing the geographic distribution of areas 1 to 9, which are used for an organized description of individual structures in the Alabama and Georgia Appalachian thrust belt. Locations of windows in the thrust belt (I to III) are also shown.

**Figure 2.2** Segments of a seismic reflection profile and interpreted cross section showing geometry of cover deformation, and of sub-decollement basement structures (modified from Thomas and Bayona, 2002). Vertical scale is in two-way travel time. Lengths of line segments correspond to lateral continuity of reflectors. The interpreted cross sections incorporate outcrop geology to show (dashed line) the shallow Rome thrust sheet and the shallow leading edge of the Helena thrust sheet, which are not clearly imaged. Note the drop to the southeast of the top of crystalline basement. See Figure 2.1 for location of seismic line and cross section 7 (Plate 2.1) that strikes parallel to the seismic profile. The arrow indicates a segment of the seismic reflection profile that allows a correlation between reflector stratigraphy and defined lithotectonic units for Paleozoic strata. Calculation of seismic velocity for each unit is based on correlation of stratigraphy from deep wells to seismic reflectors (for details, see figure 3 of Thomas, 2001). Seismic velocity for unit 1 is 4880 m/sec; for unit 2 is 6710 m/sec; for unit 3 is 5490 m/sec; and for unit 4 is 3810 m/sec.



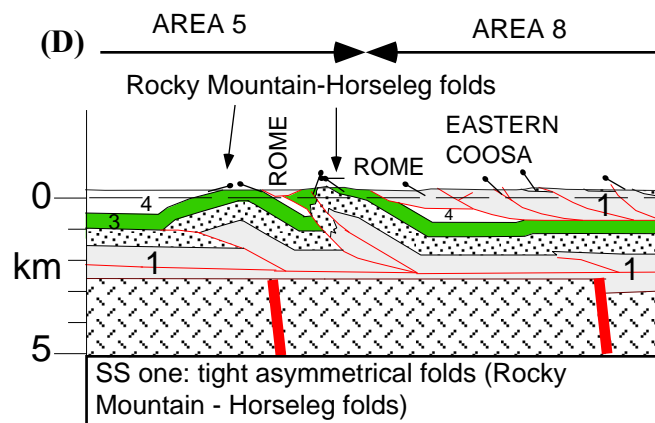
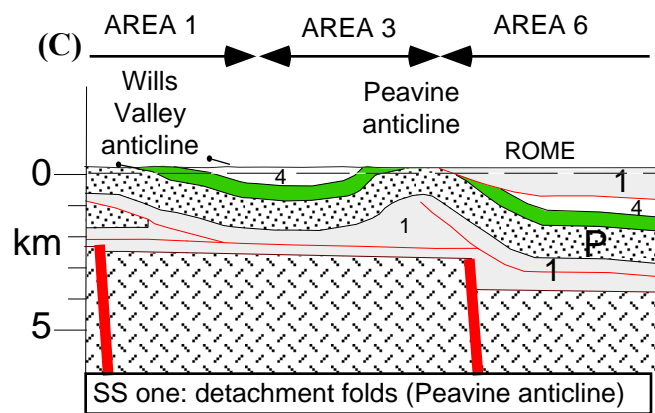
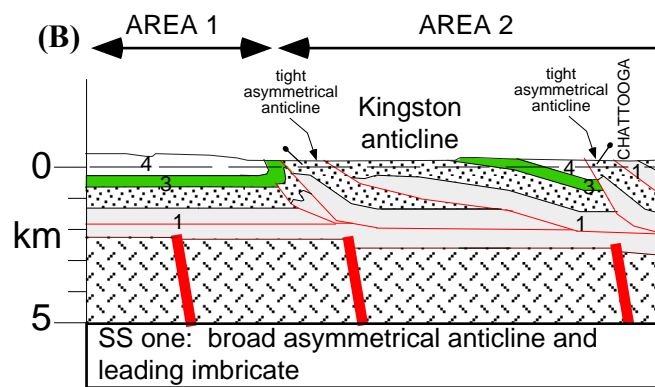
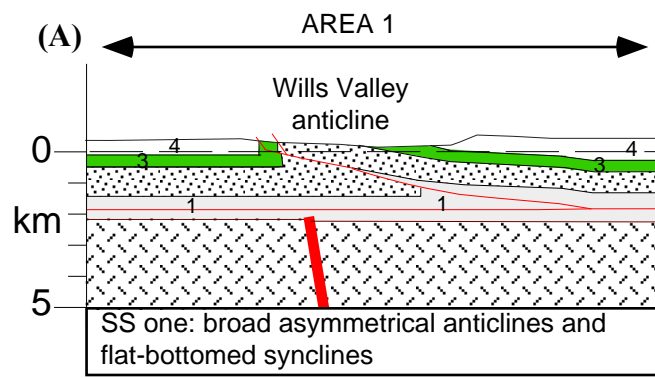


**Figure 2.3** Selected parts of the 17 structural cross sections displayed in Plate 2.1 showing representative structures of the Appalachian thrust belt in Alabama and Georgia (see Figure 2.1 for locations of cross sections). Structures are grouped into nine geographic areas, and they are identified at the top of each panel. The rectangle at the bottom of each panel indicates different structural styles (SS) illustrated in each panel. The shallow Rome thrust sheet (area 6 and structural style four) is illustrated in Figures 2.3C, D, F, and G.

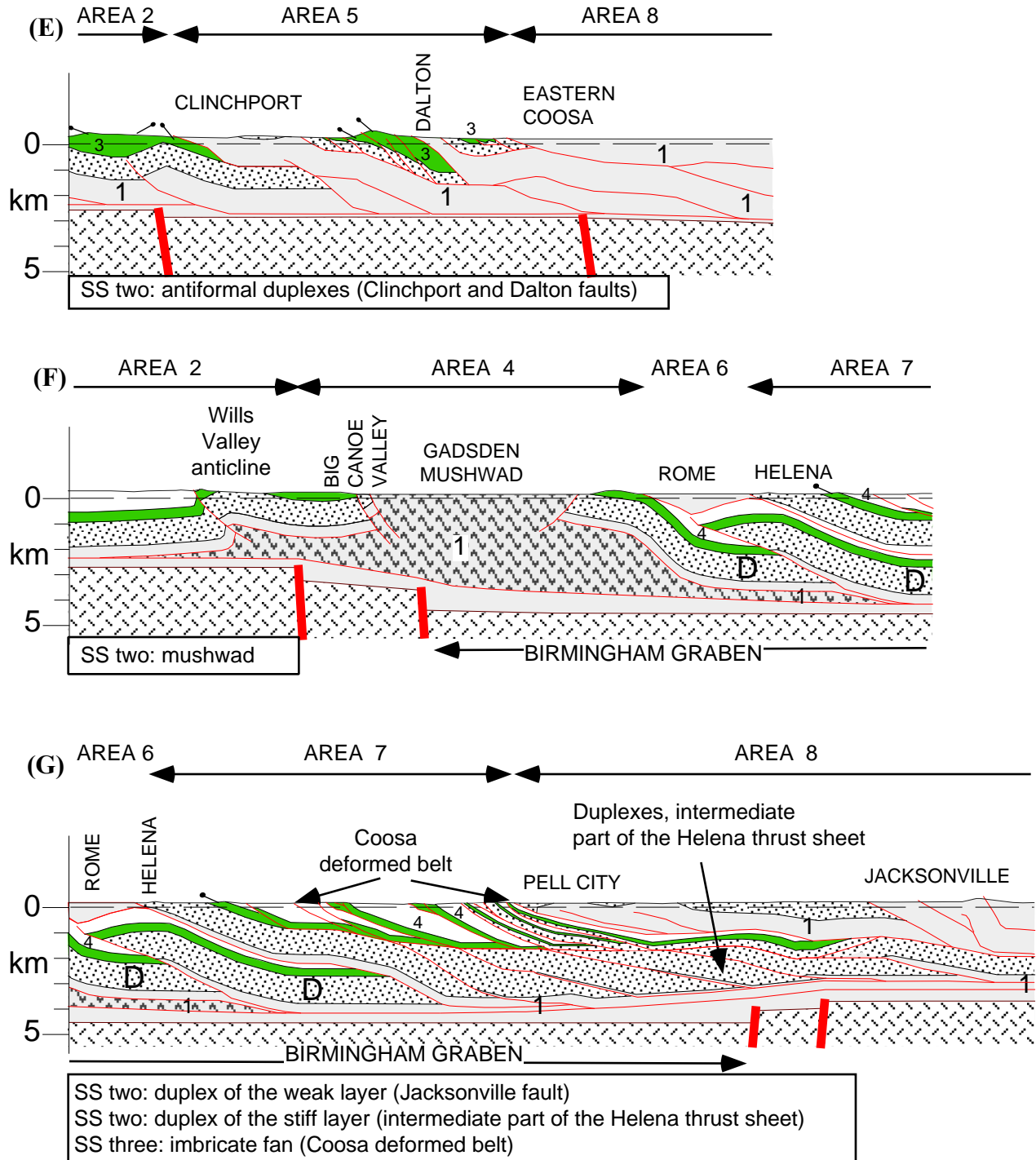
#### LITHOTECTONIC UNITS

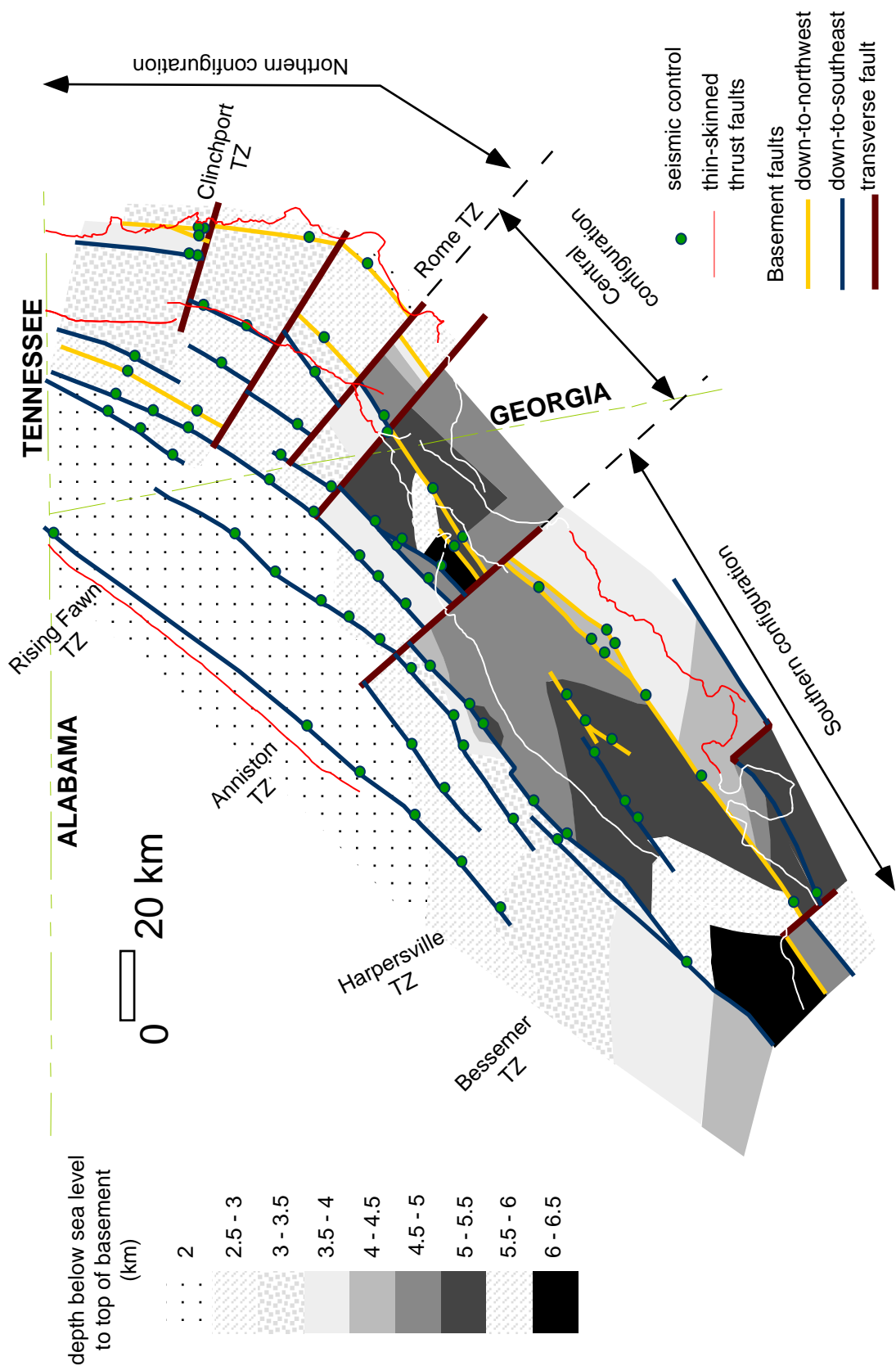
- 4 Upper Mississippian and Pennsylvanian
- 3 Middle Ordovician to Lower Mississippian
- 2 Upper Cambrian and Lower Ordovician (stiff layer)
- 1 Gadsden mushwad
- Lower and Middle Cambrian (weak layer)
- Precambrian crystalline basement

#### CROSS SECTIONS

- stratigraphic contact
- thrust fault
- basement fault
- dip of beds at surface (open circle = overturned beds)
- ROME Thrust fault
- P Peavine thrust sheet
- D Dunaway Mountain thrust sheet

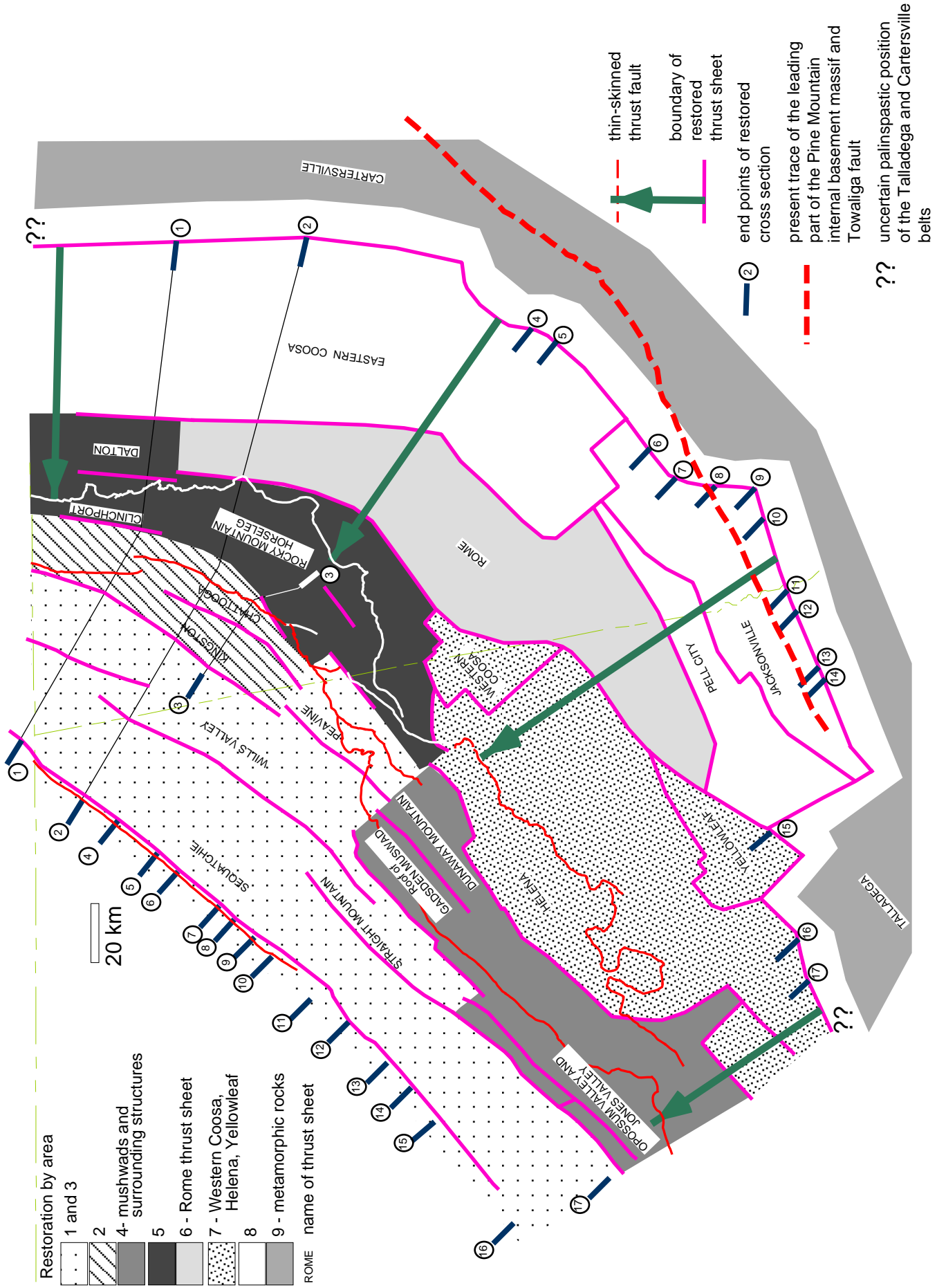
Figure 2.3 (continued)





**Figure 2.4** Map showing traces of subsurface basement faults interpreted from seismic reflection profiles, depth to top of basement, and outcrop traces of representative thrust-belt structures (as shown in Figure 2.1). Note the correspondence of transverse basement faults with location of transverse zones in the thrust belt. Abbreviation TZ= transverse zone

**Figure 2.5** Palinspastic map of the Appalachian thrust belt of Georgia and Alabama at the top of the Conasauga Formation (top of unit 1).



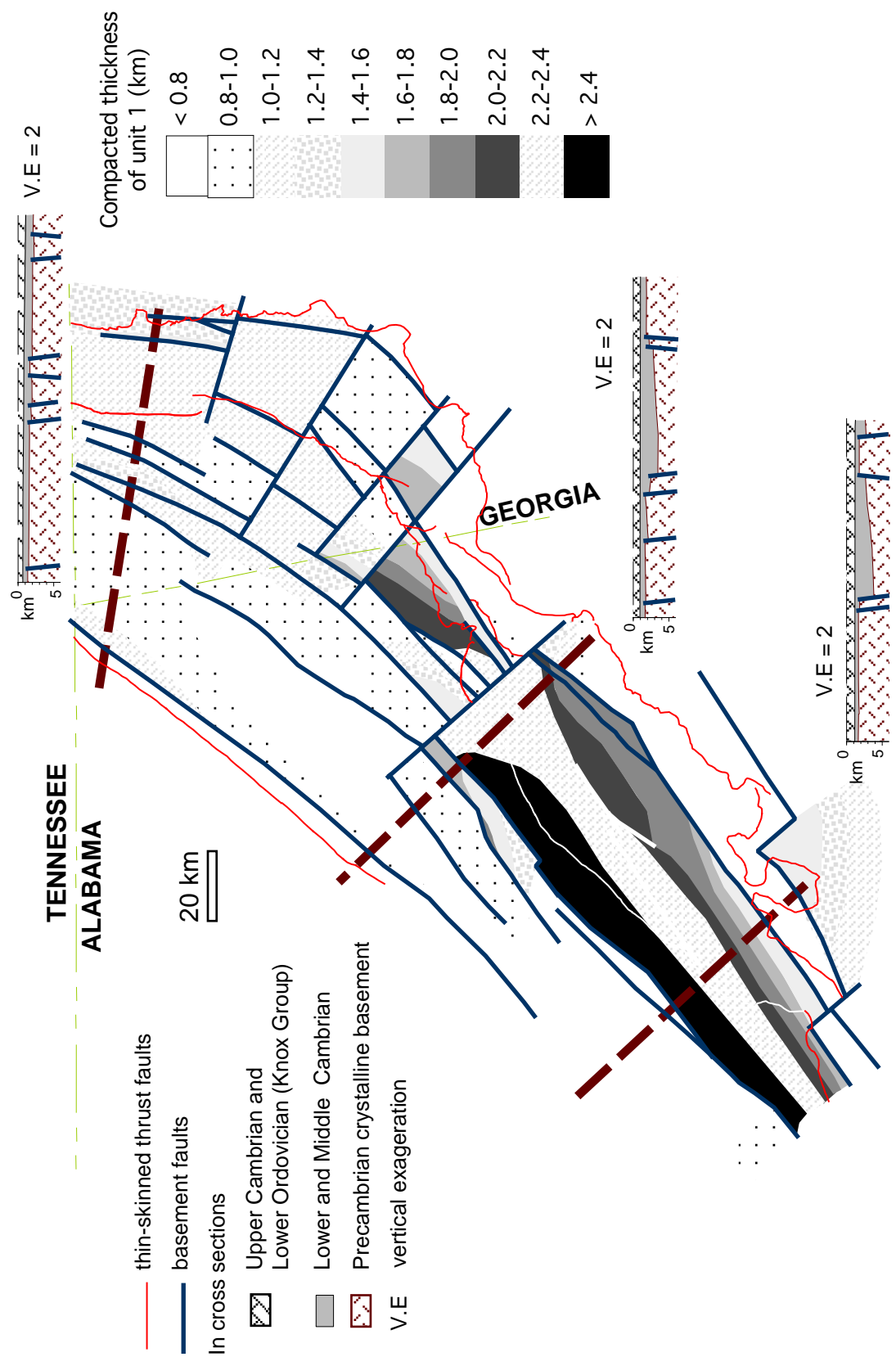


**Figure 2.6** Isopach map of compacted thickness of unit 1 in areas with seismic control. Three strike-perpendicular cross sections show the pre-deformational two-dimensional geometry of the sedimentary cover (units 1 and 2, datum is top of unit 2) and the top of basement.



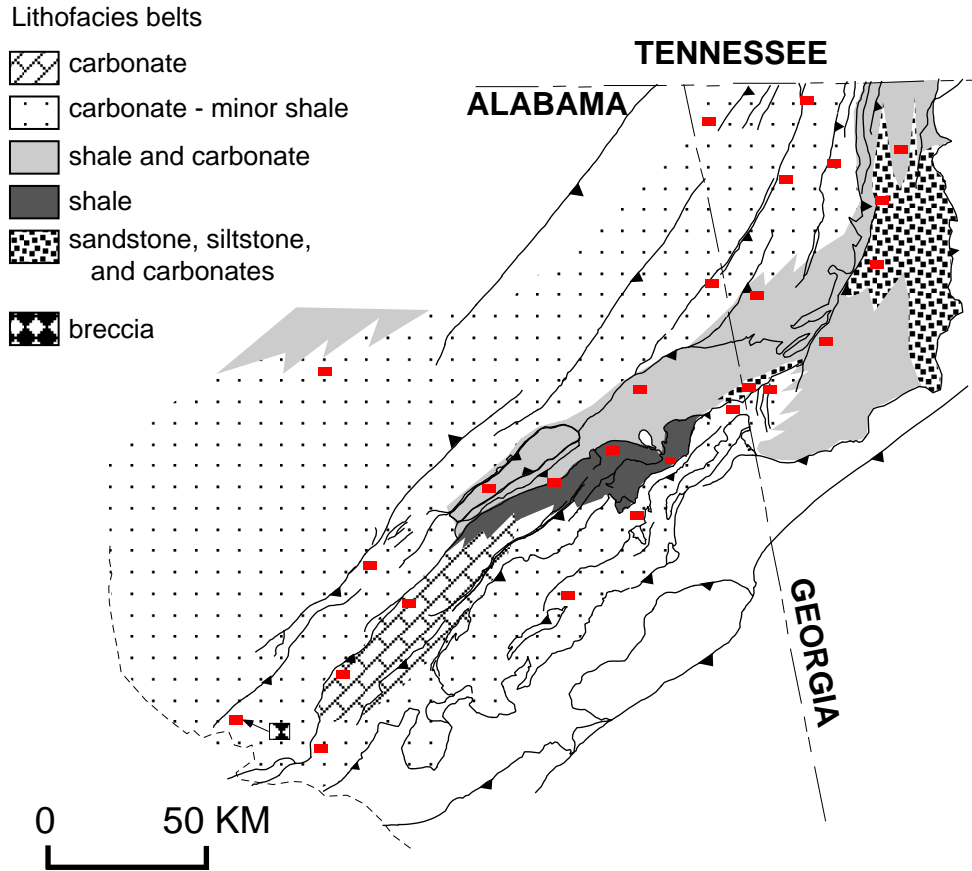


**Figure 2.7** Map of lithofacies distribution of the Conasauga Formation at present locations in the southern Appalachians. Squares are locations with outcrop or well descriptions. See Cressler (1970) and Osborne et al. (2000) for detailed description of sections.

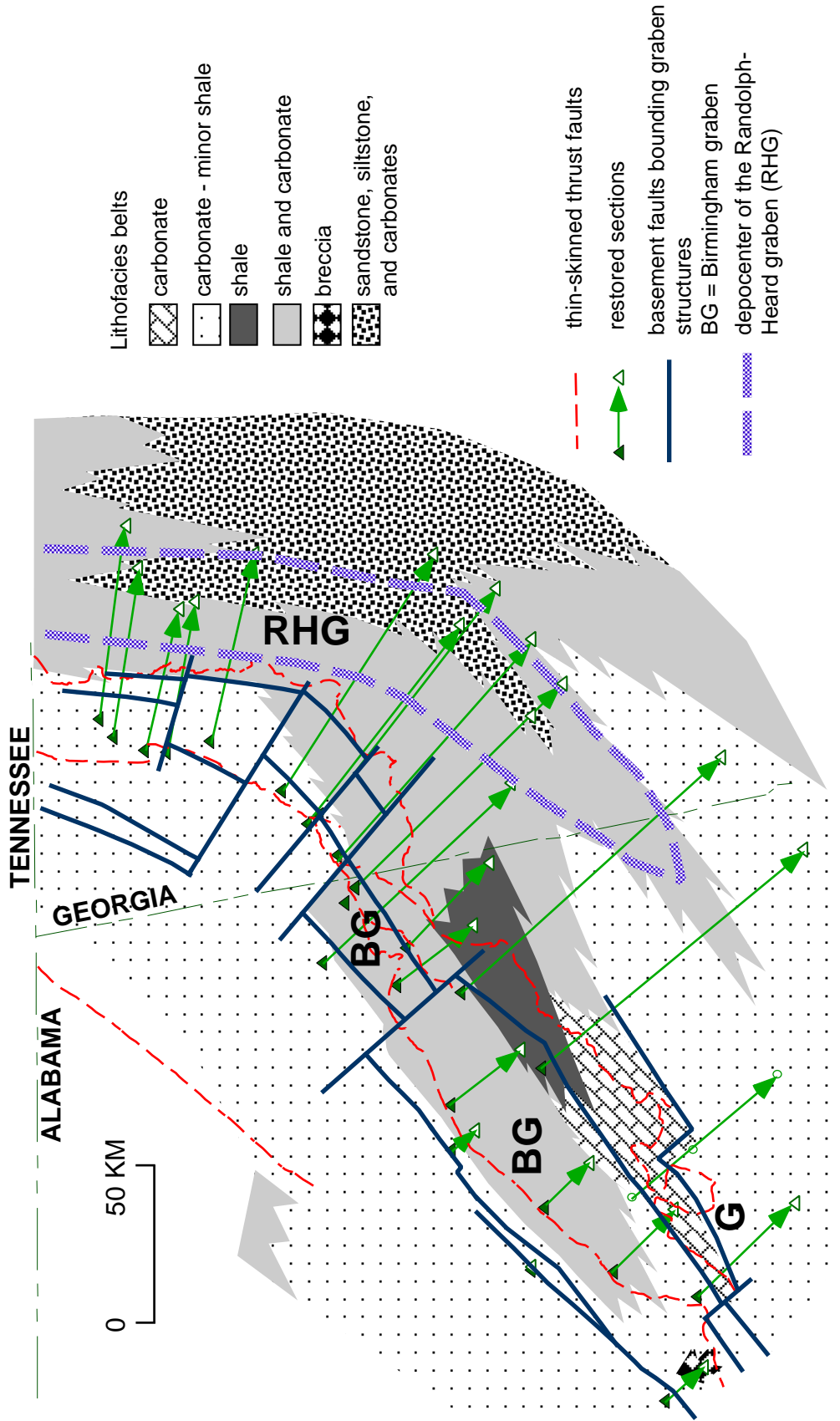


**Figure 2.8** Relationship between the palinspastic distribution of the Conasauga Formation lithofacies and the configuration of the Birmingham graben. Speculative position of the Randolph-Heard graben (RHG) is indicated by the dashed polygon. Arrows indicate the magnitude of translation of outcrops or wells that restore near or within the basement graben structures.

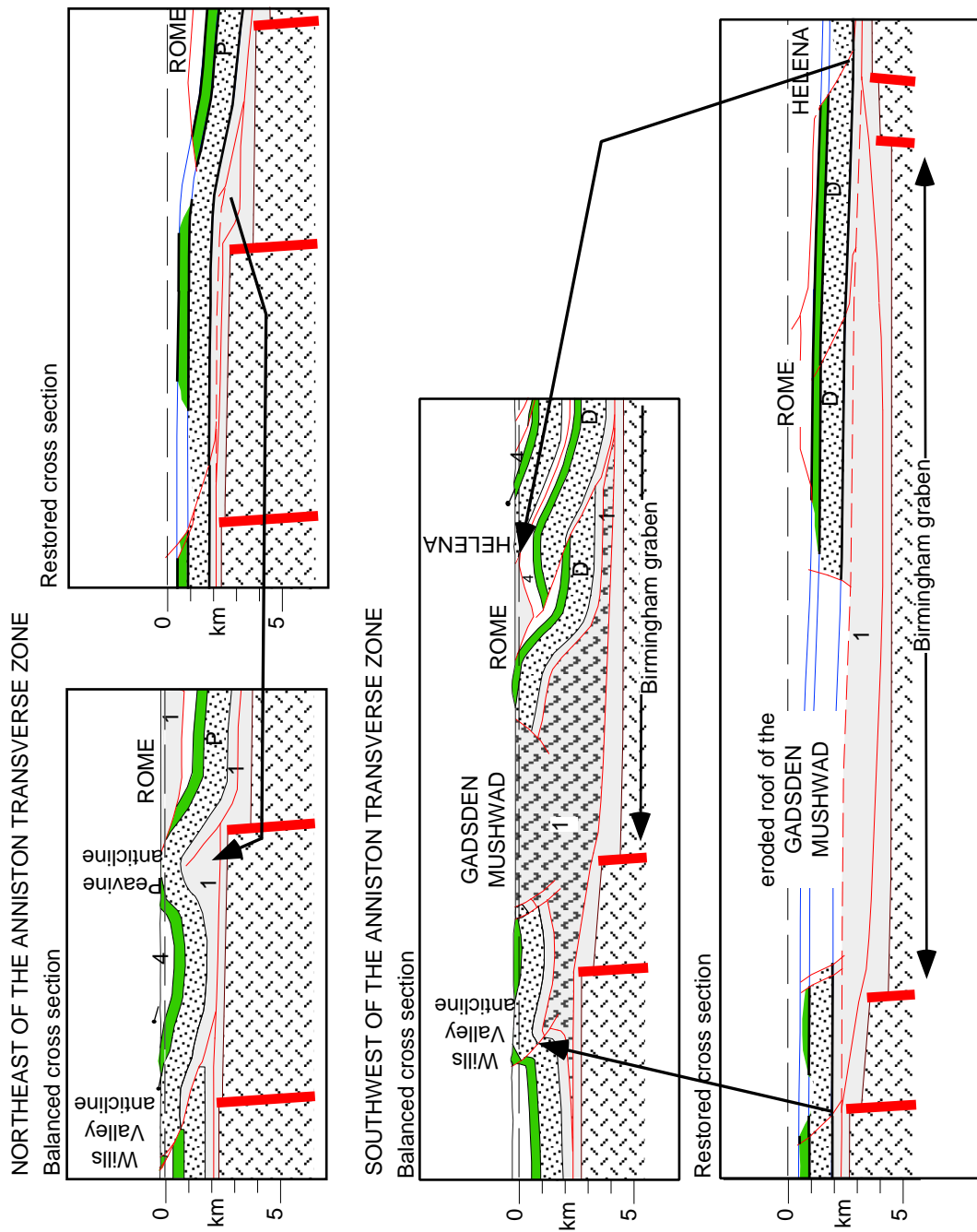


**Figure 2.9** Deformed and restored structural cross sections across part of the thrusts belt and on both sides of the Anniston transverse zone. Note the difference between the structural configurations of the top of basement, and the restored positions of strata that comprise the core of a detachment fold (upper) and the mushwad (lower). See Figure 2.3 for explanation of symbols.

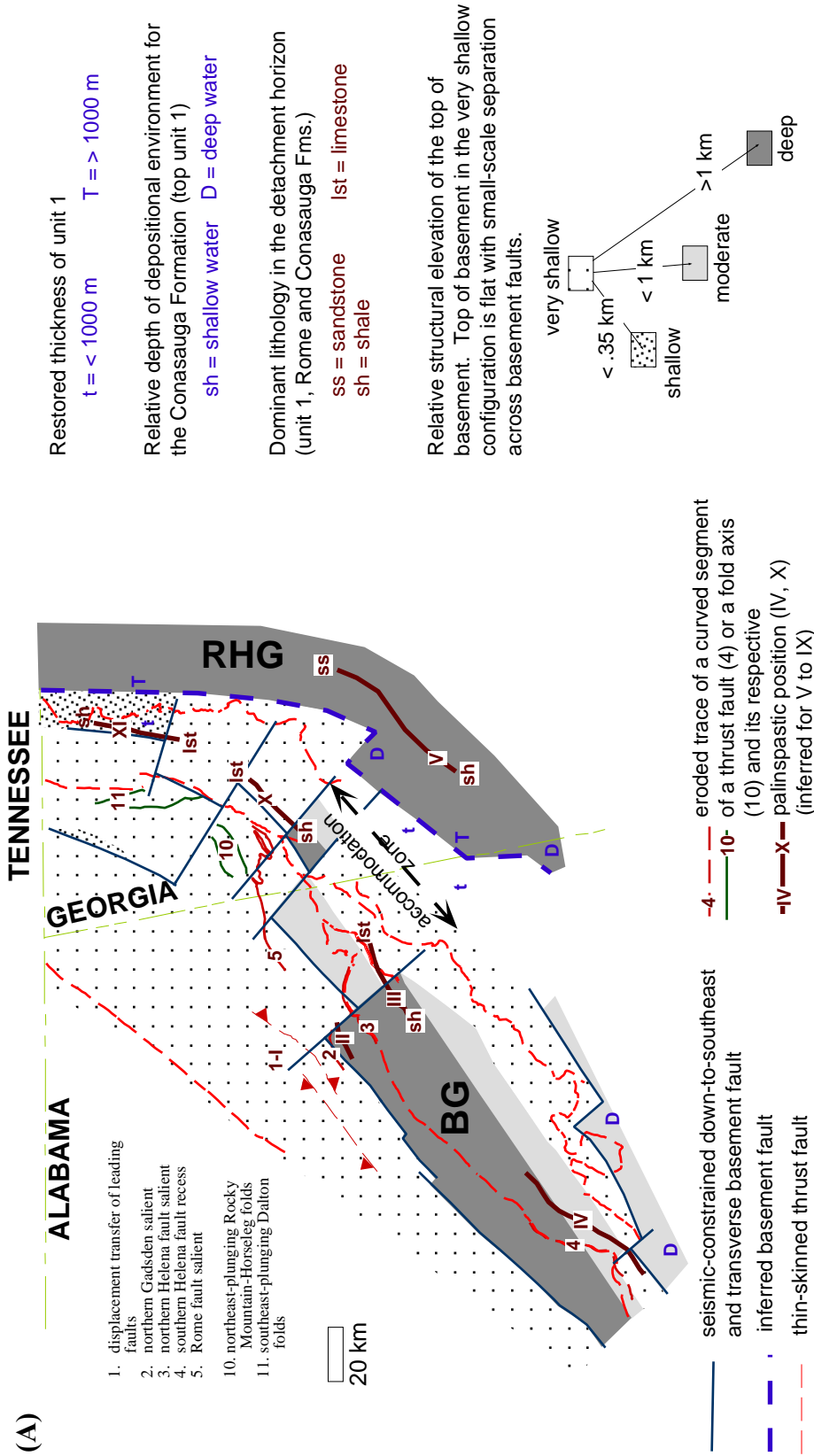


**Figure 2.10** A) Palinspastic restoration of folds and faults in the thrust belt, showing strike deviations and the relationship to the basement faults. Salients are related to southwestward deepening of the top of basement (points 2 and 3), whereas recesses are related to northeastward deepening of the top of basement (point 4). Elevation of the top of basement differs along strike across transverse basement faults of the central basement configuration. These variations in elevation of the top of basement accommodate (or transfer) the magnitude of extension between the BG and the RHG. Widening and finer lithologies of the RHG to the southwest might have contributed to the small-scale salient shape of the Rome thrust sheet (point 5).

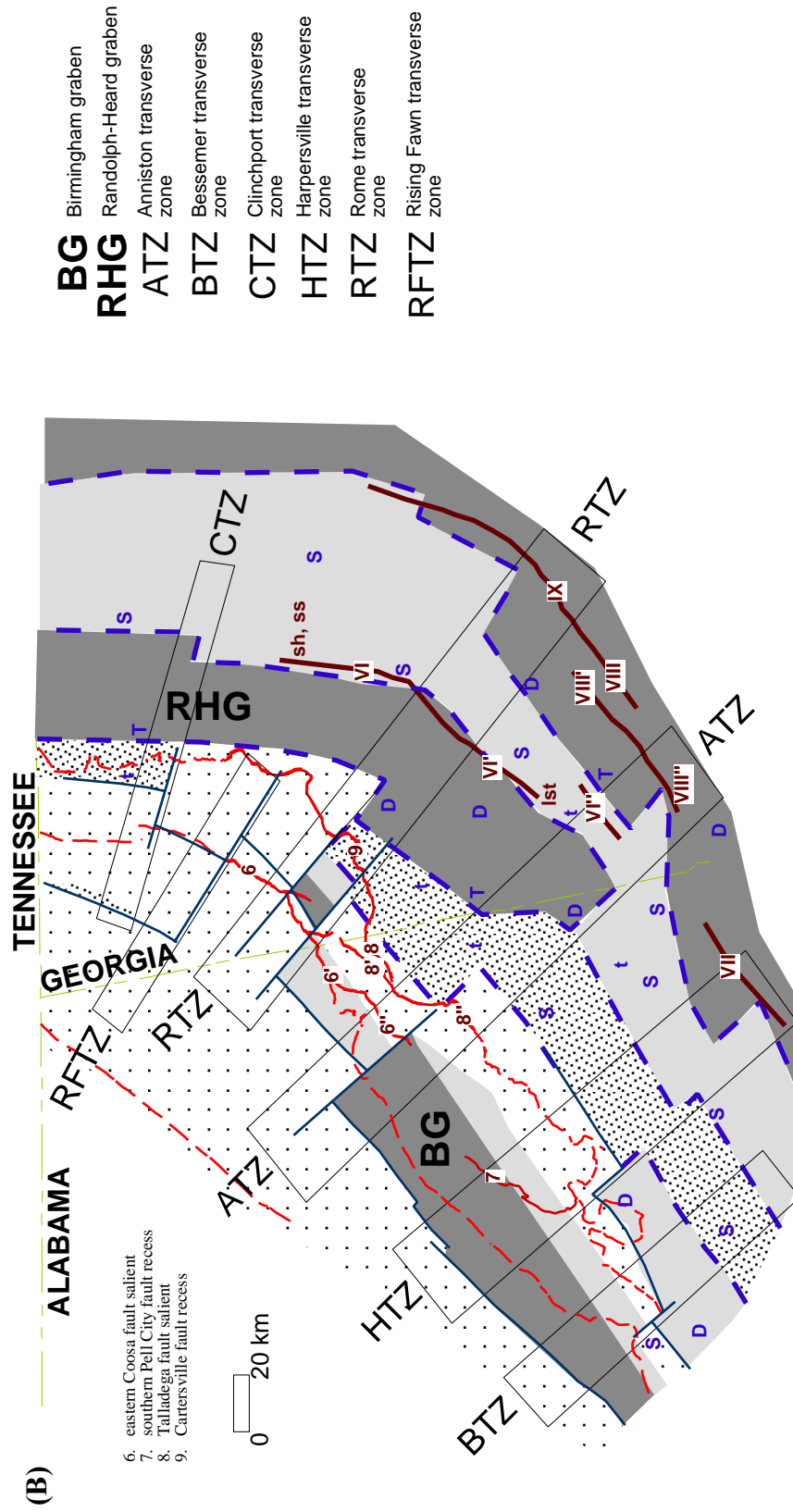


**Figure 2.10 (continued) B)** Speculative borders of the Randolph-Heard graben (RHG) and predicted locations of other basement faults southeast of the Birmingham graben. The position of each basement fault honors changes in restored thickness of unit 1, as well as contrasting lithofacies and depositional environments of the Conasauga Formation. The small-scale curvatures of trailing thin-skinned thrust faults also are considered to constrain the inferred locations of basement faults. The small-scale curvatures are from: eastern Coosa fault (points 6 and 6'), intersection between the Pell City and eastern Coosa faults (6''), southern end of Pell City (7), Talladega (8, 8' and 8''), and Cartersville fault (9). Large rectangles enclose the palinspastic position of lateral structures along the six transverse zones; note the geographic coincidence with transverse basement faults. See Figure 2.10A for explanation of symbols and codes.

Figure 2.11

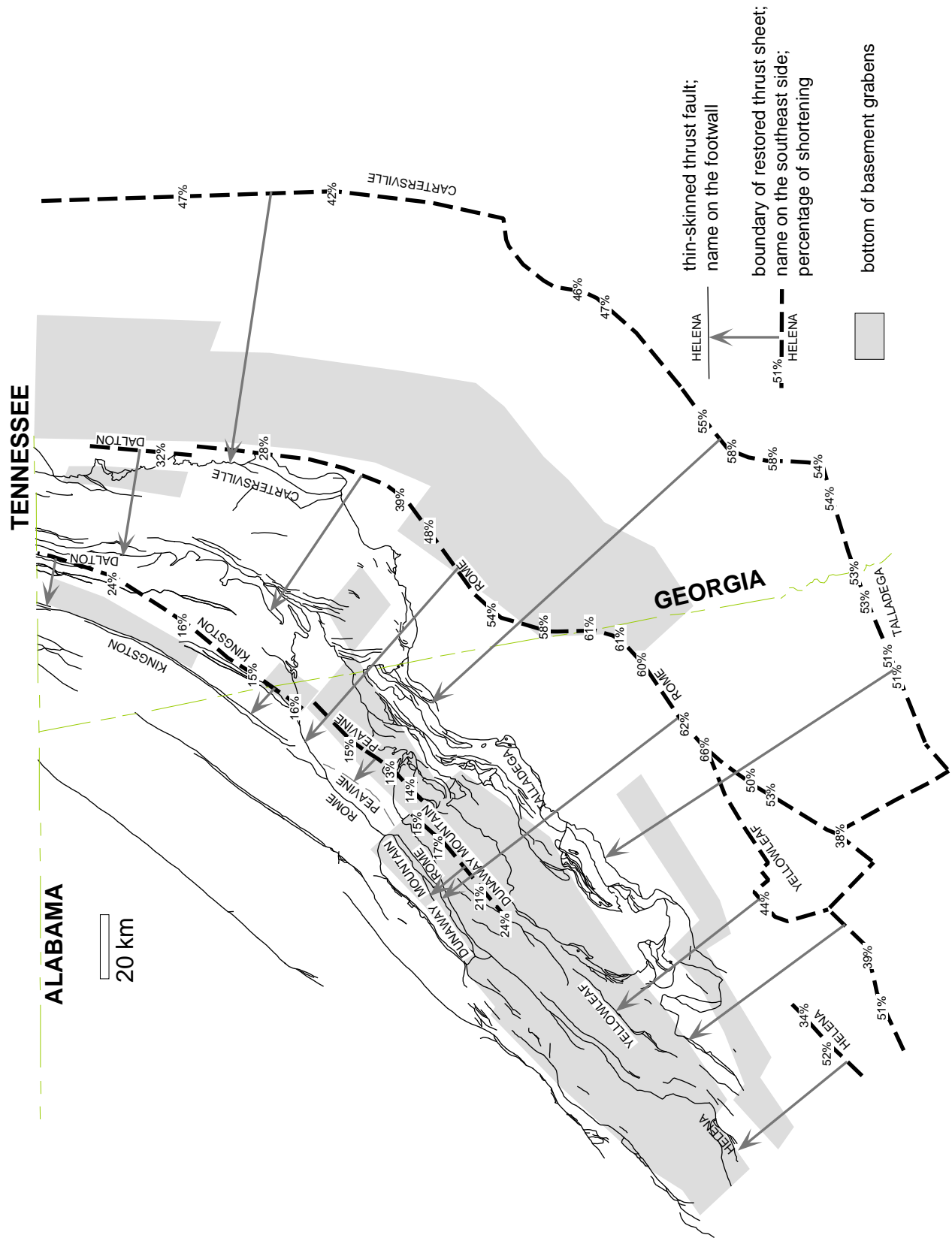


**Figure 2.11** (previous page) Along-strike variation of shortening at leading, intermediate, and trailing structures of the Appalachian thrust belt in Alabama and Georgia. Shaded polygons are the bottom of sub-décollement basement graben structures. Shortening values are the minimum because they are calculated using the present leading trace of structures on the surface (hanging-wall cutoffs are eroded) and northwestern boundary of the corresponding restored thrust sheet (construction of cross sections considers minimum amount of shortening). Leading structures are the Kingston, subsurface Peavine (thrust sheet beneath the Rome thrust sheet), and Dunaway Mountain faults. A projection of the fault to the surface (dashed line) was used for the subsurface Peavine fault. In palinspastic position, northwest boundaries of leading thrust sheets are nearly straight. However, the present trajectories of these faults indicate more shortening at the both ends (21-24%) than in the middle (13-17%). The stratigraphic thickness of unit 1 above the regional décollement is thicker at the northeastern of the Kingston fault (cross section 1, Plate 2.1) than along the rest of Kingston fault and other leading structures. More shortening at the southeastern end is caused by leading deformation of the Gadsden mudstone within the wide and deep Birmingham graben (Figure 2.3F). Intermediate structures are Dalton, Rome, Yellowleaf, and southwestern part of the Helena faults. Northwestern boundaries of these intermediate structures restore southeast of the Birmingham graben and northwest of the Randolph-Heard graben. The shortening is larger at the middle, with the least value to the northeast. The trailing structures are the Cartersville and Talladega faults. Shortening pattern is similar to intermediate structures, with more shortening in the middle and the least to the northeast.

## CHAPTER THREE

### ROLE OF BASEMENT FAULT REACTIVATION IN THE EVOLUTION OF THE DISTAL BLOUNTIAN FORELAND BASIN

#### 3.1 INTRODUCTION

Flexurally controlled subsidence of underfilled peripheral foreland basins in tropical zones leads to the growth of carbonate platforms in distal foreland zones and deposition of deep-water siliciclastic deposits in the foredeep (e.g., Papua-New Guinea; Pigram et al., 1989). Active convergence and advance of tectonic-sediment loads force the carbonate-platform and the deep-water siliciclastic systems to migrate forelandward, as recorded by the onlap of foreland deposits onto a flexurally deformed passive-margin succession (Dorobek, 1995; Sinclair, 1997). However, truncation of the former passive-margin succession and patterns of initiation of distal foreland deposition may be additionally controlled by the presence of weak zones in the foreland lithosphere, reactivation of basement faults, and cratonwide fluctuations of sea level (Figure 3.1). This chapter documents local and abrupt variations in the geometry of the passive margin-foreland unconformity, as well as in depositional patterns of Middle to Upper Ordovician distal foreland deposits along the southernmost margin of Laurentia during the Blountian orogeny, an early phase of the Taconic orogeny (Rodgers, 1953; Drake et al., 1989). Recognition of these variations in the stratigraphic record is essential for distinguishing between the plate-marginal scale migration of the flexural wave in distal zones of an underfilled peripheral foreland basin (Figures 3.1A and B), and small-scale fixed structural elements, such as reactivation of basement faults (Figure 3.1C).

Understanding the complexity of the unconformity and overlying carbonate-siliciclastic deposition in the distal foreland is essential for testing three non-exclusive models that explain anomalous depth of erosion, creation of accommodation space, and deposition in distal peripheral foreland basins (Figure 3.1). One model consists of the plate-marginal scale (~ several hundreds of km) migration of a flexural wave (backbulge-peripheral bulge-foredeep depozones of DeCelles and Giles, 1996) in a homogeneous foreland lithosphere of constant strength in space and time (Figure 3.1A) (e.g., Yu and Chou, 2001; White et al., 2002). Migration of the flexural wave across a lithosphere with weak zones (i.e., lateral strength



variations) has a different rate of migration and forebulge construction than of the preceding model. The forebulge will be positioned most of the time above a narrow weak zone and will migrate episodically, rather than continuously, from one weak zone to the next weak zone (Figure 3.1B) (Patton and O'Connor, 1988; Washbush and Royden, 1992). Another model to explain anomalous depth of erosion or onset of deposition in the distal foreland, but with more local effects (~ tens of km), is reactivation of basement faults. Reactivation of extensional basement faults as reverse faults (positive inversion; Figure 3.1C) has been related to horizontal compressional forces generated during the early stages of the orogeny, as documented in the Rocky Mountains (Meyers et al., 1992), Antler (Dorobek, 1995), and the southeastern France Alpine (Gupta and Allen, 2000). In contrast to the fixed position and early episodes of reverse faulting, extensional stresses cause normal fault activity on the foreland plate as the elastic plate bends during migration of the flexural wave (Figure 3.1A). Normal faulting may reactivate extensional faults, as in the northern Appalachians (Bradley and Kidd, 1991; Lehmann et al., 1995) and the present northwest shelf of Australia (Lorenzo et al., 1998), or reactivate thrust structures (negative inversion), as in the Pantanal wetland (Ussami et al., 1999).

Regional sea-level fluctuations also must be considered because the Middle Ordovician post-Knox unconformity is pervasive throughout the Laurentian craton (Sloss, 1963). Cratonwide erosion and restricted marine sedimentation along the edge of cratonic shelves (Harris and Repetski, 1982) document a relative drop of sea level of ~ 150 m with respect to the present sea-level position (Ross and Ross, 1995).

Distal foreland carbonate ramps are very sensitive to changes in water depth and dispersal of siliciclastic sediments (Benedict and Walker, 1978). The careful study of carbonate-ramp deposits provides evidence of dynamic changes in elevation or bathymetry of the depositional profile, as well as in discharge rates of detritus from uplifted areas (Dorobek, 1995). The lithology, stratal geometry, faunal content, faunal association, and early cementation change abruptly with a very subtle change of water depth (Steinhauff and Walker, 1996, and references therein). Causes of onset, variations, and termination of carbonate deposition include eustasy, tectonic subsidence, differential compaction, dispersal of siliciclastic sediments, and rate of carbonate production (Jones and Desrochers, 1992; Dorobek, 1995; Allen et al., 2001). In peripheral foreland settings, proximity of terrigenous influx may rapidly suppress the rate of

carbonate production as indicated by progradation of the siliciclastic wedge during later stages of foreland evolution (Walker et al., 1983; Dorobek, 1995; Sinclair, 1997).

In this chapter, I determine which of these three models, or a combination of them, explains the irregular patterns of depth of erosion of the passive-margin succession and rates of carbonate and siliciclastic distal Blountian foreland deposition. Because these rocks are presently displaced by late Paleozoic Alleghanian faults in the Appalachian thrust belt of Alabama and Georgia (Figure 3.2), a map showing the palinspastically restored position of each stratigraphic section in relation to the trace of subsurface basement faults is used for this study (see Chapter 2 for details of the construction of this map). The restored distribution of sections encompasses the northwest shoulder, intragaben, and the southeast shoulder of the intraplate Birmingham graben. This distribution of sections on the distal foreland plate permits the determination of three-dimensional variations in (1) the geometry of the post-Knox unconformity; (2) depositional systems, composition, and stratal patterns; and (3) tectonic subsidence of distal Blountian (Middle-Upper Ordovician) foreland deposits.

## **3.2 GEOLOGIC AND STRATIGRAPHIC SETTING**

### **3.2.1 Structures from the previous extensional tectonic setting**

On the basis of palinspastic restoration and stratigraphic analyses of upper Precambrian synrift and Cambrian to Lower Ordovician passive-margin deposits in the Appalachian and Ouachita orogenic belts, Thomas (1977; 1991) proposed an orthogonal zig-zag geometry of the eastern Laurentian (North American) rift margin. This margin configuration consisted of embayments (e.g., the Tennessee embayment) and promontories (e.g., the Alabama promontory) and resulted from the Blue Ridge and Ouachita rifting episodes during late Precambrian and Early Cambrian times, respectively. In Early Cambrian time, passive-margin deposition dominated along the eastern margin of Laurentia (Thomas, 1991), but extension reached intracratonic areas of the Alabama promontory forming several graben structures, such as the Birmingham graben, a structure documented by reflection seismic profiles (Figure 3.3) (Thomas, 1991; Chapter 2). Northeast-striking basement faults include faults bordering intraplate grabens and faults parallel to the plate margin. Northwest-striking basement faults separate the southern, central, and northern graben configurations of the Birmingham graben (Chapter 2). Carbonate platform deposits of the Upper Cambrian-Lower Ordovician Knox Group, which extend from

intracratonic regions to throughout west of the Blue Ridge (Thomas, 1991), have been recognized as the upper unit of the passive-margin succession in the study area.

### **3.2.2 Taconic (Blountian) orogeny and foreland deposits**

Rapid drowning of the Lower Ordovician carbonate platform, diachronous deposition of deep-water shales in proximal foreland settings, and thin beds of volcanic ash are the evidence for a collisional orogenic event along the eastern margin of Laurentia (e.g., Bradley, 1989; Drake et al., 1989; Finney et al., 1996). The southernmost depocenter along the Taconic orogen of Laurentia is spatially coincident with the Tennessee embayment of the older rifted continental margin. In the depocenter, black shales overlie carbonate-ramp deposits and grade upward in a coarsening-upward turbidite succession, reflecting drowning of the foreland plate and sediment dispersal from an orogenic terrain on the east (Shanmugam and Walker, 1978, 1980; Shanmugam and Lash, 1982; Diecchio, 1991). The Blountian clastic wedge extends southwestward from the depocenter in the Tennessee embayment onto the Alabama promontory (Thomas, 1977). Despite the general southwestward thinning and truncation of the Blountian clastic wedge (Thomas et al., 2002), correlation of graptolites indicates earlier deposition of basal synorogenic siliciclastic deposits on the Alabama promontory than on the Tennessee embayment (Bradley, 1989; Finney et al., 1996).

A very complex Blountian succession of carbonate and siliciclastic strata covers the post-Knox unconformity on the foreland plate in the Alabama promontory and southern Tennessee embayment. In this study, northwestern, intermediate, southeastern, and absent-strata lithofacies belts are distinguished on the basis of structural position within the thrust belt, age, and the order of stacking of carbonate and siliciclastic deposits (Figures 3.2 and 3.3).

The northwestern lithofacies belt consists mostly of Upper Ordovician carbonate beds and contains a complex array of lithologies ranging from mudstones to skeletal, algal, and intraclastic grainstones (Drahovzal and Neathery, 1971; Walker et al., 1983; Benson, 1986a). The association of carbonate lithologies to the northwest has been interpreted as deposition in peritidal and shallow-water carbonate platform (Ruppel and Walker, 1984; Benson, 1986b; Steinhaff and Walker, 1995). These deposits are irregularly covered by reddish tidal-flat and estuarine siliciclastic deposits (Neathery and Drahovzal, 1985; Martin, 1991).

Carbonates and red siliciclastic strata characterize the intermediate lithofacies belt. The lower part consists of karst-filling conglomerates, and peritidal and shallow-marine carbonate deposits, whereas the upper part consists mostly of red siltstone beds with some interbeds of sandstones, shales, and carbonates (Drahovzal and Neathery, 1971; Chowns and Carter, 1983). Rocks of the intermediate lithofacies belt have been interpreted as deposits of shallow-platform, estuarine, and tidal-flat environments (Ruppel and Walker, 1984; Benson, 1986b; Martin, 1991). In the Blountian foreland basin, strata of the intermediate lithofacies mark the transition between platform-carbonate deposition to the northwest and deep-water siliciclastic deposition to the southeast.

The southeastern lithofacies belt consists of Middle Ordovician carbonate beds and a thick succession of deep-water siliciclastic deposits. Southeastern carbonate strata include peritidal, and shallow- to deep-water carbonate platform deposits (Drahovzal and Neathery, 1971; Walker et al., 1983; Ruppel and Walker, 1984; Benson, 1986a). Deep-water shales and turbidites overlie the drowned carbonate succession (Ruppel and Walker, 1984; Benson, 1986b), and are truncated at the top by Devonian and Mississippian strata.

### **3.2.3 Flexural subsidence/uplift in southeastern Laurentia**

Flexural deformation models have been used to explain regional patterns of erosion on the top of the Knox Group and deposition of Middle to Upper Ordovician strata. Shanmugam and Lash (1982, 1983) and Ettensohn (1991) explained the unconformity on the top of the Knox Group by upward flexure formed in response to subduction and the building of a deformational load. Distal foreland deposition of carbonates has been related to events of lithospheric flexure in response to tectonic loading, and the overlying siliciclastic succession has been interpreted as recording basin filling and cratonward progradation of the clastic wedge (Shanmugam and Lash, 1982; Ettensohn, 1991, Sinclair, 1997). Holland and Patzkowsky (1997) suggested that soft-sediment deformation and introduction of siliciclastic sediments on Middle and Upper carbonate deposition on the Nashville dome are direct effects of the Taconic orogeny. They also linked a decrease in the rate of relative sea-level rise recorded after foreland-basin initiation with slowing of subsidence that may reflect flexural uplift of the Nashville dome.

The model of flexural uplift, but of shorter wavelength than the forebulge proposed above, also has been used to explain local irregularities in erosion, deposition, and/or diagenesis

of Ordovician strata in southeastern Laurentia. Benson (1992) proposed a forebulge to explain the deep erosion of the Knox Group in Alabama (section BI in Figure 3.2). Roberson (1994), and Steinhauff and Walker (1995) used the backbulge-forebulge model of DeCelles and Giles (1996) to explain the thicker and earlier accumulation of lowermost Middle Ordovician shallow-marine carbonates in platform-interior settings rather than in platform-margin settings. Kher (1996) proposed a forebulge to explain meteoric diagenesis in uppermost cycles of Upper Ordovician shallow-marine carbonates in Georgia (northwest of section RI in Figure 3.2).

### 3.3 METHODS

This chapter integrates data from field work, seismic reflection profiles, deep wells, and literature (published papers, theses, dissertations) to carry out stratigraphic, petrographic, and tectonic subsidence analyses in a total of 17 sections (Figure 3.2). Age control for each section is documented by conodonts (Hall, 1986; Hall et al., 1986; Shaw et al., 1990; Repetski, 1992), graptolites (Finney et al., 1996), and absolute ages of K-bentonite beds (Kolata et al., 1996, 1998). The time framework used in this study is based on the conodont-graptolite-K-bentonite correlation chart of Kolata et al. (1996) (Figure 3.4). Information related to the identification of K-bentonite beds in sections HM, HL, GU, DM, GS, and CL is in Appendix A. Identification and correlation of graptolites in sections PF, CL, EC, and AB is in Appendix B. The framework in space is given by the palinspastic map constructed for the Appalachian thrust belt of Georgia and Alabama (Chapter 2). Plates 3.1 to 3.10 include a detailed description and interpretation of depositional environments of each stratigraphic sections and show photomicrographs of selected thin sections. Definitions of lithofacies and interpretations of depositional environments used in this study are given in Tables 3.1 and 3.2, and graphic symbols are illustrated in Figure 3.5. Appendices C and D include the thickness of stratigraphic units used for tectonic subsidence analysis and a summary of descriptions of thin sections and hand samples.

Three lines of stratigraphic correlation are constructed at different settings of the plate margin and cross different structural configurations of the Birmingham graben (Figure 3.3). Line of correlation A is in the southern part of the Tennessee embayment and crosses shallow, tilted fault blocks of the northern configuration of the top of basement. Lines of correlation B and C are in the Alabama promontory and cross the wide and deep southern configuration of the top of basement.

Tectonic subsidence analysis was carried out in each section assuming that the top of Ordovician was ultimately buried to a depth of at least 4 km (from an estimate of the thickest post-Ordovician succession in the Cahaba synclinorium in the southern Appalachians, Plate 2.1). I used backstripping techniques (e.g., Sclater and Christie, 1980; Allen and Allen, 1992) to decompact the measured stratigraphic thickness; this technique assumes a lithology-dependent exponential decrease of porosity with depth, a fully saturated column of sediments, and local compensation (Airy isostasy) of sedimentary loads. Initial porosities and porosity-depth coefficients (values from Sclater and Christie, 1980) were averaged according to the percentage of each lithology in each stratigraphic interval (Appendix C). Although the assumption of Airy isostasy is inappropriate for analysis of flexural deformation (Whiting and Thomas, 1994), I intend to illustrate contrasts in tectonic subsidence curves of closely-spaced sections that restore palinspastically in distal foreland settings, and on different structural configuration of the top of basement. Tectonic subsidence analysis for each section and models of intraplate flexure were carried out using MatLab programs written by Nestor Cardozo at Cornell University. The tectonic subsidence program uses the assumptions specified above. The elastic mechanical model for flexural deformation and its assumptions are explained in Cardozo and Jordan (2001).

### **3.4 POST-KNOX UNCONFORMITY**

Lower Ordovician strata of the Knox Group dominantly underlie the post-Knox unconformity. The younger units of the Knox Group are exposed in southeastern thrust sheets (Newala and Odenville Limestones) and older units in northwestern thrust sheets (Chepultepec Dolomite and Longview Limestone) (Raymond, 1993). However, depth of erosion in intermediate sections reaches lowermost Ordovician strata (Chepultepec Dolomite, section HM in Figure 3.2) and Upper Cambrian strata (Copper Ridge Formation, sections DG, HL, and BI in Figure 3.2). These areas of deep erosion are relatively broad along strike (Cressler, 1970, 1974; Chowns and Carter, 1983; Szabo et al., 1988; Osborne et al. 1988). Seismic reflection profiles in areas near and south of BI image the anomalous thin Knox Group dipping southeast beneath the surface (see Chapter 2, cross section 16, Plate 2.1). Abrupt changes in depth of erosion are illustrated in strike-perpendicular lines A, B, and C (Figure 3.6). The depth of erosion of the post-Knox unconformity rises from lower to upper beds of the Knox Group across boundary faults of the Birmingham graben (Figure 3.6C). In fact, all sections with deeper levels of erosion

restore palinspastically inside the boundary fault systems of the Birmingham graben (sections DG, HL, BI), whereas sections with the youngest preserved record of Knox strata restore on the shoulders of the graben system (e.g., sections AB, GS, RI).

### **3.5 MIDDLE AND UPPER ORDOVICIAN STRATIGRAPHY**

The following descriptions of lithofacies, ages, thicknesses, and interpreted depositional environments cite important variations in the stratigraphy, using as a location reference the subsurface trace of northwestern and southeastern boundary fault systems of the Birmingham graben (Figure 3.3). These variations are considered in the tectonic analysis of the distal foreland.

#### **3.5.1 Sections northwest of the northwestern fault system of the Birmingham graben**

**3.5.1.1 Units, thickness, and age.** Middle and Upper Ordovician strata of sections CH, RI, GU, SS, and ST consist mostly of carbonate beds of the northwestern lithofacies belt, and represent the thickest record of distal carbonate beds in the Blountian foreland. In general, the thickness among these sections decreases southward from 504 m at section CH to 234 m at section ST. The stratigraphic thickness also thins northwestward, and at a distance of 80 km (out of the study area) is less than 190 m (Kidd, 1975). All the sections are considerably thicker than adjacent sections to the southeast (Figures 3.7 to 3.9). Conodont analyses of basal beds of the Chickamauga Group in Georgia (Pond Spring Formation, Shaw et al., 1990; Repetski, 1992) indicate initiation of carbonate deposition in late Middle Ordovician time (between *H. holodentata* and *C. sweeti* zones, upper Whiterockian). Conodonts and body fossils recovered from the Chickamauga and Sequatchie units suggest nearly continuous deposition in Late Ordovician (Mohawkian and Cincinnati) time. The lack of latest Ordovician (uppermost Cincinnati) fauna and truncation of uppermost beds of the Sequatchie Formation document the Ordovician and Silurian unconformity in section RI (Rindsberg and Chowens, 1986; Phillips and Hall, 1993).

**3.5.1.2 Lithology.** The lower units of the Chickamauga Limestone (Pond Spring, Mufreesboro, Ridley, Lebanon, and Carters in section CH, Figure 3.7; Stone River in sections GU, SS, and ST, Figures 3.8 and 3.9) are poorly exposed and consist of mud-dominant lithofacies (e.g., micritic matrix in mudstones to wackestones, and packstones with peloids,

intraclasts, and green algae) with intervals of skeletal limestones that are thicker, less dolomitic, and more abundant up section (strata between surfaces 1 and 8 in section CH-RI, Figure 3.7). The basal beds include conglomerates with chert and dolomite clasts, and slump-folded structures (Milici and Smith, 1969; Chowns et al., 1992). In these lower units, thick successions of dolomitic limestone beds with peloids and intraclasts dominate over skeletal wackestones to packstones with ostracods, brachiopods, crinoids, mollusks, trilobites, and bryozoans. The dominant lithology is interbedded with reddish bioturbated limestone beds, varicolored shales, and thin skeletal grainstones (Milici and Smith, 1969; Chowns et al., 1992; Phillips, 1996). The uppermost beds of the Carters Limestone consist of interbedded fenestral mudstones and wackestones with intraclasts and mudcracks, and the succession contains the Deicke and Millbrig K-bentonite beds (Milici and Smith, 1969; Chowns, 1989). Equivalent beds in the subsurface (strata below surface 8 in sections GU-SS and ST, Figures 3.8 and 3.9) are dolomitic limestone beds in the lower half with rounded sand grains near the base; whereas in the upper half, limestone beds are more crystalline and some are skeletal (Kidd, 1975).

The upper units of the Chickamauga Limestone and the overlying units to the west and southwest (strata between surfaces 8 and 11 in Figures 3.7 and 3.8) include the transition from carbonate to siliciclastic deposition in this area. An important increase in the concentration of fossils, mostly of bryozoans, crinoids, *Tetradium* corals, and red algae, is recorded in beds a few meters above surface 8 in the composite section CH-RI (Figure 3.7) (Milici and Smith, 1969; Phillips, 1996) and above surface 9 in the composite section GU-SS (Figure 3.8) (Neathery and Drahovzal, 1985). These skeletal limestone beds are interbedded with dolomitic and mud-dominant limestone beds (Milici and Smith, 1969; Neathery and Drahovzal, 1985). In the middle of the section, the mud-dominant carbonate lithofacies change upward to calcareous siltstones, sandstones, and shales (mixed lithologies of the lower Sequatchie Formation, and Inman Formation and Leipers Limestone) with fenestral textures, ubiquitous bioturbation, and mudcracks (Neathery and Drahovzal, 1985; Rindsberg and Chowns, 1986). However, this upward change is not observed in other sections farther west (west of SS and GU in Figure 3.3), where fine-grained calcareous deposits dominate (Leipers Limestone; Neathery and Drahovzal, 1985).

The uppermost part of the composite sections CH-RI and GU-SS (beds between surface 10 and 11 in Figures 3.7 and 3.8) consists of phosphatic calcarenites and calcareous siltstones



with low degree of bioturbation and abundant body fossils (brachiopods, bivalves, bryozoans, crinoids) (Neathery and Drahovzal, 1985; Martin, 1991). In sections CH, RI, and north of sections GU and SS, this succession is capped by a distinctive phosphatic crust, and is overlain by shales, bioturbated sandy mudstones, and muddy sandstones with phosphate grains and less diverse and abundant body fossils than the underlying unit (Martin, 1991). This fine-grained siliciclastic succession grades laterally northwestward (outside the study area) to phosphatic calcarenites (Martin, 1991), and a succession of interbedded limestone and shales (Neathery and Drahovzal, 1985).

### 3.5.2 Sections inside the graben

**3.5.2.1 Units, thickness, and age.** Middle and Upper Ordovician strata that restore inside the Birmingham graben consist of the Chickamauga Limestone and Sequatchie Formation in the southern sections BI, BR, and DM; whereas to the north, sections DG and HL include mostly red siliciclastic units of the Greensport and Sequatchie Formations. Stratigraphic thickness in these sections decreases southwestward from 268 m at section DG to 96 m at section BI, and are approximately half as thick as sections to the northwest and southeast (Figures 3.7, 3.8, and 3.9). The lowest carbonate beds are not older than latest Middle Ordovician in section BI (*C. sweeti* zone, upper Whiterockian, Hall et al., 1986; Roberson, 1988) and earliest Late Ordovician in section BR (*E. quadridactylus* zone, lower Mohawkian, Hall et al., 1986). Conodonts in section BR (Raymond, 1973) and brachiopods (*Platystrophia*) found in upper beds in section DG, which are similar to those reported for the Leipers Formation in Tennessee (Wilson, 1949), document Upper Ordovician (Cincinnatian) rocks (Frank Ettensohn, 2002 personal communication to G. Bayona). In section BI, an unconformity is documented between the uppermost beds of the Chickamauga Limestone of middle Late Ordovician age (*P. undatus* zone, middle Mohawkian) and the less-than-one-meter-thick Sequatchie Formation of late Late Ordovician age (late Cincinnatian, Drahovzal and Neathery, 1971). In section BI, strata of the Sequatchie Formation are locally distributed (Drahovzal and Neathery, 1971) and truncate at least 1 m of the underlying Chickamauga strata (Benson and Stock, 1986). An angular discordance of 1.6 degree with a dip direction to the southeast is reported between upper beds of the Ordovician and basal beds of the Silurian Red Mountain Formation (Thomas, 1986) at section BI.

**3.5.2.2 Lithology.** Basal beds of sections BI, BR, DM, and HL include a very complex array of lithofacies of (1) clast- and matrix-supported chert-clast conglomerates; (2) dolomitic mudstones with isolated chert clasts and chert conglomerate beds; (3) red to green siltstones and shales; and (4) red fenestral intraclastic limestones with chert clasts interbedded with thin beds of muddy skeletal limestones with diverse fauna (Drahovzal and Neathery, 1971, Chowns and Carter, 1983; Roberson, 1988; Garry, 2002). Stratigraphic thickness ranges from 0 to 21 m in very short distances (Drahovzal and Neathery, 1971, Roberson, 1988). Mudcracks, fenestral textures, burrows, and sparse gastropods, ostracods, and trilobites fragments are common in dolomitic mudstones. These heterogeneous basal beds have been grouped into the Atalla Chert Conglomerate Member of the Chickamauga Limestone.

A heterogeneous association of carbonate lithofacies is found in southern sections BR, DM, and BI and between the basal beds with chert clasts and the beds that contain the Millbrig or Deicke K-bentonite (surface 8 in Figures 3.7, 3.8, and 3.9). Lower carbonates of the Chickamauga Limestone consist of dolomitic mudstone to packstones with peloids, intraclasts, oncoids, and sparse fauna (mainly ostracods and gastropods). In section DM, this lithofacies persists up to the Millbrig K-bentonite bed. In section BR, medium to thick beds of skeletal and peloidal wackestones to packstones with more abundant and diverse fauna are interbedded with mud-dominant, dolomitic limestone beds (surface 7 in Figure 3.8). The latter lithology dominates in the interval that contains the Millbrig K-bentonite level. In section BI, the interbeds of skeletal and peloidal wackestones to packstones include skeletal grainstones as much as 32 m thick with bryozoan-sponge-algal bioherms (Benson, 1986a), but these skeletal limestone beds pass up section to dolomitic limestone beds below the Millbrig K-bentonite bed (Figure 3.9). Fenestral textures, burrows, and mudcracks are common in mud-dominated and dolomitic limestone beds at section BI (Drahovzal and Neathery, 1971; Benson, 1986a). Sedimentary structures in the skeletal-peloidal limestone beds include horizontal and ripple lamination, wavy bedding, and local cross bedding in grainstone beds.

Another distinctive lithofacies association between the basal beds with chert clasts (or the post-Knox unconformity) and the Millbrig or Deicke K-bentonite corresponds to siliciclastic beds of the Greensport Formation and Colvin Mountain Sandstone in northern sections HL and DG (Figure 3.7) (Chowns and Carter, 1983). The Greensport Formation in section HL includes several coarsening-upward successions with red shales, siltstones, and red dolomitic mudstones

in the lower part; argillaceous and fine-grained subarkoses to arkoses interbedded with sandy siltstones in the middle; and fine-to-coarse grained subarkoses and quartzarenites interbedded with sandy siltstones and thin beds of K-bentonite at the top. Mudcracks are common in sandy siltstones. Bioturbation is more pervasive in the middle and upper parts. Horizontal, wavy ripple, and heterolithic lamination dominates in lower sandstone beds, whereas medium sets of cross beds are in the upper sandstone beds.

Overlying the Deicke K-bentonite bed (Haynes, 1994) is the 10-meter-thick, conglomeratic quartzarenite Colvin Mountain Sandstone (Chowns and Carter, 1983). In section DM, to the south, the quartzarenite unit is less than 5 m thick and overlies the dolomitic limestone succession and the Millbrig K-bentonite bed. The Colvin Mountain Sandstone is characterized by trough and planar cross beds, horizontal bedding, scour and fill structures, bimodal sand-size distribution in some beds, and vertical burrows as much as 60 cm deep. Bentonite beds have not been identified in section DG, and surface 8 is placed in an interval of slightly calcareous shale to silty shale. In section DG, strata between the post-Knox unconformity and surface 8 consist of calcareous and siliceous sandy siltstones interbedded with fine-grained argillaceous subarkoses and thin dolomitic mudstones. Sandstone beds and sandy siltstones have ripple, flaser, and heterolithic laminations; mudcracks and bioturbation are very common in this interval.

Strata between the K-bentonite interval and the post-Ordovician unconformity (surfaces 8 and 11 in Figures 3.7, 3.8, and 3.9) correspond mainly to the Sequatchie Formation. Lithofacies and sedimentary structures are very similar to those described for sections CH-RI and GU-SS. Calcareous lithologies with thin interbeds of fine-grained mixed siliciclastic and carbonate beds dominate to the west and south (section BR); mixed carbonate-siliciclastic lithologies increase considerably to the east (section DM), and siliciclastic beds dominate to the north (sections DG and HL). In sections BI and BR, dolomitic limestone beds pass up section abruptly to skeletal and peloidal wackestones to grainstones. In section BR, mixed lithologies with ripple lamination and mudcracks and dolomitic limestone beds cover skeletal limestone beds (e.g., beds above surface 9 in section BR, Figure 3.8). Quartzarenite beds of the Colvin Mountain Sandstone in sections DM and HL separate the very similar red silty lithologies of the Greensport and Sequatchie Formations. In section DG, quartzarenites of the Colvin Mountain Sandstone are absent making a contact between those stratigraphic units difficult to place. In section DG, the

uppermost beds grade from dolomitic sandstone beds with brachiopods, to mixed siliciclastic-carbonate mudstones in the middle, and fine- to coarse-grained, cross-bedded quartzarenites to the top.

Coarse-grained beds of distinct lithologies and with phosphates interbedded with red siltstones are found toward the top of all the sections and underlying dark-colored siliciclastic mudstone and thin bedded fine-grained sandstones with ripple and hummocky cross beds of the Red Mountain Formation. Coarse-grained lithofacies vary from (1) skeletal grainstones in section BI; (2) cross-bedded, skeletal grainstone capped by fine- to coarse-grained phosphatic arenites with skeletal fragments (bryozoans, red algae, crinoids), quartz, and feldspar fragments in section BR; (3) quartzose sandstone with bryozoan fragments in section DM; and (4) quartzarenites in section HL and DG.

### **3.5.3 Equant calcite cements in carbonate rocks of the Chickamauga Limestone and Sequatchie Formation**

Distinctive styles of meteoric diagenesis have been documented in strata of the Chickamauga and Sequatchie units on the basis of petrography and geochemistry (Tobin and Walker, 1994; Kher, 1996). In sections CH and BR and in all lithofacies of the Chickamauga Limestone, 75-80% of the porosity is associated with equant (drusy) calcite, and paragenic relations indicate precipitation in shallow to moderate depths (Kher, 1996). In section BI and Tidwell Hollow (50 km northeast of BI), thick-cross bedded skeletal grainstones (bioherms) also show equant calcite cements (Tobin and Walker, 1994). Stable-isotope (oxygen and carbon) and trace-element compositions of the equant (drusy) calcite suggest a component of meteoric water mixing with marine-like fluids. Because spar cements are petrographically and geochemically similar throughout the vertical succession, Kher (1996) inferred a synchronous event of precipitation in a subsurface meteoric phreatic diagenetic environment. Tobin and Walker (1994) compared early cements pattern of bioherm deposits of the Chickamauga Limestone and deposits underlying the post-Ordovician unconformity and concluded that meteoric cementation in bioherm facies occurred before the development of the post-Ordovician unconformity.

In contrast, early meteoric diagenesis is not pervasive in uppermost beds of the Chickamauga Limestone at section BI (Tobin and Walker, 1994) and Sequatchie Formation at the northwestern corner of Georgia (Kher, 1996). In section BI, equant calcite cements have

high Fe and Mn values, and Tobin and Walker (1994) interpreted this cement as precipitation in a meteoric phreatic lens that developed during the erosion of upper Chickamauga strata. Meteoric diagenesis is local and restricted to the upper beds of a shoaling-upward succession in the upper phosphatic calcarenites and calcareous siltstones of the Sequatchie Formation in areas northeast of section RI and northwest of section CH (Kher, 1996). Cements at the top of equivalent phosphatic calcarenites in section RI do not allow the interpretation of subaerial diagenesis (Kher, 1996). Physical features of exposure are not evident at this contact, and the interpretation of subaerial diagenesis is based exclusively on observations under the microscope (Kher, 1996).

### **3.5.4 Sections southeast of the southeastern fault system of the Birmingham graben**

**3.5.4.1 Units, thickness, and age.** Middle and Upper Ordovician carbonate strata restoring southeast of the Birmingham graben consist of the Lenoir, Little Oak, and Holston Limestones. The carbonate succession is overlain by the Athens Shale in southern sections PF, AB, and CL; by red siliciclastic beds of the Greensport-Colvin Mountain-Sequatchie units in sections GS and HM, and mixed carbonate-siliciclastic Ottosee Formation in the northern section RH. Measured stratigraphic thickness for these sections is incomplete because of truncation of upper strata at the post-Ordovician unconformity (sections GS, AB, CL, and PF) or erosion on the present land surface (sections HM and RH). Regardless of the incomplete preservation, these sections are thicker, and the lower beds are older than those in the adjacent sections to the northwest. A significant decrease in thickness is shown by sections RH and CL (Figures 3.7 and 3.9, respectively) that restore progressively farther southeast from the Birmingham graben. Conodonts in basal carbonate beds in section PF yield a late Middle Ordovician (*C. friendsvillensis* zone, middle Whiterockian) age (Shaw et al., 1990).

Conodonts and graptolites reported in the Lenoir-Athens contact of locality CL are one zone older than the conodonts and graptolites reported in sections PF and AB to the northwest (Hall et al., 1986; Finney et al., 1996). The difference in age of the Lenoir-Athens contact documents the diachronous drowning of the carbonate platform during late Middle Ordovician and early Late Ordovician time (Figure 3.9) (Finney et al., 1996). In section GS, conodont studies in the Lenoir Limestone yield sparse fauna in the lower beds, an earliest Late Ordovician age (*C. sweeti* zone, uppermost Whiterockian) for middle and upper beds (Tom Shaw, written

communication to Ed Osborne, 1987), and middle to late Late Ordovician age (*B. confluens* to *A. ordovicicus* zones, late Mohawkian to middle Cincinnati) for the upper part of the Sequatchie Formation (Raymond, 1973). Ages for stratigraphic units in northern sections HM and RH (Lenoir, Holston, and Ottosee) are assigned by lithostratigraphic correlation with equivalent units in southern Tennessee (Bergström, 1973, 1977).

**3.5.4.2 Lithology.** The vertical association of lithofacies in basal beds of the carbonate interval is very complex and varies from place to place, even within the same section. The most dominant lithology is fenestral and mud-rich limestones with sparse fauna (ostracods and gastropods) with isolated sand-size fragments of quartz and chert. This lithology has been identified in all sections as the Mosheim Member of the Lenoir Limestone, and thickness varies from 0 to 30 m. Lowermost beds also locally includes: (1) argillaceous and dolomitic mudstone to wackestone with dolomite conglomerates at the base and isolated cross beds in upper beds (section PF, Shaw et al., 1990); (2) chert conglomerates (section AB, Drahovzal and Neathery, 1971); (3) intraclastic and skeletal wackestone to grainstone with chert clasts (in areas near sections AB and GS, Roberson, 1988; Osborne, 1996); (4) peloidal, intraclastic, algal wackestone to packstone and limestone conglomerate (sections CL and GS, Bearce, 1999); and (5) red, mudcracked, mixed siliciclastic and limestone lithologies (section HM; Randy Kath, written communication to G. Bayona, 2001).

The carbonate interval of the Lenoir Limestone overlying the Mosheim Member and underlying fine-grained siliciclastic deposits (surfaces 3 and 6 in Figures 3.7, 3.8, and 3.9) changes along strike from algal, intraclastic and mud-dominant limestone beds on the south and west to more skeletal limestone beds to the northeast. The Lenoir Limestone in sections PF and CL consists of argillaceous, peloidal, algal (*Calcisphere*, *Nuia* and *Girnavella*), intraclastic wackestone to packstone. Interbeds of skeletal limestone with more diverse and abundant fauna (crinoids, trilobites, brachiopods, and mollusks) and intensity of bioturbation increase upsection. Uppermost beds of the Lenoir Limestone in section PF consist of well sorted, skeletal grainstone (crinoids, bryozoans, brachiopods, sponges, mollusks, and trilobite fragments; Pratt Ferry beds of Drahovzal and Neathery, 1971). In section CL, thin calcareous beds are interbedded in the upper part of the section with skeletal, intraclastic wackestones. The uppermost part of the section CL consists of horizontal-laminated, bioclastic debris with internal normal grading, mixed argillaceous skeletal wackestones to grainstones, and calcareous black shales. Time-equivalent

carbonate beds to the northwest have been named the Little Oak Limestone. This carbonate unit is well exposed in section AB and consists of a very uniform succession of argillaceous, dark-gray, intraclastic, algal (*Nuia*, *Girnavella*, *Calcisphere*, *Dasyclads*), and skeletal wackestones to packstones with more diversity of skeletal grains (Drahovzal and Neathery, 1971 reports a few graptolites) than in the underlying Lenoir strata (Osborne, 1996). Chert nodules, thin chert interbeds and slump-folded strata are observed locally in the upper beds of the Little Oak in section AB. In section GS, the carbonate interval is dolomitic, with diverse fauna (bryozoan, crinoids, brachiopods, trilobite) and algae (*Nuia*, *Girnavella*, *Solenopora*) at the bottom, and less diverse fauna (*Tetradium*, mollusks, ostracods, trilobites), fenestral, and algal-laminated dolomite toward the top. Isolated pebbles of chert have been reported only in one medium bed at the middle of the section (Drahovzal and Neathery, 1971). Bedding contacts and internal lamination in all these sections are stylonodular, with local high amplitude and high concentration of shaly residue (Bearce, 1999).

In northern sections HM and RH, carbonate beds are grouped into two groups. One group includes mud-dominant lithofacies of the Lenoir Limestone as described in section GS. The other group includes coarse-grained limestones. In section HM, oncolitic and skeletal (mostly crinoids) limestones are interbedded with the Lenoir mud-rich lithologies. The coarse-grained lithologies are massive at the base, and have more ripple laminations and cross beds at the top. In section RH, the Holston Limestone (Cressler, 1974; or Rockwell and Chapman Ridge Formations of Caldwell, 1992) consists of oncolitic limestones, calcarenites, and cross-bedded skeletal grainstones (Cressler, 1974; Caldwell, 1992). The uppermost beds in section RH are coarse-grained mixed crinoid and bryozoan grainstones with quartz-rich laminations and red calcilutite in the matrix (Caldwell, 1992). Sedimentary structures include planar and trough cross-beds.

Overlying the carbonate interval and underlying the Millbrig-Deicke K-bentonite beds is a dominant siliciclastic interval of fine-grained sediments, but of differing lithofacies assemblage along strike. In southern sections AB and CL, graptolite-bearing siliciclastic black shales overlie the interbedded calcareous shales and argillaceous skeletal limestone lithofacies. In section PF, graptolite-bearing and calcareous black shales with slump-folded structures (Ferrill, 1989) and isolated hummocky cross beds pass up section to laminated, argillaceous calcareous mudstones with fine-grained bioclastic debris composed of bryozoans, brachiopods, and trilobites (Finney,

1977). Farther northeast in sections GS and HM, the transition between carbonate and siliciclastic lithofacies is more gradual. In section GS, dolomitic limestones are interbedded with gray and red calcareous and siliciclastic shales and shaly siltstones; whereas in section HM, argillaceous skeletal grainstones and packstones are interbedded with dark-colored shales.

Shales and siltstones are overlain by a lithofacies assemblage similar to the one described for sections DG and HL, a succession that consists of siltstones, subarkoses, quartzarenites, and K-bentonites of the Greensport Formation and Colvin Mountain Sandstone. Thin to medium beds of dolomitic mudstones and intraclastic-skeletal debris deposits appear locally in the middle of the section, overlying surface 7 in sections HM and GS (Figures 3.7 and 3.8). In section GS, intraclastic and skeletal debris-like deposits truncate underlying strata, and in both sections HM and GS the debris-like deposits separate calcareous beds below from siliciclastic deposits above with thin laminae of K-bentonite beds. Overlying the skeletal grainstone with quartz-rich laminae in section RH is a succession of calcareous laminated mudstones, sandstones, and shales of the Ottosee Formation (Caldwell, 1992). The framework of the sandstones includes quartz, calcareous intraclasts, trilobites, bryozoans, brachiopods, and peloids; the more common sedimentary structures are wavy and heterolithic laminations.

Deposits overlying the Millbrig-Deicke K-bentonite interval are preserved only in section GS, and correspond to uppermost beds of the Colvin Mountain Sandstone grading abruptly to strata of the Sequatchie Formation. In the transitional contact, quartzarenite beds of the Colvin Mountain Sandstone are bioturbated, have trace amounts of crinoids in some laminae, and the geometry of beds is cuneiform with sets of lateral accretion. The lithofacies assemblage of the Sequatchie Formation in section GS is dominated by red laminated mudstones and siltstones at the base; red, fine-grained mixed carbonate and siliciclastic lithofacies in the middle; and dolomitic mudstones to wackestones to the top. Mudcracks and rip-up clasts are common in the intermediate interval.



## **3.6 STRATIGRAPHIC CORRELATION, DEPOSITIONAL ENVIRONMENTS, AND STACKING PATTERNS**

### **3.6.1 Definition of stratigraphic surfaces of correlation**

The key for stratigraphic correlation in strata with a high diversity of lithofacies is the identification of chronostratigraphic surfaces that may be connected across different depositional systems. Eleven stratigraphic surfaces are identified, and the definition of each surface in sequential order is given in Table 3.3. Surfaces 4, 7, 8, and 9 have the best spatial and chronostratigraphic constrains. We use these surfaces, in addition to the lower and upper unconformities, to divide the Middle and Upper Ordovician succession into five stratigraphic intervals.

**3.6.1.1 Unconformities.** Onset of post-Knox deposition is highly diachronous and very irregular across the study area. Two regional patterns in the onset of deposition are observed: (1) deposition in sections restoring inside the graben began later (at least 5 m.y.) than in adjacent sections restoring both northwest and southeast, and (2) lowermost Blountian strata are younger northeastward along strike. Because of the diachroneity of initiation of Blountian foreland deposition, the post-Knox unconformity surface is covered by beds that range from stratigraphic levels of correlation 1 through 5 in the study area. The uppermost surface (11) is the post-Ordovician unconformity and separates Ordovician strata from the Silurian Red Mountain Formation (Chowns and McKinney, 1980) or Devonian strata in southeastern sections PF, CL, AB, and EC.

**3.6.1.2 Termination of carbonate-platform deposition.** The abrupt, transitional, or gradual contact between carbonate and siliciclastic deposits may be used as a surface of lithostratigraphic correlation. However, biostratigraphic data indicate that this contact is highly diachronous (Hall et al., 1986; Finney et al., 1996) and follows a cratonward (surface 3 in sections CL and AB) and northeastward (compare surface 3 in section CL, Figure 3.9; and surface 6 in section HM, Figure 3.7) trend in sections restoring southeast of the graben. Surfaces 1 and 2 correspond to the abrupt drowning of the carbonate platform (platform submerged below the euphotic zone, Schlager, 1981) in proximal parts of the foreland (Finney et al., 1996). Drowning in the southern sections PF, AB, and CL corresponds to surface 3. Termination of carbonate deposition in section GS (surface 5) and the northern sections HM and RH (surface 6)

might be related to combined effects of deepening and influx of terrigenous sediments. Surface 10 near the top of the Ordovician succession marks the onset of a very gradual progradation of terrigenous detritus and deepening of the carbonate platform.

**3.6.1.3 Regional marine-flooding surfaces.** Boundaries of third-order depositional cycles (tens to hundred of meters thick and ~ 3 m.y. in duration) define a surface used for stratigraphic correlation in carbonate platforms (e.g., Steinhaff and Walker, 1995, 1996). Meter-scale shoaling-upward successions (or parasequences) in carbonate and siliciclastic successions are bounded by marine-flooding surfaces (Van Wagoner et al., 1990). However, marine-flooding surfaces separating meter-scale successions in the Middle to Upper Ordovician carbonate platform are of more local extent and very difficult to use for stratigraphic correlation (Steinhaff and Walker, 1996). Vertical stacking of meter-scale successions (or parasequence sets) can be used to determine whether deposits within a depositional system are vertically progradational, aggradational, or retrogradational. A progradational parasequence set in the Middle to Upper Ordovician carbonate platform of southern Laurentia consists dominantly of shallow-ramp, subtidal deposits grading upward to peritidal and very shallow marine deposits (Steinhaff and Walker, 1996).

In this study, regional marine-flooding surfaces are called at boundaries of parasequence sets recognizable in carbonate and siliciclastic depositional systems, have a regional extend (Figure 3.4), and are within the same or equivalent conodont zone. Three surfaces of regional marine flooding are identified (surfaces 4, 7, and 9; Figures 3.7 and 3.8; Table 3.3). The internal array of meter-scale successions, time duration (Table 3.3), and thickness of strata between surfaces 4 and 7 (Interval II) and 7 and 9 (Intervals III and IV) suggest that these surfaces are boundaries of third-order sea-level cycles or sequences (e.g., Van Wagoner, 1990).

**3.6.1.4 K-bentonites.** Several K-bentonite beds have been identified within the Middle and Upper Ordovician succession in Alabama and Georgia (Haynes, 1994; Kolata et al., 1996). The Millbrig and the Deicke K-bentonite beds have been identified using petrography and geochemical analysis both in the carbonate and siliciclastic successions (Haynes, 1994).

Because of rapid deposition and widespread distribution, these beds have been considered to be the best surfaces for stratigraphic correlation (e.g., Kolata et al., 1996, 1998). For this reason, the Millbrig K-bentonite bed (or the Deicke where Millbrig is missing) is used as a boundary between intervals III and IV, and as the datum for stratigraphic correlation.

**3.6.1.5 Chronostratigraphic surfaces.** With the exception of the K-bentonite beds (surface 8), the other ten surfaces have varying degrees of diachroneity, but they are within the range of one conodont or graptolite zone (Figure 3.4). Of the eleven stratigraphic surfaces, only three regional marine-flooding surfaces and one K-bentonite bed might be correlated between depositional systems. These four surfaces are used to divide the Middle and Upper Ordovician succession into five stratigraphic intervals, numbered I through V in Figures 3.7, 3.8, and 3.9.

### **3.6.2 Strata and depositional systems of Interval I (upper Middle to lower Upper Ordovician)**

**3.6.2.1 Distribution and thickness.** Strata of this interval are bounded by the post-Knox unconformity at the base and the regional marine-flooding surface 4 at the top. This interval is thick in southern sections PF, AB, and CL (Figure 3.9) and is very thin and scattered in northern sections CH, RI, HM, RH, and GS (Figures 3.7 and 3.8). All these sections restore outside the Birmingham graben. Of the sections that restore inside the graben, a thin and very variable accumulation of the Atalla Chert Conglomerate Member of the Chickamauga Limestone in section BI yields conodonts (Hall et al., 1986) that indicate initiation of deposition at this locality in the later part of Interval I.

**3.6.2.2 Depositional environments and stacking patterns.** Lithofacies of basal beds in sections CH, RI, HM, RH, BI, AB, PF, and CL vary both vertically and laterally, but are suggestive of very shallow marine to supratidal environments. Irregular and scattered distribution of chert and dolomite conglomerate beds overlying the post-Knox unconformity have been interpreted as the filling of karst topography (e.g., Drahovzal and Neathery, 1971). Benson (1986b) interpreted the dolomitic, fenestral, mud-rich limestone beds of the Mosheim Member as the record of peritidal environments; a similar interpretation is valid for reddish mudcracked mixed lithologies for lower beds in sections CH, RI, HM, and BI (e.g., Roberson, 1988; Chowns et al., 1992). Intraclastic and skeletal wackestones to packstones and peloidal, intraclastic, algal packstones are more indicative of intertidal to very shallow subtidal environments (Benson, 1986b; Roberson, 1988). The wide variation in lithologies and depositional environments may be an indication of the irregular topography associated with the post-Knox unconformity (e.g., Roberson, 1988).

In contrast to the diversity of lithofacies in basal strata, the lithofacies association of the main body of limestone beds between surfaces 1 and 3 (i.e. Lenoir Limestone) in southern sections PF, AB, and CL, and in sections RH and GS is more homogeneous. The main body of limestone consists of argillaceous, peloidal, intraclastic wackestones to packstones with more diverse and abundant body fossils and algae than the underlying strata. A restricted subtidal lagoonal environment with water depths in the photic zone and below wave base is indicated by the abundance of algae (e.g., *Nuia*, *Girnavella*), the presence of more diverse body fossils, bioturbation, and absence of shallow-water sedimentary structures. Deposition in low-energy regimes is interpreted from the abundance of micrite and argillaceous detritus forming the characteristic stylonodular structures in these beds. Lagoonal environments reached its maximum water depths near section AB, as interpreted from the association of argillaceous limestones with few graptolites in the Little Oak Limestone. A subtidal lagoonal environment also has been proposed for algal-bearing beds of the Lenoir Limestone in Tennessee (Walker, 1977) with water depths between 20 to 50 m (Benedict and Walker, 1978). Interbeds of fenestral and dolomitic mudstones to wackestones are common and are fundamental to the identification of meter-scale shoaling-upward successions. These successions suggest an aggradational to slight progradational stacking pattern of deposition (e.g., section PF in Figure 3.9). In section CH, strata overlying basal deposits consist of dolomitic peloidal mudstones and wackestones, bioturbated limestone beds, and shales with a low faunal content. Chowns et al. (1992) interpreted these deposits as restricted subtidal-lagoonal environment.

The upper beds of the Lenoir Limestone have an increase in normal-marine water skeletal (e.g., crinoids and bryozoans; Jones and Desrochers, 1992) fragments and decrease of chert clasts, mud particles, green algae, and mollusk fragments. The up section change in allochems and matrix suggests deposition in more open-marine waters than lagoonal restricted waters. These skeletal-rich beds pass upward at an abrupt transitional contact to deep-water, graptolite-bearing black shales, recording the drowning of the carbonate platform (surface 3). Near surface 3, K-bentonite beds and slump-folded strata in sections PF, AB, and CL record platform instability (drowning) associated with active tectonic activity at the plate margin. Correlation using the boundary between *P. serra* and *P. anserinus* conodont zones, and the *C. sweeti* zone (as interpreted by Hall et al., 1986) indicate the lateral continuity of peritidal (section BI), lagoonal (section AB), shallow to deep carbonate ramp (sections PF and CL), and basinal

deposition (sections CL and EC) (Figure 3.10A). This southeast-dipping depositional profile is confirmed by the abrupt contact between carbonate and siliciclastic shales in sections AB, CL, and EC. A deep carbonate ramp environment is recorded in section PF by calcareous graptolite-bearing calcareous shales with isolated hummocky cross beds that grade up section to calcareous mudstones.

In general, interval I records the onset of peritidal to very-shallow marine carbonate deposition in areas outside of the Birmingham graben. Aggradational to progradational carbonate deposits in sections on the southeast are interpreted as deposition in peritidal to subtidal lagoonal environments, whereas peritidal deposits dominate to the north. Drowning of the carbonate platform in southern sections is diachronous, and accompanied by thin accumulation of K-bentonite beds and soft-sediment deformation of carbonate beds. Deep-water black shale deposits in southeasternmost sections are of the same age as shallow-marine, lagoonal, and peritidal deposits to the northwest and northeast (Figure 3.10A).

### **3.6.3 Strata and depositional systems of Interval II (lower Upper Ordovician)**

**3.6.3.1 Distribution and thickness.** Interval II is recorded in all sections with the exception of southern sections AB, CL, and EC, where the post-Ordovician unconformity truncates the upper strata of Interval I. Regional marine flooding surfaces 4 and 7 are the lower and upper boundaries of this interval. Interval II includes: (1) an increment in the rate of deposition in sections restoring northwest of the Birmingham graben (Figure 3.7); (2) thin accumulation in sections restoring inside the graben (Figures 3.7, 3.8, and 3.9); and (3) termination of carbonate-platform deposition in sections GS, HM, and RH. In contrast to the southward trend of thickening of Interval I, deposits of interval II thicken northward and thin abruptly in sections restoring inside the Birmingham graben.

**3.6.3.2 Depositional environments and stacking patterns.** Encroachment of deposition in interval II is recorded by a heterogeneous array of carbonate depositional systems and the influx of siliciclastic detritus from the east. Deep-water carbonate ramp environments are documented by laminated argillaceous carbonate mudstones interbedded with calcareous shales in the upper part of section PF. Bioherms and skeletal-peloidal limestones in section BI indicate the equivalent shallower and open-marine section of the carbonate ramp. Bioclastic debris beds in section PF might be derived from the area around section BI, where production of open-

marine fauna was high and diverse. Following the northward shallowing of the carbonate platform, dolomitic mudstones to packstones with peloids, intraclasts, algae, and sparse fauna in sections BR, DM, GS, HL, and CH are the record of subtidal lagoonal to peritidal deposition. Fenestral and mudcrack structures document very shallow marine deposition and exposure (Benson, 1986b).

Termination of carbonate-platform deposition in sections GS, HM, and RH (southeast of the Birmingham graben) is more gradual and in shallower and more oxygenated water depths than in sections AB, CL, EC, and PF of Interval I. Up section decrease of faunal diversity, fenestral structures and algal-laminated dolomitic mudstones to the top of the Lenoir in section GS document dominance of low-energy supratidal to intertidal environments. In contrast, cross-bedded, skeletal and quartz-rich, coarse-grained carbonates in sections HM and RH indicate deposition in more open, high-energy, shallow-ramp environments. Interbedding of the carbonate lithologies with shales and siltstones documents the influx of terrigenous detritus from the east and deposition in a low-energy subtidal to shallow-shelf environment (Drahovzal and Neathery, 1971). The influx of fine-grained terrigenous detritus did not reach areas around sections CH, RI, BR, and BI, where carbonate deposition continued. Coarsening-upward siliciclastic successions in sections GS and HM, up section increase of bioturbation and ripple laminations, and mudcracks in sections HL and HM indicate shoaling cycles in the shallow clastic shelf. Thin carbonate and mixed lithologies in section RH suggest shallow depositional conditions that favored episodic production of carbonates (Figure 3.10B).

Depositional environments of interval II include a shallow- to deep-water carbonate ramp to the south and southeast and shallow-marine to peritidal environments to the north and northwest (Figure 3.10B). Aggradational to progradational patterns of deposition dominated in carbonate and siliciclastic depocenters. The east-to-northeastward shift from shallow-ramp carbonate to low-energy clastic shelf illustrates the process of termination of carbonate production in shallow environments. Lack of soft-sediment deformation and K-bentonite beds also suggest a period of tectonic stability. Patterns of fine-grained clastic deposition are progradational with coarser-grained, bioturbated, and ripple-laminated strata toward the top. Phosphate detritus in both carbonate and siliciclastic deposits are irregularly distributed in this interval.

### **3.6.4 Strata and depositional systems of Interval III (lower Upper Ordovician)**

**3.6.4.1 Distribution and thickness.** Interval III encompasses strata bounded by the regional marine flooding surface 7 at the base and by the Millbrig or Deicke K-bentonite at the top (surface 8) (Figures 3.7, 3.8, and 3.9). In this interval, the migration of carbonate and siliciclastic depocenters characteristic of underlying intervals ended; consequently, carbonates and siliciclastic deposition continued in the same areas as for upper deposits of Interval II (Figures 3.10B and C). Stratigraphic thickness of interval III decreases toward sections restoring inside the graben and increases northward.

**3.6.4.2 Depositional environments and stacking patterns.** Up section increase of peloidal and intraclastic dolomitic limestone beds with fenestral and mudcrack structures over transgressive shallow-marine carbonate strata suggest shoaling and progradation of peritidal environments in sections to the northwest of the southeast boundary of the Birmingham graben, with exception of section DG. At the base of interval III in sections HM, RH, and GS, skeletal and intraclastic debris-like deposits, slump-folded strata, and slight truncation of underlying strata indicate either an event of carbonate platform instability or a marine transgression (i.e. transgressive lag deposit). Up section prevalence of sandy siltstones and subarkosic sandstones, increase of bioturbation, and mudcracks indicate subtidal to intertidal environments of deposition in sections southeast of the Birmingham graben (DG, HL, HM, RH, and GS). In general, progradational deposition is basinwide and documented in carbonate depocenters northwest of the Birmingham graben (sections CH, RI, SS, GU, and ST), in sections inside the graben to the south and with carbonate rocks (sections BR, DM, and BI), and in sections southeast of the Birmingham graben in the siliciclastic depocenter (DG, HM, RH, HL, and GS) (Figures 3.7, 3.8, and 3.9).

The sharp contact of the Colvin Mountain Sandstone with underlying strata indicates an abrupt change in depositional conditions accompanied by an increase in coarse-grained sediment supply and thin accumulation of K-bentonite beds (Figure 3.10C). Strata underlying the contact range from peritidal carbonates in section DM to bioturbated sandy siltstones and sandstones in sections HM, HL, and GS; these deposits represent shallow-water deposition in a low- to moderate-energy regime. In contrast, quartzarenites overlying the contact show planar and trough cross beds, have bimodal sand-size distribution in some lower beds, and are texturally and compositionally mature (Jenkins, 1984). Elongated vertical burrows in upper beds suggest a

shallowing-upward trend of deposition in high-energy regimes. All these criteria suggest alternate high- to moderate-energy regime in shallow-marine environments.

The sharp change on depositional conditions between Greensport and Colvin Mountain units is diachronous and younger to the northeast and northwest. The change is positioned below the Millbrig-Deicke K-bentonite interval in section GS, within the K-bentonite interval in sections DM and HL, and above the K-bentonite interval in section HM. In palinspastic maps, quartzarenites of the Colvin Mountain Sandstone form a northeast-striking narrow belt of shallow-marine sand bars that separates fine-grained subtidal siliciclastic deposits on the southeast from peritidal carbonate deposition on the northwest (Figures 3.7, 3.8, and 3.10C). Shallow-marine sand bars correlate along-strike with subtidal, quartzose, medium-grained sand ridges and sandy siltstones of the Greensport Formation. Previous studies have interpreted these quartzarenites as shallow-marine sand bars reworked by tidal and longshore currents (Chowns and Carter, 1983; Jenkins, 1984). This event of change in energy migrates from the southeast (section GS) to sections in the north and west (Colvin Mountain Sandstone is in interval IV in sections DM and HM). A similar distribution of sand and gravel bars striking parallel to the foreland, and separating carbonate production on one side from tidal-dominated deltaic deposition on the other side is documented in the Gulf of Papua foreland basin (Harris et al., 1996).

Interval III records shallowing of carbonate and siliciclastic depositional systems after an event of platform instability, and the resume of volcanic activity as documented by the numerous K-bentonite beds in the latest part of this interval. A localized and diachronous event of along-strike migration of sand bars is recorded in the siliciclastic depocenter, and it is associated with an increase in rate of supply of coarse and very mature sediments.

### **3.6.5 Strata and depositional systems of Interval IV (lower-middle Upper Ordovician)**

**3.6.5.1 Distribution and thickness.** Interval IV encompasses strata bounded by the Millbrig K-bentonite bed (surface 8) at the base and the regional marine-flooding surface 9 at the top (Figures 3.7, 3.8, and 3.9). In section DG, where K-bentonite beds have not been reported, surface 8 is located at the base of a thick interval of red calcareous silty shales and siltstones that are interpreted to represent deepening of the basin floor (Figure 3.7). The depocenter of siliciclastic deposition continued nearly in the same areas as for upper deposits of interval III,



whereas the depocenter of carbonate deposition migrated slightly northeastward (Figure 3.10C and D). Although stratigraphic thickness of interval IV thickens northward, as documented for intervals II and III, stratigraphic thinning toward sections inside the Birmingham graben is minimal in southern areas and abrupt in northern areas. Maximum values of thickness are recorded in section CH, where carbonate deposition dominates.

**3.6.5.2 Depositional environments.** A diachronous deepening and increase of energy of depositional conditions is recorded by a change from prograding peritidal carbonates of interval III to locally cross-bedded, skeletal, peloidal, and intraclastic wackestones to packstones beds near the base of interval IV, reflecting a deepening of the basin floor. The change to deeper water deposition is positioned at different levels above the Millbrig K-bentonite, documenting the diachroneity of a marine-flooding surface. In section BI, surface 8 records the transition (Figure 3.9); in section CH, the transition is 2 m above surface 8 (Figure 3.7); in section BR is 6 m above the Millbrig K-bentonite (Figure 3.8). Calcareous shales and siltstones overlying a succession of siltstones and fine-grained sandstones in section DG (Figure 3.7), in addition to deposition of Colvin Mountain quartzarenite beds in sections DM and HM, indicate the diachronous event of sand bar migration in siliciclastic depocenters.

After the event of deepening in the carbonate ramp, a regional shoaling occurred in both carbonate and siliciclastic depocenters. Micritic and dolomitic limestone beds with mudcracks in sections GU and BR, and fine-grained mixed lithologies interbedded with mudcracked dolomitic mudstones in sections DM and GS document the dominance of very shallow, peritidal deposits near the top of interval IV. In section DG, the up section change from laminated shales to bioturbated siltstones and fine arkosic sandstones with mudcracks document the shoaling of depositional conditions toward surface 9. Limited exposures of siltstones and thin beds of fine-grained sandstone in sections HL, DM, and GS suggest the dominance of low-energy regime of deposition in siliciclastic depocenters. The progradational pattern of deposition is also observed in the lower part of carbonate beds of the thick section CH; however, the up section increase in abundance and diversity of skeletal fragments suggest gradual deepening and deposition in more open waters, and a change from progradational to more aggradational and retrogradational patterns of deposition.

Interval IV documents waning of volcanic activity, slight deepening in the carbonate ramp, and the continuation of the diachronous migration of high-energy depositional settings that

initially affected siliciclastic depocenters southeast of the subsurface Birmingham graben (top of Interval III), and then affected carbonate depocenters located inside and northwest of the subsurface Birmingham graben (lower Interval IV). Progradation of shallow-marine and peritidal deposits and variable low influx rates of sediment supply from the east favored the resumption of production of carbonates in sections to the east (Figure 3.10D).

### **3.6.6 Strata and depositional systems of Interval V (middle-upper Upper Ordovician)**

**3.6.6.1 Distribution and thickness.** The upper interval V is bounded by the regional marine-flooding surface 9 and the post-Ordovician unconformity (Figures 3.7, 3.8, and 3.9). In this interval, the siliciclastic depocenter migrated cratonward and mixed with carbonate deposits, anticipating the termination of the Ordovician carbonate platform in distal foreland settings. The northward thickening trend of strata continues in this interval. Truncation at different levels of upper Ordovician strata at the post-Ordovician unconformity does not allow the definition of thickness trends in a northwest-southeast direction.

**3.6.6.2 Depositional environments and stacking patterns.** Strata between surfaces 9 and 10 show shoaling of both carbonate and fine-grained mixed carbonate-siliciclastic deposits. In sections restoring northwest of the Birmingham graben and section BR, strata between surfaces 9 and 10 consist of skeletal grainstones and packstones passing up section to fenestral dolomitic limestone beds and mixed, fine-grained lithologies with mudcracks. In sections DM and GS, shoaling is indicated by the up section decrease of reddish, bioturbated, fine-grained mixed lithofacies and increase of dolomitic limestone beds. The superposition of these lithofacies constitutes shoaling-upward successions with subtidal deposits at the bottom and shallower marine to peritidal deposits toward the top (Chowns et al., 1992; Phillips, 1996).

Lithofacies assemblages of strata above surface 10 change both vertically and laterally in short distances (Figure 3.10E). Phosphatic cross-bedded skeletal grainstones, skeletal dolomitic sandstone beds, bioturbated shales, and cross-bedded quartzarenites overlie surface 10 in sections northwest of the southeastern fault system of the Birmingham graben (e.g., RI, DG, HL, GU, BR, DM, and BI), suggesting deepening of the platform and abrupt, lateral changes in the energy of deposition. Overlying these coarse-grained beds in section DG are coarsening-upward siltstones and cross-bedded quartzarenites. In section RI, the coarse-grained succession is capped by a phosphatic crust and overlain by bioturbated shales and sandstones; these two

features indicate a shift from high to low energy regimes of deposition. The abrupt changes in lithofacies assemblages above surface 10 have been interpreted as a dynamic shift of depositional conditions from a shallow carbonate platform to lagoon and riverine estuary environments to the east (Rindsberg and Chowms, 1986; Martin, 1991).

Deposits of Interval V record the cratonward progradation and encroaching of siliciclastic deposits over locations previously dominated by carbonate deposition and above or northwest of the subsurface Birmingham graben structure.

### **3.7 TECTONIC SUBSIDENCE OF THE DISTAL FORELAND**

Curves of total and tectonic subsidence for sections restoring in middle and distal foreland settings illustrate different behaviors of the top of basement during Middle and Late Ordovician deposition. Figure 3.11 shows representative curves of total and tectonic subsidence for sections restoring northwest, inside, and southeast of the Birmingham graben. Total subsidence curves may be divided into four segments. The first segment has a negative slope and corresponds to thermal subsidence, as recorded by upper beds of the Knox Group along the southern margin of Laurentia (Thomas and Astini, 1999). The second segment is flat and corresponds to the post-Knox unconformity. The third segment is again downslope and is between the post-Knox unconformity and the Millbrig and Deicke K-bentonite beds (surface 8). The fourth segment is between the K-bentonite beds and the top of the Silurian, where the total subsidence curve has a gentle downslope, with exception of section DG that follows the geometry of the third segment.

Tectonic subsidence curves show a different geometry than total subsidence curves, and a total of five segments (segments a to e, Figure 3.11) is recognized after the segment of thermal subsidence of the Knox Group and before Silurian. Sections restoring inside the graben (e.g., sections DG and BI, Figure 3.11A) have a deeper level of erosion at the post-Knox unconformity than sections in adjacent blocks (e.g., sections CH-RI, GS, or PF). The minimum amount of erosion of upper Knox strata is represented by segment a in sections CH-RI, GS, and PF. For sections DG and BI, an estimated amount of uplift (difference in thickness of preserved Knox strata between adjacent sections; compacted for lower boundary and uncompacted for upper boundary) was calculated and included in the tectonic subsidence diagrams (segment b in Figure

3.11A). As a result, the basement in sections DG and BI rises during time of the post-Knox lacuna with respect to sections restoring outside the graben.

Two inflections of the tectonic curve (segments c and d) previous to deposition of Millbrig-Diecke K-bentonite beds are observed in the tectonic subsidence curves for composite section CH-RI (northwest of the graben, Figure 3.11A) and section PF (southeast of the graben, Figure 3.11B). The first and more gentle downslope geometry of segment c is related to subsidence and the early onset of peritidal and shallow-marine deposition in both areas (Interval I); the second downslope is of segment d and corresponds to the onset of black shale deposition in section PF (Interval I) and an increase in the rate of carbonate deposition in composite section CH-RI (Intervals II and III). Segment d in section PF corresponds to the passage of the flexural wave that also affected sections CH-RI to a lesser degree. Therefore, subsidence of segment d is related to lithospheric flexure. Tectonic subsidence of segment c is related to an earlier event that affected sections restoring at both sides of the Birmingham graben. Tectonic subsidence curves for sections DG, GS, and BI have an initial gentle downslope trend before the K-bentonite interval that may be equivalent to segment d in sections CH-RI.

The gentle downslope segment d is followed by flattening and/or upslope trend of segment e toward the top of the Ordovician. Segment e is observed in sections restoring outside of the Birmingham graben (sections GS and CH-RI) and inside the Birmingham graben (sections DG and BI). The upslope trend records uplift of the top of basement coeval with the cratonwide rise of sea level (Bond and Kominz, 1991). This event of uplift is better recorded in section BI, where the angular unconformity between Upper Ordovician strata of the Chickamauga Limestone and the Silurian strata indicates erosion and tilting (1.6-degree to the southeast) of the Chickamauga Limestone. In the other sections, the magnitude of the rise of the top of basement in sections GS and DG is higher than sections BR and CH-RI to the northwest (Appendix C). In the Silurian, the curve stays flat for sections CH-RI, BI, and GS, and bends down for section DG. The latter downslope in section DG documents an increase of tectonic subsidence only in the northeasternmost section of the study area.

### **3.8 DISCUSSION**

In this section, we discuss the effects of basement fault reactivation, flexural subsidence, and eustasy in the geometry of the post-Knox unconformity, patterns of carbonate and

siliciclastic deposition, generation and distribution of uplifted areas, and tectonic subsidence for the distal Blountian foreland basin.

### **3.8.1 Lacuna geometry and stratigraphic patterns associated to early forebulge migration**

Initial migration of the flexural wave creates a characteristic pattern of erosion and/or deposition on the foreland plate (Figure 3.1A and B). In the western Taiwan (Yu and Chou, 2001) and north Alpine foreland basins (Crampton and Allen, 1995), the regional basal unconformity has a chronostratigraphic gap increasing forelandward and with the maximum gap at the flexural bulge. This distinctive forelandward increase of the lacuna reflects the forward migration of the flexural wave. Besides of the time-transgressive onlap of foreland strata on flexurally-deformed passive-margin strata, the forebulge has an orogen-parallel orientation (Yu and Chou, 2001; White et al., 2002). In contrast, the growth of a semi-fixed forebulge (Figure 3.1B) causes deep truncation of passive-margin strata in very narrow areas, as documented in the Apennine foreland basin (Washbush and Royden, 1992) and in the Oman Mountain foredeep (Patton and O'Connor, 1988).

In distal foreland settings, early stages of deposition of underfilled foreland basins are characterized by development of a carbonate platform deepening toward the orogen (Dorobek, 1995). Distal foreland stratal architecture of carbonate beds allows the differentiation between a migrating and a semi-fixed forebulge. Cratonward migration of the flexural wave causes increasing subsidence rates at progressively more distal foreland localities, backstepping and drowning of the carbonate platform on localities facing the hinterland, and the reactivation of older basement faults as normal faults (Figure 3.1A). In contrast, the growth of a semi-fixed forebulge is associated with: (1) an abrupt lateral change from shallow-water to deep-water carbonate deposition at both sides of a pronounced bulge; (2) narrowing and steepening of the foredeep and backbulge depozones; and (3) if the bulge becomes exposed, unroofing of the passive-margin succession (Figure 3.1B).

As discussed in section 3.2.3, the model of flexural wave migration has been postulated to be the principal factor in controlling the origin of the basal unconformity (or post-Knox unconformity), irregular Middle Ordovician deposition in the distal foreland, and backstepping of Middle and Upper Ordovician carbonate-ramp deposits. The lacuna geometry and early patterns of distal foreland uplift and carbonate deposition, as discussed below, indicate that

neither a migrating nor a semi-fixed forebulge played a primary control in the early evolution of the distal foreland. However, migration of the flexural wave did play an important role on deposition in subsequent stages of distal foreland evolution.

### **3.8.2 Geometry of the post-Knox unconformity and intraforeland uplifts**

The cratonwide post-Knox unconformity shows the greatest magnitude of the lacuna in sections DG, BR, DM, and BI, which restore inside the Birmingham graben (Figure 3.6). The chronostratigraphic gap increases from ~ 9 m.y. in section AB to more than ~ 32 m.y. in section BI, and the unconformity truncates at least 472 m (compacted thickness) of the Knox Group in section BI. Palinspastic restoration of the thin Knox interval imaged in seismic reflection profiles indicates that the abrupt change in the lacuna geometry occurs across the southeastern fault boundary system of the Birmingham graben (cross section 16, Plate 2.1). A similar magnitude of change in the lacuna and depth of erosion across the northwestern fault boundary system of the Birmingham graben is documented between sections DG and RI. The contrasting geometry of the lacuna between sections BI and AB in the south, and sections RI and DG in the north may not be explained solely by eustasy, where maximum erosion is expected either at the paleoshelf edge in incised channels (e.g., Van Wagoner et al., 1990) or toward the craton, where the rocks would be exposed longer (Bond and Kominz, 1991). A semi-fixed forebulge above the Birmingham graben (i.e., the graben as a weak segment of the lithosphere) may explain the deep erosion of the Knox Group, but it does not explain the early and thick accumulation of deep lagoonal carbonate deposits with chert clasts at both sides of the Birmingham graben.

Tectonic inversion of the graben (Figure 3.1C) provides a better explanation for the lacuna geometry, patterns of early deposition on the distal foreland, supply of conglomerate clasts, and recharge of meteoric waters. Positive relief of the inverted upthrown block (former Birmingham graben) caused the deep truncation of Knox strata and the late onset of deposition in sections restoring inside the Birmingham graben. The thick and mappable record of karst-filling chert conglomerates in sections restoring inside the graben indicates deep weathering of limestone and chert beds of the Knox Group in inverted upthrown blocks. In contrast, less weathering of the Knox Group and early deposition occurred in inverted downthrown blocks (former shoulders of the Birmingham graben). Limestone-conglomerate clasts in sections CH, RI, AB, CL, and PF indicate short time of exposure below the basal conglomerates in inverted

downthrown blocks. Gravel-sized chert and limestone clasts, and sand-size monocrystalline quartz embedded in shallow-marine and lagoonal carbonate deposits of sections CH, RI, AB, CL, and PF indicate the nearby presence of uplifted areas. Karst topography in uplifted blocks bounded by faults should have facilitated nearly vertical filtration of meteoric waters to subsurface aquifers that contributed to early cementation in carbonate strata of the Chickamauga Limestone (Tobin and Walker, 1994; Kher, 1996).

An alternative explanation is to consider the intraplate uplift as bounded by normal faults (flexural profile of time 2 in Figure 3.1A). As the foreland plate bends and the flexural wave migrates, flexural normal faults will reactivate older basement structures and uplift segments of the distal foreland carbonate platform. The coincidence in position between uplift blocks and the Birmingham basement graben, lack of Middle Ordovician conglomerate clasts in limestone beds, and later record of flexural migration in early Late Ordovician time (see below) suggest that upthrown and downthrown blocks were bounded by basement-cored inversion structures rather than by flexural normal faults. These intraforeland structures record the early response of ancient structures to the new in-plane stress regime (Dorobek, 1995) caused by Blountian convergence.

### **3.8.3 Architecture of the Middle Ordovician carbonate platform**

Thickness, lithofacies assemblages, and stacking patterns of lower-middle Lenoir and lower Chickamauga strata (lower Interval I) constraints the early inversion of basement faults. In areas adjacent to inverted upthrown blocks, tectonic subsidence curves of lower carbonate deposits of the Chickamauga and Lenoir beds document an early development of carbonate depocenters on opposite sides of the inverted upthrown block (segment c in sections CH-RI and PF, Figure 3.11), previous to the steep downslope curve of flexural subsidence (segment d in Figure 3.11). Stacking patterns of lagoonal deposits are dominantly aggradational, suggesting that the rate of carbonate production kept pace with creation of accommodation space in downthrown blocks.

Local topography of the inverted graben likely distorted the marginal-scale flexure of the foreland plate. Carbonate deposits in section HM and AB are thicker and more fine-grained than adjacent sections RH and CL, respectively, to the southeast. The Middle and Upper Ordovician succession also thins northwestward away from sections ST and SS (Kidd, 1975). Stratigraphic

thinning of foreland strata suggests the presence of two small-scale foreland-like basins adjacent to the inverted upthrown block. If the inverted block is considered as a tectonic load on a continuous elastic plate (e.g., Turcotte and Schubert, 1982), the effects of loading bend the elastic plate and two asymmetrical basins are formed (Figures 3.12A and B). As this model predicts, thicker and deeper water deposition occurred in sections adjacent to the inverted structure (e.g., AB, HM, ST, and CH-RI) than in sections away from the inverted load (e.g., CL, RH). This model gives an explanation of the southeastward and northwestward thinning and shallower depositional conditions of coeval carbonate strata away from the Birmingham graben. (Figures 3.9 and 3.12B)

Latest Middle Ordovician carbonate deposition may be the combined result of basement fault inversion and distal effects of the northeastward migration of the flexural wave (Finney et al., 1996; Chapter 4). Thick lagoonal deposits as seen in sections PF and AB in Interval I (Figure 3.9) are also observed later in Interval II in section CH (Figure 3.7). Similarly, lowermost deposits above the post-Knox unconformity in the inverted upthrown block are older in section BI (Interval I; Figure 3.9) and younger to the northeast in sections DM, HL and DG (Interval II; Figure 3.7 and 3.8). Termination of carbonate deposition in the southeastern inverted downthrown block is older to the southeast (sections AB and CL) and younger to the northeast in sections GS, HM, and RH. This northeastward trend in carbonate deposition in both southeastern inverted downthrown and inverted upthrown blocks is similar to the northeastward migration of black shale deposition in the proximal foreland (Finney et al., 1996).

### **3.8.4 Upper Ordovician carbonate platform, progradation of the synorogenic clastic wedge, and eustasy**

The early signature of basin inversion in the distal foreland was subdued gradually by weathering of intraplate uplifts, fluctuations of sea level, thin accumulation of K-bentonite beds, and forelandward migration of the flexural wave that brings the sea floor into different facies zones and backsteps the zone of optimum carbonate production (Figure 3.12C) (Dorobek, 1995). The lateral change from peritidal and karst-filling deposits in section BI, lagoonal-subtidal in section AB, well-sorted skeletal grainstones in section PF, and turbidite skeletal limestones and graptolitic black shales in sections CL and EC depicts the geometry of a regionally southeast-dipping foredeep in early Late Ordovician (Figure 3.10A). In southeastern sections AB, CL, EC,



and PF, the up section increase of coarser-grained carbonate deposits in upper beds of the Lenoir Limestone followed by deposition of thin K-bentonite beds and graptolitic black shales documents the cratonward flexural wave migration, drowning of the carbonate platform in a time of input of volcanic material to the foreland basin.

However, early Late Ordovician forelandward migration of the flexural wave partially stopped above the Birmingham graben. Segment d in tectonic subsidence curves documents the regional and variable response of the top of basement to flexural subsidence in early Late Ordovician time. Segment d in flexural subsidence curves is steeper in sections restoring southeast and away of the Birmingham graben (e.g., section PF in Figure 3.11B) than in sections to the northeast (e.g. sections GS and DG) and northwest of the Birmingham graben (e.g., section CH-RI). The record of peritidal to shallow-water carbonates underlying fine-grained red siliciclastic beds and the lack of deep-water carbonates and siliciclastic beds in sections GS, HM, and RH indicate that termination of carbonate deposition may be more the result of siliciclastic influx than deepening caused by flexural subsidence (Figure 3.10B).

Tectonic subsidence and sea-level curves for deposits of Intervals III, IV, and V indicate that these deposits accumulated in a time of cratonwide rise of sea level and of regional rise of the top of basement (segment e in Figure 3.11). The regional rise of basement may reflect orogenicward migration of flexural uplift, an interpretation further supported by (1) shoaling of siliciclastic depocenters favoring deposition of shallow-marine sandy shoals of the Colvin Mountain Sandstone (Figure 3.10C); (2) later southeastward progradation of shallow-water to peritidal carbonates over siliciclastic deposits (Figure 3.10D); and (3) aggradational to retrogradational carbonate deposition in section CH-RI to the northwest (Interval IV in Figure 3.7). The migration of the flexural wave toward the orogenic belt was initially accompanied by accumulation of K-bentonite beds and high influx of sand-sized quartzose detritus followed by a decrease in influx of siliciclastic detritus to the distal foreland. Cratonwide sea-level rise of ~ 80 m (Bond and Kominz, 1991) created the conditions for the record of a submerged southeastward migration of the flexural wave, the thick and widespread record of deposition of volcanic ash beds, and the thicker and aggradational to retrogradational pattern of deposition in section CH-RI (Figures 3.7 and 3.10D).

The dynamic change related to the passage of the flexural wave is repeated in uppermost Ordovician and lowermost Silurian strata. The shallowest part of the latest Ordovician flexural

profiles is in section BI, where southeast tilting of Upper Ordovician strata caused erosion (Thomas, 1986) and iron-rich meteoric cementation (Tobin and Walker, 1994) in uppermost preserved strata of the Chickamauga Limestone. Farther to the northeast, peritidal to subtidal deposits of sections RI, GU, BR, and DM pass up section to high-energy, shallow-marine, mixed carbonate-siliciclastic deposits with evidence of early meteoric diagenesis in upper beds of shoaling-upward cycles (Kher, 1996). The siliciclastic and deep-water component of the flexural wave profile is in sections RI and DG and corresponds to prograding clastic estuarine and tidal-flat deposits (Martin, 1991). All these carbonate and siliciclastic Ordovician deposits are overlain by deeper-water shales and hummocky cross-bedded sandstones of the Silurian Red Mountain Formation with a slight increase in tectonic subsidence rates in the northern section DG (Figure 3.11A).

Geodynamic models of foreland basins explain migration of the flexural wave using two different mechanisms. Quinlan and Beaumont (1984) suggested that viscoelastic relaxation of the lithosphere is the dominant control on hinterland bulge migration between periods of crustal deformation, whereas cratonward bulge migration and generation of accommodation space in the distal foreland occur during episodes of crustal deformation. In contrast, Flemings and Jordan (1990) indicated that the flexural wave migrates hinterland at the onset of deformation using an elastic rheology of the lithosphere, whereas cratonward bulge migration and accommodation space in the distal foreland occur between periods of crustal deformation. Because a complete proximal foreland stratigraphy and the Blountian tectonic loads are not preserved (Chapter 4), there is not a direct evidence to link depositional patterns in the distal foreland with events of deformation in the Blountian orogenic belt and deposition in the proximal foreland.

This study can establish a relationship between episodes of flexural migration, accumulation of K-bentonite beds, and influx of siliciclastic detritus. The early episode of forelandward flexural migration recorded in southeastern sections (e.g., section CL) was accompanied by deposition of thin K-bentonite beds and black shales (Interval I). The episode of hinterlandward flexural migration was accompanied by deposition of the Deicke and Millbrig K-bentonite beds and an upsection decrease in influx of synorogenic detritus (Interval IV). The last event of cratonward flexural wave migration is documented by termination of carbonate deposition and initiation of deep shelf synorogenic clastic deposition of the Silurian Red Mountain

Formation. These relationships suggest that flexural wave migration was linked with active volcanism along the plate margin, and sedimentary filling of the foredeep.

Progradation of the Blountian clastic wedge was controlled by inverted upthrown blocks in the distal foreland. Distribution of the Greensport Formation and Colvin Mountain Sandstone follows the southeast boundary of the inverted Birmingham graben, suggesting local structural control of sedimentation within the siliciclastic depocenter and restricted dispersal of fine- and coarse-grained synorogenic detritus in the inverted upthrown and southeastern downthrown blocks (Figure 3.10A to D). The restricted and structurally controlled siliciclastic deposition on the southeast permitted shallow-marine carbonate deposition in the northwestern inverted downthrown block. Cratonward progradation of the clastic wedge in the latest Ordovician-Early Silurian and thicker deposition in sections restoring inside the graben in the upper part of Interval V (Figures 3.7 and 3.10E) suggest the termination of basement fault inversion in the distal foreland.

Eustatic effects in Middle and Late Ordovician deposition are defined by identification of nearly coeval regional marine flooding surfaces that affected both siliciclastic and carbonate depocenters. Surfaces 4, 7, and 9 are the lower boundaries of third-order depositional cycles (Intervals II, III, and V) that include transgressive carbonate and siliciclastic deposits and meter-scale shoaling-upward successions. Internal stacking patterns of third-order depositional cycles indicate the conformable progradation of shallow-marine and peritidal deposits. The regional marine flooding surfaces identified in this study are of regional extent, and they may be correlated with depositional sequence boundaries documented in the Tennessee platform (Steinhauff and Walker, 1995, 1996) and the Nashville dome (Holland and Patzkowsky, 1997) (Figure 3.4). However, the correlation of coeval K-bentonite beds and transgressive marine deposits near surface 8 depict the diachronous signature of marine flooding surfaces in a foreland basin.

### **3.9 CONCLUSIONS**

Patterns of carbonate, mixed, and siliciclastic deposition in the distal Blountian foreland basin and during Middle and Late Ordovician time were controlled by the interaction of basement-fault inversion, fluctuated migration of the Blountian flexural wave, and rise of sea level. Each of these factors dominated at different stages of the foreland evolution, and they are

identified by the local, plate-margin, or cratonwide effects on foreland deposition. Late Middle Ordovician inversion of a former northeast-striking basement graben (Birmingham graben) enhanced erosion of Knox strata and shaped an irregular karst relief at the post-Knox unconformity. Local bending effects of inverted upthrown blocks triggered carbonate deposition in two small-scale foreland-like basins adjacent to the active faults and in opposite sides of the inverted upthrown blocks. Deeply weathered inverted upthrown blocks supplied coarse-grained chert and quartz grains to carbonate depocenters in inverted downthrown blocks, facilitated filtration of meteoric waters to carbonate aquifers in downthrown blocks, and restricted the cratonward advance of the synorogenic clastic wedge during early and middle Late Ordovician. A geodynamic model of the inversion corroborates the link between intraplate uplift and deposition, and together with stratigraphic and provenance analyses allow to reject the model of flexural uplift as the solely mechanism to create the post-Knox unconformity in southernmost Laurentia..

Flexural subsidence related to tectonic and sediment loading along the plate margin and influx of siliciclastic detritus strongly contributed to the diachronous termination of carbonate platform deposition in the study area. In the southeastern inverted downthrown block, flexural drowning of the carbonate platform at the southeastern end and influx of terrigenous clastic detritus at the northeastern end caused the diachronous termination of carbonate deposition in early Late Ordovician time. Tectonic subsidence curves, shoaling stratigraphic patterns in siliciclastic depocenters, and southeastward progradation of carbonate beds indicate an event of hinterlandward migration of the flexural wave during the middle to late Late Ordovician time. These first two events of flexure are accompanied by deposition of volcanic ash material. The combined effects of cratonwide sea-level rise and hinterlandward forebulge migration created the conditions for continuous shallow-water deposition and the record of shoaling-upward successions forming third-order depositional cycles in both siliciclastic and carbonate depocenters. Termination of carbonate-platform deposition in the inverted upthrown block and northwestern downthrown block is linked to the cratonward progradation of synorogenic siliciclastic deposits, first during early and middle Late Ordovician and later during the latest Ordovician and early Silurian. The latter is associated with the forelandward passage of the flexural wave that also tilted and eroded Upper Ordovician strata in southern sections.

**Table 3.1** Explanation of lithofacies codes and lithofacies interpretations for carbonate and mixed carbonate and siliciclastic deposits.

		<b>Lithology code</b>	<b>Rock name (Dunham, 1962)</b>	<b>Energy, Water depth</b>	<b>Environment of deposition. Dominant framework grains. Structures</b>
<b>CARBONATES</b> L= Limestone D= Dolomite	Lm, LDm, Dm = micrite-dominant constituents	Lmm, LDmm Dmm	Mudstone to wackestone	Low < 4 m	Supratidal to intratidal. Peloids, intraclasts, algae, restricted fauna. Fenestral, ripple and horizontal laminated, mudcracks, bioturbated.
		Lmms, LDmms Dmms	Mudstone to wackestone	Generally low < 16 m	Supratidal to subtidal (lagoon). Restricted fauna fragments of conglomerate size. Massive, fenestral.
		Lmo, LDmo	Wackestone to grainstone	Low to high < 16 m	Supratidal to shallow subtidal. Algae, oncoids, peloids, intraclasts, minor skeletal (mixed fauna). Massive, fenestral, ripple lamination, stylonodular.
		Lmi, LDmi	Wackestone to packstone	Moderate to high < 64 m	Intratidal to shallow subtidal with restricted circulation (lagoon). Intraclasts dominantly of Lmo lithologies. Massive, bioturbated, stylonodular, poor sorting.
		Lmr, LDmr	Wackestone to packstone	Low to moderate < 16 m	Shallow to intermediate subtidal, ramp or lagoon. Mixed restricted and open-water skeletal fragments, minor algae and peloids. Massive, stylonodular, fenestral.
		Lms	Wackestone to grainstone	Moderate to low < 64 m	Subtidal, open-marine circulation (shallow ramp). Open-marine fossils, trace of algae, intraclasts and peloids.
		Lml	Mudstone to wackestone	Generally low < 256 m	Massive, laminated, cross beds, stylonodular, bioherms. Intermediate to deep ramp. Thin horizontal lamination, internal grading and thin beds of Lss and Sb.
		Dsm	Coarse-crystalline dolomite		Non-skeletal. Massive. Original components must have been destroyed during dolomitization.
		Lso	Grainstone	Moderate to high < 16 m	Shallow ramp, shoals, tidal bars. Ooids, algae, trace of skeletal fragments, quartz. Cross beds, normal grading, lamination.
		Lss	Packstone to grainstone	Moderate to high < 16 m	Shallow ramp, shoals, tidal bars. Open-marine skeletal fragments, sand-size quartz. Massive, cross beds, good sorting.
		Lsp	Packstone to grainstone	Moderate to low < 16 m	Very shallow, intratidal to subtidal. Peloids and intraclasts, rare skeletal grains. Lamination, cross beds, good sorting.
		Lsi, Dsi	Packstone to grainstone	Moderate to high < 16 m	Very shallow, intratidal to subtidal. Intraclasts and open-marine skeletal grains, sand-size quartz. Massive, horizontal- and cross-bedded, good to moderate sorting.
		restricted-water skeletal fragments: ostracods, trilobites, mollusks, brachiopods, coral <i>Tetradium</i> , crinoids, green algae, oncoids open-marine skeletal fragments: brachiopods, trilobites, crinoids, bryozoans, corals, red algae			
<b>MIXED LITHOLOGIES</b> LS (carbonate dominant); SL (siliciclastic dominant)		<b>Lithology code</b>	<b>Dominant carbonate and siliciclastic lithologies</b>	<b>Energy, Water depth</b>	<b>Environment of deposition. Dominant framework grains. Structures</b>
		LSbs, SLbs	Lml, Lms, Lss, Sb	Low < 1024 m	Deep-water ramp, distal carbonate turbidites. Graptolites. Horizontal lamination, soft-sediment deformation.
		LSf, SLf	LDmm, Ldmo, Lml, Sfsm, Sfm, calcisiltite	Generally low < 16 m	Intertidal, subtidal lagoon. Trace of skeletal grains. Mottled, diverse degree of bioturbation, massive, ripples and horizontal lamination, cross beds, mudcracks.
		LSci, SLci	Lmi, Lms, Ssm, Sgcg conglomerate	High < 64 m	Subtidal, debris-flow deposit. Massive, cross-bedded, matrix- to clast-supported, bioturbated, argillaceous, matrix of LSf, Sfsm, Ssm.
		LSes, SLcs	Lss, Lms, Sst, Ssp, Ssm, Sgcg conglomerate	High < 16 m	Very shallow ramp, shoals, tidal bars. Open-marine skeletal fragments, trace of peloids and intraclasts. Cross beds, cuneiform and lenticular beds, clast-supported.

**Table 3.1** (previous page) Explanation of lithofacies codes and lithofacies interpretations for carbonate and mixed carbonate and siliciclastic deposits. The codes have uppercase letters to indicate which is the dominant composition of each lithofacies (L=limestone, D=dolomite, S=siliciclastic (see Table 3.2)). Mixed lithofacies have two uppercase letters (LD=dolomitized limestone; LS=carbonate-siliciclastic). In only carbonates lithofacies, the first lowercase letter indicates either micritic (m) or sparry (s) lithologies. The second and third lowercase letter(s) denote important components or structures of the lithofacies: p =peloidal, i =intraclastic, o =non-skeletal allochems, r = association of skeletal fragments indicates restricted-water environments (ostracods, trilobites, mollusks, brachiopods, *Tetradium*, crinoids, green algae, oncoids), s = association of skeletal fragments indicates open-marine environments (brachiopods, trilobites, crinoids, bryozoans, corals, red algae), l=laminated, m=massive. In mixed lithologies, the lowercase letters indicate: bs = interbedding with black shales, f = fine-grained lithologies, ci = coarse-grained intraclastic, cs = coarse-grained skeletal.

**Table 3.2** Explanation of lithofacies codes and lithofacies interpretations for siliciclastic deposits. The code uses the uppercase letter “S” to identify the lithofacies as siliciclastic. The first lowercase letter denotes the grain size: g = gravel-size deposits, s = sand-size deposits, f = silt-size deposits, b = shale deposits. The second and/or third lowercase letters denote an important structure, as described in the table, and allow the identification of each lithofacies.

<b>Lithology code</b>	<b>Dominant grain size</b>	<b>Structures</b>	<b>Interpretation. Range of depositional environments</b>
Sgmm	Gravel, matrix-supported	Massive to weak grading	Plastic debris flow. Subaerial to submarine fans
Sgmg	Gravel, matrix-supported	Inverse to normal grading	Pseudoplastic debris flow. Subaerial to submarine fans
Sgmh	Gravel, matrix-supported	Crude horizontal bedding	Hyperconcentrated flow. Subaerial to submarine fans
Sgcg	Gravel, clast-supported	Normal grading	Hyperconcentrated flow. Subaerial to fan deltas
Sgcm	Gravel, clast-supported	Massive to crude horizontal bedding	Clast-rich debris flow, pseudoplastic debris flow, hyperconcentrated flow. Fan deltas
Sgh	Gravel, clast-supported	Crudely- to horizontally bedded, Imbrication	Longitudinal bedforms; lag or sieve deposits. Subaerial unconfined water flows
Sgt	Gravel, stratified	Trough cross-beds	Transverse bedforms, channel fill. Fluvial to fan deltas
Sgp	Gravel, stratified	Planar cross-beds	Transverse bedforms, deltaic growths from older bar remnants. Fluvial to fan deltas
Sst	Sand, fine to very coarse, locally pebbly. (i= bimodal grain size distribution)	Solitary or grouped trough cross-beds	Sinuuous-crested and linguoid 3-D dunes.
Ssti			Fluvial, subtidal, longshore bars
Ssp	Sand, fine to very coarse, locally pebbly. (i= bimodal grain size distribution)	Solitary or grouped planar cross-beds	Transverse and linguoid 2-D dunes. Fluvial, subtidal, longshore bars
Sspi			
Sse	Sand to pebble	Sigmoidal or ellipsoidal bedding	Lateral accretion. Fluvial to subtidal bars
Ssr	Sand, fine to coarse	Ripple cross-lamination (current or oscillatory)	Ripples (lower flow regime). Fluvial to deep-water turbidites
Ssh	Sand, fine to very coarse, locally pebbly. (i= bimodal grain size distribution)	Horizontal lamination with parting or streaming lineation	Plane-bed flow (critical flow). Fluvial to deep-water turbidites
Sshi			
Ssl	Sand, fine to very coarse, locally pebbly	Low-angle (<15°) cross-beds	Scour fills, humpback or washed-out dunes, antidunes. Fluvial
Sss	Sand to pebble	Broad, shallow scours	Scour fill. Fluvial, subtidal, longshore bars
Ssm	Sand, fine to coarse	Massive, or faint lamination	Sediment-gravity flow deposits. Fluvial to deep-water turbidites
Ssw	Sand, fine to coarse	Wave ripples and planar cross-beds	Sand dunes reworked by wave-dominated currents. Intratidal to shallow shelf
Ssb	Sand, fine	Hummocky cross-beds	Wave-dominated currents (storm currents). Shallow shelf
Sshe	Sand, mud	Heterolithic lamination, lenticular lamination	Continuing change from suspension to lower flow regime. Intratidal to shallow shelf
Ssfl	Sand, mud	Flaser or thin horizontal lamination	Deposition and/or erosion of mud laminae. Fluvial, intratidal, shallow shelf

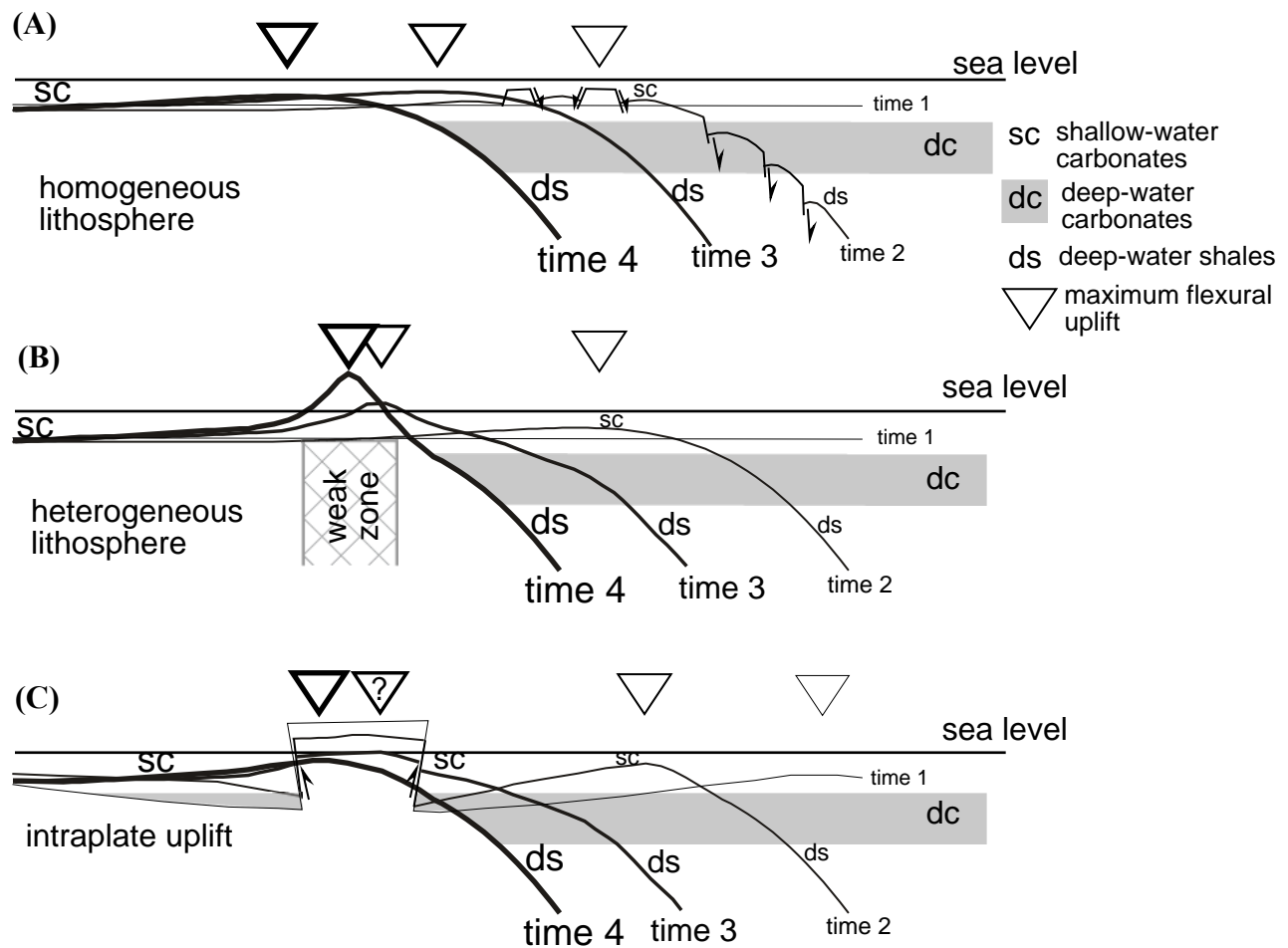
**Table 3.2 (continued).**

Sfl	Sand, mud, slightly calcareous	Fine lamination, very thin lenses of sandstones, ripples, rare skeletal fragments (mollusks, brachiopods, bryozoans)	Overbank, abandoned channel, or waning flood deposits, intermediate-water suspension. Fluvial to deep-water turbidites
Sfsm	Sand, mud	Massive, leached carbonate, mottled by bioturbation, thin lenses of Ssm, Sss	Suspension in intermediate waters. Fluvial to intratidal
Sfm	Mud	Massive, faint lamination, dolomitic, desiccation cracks	Suspension in intermediate waters; overbank, abandoned channel, or drape deposits. Fluvial to intratidal
Sb	Black shale	Fissil, organic, calcareous and non-calcareous, graptolites	Suspension in deep water. Offshore and slope suspension; distal tail of submarine fans



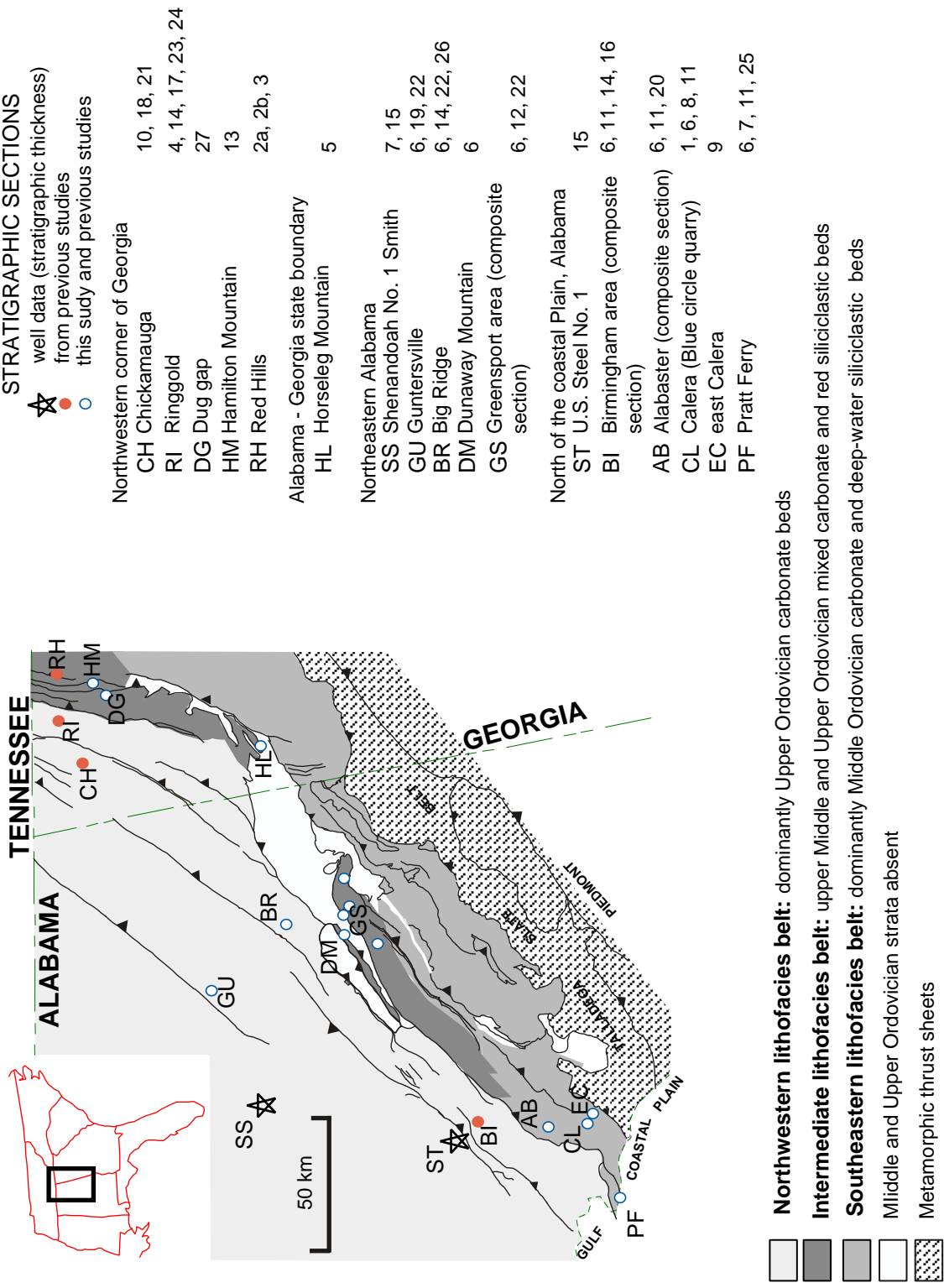
**Table 3.3** Explanation of key stratigraphic surfaces. Abbreviations for stratigraphic sections are explained in Figure 3.2.

	Age	Significance of the event in carbonate and mixed lithologies successions (sections restoring northwest of and inside the graben)	Significance of the event in siliciclastic successions (sections restoring southeast of and inside the graben)
11		<b>Post-Ordovician unconformity. Total to partial drowning</b> of the Ordovician platform.	<b>Post-Ordovician unconformity.</b> Regional onset of fine-grained, siliceous to calcareous shales deposition of the Silurian Red Mountain Formation with thin interbeds of hummocky, fine-grained sandstones.
10	late Late Ordovician (Cincinnatian, ca 446)	<b>Marine flooding</b> and shoaling with deposition of coarser-grained, phosphatic, skeletal carbonates (at BI, BR), mixed lithologies (at GU, BR, RI), and quartzarenites (at DG, HL, DM) ( <i>A. ordovicicus</i> zone).	
9	middle Late Ordovician (Mohawkian – Cincinnatian, ca. 451)	<b>Limited subaerial exposure followed by regional marine flooding</b> above surface 8 in carbonate lithologies at CH, GU, and BR; and mixed lithologies at GS ( <i>P. tenuis</i> to <i>B. confluens</i> ).	<b>Regional marine flooding</b> between surfaces 8 and 10 at DG.
8	ca 454 Ma	<b>Millbrig and Deicke K-bentonite interval</b> in dolomitic limestones at CH, BR, and BI.	<b>Millbrig and Deicke K-bentonite interval</b> in red siltstones at HM, at the base of quartzarenite deposits at HL and DM; and toward the top of the quartzarenite interval in GS.
7	early Late Ordovician (middle Mohawkian, ca 456)	<b>Subaerial exposure followed by regional marine flooding</b> below surface 8 at CH, BR, and BI (upper <i>E. quadridactylus</i> to lower <i>B. compressa</i> zones).	<b>Subaerial exposure followed by regional marine flooding</b> below surface 8 at HM, HL, DM, GS, and PF ( <i>C. bicornis</i> zone). Resurgence of limestone deposition in section E.
6	Late Ordovician (late Mohawkian)	Marine flooding in southern sections BI and BR ( <i>E. quadridactylus</i> zone).	Coarsening-upward and shallowing, <b>termination of carbonate deposition</b> , and onset of fine-grained siliciclastic deposition in northern sections D and E ( <i>P. gerdae</i> zone).
5	Late Ordovician (late Mohawkian)	Marine flooding in BI ( <i>P. aculeata</i> zone) and onset of carbonate deposition in BR (older than <i>E. quadridactylus</i> zone). Inferred latest onset of deposition in DG, SS, GU, DM, and ST.	Shoaling, <b>termination of carbonate deposition</b> , and onset of fine-grained siliciclastic deposition in section GS (younger than <i>P. Sweeti</i> conodont zone).
4	Middle-Late Ordovician (ca. 458)	<b>Subaerial exposure followed by regional marine flooding</b> in section BI (upper <i>C. Sweeti</i> to lower <i>P. aculeata</i> zones).	<b>Regional marine flooding</b> in southern section Q ( <i>N. gracilis</i> to <i>C. bicornis</i> zones).
3	Middle-Late Ordovician (ca. 458)	<b>Onset of carbonate deposition</b> at BI ( <i>C. sweeti</i> zone) and inferred for GS, HM, and RH ( <i>P. serra</i> zone).	<b>Drowning</b> of the carbonate platform and graptolitic, black shales deposition at AB and CL; slight shoaling and <b>drowning</b> at PF (top of <i>G. teretiusculus</i> to <i>N. gracilis</i> zones; Finney et al., 1996).
2	late Middle Ordovician (upper Whiterockian, ca. 463)	<b>Onset of carbonate deposition</b> at the northern section RH ( <i>P. serra</i> zone) and uncertain for section HM. Marine flooding events may have been recorded in the carbonate interval at CH, RI, PF, AB, and CL.	<b>Drowning</b> of the carbonate platform and graptolitic, calcareous shales deposition ( <i>D. teretiusculus</i> zone) at areas eastward of RH (Finney et al., 1996).
1	late Middle Ordovician (middle Whiterockian, ca 466-464 Ma)	<b>Localized onset of carbonate deposition</b> at CH (H. holodontata to <i>C. sweeti</i> zones), PF ( <i>C. friendsvillensis</i> zone), and uncertain at RI, AB, and CL.	<b>Drowning</b> of the carbonate platform and graptolitic shales ( <i>D. purchisoni</i> zone) deposition at areas eastward of CL, GS, and HL (Finney et al., 1996).
		<b>Post-Knox unconformity.</b> This surface incorporates surfaces 1, 2, 3, 4, or 5 due to the diachronous onset of carbonate deposition in the distal foreland.	<b>Post-Knox unconformity.</b> This surface either corresponds to surface 1 or is less than 20 m below of surfaces 1 or 2. Resume of peritidal to shallow-marine deposition in proximal foreland settings in northwestern Georgia and Tennessee.



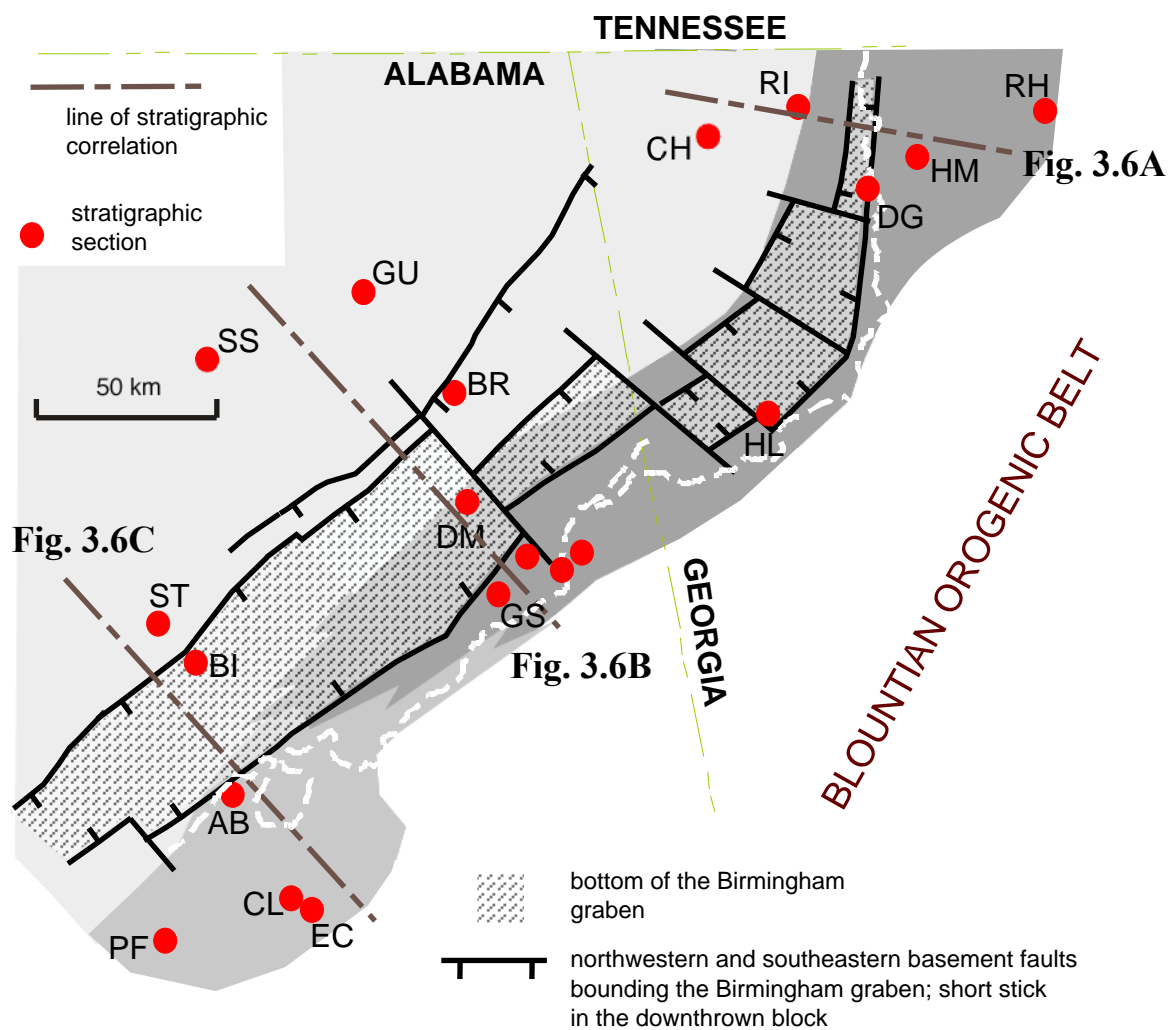
**Figure 3.1** Illustration of the flexural geometry and distribution of depositional settings through time for three different configurations of the distal foreland lithosphere (not to scale). These hypothetical profiles are constructed assuming that time intervals (e.g., time 2 to time 3, time 3 to time 4) are the same, a marginal load advances to the left beginning at time 2, and sea-level position is fixed. (A) In a homogeneous lithosphere, the flexural wave migrates cratonward at a consistent rate. Flexurally-induced irregularities, such as flexural normal faults (shown only in profile for time 2 for simplicity), develop as the flexural wave migrates. The carbonate platform shallows, may be exposed to subaerial settings, and later deepens as the flexural wave and flexurally-induced irregularities place the foreland plate at different water depths. (B) Weak zones in the lithosphere affect the rate of cratonward migration and geometry of the bulge (e.g., Patton and O'Connor, 1988; Washbush and Royden, 1992). The bulge is locked above the weak zone for longer intervals of time because the plate bends more easily in weak segments than in stiff segments. As a result, the bulge will have a narrower and higher amplitude than the forebulge predicted in flexural models. Additionally, the foredeep will narrow and deepen with time. As the bulge grows with time, shallow-water carbonates and underlying strata are exposed to the surface, whereas the carbonate platform on the foredeep side of the weak zone is drowned rapidly. (C) Intraplate uplifts generated prior to marginal loading at time 1, such as inversion of a pre-existing graben structure (e.g., Dorobek, 1995; this chapter), may also interfere with the geometry and rate of migration (as in B) of the marginal flexural wave. Prior to the arrival of the flexural wave and flexurally-induced irregularities, deep erosion of the passive-margin succession occurs within inverted upthrown blocks, whereas thick successions of carbonates (dc and sc) are deposited in downthrown blocks. As the flexural wave advances, the intraplate uplift obscures the position of the flexural uplift (time 3) and becomes less evident with time (time 4).

Figure 3.2



**Figure 3.2** (previous page) Location of study sections and distribution of lithofacies belts of the Middle and Upper Ordovician strata in the Appalachian thrust belt of Georgia and Alabama.

References to sources of stratigraphic sections are listed in alphabetic order: 1) Bearce, 1999; 2a) Bergström, 1973; 2b) Bergström 1977; 3) Caldwell, 1992; 4) Chowns, 1972; 5) Chowns and Carter, 1983; 6) Drahovzal and Neathery, 1971; 7) Ferrill, 1989; 8) Finney et al., 1996; 9) Guthrie, 1994; 10) Hall, 1986; 11) Hall et al., 1986; 12) Jenkins, 1984; 13a) Kath et al., 1994; 13b) Randal L. Kath, written communication, 2001; 14) Kher, 1996; 15) Kidd, 1975; 16) Lee, 1983; 17) Martin, 1991; 18) Milici and Smith, 1969; 19) Neathery and Drahovzal, 1985; 20) Osborne, 1996; 21) Phillips, 1996; 22) Raymond, 1973; 23) Repetski, 1992; 24) Rindsberg and Chowns, 1986; 25) Shaw et al., 1990; 26) Ward, 1983; 27) Zeigler, 1988.



**Figure 3.3** Palinspastic location of study sections, lines of stratigraphic correlation, and distribution of study sections and lithofacies belts in relation to mapped subsurface basement faults and the Birmingham basement graben (palinspastic map from Chapter 2). White dashed line corresponds to the present eroded trace of the Talladega and Cartersville faults. See Figure 3.2 for explanation of lithofacies belts.

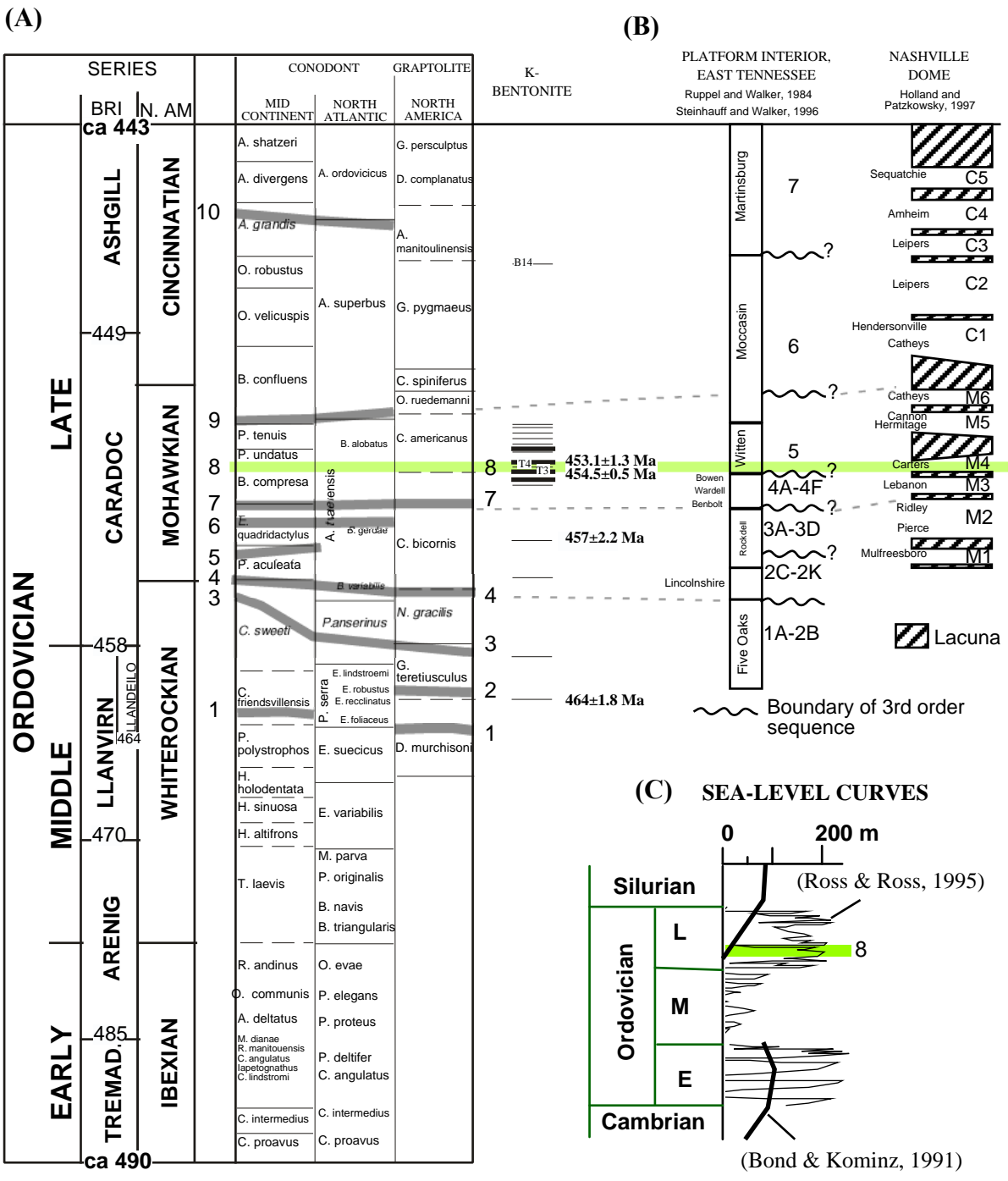
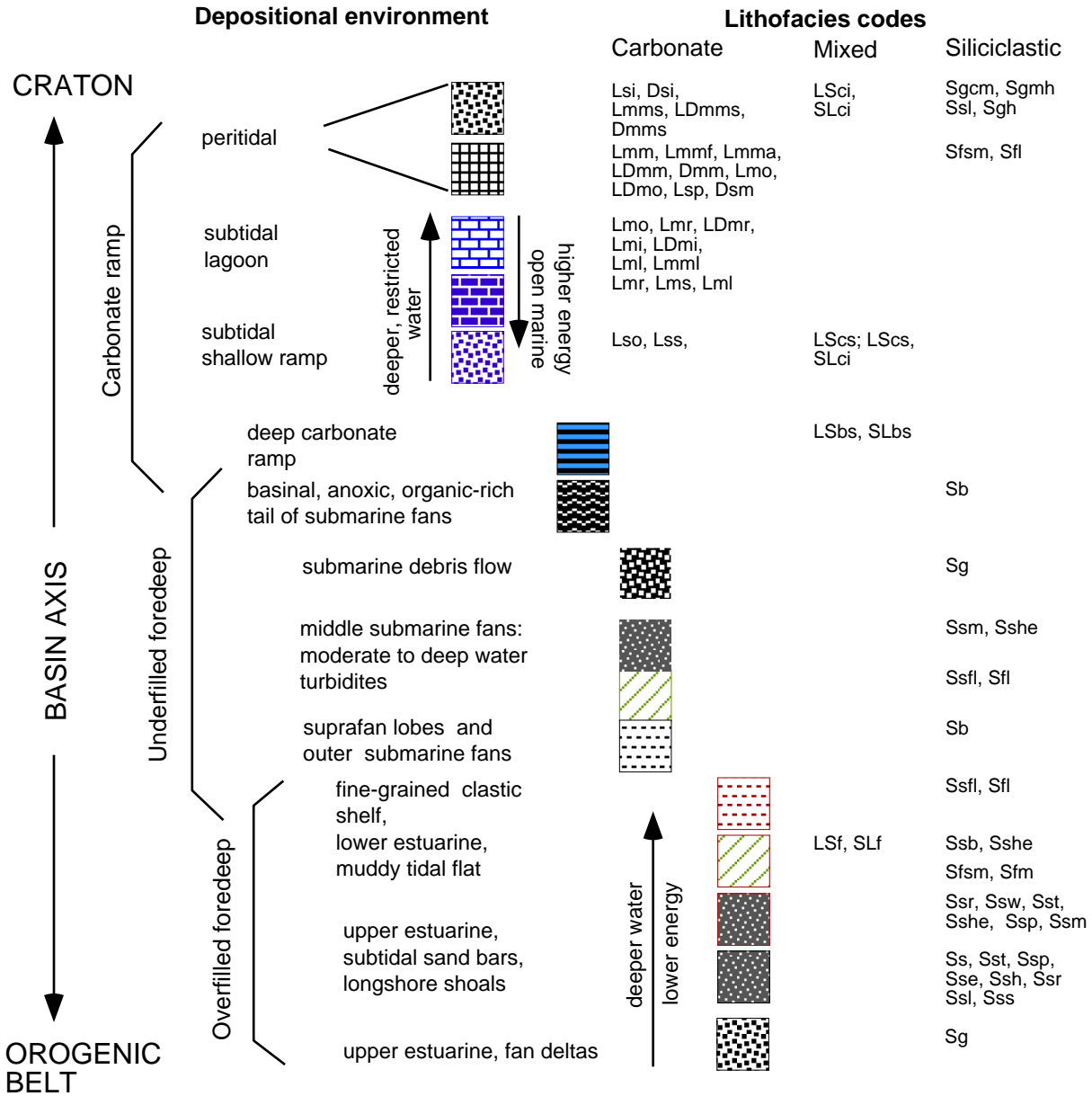


Figure 3.4

**Figure 3.4** (previous page) (A) Ordovician series (from Webby, 1998) and correlation of conodont zones, graptolite zones, and K-bentonite beds (modified from Kolata et al., 1996); radiometric ages of Mohawkian K-bentonites from Kolata et al. (1996, 1998), and of older K-bentonites from correlations made by Finney et al. (1996). Also are shown the positions of the stratigraphic surfaces discussed in the text (numbers 1 to 10, see Table 3.3 for definition of each of these surfaces). (B) Third-order depositional sequences established in the platform interior of northeastern Tennessee and the Nashville dome. (C) Proposed Ordovician sea-level curves. Ross and Ross (1995) curve is based on third-order stratigraphic sequences from several key sections in North America. Bond and Kominz (1991) curve is relative to a section in the stable Iowa craton. The latter curve was used in constructing tectonic subsidence curves. The stratigraphic position of surface 8 is shown for reference.



**Figure 3.5** Key to facies for stratigraphic columns in Figures 3.7, 3.8, and 3.9. Explanation of lithofacies codes is given in Tables 3.1 and 3.2.



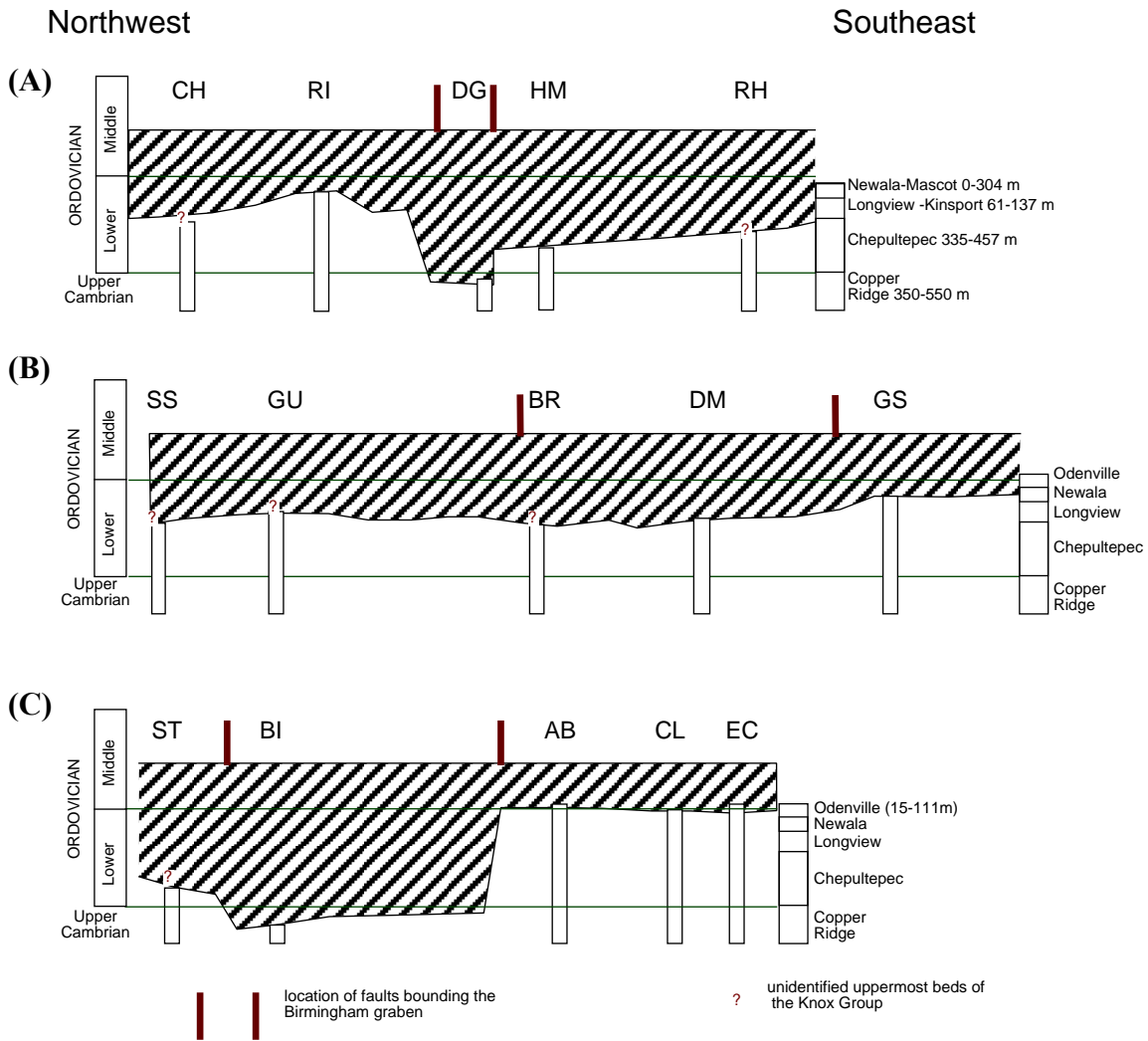


**Figure 3.6** Geometry of the truncation of passive-margin strata of the Knox Group in the distal Blountian foreland basin. See Figure 3.3 for location of lines of correlation. Thicknesses of Knox units are from Raymond (1993) and Chowns et al. (1992). (A) Depth of erosion rises northwestward from Copper Ridge beds in section DG (Cressler, 1974) to upper Lower Ordovician beds of the Mascot Dolomite unit in section RI (Chowns et al., 1992; Repetski, 1992). (B) Depth of erosion rises southeastward from beds in the Longview (section DM) to beds in the Newala Limestone (section GS) (Drahovzal and Neathery, 1971). (C) Depth of erosion rises southeastward from beds in the Copper Ridge (section BI) to beds in the Odenville Limestone (section AB). The anomalous thin Knox interval identified in section BI extends southeastward in the subsurface, as imaged by seismic reflection profiles and structural cross sections southeast of section BI (e.g., cross section 16, Plate 2.1). Note that sections with maximum and minimum amount of Knox truncation are adjacent to each other and restore on different sides of basement faults.

**NORTHWEST OF THE GRABEN**

**LINE OF CORRELATION**

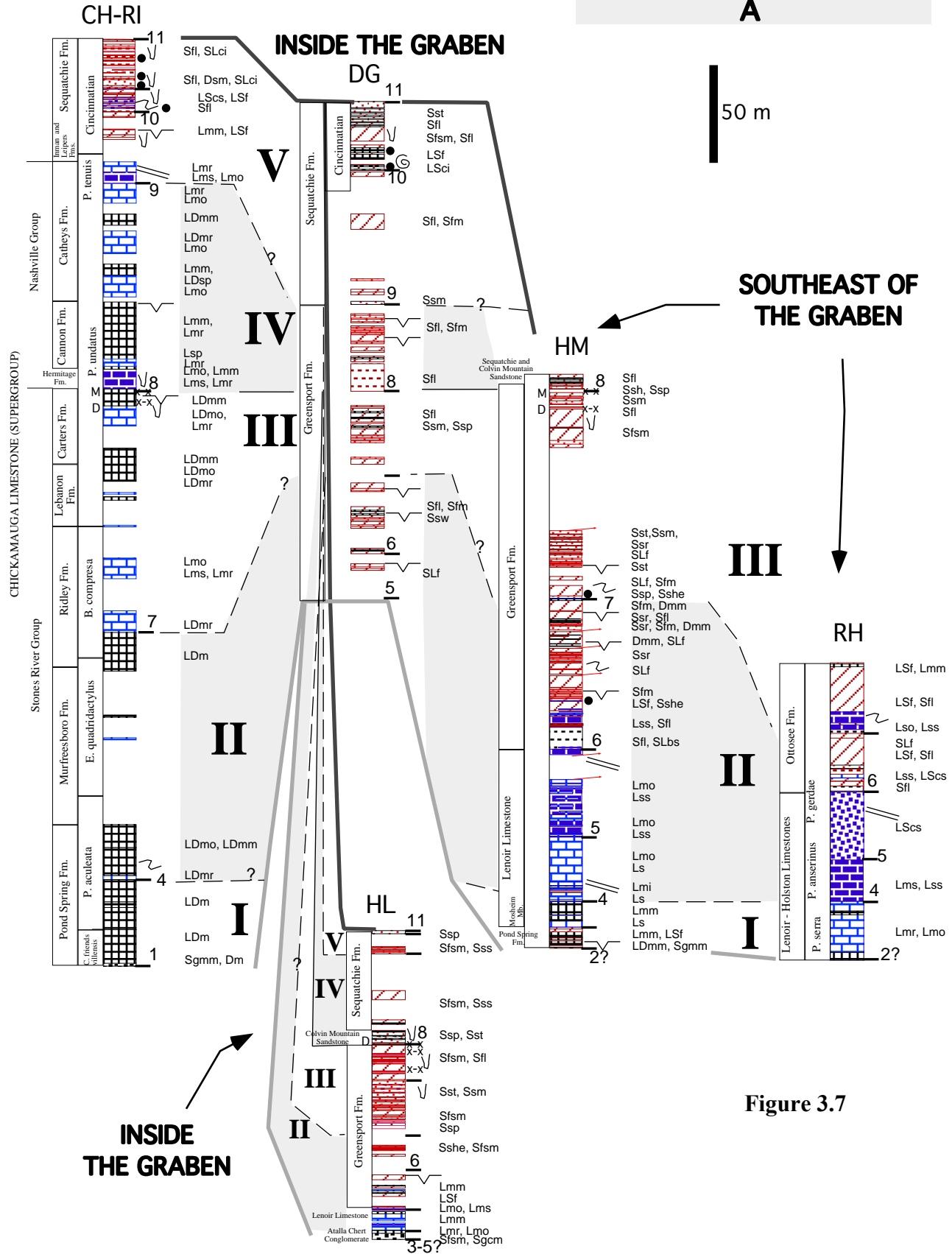


**Figure 3.7** (previous page) Line of stratigraphic correlation A (including section HL, which is southwest of line A) showing stratigraphic units, biostratigraphic data, lithofacies, stratigraphic correlation surfaces (numbers 1 to 10), and stratigraphic intervals (numbers I to V). Note the dominance of siliciclastic deposits to the southeast in sections HM and DG; the thinner succession in sections DG, HL, and RH; and the thick carbonate succession in the composite section CH-RI. The datum for stratigraphic correlation is the stratigraphic interval containing the Millbrig (where Millbrig is absent, the Deicke) K-bentonite. See Figure 3.3 for location of line of correlation A, Figure 3.5 and Tables 3.1 and 3.2 for facies codes, and Figure 3.2 for key code of sections.

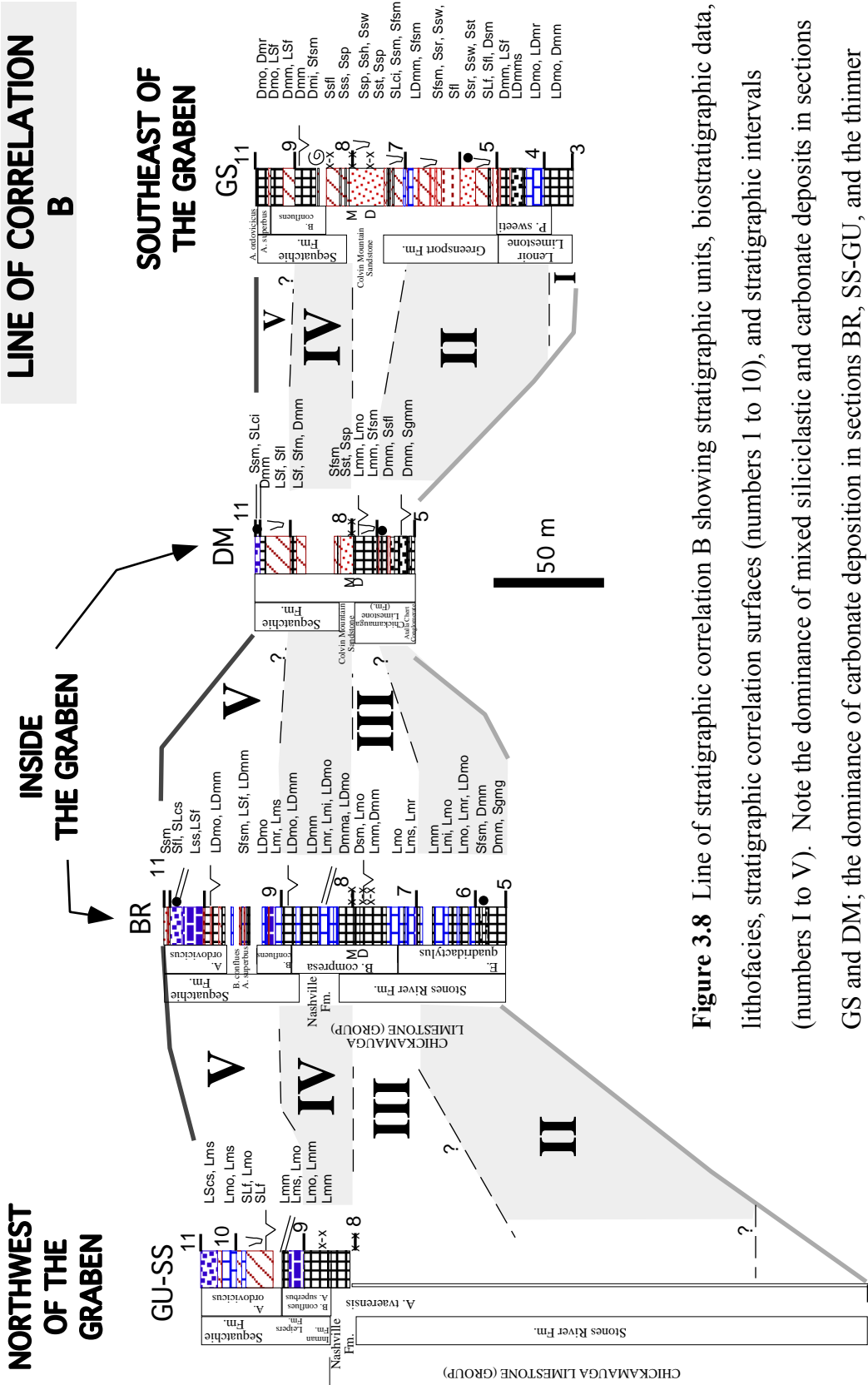


**Figure 3.8** Line of stratigraphic correlation B showing stratigraphic units, biostratigraphic data, lithofacies, stratigraphic correlation surfaces (numbers 1 to 10), and stratigraphic intervals (numbers I to V). Note the dominance of mixed siliciclastic and carbonate deposits in sections GS and DM; the dominance of carbonate deposition in sections BR, SS-GU, and the thinner succession in sections BR and DM. The datum for stratigraphic correlation is the stratigraphic interval containing the Millbrig K-bentonite. See Figure 3.3 for location of line of correlation A, Figure 3.5 and Tables 3.1 and 3.2 for facies codes, and Figure 3.2 for key code of sections.

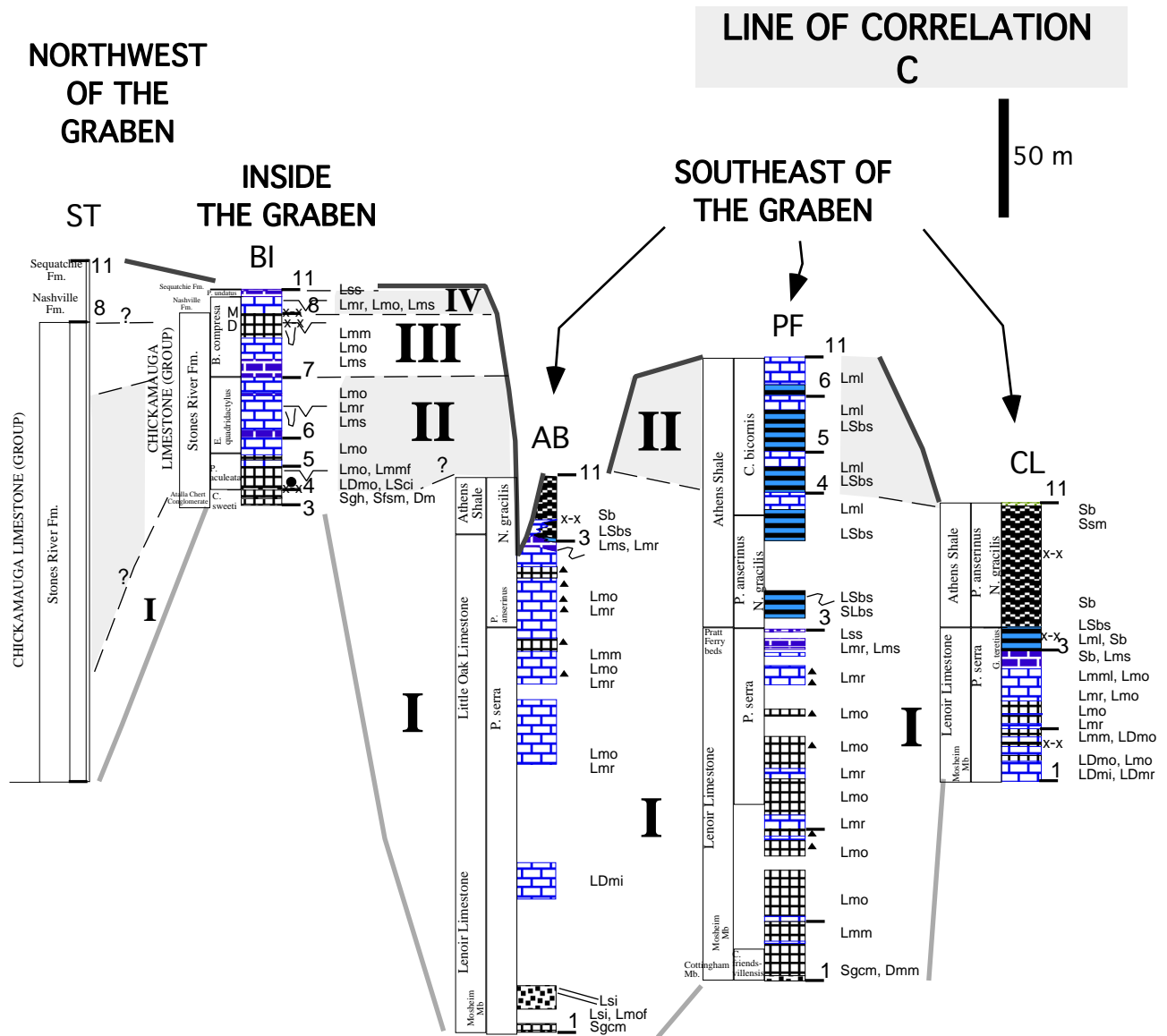


**Figure 3.9** Line of stratigraphic correlation C showing stratigraphic units, biostratigraphic data, lithofacies, stratigraphic correlation surfaces (numbers 1 to 10), and stratigraphic intervals (numbers I to V). Note the dominance of carbonate deposits in northwestern sections BI and AB; the sharp contact between shales and carbonate successions in sections AB, CL, and PF, and the thinner succession in section BI. The datum for stratigraphic correlation is the inferred position in the stratigraphic column of the boundary between *P. anserinus* -*P. Serra* conodont zones. See Figure 3.3 for location of line of correlation A, Figure 3.5 and Tables 3.1 and 3.2 for facies codes, and Figure 3.2 for key code of sections.

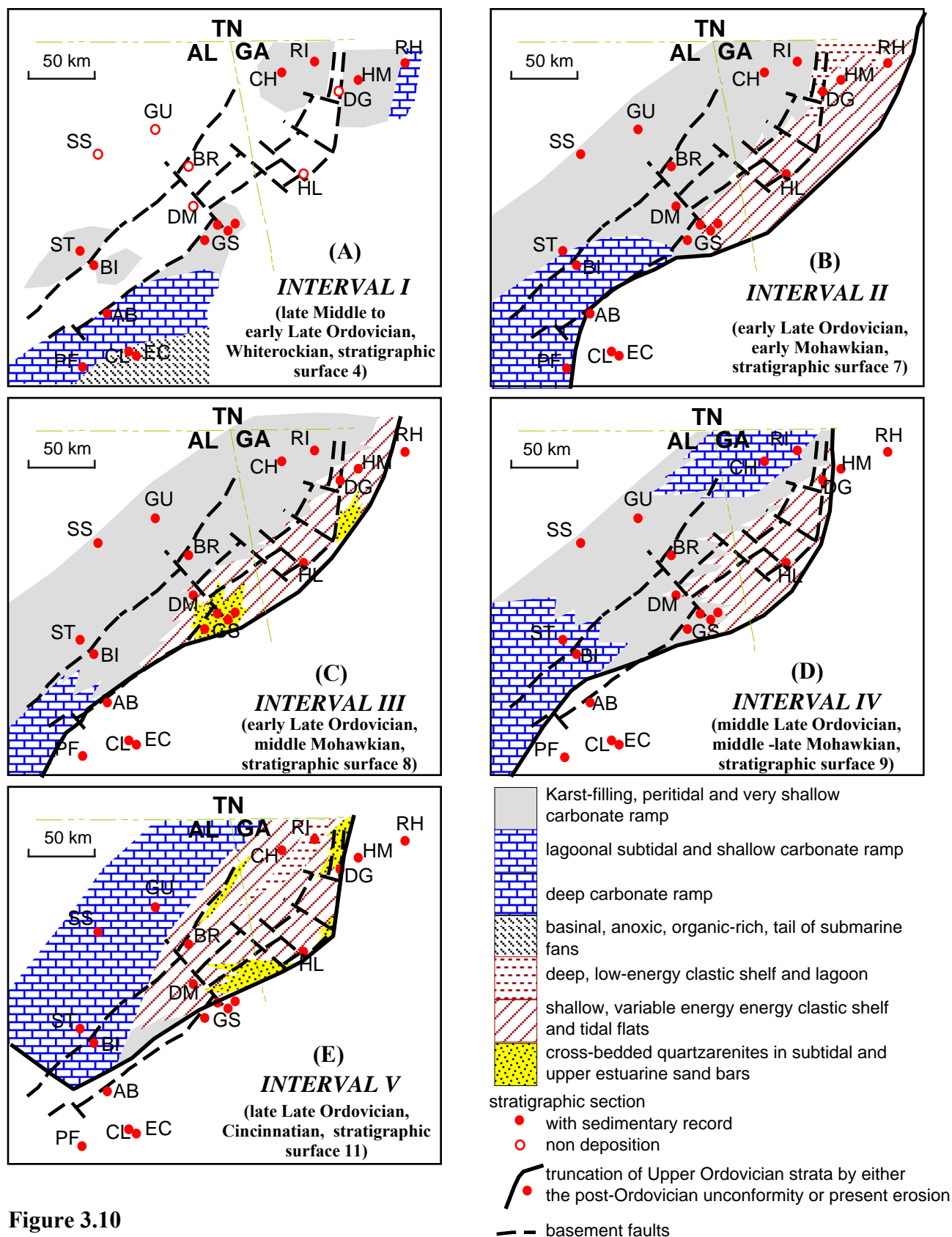


Figure 3.10

**Figure 3.10** (previous page) Paleogeographic maps showing evolution of depositional environments in the distal foreland basin through the Middle and Late Ordovician. Each map represents the time of deposition for strata underlying the stratigraphic surface indicated. Note the role of inversion of basement faults of the Birmingham graben system in the early distribution of depocenters (Interval I), and stopping the cratonward progradation of the Blountian clastic wedge on the southeast (Intervals I to IV). Siliciclastic depocenters migrated northeastward and are shallower on the northeast (Intervals I to IV). The clastic wedge prograded across the inverted Birmingham graben in Interval V. See Figure 3.2 for key code of sections.

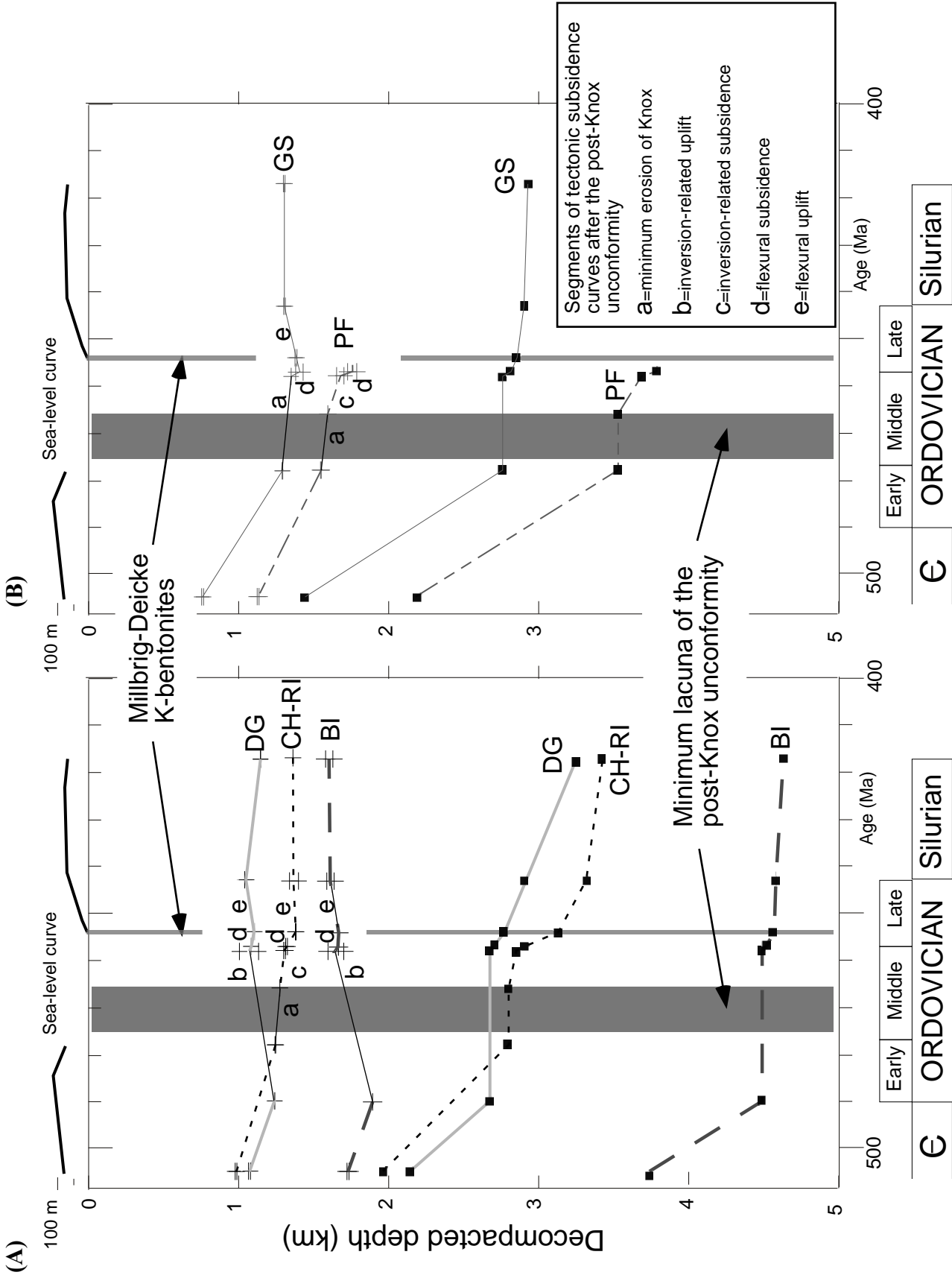
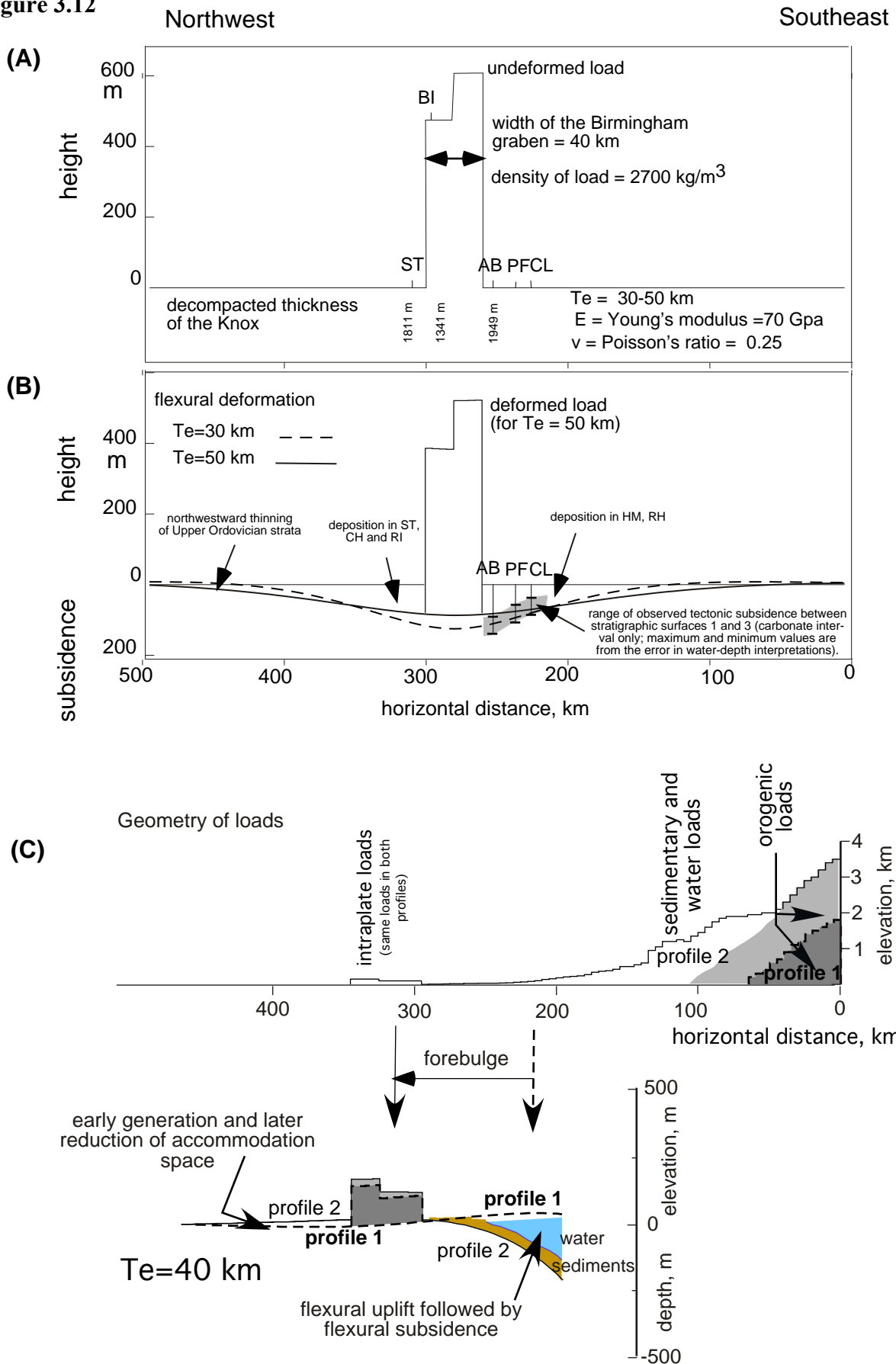


Figure 3.11



**Figure 3.11** (previous page) (A) Total and tectonic subsidence curves (lower and upper curves, respectively) for representative sections restoring along the northwestern shoulder of the Birmingham graben (composite section CH-RI) and inside the graben (sections BI and DG). (B) Total and tectonic subsidence curves (lower and upper curves, respectively) for representative sections restoring southeast of the Birmingham graben (sections GS and PF). Cross symbols in tectonic subsidence curves correspond to the error in determination of water-depth for the uppermost strata of each interval. Definitions of water-depth criteria are from Steinhauff and Walker (1996). Correction for sea-level fluctuations uses the sea-level curve relative to the Iowa craton (Bond and Kominz, 1991) in order to give a minimum estimate of relative sea-level fluctuation along the plate margin. See text for discussion of the patterns of tectonic and total subsidence.

Figure 3.12



**Figure 3.12** (previous page) Effects of tectonic loads in an intraplate setting, assuming that the load consists of the inverted Birmingham graben at early phases of deposition of Interval I (late Middle Ordovician). (A) Flexural models indicate bending of a continuous elastic lithosphere by effects of tectonic loading (Turcotte and Schubert, 1982). Geometry of the load corresponds to the width of the Birmingham graben (from seismic data and thickness of Cambrian strata); the height of the load to the half northwest is from the difference in decompacted thickness of the Knox Group between sections ST and BI, and for the half southeast between BI and AB. Values of 30 and 50 km were chosen as reasonable boundary values for the elastic thickness of the continental lithosphere (e.g., Cardozo and Jordan, 2001). Other model input parameters are specified in the diagram. This flexural model does not consider the effects of reactivation of other faults and the distal effects of flexural subsidence by loading at the plate margin. (B) Predicted flexural deformation curves are within the range of the tectonic subsidence calculated for sections AB, PF, and CL (shown in Figure 3.11B). This hypothetical model predicts the creation of two small-scale foreland-like basins adjacent to the inverted block (Figure 3.10A), which geometry will depend on the geometry of the inverted upthrown block. In section ST, lack of biostratigraphic data does not permit the calculation of tectonic subsidence for Interval I. This model also explains early carbonate deposition in sections CH-RI, HM, and RH, and deep truncation of Knox strata in section DG. A better match in the geometry of the depocenter would be obtained if the following factors, among others, were considered: angle of the faults (e.g., Zhang and Bott, 2000) and rate of erosion of the tectonic load (e.g., Crampton and Allen, 1995). (C) Hypothetical model showing the effects on distal foreland deposition by interaction between intraplate flexure and the migration of the marginal flexural wave (note that intraplate uplift has less relief than A and has the same geometry for profiles 1 and 2). Initial overlap of intraplate and marginal flexural profiles creates anomalous patterns of deposition northwest of the intraplate uplift (profile 1). Forelandward migration of the marginal flexural wave by advance of tectonic and depositional loads (profile 2) reduces the anomalous accommodation space northwest of the intraplate uplift (e.g., in section CH-RI, middle Interval I) and creates accommodation space southeast of the intraplate uplift by flexural subsidence.

## CHAPTER FOUR

### INFLUENCE OF PRE-EXISTING STRUCTURES ON FOREDEEP STRATIGRAPHY, SUBSIDENCE, AND PROVENANCE OF THE BLOUNTIAN FORELAND BASIN

#### 4.1 INTRODUCTION

In peripheral foreland basins, coeval drowning and exposure of different parts of the former platform have been attributed to tectonic and sediment loading along the collisional margin (e.g., Beaumont, 1981; Jordan, 1981; Dorobek, 1995; Sinclair, 1997). The drowned platform becomes the foredeep zone of the foreland basin, which is bounded by the frontal tip of the orogenic belt on the collisional side and the forebulge on the craton side (DeCelles and Giles, 1996). Temporal and spatial variations of flexurally controlled subsidence of the foredeep have been constrained mainly by the effects of crustal loads and the underlying lithosphere. The uneven distribution of crustal loads on the plate margin are controlled by the temporal and spatial variations of tectonic shortening (e.g., Whiting and Thomas, 1994; DeCelles and Mitra, 1995; DeCelles and DeCelles, 2001), exhumation (Fleming and Nelson, 1991), climate (Horton, 1999), and/or sediment supply. The underlying lithosphere has also spatial and temporal variations in strength, which are a function of its thermal state (e.g., Beaumont, 1981; Stockmal et al., 1986), can be affected by pre-existing variations in lithospheric strength (e.g., Patton and O'Connor, 1988; Cardozo and Jordan, 2001), or inelastic yielding of the deep continental lithosphere during flexural bending (Waschbush and Royden, 1992; Lorenzo et al., 1999; Tandon et al., 2000). Geodynamic modeling of the lithosphere depends strongly on the choice of rheological properties assumed for the lithosphere (i.e., uniform elastic, uniform viscoelastic, or temperature-dependent viscosity models; Quilan and Beaumont, 1984) and if the foreland plate is infinite (continuous) or broken. Subsurface loads acting on the subducted slab (Royden et al., 1987) and dynamic loading by viscous mantle corner flow associated with subduction (Gurnis, 1992) are other mechanism proposed to explain tectonic subsidence of the lithosphere.

In general, all these models ignore the role of inherited structural and compositional configuration of the rifted margin (e.g., zig-zag geometry of the Laurentian margin of Thomas, 1977, 1991, 1993) in the three-dimensional evolution of the orogenic thrust belt and foreland basin. This study considers the role of reactivation of rift-related marginal and intraplate faults

in subsidence and sedimentary filling of a peripheral foreland basin, as well as the influence of those structures in foreland-plate and orogenic-belt deformation (Figure 4.1). Reactivation of pre-existing structures, such as intraplate grabens, transverse basement faults, and normal faults in promontories and embayments needs somehow be included in the three-dimensional analysis and geodynamic modelling of foreland basins.

There is a growing recognition of the effects of pre-existing structures in the evolution of foreland basins. Offsets of foreland depocenters and forebulges in the Apennine foreland plate occur across faults that trend nearly perpendicular to the mountain belt (Royden et al., 1987). Reactivation of faults trending at high angles to the collisional margin also has provided an efficient mechanism to explain differential subsidence, sand percent, and sequence distribution along the Taconic foreland in the north-central Appalachians (Castle, 2001). Bradley and Kidd (1991) and Lehmann et al. (1995) have suggested flexural reactivation of basement faults striking parallel to the collisional margin to explain the rapid subsidence and abrupt shift from shallow- to deep-water deposition in the northern Taconic foreland basin. Gupta and Allen (2000) recognized reactivation of basement structures as the primary control on the geometry of the basal unconformity and deposition in the distal Alpine foreland basin. Similarly, intraplate normal basement faults in the southeastern corner of Laurentia striking parallel to the margin were reactivated as reverse structures during early pulses of the Taconic orogeny (Chapter 3) and controlled both erosion and depositional patterns in the distal foreland.

The structural and stratigraphic configuration of the continental margin is a dominant factor in the evolution of orogenic belts (Thomas, 1977; Macedo and Marshak, 1999). Spatial and temporal changes in thrust-belt deformation are recorded in the geometry and composition of foreland strata adjacent to the thrust belt (Figure 4.1). The regional recess and salient geometry of the Appalachian thrust belt (Thomas, 1977) has been kinematically linked to the basin geometry and stratal composition of the rifted margin of Laurentia (Thomas, 1991). Salients of the thrust belt include the thick sedimentary successions of the embayments; in contrast, recesses of the thrust belt formed in the promontories, where the sedimentary cover is thinner than in the embayments (Thomas, 1977). In the Appalachians and other thrust belts, salients have less internal shortening and broader critical wedges than in recesses (e.g., Macedo and Marshak, 1999; Marrett and Aranda-Garcia, 1999). Total shortening in cross sections across the Tennessee salient is in average 10% less than in cross sections across the Alabama recess (Figure

2.11 in Chapter 2). Higher deformation in recesses than in salients of the orogenic belt may cause along-strike changes in the geometry and depth of erosion of the mountain belt. Because peripheral foreland-basin geometry is dominantly influenced by geometry of orogenic loads (e.g., Stockmal et al., 1986), along-strike variation of foredeep geometry may reflect the along-strike recess-salient geometry of the orogenic belt (Figure 4.1).

In this chapter, stratigraphic, tectonic subsidence, and provenance analyses of proximal and middle Blountian foreland strata are used to establish whether along-strike variations on foredeep stratigraphy are somehow influenced by the pre-existing configuration of the plate margin of southern Laurentia. Blountian strata are involved in the Alabama and Georgia Appalachian thrust belt (Figure 4.2), but they restore palinspastically on the transition between the Alabama promontory and Tennessee embayment of the southeastern Laurentia margin (Figures 4.1 and 4.3) (Chapter 2).

## **4.2 GEOLOGIC AND STRATIGRAPHIC SETTING**

### **4.2.1 Structures from the previous extensional tectonic setting**

On the basis of palinspastic restoration and stratigraphic analyses of upper Precambrian synrift and Cambrian to Lower Ordovician passive-margin deposits in the Appalachian and Ouachita orogenic belts, Thomas (1977, 1991) proposed an orthogonal zig-zag geometry of the eastern Laurentian (North American) rift margin. Although for latest Early Ordovician the eastern margin of Laurentia was covered by a shallow carbonate platform after more than 40 m.y. of passive-margin deposition (Thomas, 1977, 1991), the underlying basement configuration of the Laurentian margin differs along-strike from embayments (e.g., the Tennessee embayment, Figure 4.1B) to promontories (e.g., the Alabama promontory, Figure 4.1B'). The embayment-promontory configuration resulted from the Blue Ridge and Ouachita rifting episodes during late Precambrian and Early Cambrian times, respectively (Thomas, 1991). Extension in Cambrian time reached intracratonic areas of the Alabama promontory forming several graben structures, such as the Birmingham graben (Figures 4.1 and 4.3). The structural configuration of the intraplate Birmingham graben changes along strike across several transverse basement faults (Chapter 2) forming an accommodation or transfer zone typical of continental rifts (Moustafa, 2002; Younes and McClay, 2002). This accommodation zone strikes parallel with and likely

connects with the Georgia transform fault system that separates the Alabama promontory and Tennessee embayment in the plate margin (Figure 4.1) (Thomas, 1993).

#### **4.2.2 Taconic (Blountian) orogeny and foreland deposits**

Rapid drowning of the Lower Ordovician carbonate platform, diachronous deposition of deep-water shales in proximal foreland settings, and thin beds of volcanic ash are the evidence for a collisional orogenic event along the irregular eastern margin of Laurentia (e.g., Bradley, 1989; Drake et al., 1989; Finney et al., 1996). The southernmost depocenter along the Taconic orogen of Laurentia is spatially coincident with the Tennessee embayment of the older rifted continental margin (Thomas, 1977). In the depocenter, black shales overlie Middle Ordovician carbonate-ramp deposits and grade upward in a coarsening-upward turbidite succession, reflecting drowning of the foreland plate and sediment dispersal from an orogenic terrain on the east (Shanmugam and Walker, 1978, 1980; Shanmugam and Lash, 1982; Diecchio, 1991). The Blountian clastic wedge thins southwestward from the depocenter in the Tennessee embayment onto the Alabama promontory (Thomas, 1977; Thomas et al., 2002). However, the ages of basal synorogenic siliciclastic deposits show that orogeny along the Alabama promontory began somewhat earlier than farther north along the southern part of the Laurentian margin (Bradley, 1989; Finney et. al., 1996).

A very complex Blountian succession of carbonate and siliciclastic strata covers the post-Knox unconformity on the foreland plate in the Alabama promontory and southern Tennessee embayment (Chapter 3). In this study, northwestern, intermediate, southeastern, and absent strata lithofacies belts are distinguished on the basis of structural position within the thrust belt, age, and the order of stacking of carbonate and siliciclastic deposits (Figures 4.2 and 4.3).

The northwestern lithofacies belt corresponds to the distal zone of the Blountian foreland and is described in detail in Chapter 3. This lithofacies belt consists mostly of Upper Ordovician carbonate beds and contains a complex array of lithologies ranging from mudstones to skeletal, algal, and intraclastic grainstones (Drahovzal and Neathery, 1971; Walker et al., 1983; Benson, 1986a). The association of carbonate lithologies on the northwest has been interpreted as recording deposition on a peritidal and shallow-water carbonate platform (Ruppel and Walker, 1984; Benson, 1986b; Steinhaff and Walker, 1995) (chapter 3). These deposits are irregularly

covered by reddish tidal-flat and estuarine siliciclastic deposits (Neathery and Drahovzal, 1985; Martin, 1991).

Carbonates and red siliciclastic strata characterize the intermediate lithofacies belt. The lower part consists of karst-filling conglomerates, peritidal and shallow-marine carbonate deposits, whereas the upper part consists mostly of red siltstone beds with some interbeds of sandstones, shales, and carbonates (Drahovzal and Neathery, 1971; Chowns and Carter, 1983). Rocks of the intermediate lithofacies belt have been interpreted as deposits of shallow-platform, estuarine, and tidal-flat environments (Ruppel and Walker, 1984; Benson, 1986b; Martin, 1991). In the Blountian foreland basin, strata of the intermediate lithofacies mark the transition between platform carbonate deposition to the northwest and deep-water siliciclastic deposition to the southeast.

The southeastern lithofacies belt consists of Middle Ordovician carbonate beds and a thick succession of deep-water siliciclastic deposits. Southeastern carbonate strata include peritidal, and shallow- to deep-water carbonate platform deposits (Drahovzal and Neathery, 1971; Walker et al., 1983; Ruppel and Walker, 1984; Benson, 1986a). Deep-water shales and turbidites overlie the drowned carbonate succession (Ruppel and Walker, 1984; Benson, 1986b), and are truncated at the top by Devonian and Mississippian strata.

On the northwestern side of the southeastern lithofacies belt, Middle Ordovician to Silurian strata are absent. In the palinspastic map, localities with no Blountian or Silurian stratigraphic record (i.e., sections with Devonian or Mississippian strata resting on Lower Ordovician strata) form a gap of ~ 111 km with a linear (Figure 4.3). Sections northwest of the linear gap include Middle Ordovician carbonates of the southeastern lithofacies (sections GS and RL in Figure 4.3), and sections southeast of the linear gap include either only Middle Ordovician black shales (section CB) or carbonates and black shales (section FC). Sections southwest of the gap have either mostly carbonates (e.g., sections AA and AB in Figure 4.3) or the same succession of carbonates grading abruptly to deep-water black shales (section CL in Figure 4.3). The vertical and lateral change from shallow-marine carbonates to deep-water shales, as recorded in sections southeast and southwest of the gap, is a common characteristic of underfilled peripheral foreland basins (Sinclair, 1997). Therefore, I infer that Middle Ordovician deposits were originally accumulated on a homogeneous southeast-dipping foredeep, and that the



linear gap formed after Ordovician deposition, probably because of reactivation of basement structures.

#### **4.2.3 Previous subsidence studies in the central-southern Taconic foreland**

Several studies have used a model of lithospheric flexure associated with tectonic loading on the eastern margin of Laurentia as the primary mechanism driving subsidence for the foreland of the Blountian and Taconic orogeny (Shanmugam and Lash, 1982; Quinlan and Beaumont, 1984; Beaumont et al., 1988, Ettehnsohn, 1991; Diecchio, 1993). However, the northwestern extent of the Blountian foredeep is controversial. A thin succession of distal mixed carbonate-siliciclastic strata that separates a deeper and more clastic-rich basin to the southeast (foredeep) from thick, shallow-marine carbonates to the northwest was interpreted by Diecchio (1993) and Roberson (1994) as evidence of the Blountian forebulge. Diecchio (1993) suggested that buried graben-fill successions in the distal foreland played an active role in subsidence (i.e., sediment load subsidence), creating the conditions for the thick record of shallow-marine carbonates northwest of the forebulge. Walker et al. (1983) considered that high depositional rates of carbonates and siliciclastic deposits at opposite sides of the foreland plate created a zone of thin deposition (slow depositional rates) between carbonate and siliciclastic depocenters. Quinlan and Beaumont (1984), Beaumont et al. (1988), and Etensohn (1991) include both carbonate and siliciclastic deposits within the foredeep zone. None of these studies considered the effects of reactivation of pre-existing structures in the foreland plate.

#### **4.2.4 Provenance in the central-southern Taconic foreland**

Provenance data are available from conglomerates and sandstones within the Blountian clastic wedge near and to the northeast of the depocenter in the Tennessee embayment. Coarse conglomerate beds distributed at various stratigraphic levels of proximal foreland strata and in several localities along strike consist dominantly of clasts of carbonate rocks, with subordinate clasts of sandstones and siltstones, and trace amounts of volcanic (greenstones) and Precambrian (Grenville) basement clasts (Kellberg and Grant, 1956; Cressler, 1970; Rader and Gathright, 1986). This clast population indicates that nearby source areas included the Lower Cambrian-Lower Ordovician passive-margin succession of the Laurentian margin, as well as late Precambrian synrift clastic sedimentary rocks and synrift volcanic rocks. Sandstone composition

of the Blountian clastic wedge is dominated by monocrystalline quartz, plagioclase, and sedimentary rock fragments (Mack, 1985). This association of sand-size detritus indicates sources composed primarily of sedimentary rocks and subordinate amounts of low-grade metamorphic rocks and plagioclase-rich plutonic rocks and/or gneiss (Mack, 1985). Sandstones also contain detrital grains of carbonate rocks, and an extrabasinal source of detrital carbonate grains rather than intrabasinal allochems is consistent with the clast population of the conglomerates (Mack, 1985). Matching heavy-mineral associations between sandstones of the Upper Ordovician Bays Formation and Lower Cambrian and late Precambrian siliciclastic rocks in northeastern Tennessee indicates supply from Laurentian sedimentary rocks and Precambrian crystalline basement (Cummings, 1965). Farther to the northeast, sandstones of the Upper Ordovician Martinsburg Formation (clastic wedge in the Pennsylvanian embayment) contain volcanic rock fragments; and percentages of pelitic, low-grade metamorphic, chert, and plagioclase fragments are higher than in the Blountian sandstones (Mack, 1985).

Whole-rock chemical analysis in Middle and Upper Ordovician samples from the southern-central Appalachians indicates supply from terranes with more diverse rock composition. Whole-rock chemical composition of Blountian and Taconic (clastic wedge in the Quebec embayment) mudstones indicates an increase in the ratio of mafic to felsic elements with time suggesting supply from mafic rocks within colliding terranes (Andersen, 1995). This increase is higher in the Taconic clastic wedge in the Quebec embayment than in the Blountian clastic wedge in the Tennessee embayment (Andersen, 1995).

Sedimentary provenance analysis using initial  $^{143}\text{Nd}/^{144}\text{Nd}$  ratios ( $\epsilon_{\text{Nd}}$ ) have been used in the southern Appalachians to determine an average age of regional source areas. This approach assumes that major chemical fractionation of the Sm-Nd system occurs during differentiation of material from the mantle and incorporation into the continental crust (Taylor and McLennan, 1985). The advantage of Nd isotopes for provenance analysis is the low diagenetic effects affecting the Sm/Nd ratios after deposition, coherent behavior of Nd isotopes in clastic sediments during transport, and the ability to differentiate sources if their crustal ages are  $> 100$  m.y. (Gleason et al., 1994). Nd-isotopic composition of Middle and Upper Ordovician deposits of the southern-central Appalachians and Ouachita Mountains reflects an isotopic shift, which has generated controversy in the interpretation of source and paleodrainage of Middle and Upper Ordovician sediments deposited along the southern margin of Laurentia and the Ouachita

embayment (Gleason et al., 1994, 1995a, 1995b, 1997, 2002; Thomas, 1995, 1997; Andersen and Samson, 1995). The rapid up section increase of Nd-isotopic composition at ~ 465-455 Ma from  $\epsilon_{Nd} = -15$  to  $\epsilon_{Nd} = -7$  contrasts with the homogeneous composition after 450 Ma (Gleason et al., 2002). This isotopic shift is recorded earlier in Blountian sediments than in sediments in the Ouachita Mountains to the southwest (Gleason et al., 2002) or in other Taconic sediments to the north (Gleason et al., 1995b; Andersen and Samson, 1995). The increase in Nd-isotopic ratios is greater in Blountian sediments than in Taconic sediments, indicating greater influence of juvenile source rocks in the south than in the north (Andersen and Samson, 1995).

The abrupt change of isotopic signature has been interpreted as the result of delivery of detritus from a combined Archean-Grenville crust (more negative  $\epsilon_{Nd}$ ) to sources composed mainly of Grenville rocks (more positive  $\epsilon_{Nd}$ ) (Andersen and Samson, 1995; Gleason et al., 2002). Using Nd isotopes and U-Pb ages of single detrital zircons, Gleason et al. (2002) indicate that Middle and Upper Ordovician sediments in the Ouachita region were delivered from the Appalachian Taconic highlands with a dominant Grenville component. Andersen and Samson (1995) suggest juvenile sediment being delivered from uplifted Grenville crust probably combined with exotic terranes, such as volcanic arcs. Thomas (1997) argued that the homogeneous Nd-isotopic composition after 450 Ma contrasts with along-strike heterogeneity of lithotectonic composition of the orogenic belt.

#### **4.2.5 Blountian allochthonous terranes in the southern Appalachians**

Late Paleozoic (Alleghanian) dextral strike-slip and thrusting in the southern Appalachians (Hatcher et al., 1989; Hatcher, 1999) obscure the identification of possible Blountian allochthonous terranes and loads in the southern Appalachians. Southeast of the unmetamorphosed Appalachian thrust belt, the Talladega Slate belt and the Pine Mountain internal massif contain lower Paleozoic Laurentian rocks (Tull, 1998, 2002; Steltenpohl and Tull, 2002). Because Blountian provenance studies have suggested that sediment sources had exposed Grenville basement, these two metamorphic complexes cannot be considered as source areas or tectonic loads for the Blountian orogeny. Farther northeast, tectonic loads for the Taconic orogeny have been proposed by accretion of the Piedmont arc in east-dipping subduction collision (Hatcher, 1999), followed by accretion of the peri-Gondwana Carolina terrane (Hibbard, 2000).

The Blountian highlands have been proposed as the site of Middle and Upper Ordovician volcanism, even though the position of the volcanic arc in the southern Appalachians is unknown. K-bentonite beds are thicker, more numerous, and coarser in the southern Appalachians suggesting that source volcanoes were situated near the southern and central margin of Laurentia (Kolata et al., 1996). Trace element analyses of K-bentonites indicate that parent magmas were highly evolved felsic calc-alkaline, more likely produced by melting of continental crust (Kolata et al., 1996, 1998).

### **4.3 METHODS**

In this chapter, I integrate data from field work, seismic reflection profiles, deep wells, and literature (published papers, theses, dissertations) to carry out stratigraphic, provenance, and tectonic subsidence analyses in a total of 17 sections (Figure 4.2). Age control for each section is documented by conodonts (Bergström, 1973, 1977; Hall et al., 1986; Shaw et al., 1990), graptolites (Finney et al., 1996), and absolute ages of K-bentonite beds (Kolata et al., 1996, 1998). The time framework used in this study is based on the conodont-graptolite-K-bentonite correlation chart of Kolata et al. (1996) (Figure 4.4). Information related to the identification of K-bentonite beds in sections HM, HL, RK, GU, DM, GS, and CL is in Appendix A. Identification and correlation of collection of graptolites in sections PF, CL, EC, AB, HV, and LM is in Appendix B. The framework in space is given by the palinspastic map constructed for the Appalachian thrust belt of Georgia and Alabama (Chapter 2). Definitions of lithofacies and interpretations of depositional environments used in this study are given in Tables 4.1 and 4.2, and graphic symbols are illustrated in Figure 4.5. Plates 4.2 and 4.3 include a detailed description and interpretation of depositional environments of the stratigraphic sections in CI and RK. Appendices C and D include the thickness of stratigraphic units used for tectonic subsidence analysis and a summary of descriptions of thin sections and hand samples.

Two lines of along-strike stratigraphic correlation of the middle to distal Blountian foreland are constructed to illustrate differences in depositional architecture among the Alabama promontory, the accommodation zone, and the Tennessee embayment (Figures 4.6 and 4.7). Stratigraphic columns and estimation of thickness of proximal Blountian deposits are from regional and local structural cross sections (Figures 4.8 to 4.10). Plate 4.1 shows four strike-perpendicular stratigraphic correlations that connect the information of stratigraphic columns in

the distal and middle foreland discussed in Chapter 3 (Plates 3.1 to 3.10) with the sections in the proximal foreland (Plates 4.2 and 4.3). The key for stratigraphic correlation among sections in the middle foreland or between sections in the proximal and middle foreland is the identification of chronostratigraphic surfaces that may be connected across different depositional systems. Eleven chronostratigraphic surfaces were identified, and they correspond to unconformities, termination of carbonate deposition, marine flooding surfaces, and K-bentonites. Definition of each surface in sequential order is given in Table 4.3. A more detailed explanation of these surfaces is in Chapter 3.

Provenance analyses were carried out for distal, middle, and proximal Blountian sandstone and mudstone deposits. Eighty-one thin sections of fine to medium sandstones, selected from a total of 132 thin sections, were point-counted utilizing 300 framework points per thin section and using the Gazzi-Dickinson method (e.g., Ingersoll et al., 1984). Thin sections were stained for identification of plagioclase and potassium feldspars. Detrital modes exclusive of carbonate grains were calculated from the point-count results following the technique of Dickinson (1985) (Table 4.4). The 81 thin sections were grouped in 20 sandstone groups according to location and stratigraphic position (Table 4.5) in order to establish spatial and temporal variations in sandstone composition of the Blountian clastic wedge (Plates 3.1 to 3.10 and 4.2 to 4.4 show photomicrographs of selected thin sections next the stratigraphic columns). The mean and standard deviation of each group was plotted in QFL and QmFLt ternary diagrams of Dickinson (1985) (Figures 4.6B and 4.9D). Six samples of shales were selected at different stratigraphic positions within the Blountian clastic wedge in the Alabama promontory for determination of Nd-isotopic composition. These samples were analyzed by James D. Gleason at the University of Michigan. Procedures are explained in Gleason et al. (1995b, 2002, in prep.).

Tectonic subsidence analysis was carried out in each section assuming that the top of Ordovician was ultimately buried to a depth of at least 4 km. (from an estimate of the thickest post-Ordovician succession in the Cahaba synclinorium in the southern Appalachians). I used backstripping techniques (e.g., Sclater and Christie, 1980; Allen and Allen, 1992) to decompact the measured stratigraphic thickness; this technique assumes a lithology-dependent exponential decrease of porosity with depth, a fully saturated column of sediments, and local compensation (Airy isostasy) of sedimentary loads. Initial porosities and porosity-depth coefficients (values

from Sclater and Christie, 1980) were averaged according to the percentage of each lithology in each stratigraphic interval (Appendix C). Although the assumption of Airy isostasy is inappropriate for analysis of flexural deformation (Whiting and Thomas, 1994), I intend to illustrate contrasts in tectonic subsidence curves of sections that restore palinspastically in the middle and proximal foreland zones, and on the Alabama promontory and Tennessee embayment. Tectonic subsidence analysis for each section was carried out using a MatLab program written by Nestor Cardozo at Cornell University. The elastic mechanical model for flexural deformation and its assumptions are explained in Cardozo and Jordan (2001).

#### **4.4 MIDDLE FORELAND STRATIGRAPHY AND COMPOSITION OF SILICICLASTIC DEPOSITS**

##### **4.4.1 Units, thickness, and age**

Middle and Upper Ordovician carbonate strata restoring southeast of the Birmingham graben consist of the Lenoir, Little Oak, and Holston Limestones. The carbonate succession is overlain by the Athens Shale in sections restoring on the southeasternmost part (e.g., in sections AB, CL, CI); by red siliciclastic units of the Greensport-Colvin Mountain-Sequatchie succession in sections near the Birmingham graben (e.g., sections GS and HM), and by the mixed carbonate-siliciclastic Ottosee Formation in section RH (Figure 4.3). Measured stratigraphic thickness for some sections is incomplete because of truncation of upper strata at the post-Ordovician unconformity (sections HL, GS, RL, AB, CL, EC, PF) or erosion on the present land surface (sections HM and RH). In general, stratigraphic thickness is greater at both the northeast and southwest ends of the line of correlation HM-HL-GS-AB (Figure 4.6). Conodonts in basal carbonate beds in section PF yield a late Middle Ordovician age (*C. friendsvillensis* zone, middle Whiterockian) (Shaw et al., 1990). Conodonts and graptolites reported at the Lenoir-Athens contact of locality CL are one zone older than the conodonts and graptolites reported in sections PF and AB to the northwest (Figure 4.6; Hall et al., 1986; Finney et al., 1996). The difference in age of this contact documents the diachronous northwestward drowning of the carbonate platform during late Middle Ordovician and early Late Ordovician time (Finney et al., 1996). In section GS, conodont studies in the Lenoir Limestone yield an earliest Late Ordovician age (*C. sweeti* zone, uppermost Whiterockian) for middle and upper beds (Tom Shaw, written communication to Ed Osborne, 1987). The difference in conodont ages of upper Lenoir beds

between sections AB and GS documents the diachronous northeastward termination of carbonate deposition (Figure 4.6). For section GS, middle to late Late Ordovician conodonts (*B. confluens* to *A. ordovicicus* zones, late Mohawkian to middle Cincinnati) have been reported for the upper part of the Sequatchie Formation (Raymond, 1973). Ages for stratigraphic units in northern sections (Lenoir, Holston, and Ottosee) are assigned by lithostratigraphic correlation with equivalent units in southern Tennessee (Bergström, 1973, 1977).

#### 4.4.2 Lithology

The vertical association of lithofacies in lowermost beds of the carbonate interval is very complex and varies from place to place. The dominant lithology is fenestral and mud-rich limestones with sparse fauna (ostracods and gastropods) with isolated sand-size fragments of quartz and chert. This lithology has been identified in all sections as the Mosheim Member of the Lenoir Limestone, and thickness varies from 0 to 30 m. Lowermost beds also locally includes: (1) argillaceous and dolomitic mudstone to wackestone with dolomite conglomerates at the base and isolated cross beds in upper beds (section PF, Shaw et al., 1990); (2) chert conglomerates (section AB, Drahovzal and Neathery, 1971); (3) intraclastic and skeletal wackestone to grainstone with chert clasts (in areas near sections AB and GS, Roberson, 1988; Osborne, 1996); (4) peloidal, intraclastic, algal wackestone to packstone and limestone conglomerate (sections CL and GS, Bearce, 1999); and (5) red, mudcracked, mixed siliciclastic and limestone lithologies (section HM; Randy Kath, written communication to G. Bayona, 2001).

The carbonate interval of the Lenoir Limestone overlying the Mosheim Member and underlying fine-grained siliciclastic deposits (surfaces 3, 5 and 6 in Figure 4.6) changes along strike from algal, intraclastic, and mud-dominant limestone beds in sections at the Alabama promontory and accommodation zone to more skeletal limestones in sections at the Tennessee embayment. The Lenoir Limestone in sections PF and CL consists of argillaceous, peloidal, algal (*Calcisphere*, *Nuia* and *Girnavella*), intraclastic wackestone to packstone. Interbeds of skeletal limestone with more diverse and abundant fauna (crinoids, bryozoans, sponges, trilobites, brachiopods, and mollusks) and intensity of bioturbation increase up section. Uppermost beds of the Lenoir Limestone in section PF consist of well sorted, skeletal grainstone (crinoids, bryozoans, brachiopods, sponges, mollusks, and trilobite fragments; Pratt Ferry beds of

Drahovzal and Neathery, 1971). In section CL, thin calcareous beds are interbedded in the upper part of the section with skeletal, intraclastic wackestones. Time-equivalent carbonate beds to the northwest have been named the Little Oak Limestone. This carbonate unit in sections AB and RL consists of argillaceous, dark-gray, intraclastic, algal (*Nuia*, *Girnavella*, *Calcisphere*, *Dasyclads*), and skeletal wackestones to packstones with more diversity than in the underlying Lenoir strata (Drahovzal and Neathery, 1971; Osborne, 1996). Chert nodules, thin chert interbeds and slump-folded strata are observed locally in the upper beds of the Little Oak in section AB. In section GS, the carbonate interval is dolomitic, with diverse fauna (bryozoan, crinoids, brachiopods, trilobite) and algae (*Nuia*, *Girnavella*, *Solenopora*) at the bottom, and less diverse fauna (*Tetradium*, mollusks, ostracods, trilobites), fenestral, and algal-laminated dolomite toward the top. In section HL, the carbonate interval is the thinnest in the middle foreland (Figure 4.6) and consists mainly of very argillaceous intraclastic, skeletal, algal packstone. Bedding contacts and internal lamination in all these sections are stylonodular, with local high amplitude and high concentration of shaly residue (Bearce, 1999).

In northern sections HM and RH, carbonate beds are divided into two groups. One group includes mud-dominant lithofacies of the Lenoir Limestone as described in section GS. The other group includes coarse-grained limestones. In section HM, oncolitic and skeletal (mostly crinoids) limestones are interbedded with the Lenoir mud-rich lithologies. The coarse-grained lithologies are massive at the base, and have more ripple laminations and cross beds at the top. In section RH, the Holston Limestone (Cressler, 1974; or Rockwell and Chapman Ridge Formations of Caldwell, 1992) consists of oncologic limestones, calcarenites, and cross-bedded skeletal grainstones (Cressler, 1974; Caldwell, 1992). The uppermost beds in section RH are coarse-grained mixed crinoid and bryozoan grainstones with quartz-rich laminae and red calcilutite in the matrix (Caldwell, 1992). Sedimentary structures include planar and trough cross-beds.

Overlying the carbonate interval and underlying the Millbrig-Deicke K-bentonite interval (surface 8 in Figure 4.6) is a dominant siliciclastic interval of fine-grained sediments, but of differing lithofacies assemblage along strike. In southern sections AB and CL, graptolite-bearing siliciclastic black shales overlie the interbedded calcareous shales and argillaceous skeletal limestone lithofacies. In section PF, graptolite-bearing calcareous black shales with slump-folded structures (Ferrill, 1989) and isolated hummocky cross beds pass up section to laminated,



argillaceous calcareous mudstones with fine-grained bioclastic debris beds composed of bryozoans, brachiopods, and trilobites (Finney, 1977). Farther northeast in sections GS, HL, and HM, the transition between carbonate and siliciclastic lithofacies is more gradual. In sections GS and HL on the accommodation zone, dolomitic limestones are interbedded with gray and red calcareous and siliciclastic shales and shaly siltstones. In section HM on Tennessee embayment, argillaceous skeletal grainstones and packstones are interbedded with siliciclastic shales. In section RH, a succession of calcareous laminated mudstones, sandstones, and shales of the Ottosee Formation overlies the skeletal grainstone with quartz-rich laminae (Caldwell, 1992). The framework of the sandstones includes quartz, calcareous intraclasts, trilobites, bryozoans, brachiopods, and peloids; the more common sedimentary structures are wavy and heterolithic laminations.

Shales and siltstones in sections GS, HL, and HM are overlain by siltstones, sandstones, and K-bentonites of the Greensport Formation and Colvin Mountain Sandstone (Figure 4.6). The Greensport Formation includes several coarsening-upward successions with red shales, siltstones, and red dolomitic mudstones in the lower part; argillaceous and fine-grained subarkoses to arkoses interbedded with sandy siltstones in the middle; and fine- to coarse-grained subarkoses and quartzarenites interbedded with sandy siltstones at the top. Bioturbation is more pervasive in the middle and upper parts. Horizontal lamination, wavy ripples, and heterolithic lamination dominates in lower sandstone beds, whereas medium sets of cross beds are in the upper sandstone beds. Mudcracks are common in sandy siltstones in section HM at the Tennessee embayment. Thin to medium beds of dolomitic mudstones and intraclastic-skeletal debris beds with red sandy siltstone matrix appear locally in the middle of the section, overlying surface 7 in sections HM and GS (Figure 4.6). In section GS, these debris beds truncate underlying strata; and in section HM, slump-folded beds are in this interval. In both sections HM and GS, the debris beds separate calcareous beds below from siliciclastic deposits above.

The Colvin Mountain Sandstone is characterized by trough and planar cross beds, horizontal bedding, scour and fill structures, bimodal sand-size distribution in some beds, and vertical burrows as much as 60 cm deep. This unit pinches out laterally to the northeast and southwest of sections HM and GS, respectively (Figure 4.6). In the distal foreland, and using the Deicke and Millbrig K-bentonite for correlation of sections BI-DM-DG (Figure 4.7), the thin Colvin Mountain wedge grades southwestward to shallow-water carbonate deposits in section

BI. In the same line of correlation and on the Tennessee embayment, the Greensport Formation thickens northeastward and directly overlies the post-Knox unconformity (Chapter 3).

Deposits overlying the Colvin Mountain Sandstone correspond to strata of the Sequatchie Formation and are best recorded in section GS and in distal foreland sections (Figures 4.6 and 4.7). The lithofacies assemblage in section GS is dominated by red laminated mudstones and siltstones at the base; red, fine-grained, mixed carbonate and siliciclastic lithofacies in the middle; and dolomitic mudstones to wackestones toward the top. Mudcracks and rip-up clasts are common in the middle Sequatchie Formation. In sections DG and DM, the Sequatchie Formation thickens and is coarser northeastward. In addition to the lithofacies association described for section GS, Sequatchie beds in sections DG and DM include medium-grained quartzarenites and mixed siliciclastic and carbonate deposits toward the top (Figure 4.7) (Martin, 1991; Zeigler, 1988; Chapter 3).

#### **4.4.3 Composition of conglomerates and sandstones.**

In middle foreland strata, clast-supported conglomerate beds have a scattered distribution and are mostly in basal beds of the Lenoir Limestone (Figure 4.6). Clast composition is oligomictic, but varies from locality to locality. In section PF, dolomite and lime mud clasts dominate, and the matrix consists of dolomitic mud (Shaw et al., 1990). In section CL, limestone clasts are in a calcareous mud matrix (Bearce, 1999). In section AB, chert and quartzite clasts are in a calcareous silt matrix (Drahovzal and Neathery, 1971). In section HL, angular chert fragments are in red mudstones and shaly limestones (Chowns and Carter, 1983). In other localities where basal chert-conglomerate beds are best exposed (i.e., the Atalla Chert Conglomerate Member of the Chickamauga Limestone near BR and BI sections), the sand-size matrix of the chert-conglomerate consists of chert (27-60%) and monocrystalline quartz (40-67%) grains with calcareous and silica cement (sandstone group 15; Table 4.5 and Figure 4.6).

Fine- to medium-grained sandstones in the middle foreland have composition ranging from arkoses to quartzarenites (sandstone groups 9 to 14 and 16 to 20; Table 4.5 and Figure 4.6). Framework grains consist, in order of abundance, of monocrystalline quartz (44-99%), plagioclase (0-26%), unidentified feldspar (includes albitized plagioclase and feldspar partly replaced by calcite, 0-20%), potassium feldspar (0-13%), non-foliated polycrystalline quartz (0-8%), sedimentary lithic fragments (0-8%), metamorphic lithic fragments (0-7%), unidentified

lithic fragments (0-5%), foliated polycrystalline quartz (0-4 %), and chert (0-2%). Volcanic and plutonic lithic fragments are identified in trace amounts. The dominance of monocrystalline quartz in these units is illustrated by the very small switch in position of group mean values in QFL and QmFLt diagrams (Figure 4.6). In a single feldspar grain, albitization was identified by yellow and pink stains with irregular dissolution-like borders, irregular change from twinned to untwinned feldspar, and chessboard albite (e.g., Walker, 1984). Sedimentary lithic fragments are mainly siltstones and shale fragments, whereas metamorphic lithic grains are quartz-mica phyllites. Matrix and cements constitute between 15 and 35% of the thin sections. Clay, silt, calcite, dolomite, hematite, micas, and glauconite are the dominant interstitial constituents in the Greensport and Sequatchie Formations, whereas quartz, oxides, clay, and silt dominate in the Colvin Mountain Sandstone.

Sandstone composition varies both vertically and laterally in middle foreland strata, being more quartzose in coarser grained beds of the Colvin Mountain Sandstone and Sequatchie Formation. Sandstone beds of the Greensport Formation are arkosic to subarkosic in lower and middle beds (sections GS and HL; sandstone groups 9, 10, and 13; Figure 4.6) and subarkosic to quartzarenitic in upper beds (sections HM, HL, and DM; sandstone groups 11, 12, and 14). The Colvin Mountain Sandstone in sections HM, HL, and GS consists mostly of quartzarenites (Jenkins, 1984) (sandstone groups 16 and 18), although subarkoses are found in sections GS and DM (sandstone group 17). Sandstones of the Sequatchie Formation are subarkosic to quartzarenitic in sections DG (Zeigler, 1988) and HL (sandstone group 20), as well as in samples from sections BR, DM, and GS (sandstone group 19). Skeletal fragments (algae, bryozoans, crinoids), and phosphates are also present in medium-to-coarse sandstone beds at the top of the Sequatchie Formation in section BR.

## **4.5 PROXIMAL FORELAND STRATIGRAPHY AND COMPOSITION OF SILICICLASTIC DEPOSITS**

### **4.5.1 Units, thickness, and age**

Middle and Upper Ordovician units in the proximal foredeep zone include the Lenoir Limestone, Athens Shale, Rockmart Slate, and Chota Formation. Although Blountian strata restoring palinspastically to the southeast are thicker than Blountian strata to the northwest, complexity of Alleghanian structures (e.g., in section AA and AA'), truncation of upper strata at

the post-Ordovician unconformity (sections RK and FM), or erosion on the present land surface (sections CI, LM, FC, and HV) preclude an estimate of the complete thickness. I calculate values from structural cross sections and geologic maps of > 605 m in section CI (Figure 4.8), 350 m in section RK (Sibley, 1983), and several hundred meters in sections LM, FC, and HV (Figure 4.10). In addition to complex deformation, lack of biostratigraphic control in most of the proximal foreland succession does not allow constraints on the stratigraphic column constructed from structural cross sections. Conodonts collected in metamorphosed carbonate beds of the Lenoir Limestone in section RK (*E. foliaceus*, middle Whiterockian, Bergström, 1973), and graptolites of the overlying Rockmart Slate in section RK and in the Athens shale in sections LM, FC, and HV (*D. purchisoni* zone, middle Whiterockian, Finney et al., 1996) document the oldest record of Middle Ordovician deposition in the southern corner of Laurentia. Graptolites reported in Athens beds of section CI (*G. teretiusculus* zone, middle-late Whiterockian, Finney et al., 1996) indicate diachronous drowning of the platform parallel to the plate margin. The youngest age documented for proximal foreland deposits comes from graptolites in section RK (*G. teretiusculus* zone, middle-late Whiterockian, Cressler, 1970 (graptolites identified by William B. Berry)), and in the Athens Shale in section FM (*N. gracilis* zone, late Whiterockian, Appendix B).

#### 4.5.2 Lithology

Absence or thin and irregular distribution of the Lenoir Limestone characterizes the basal beds of the proximal foreland on the Alabama promontory. In section HV, the Lenoir Limestone has not been reported, and the black shales overlie Newala and Odenville beds of the Knox Group (Thomas and Drahovzal, in prep.). In section FC, the Lenoir Limestone consists of ~ 38 m of fenestral mudstones (i.e., Mosheim Member) and mud-dominated limestones with gastropods, brachiopods, cephalopods, and trilobites (Ed Osborne, written communication to G. Bayona, 2001). In sections CB and LM, the Lenoir Limestone has not been reported. In section FM on the accommodation zone, thin to medium beds of highly fractured, mud-dominated, black limestones are juxtaposed with highly deformed black shales with slaty cleavage; this succession overlies structurally undifferentiated units of the Knox Group (Osborne et al., 1988; Thomas and Drahovzal, in prep.). In section RK, the Lenoir Limestone is < 20 m and contains lithologies similar to those described for section FC, but with foliation (i.e., flattened fenestral textures).

Other lithologies of the Lenoir Limestone correspond to dolomite-conglomerates, ferruginous intraclastic and algal limestone beds with brachiopods, trilobites, mollusks, and phosphate grains (Figure 4.9C). These last lithologies have very local distribution and have been assigned to the Deaton Member (Cressler, 1970). The Lenoir Limestone in section CI on the Tennessee embayment is 5 m thick and consists of peloidal to intraclastic packstone and grainstone interbedded with fenestral peloidal mudstones.

Middle Ordovician strata overlying either the Lenoir Limestone or Knox strata consist uniformly of graptolite-bearing black shales of the Athens Shale or black slate of the Rockmart Slate. Calcareous content in shales varies along strike. Calcareous shales have not been reported in sections restoring on the Alabama promontory and in section FM (Figure 4.3). In section RK on the accommodation zone, calcareous black slates are interbedded with siliciclastic black slates. In section CI on the Tennessee embayment, laminated dolomitic dark gray silty shales and siltstones are the dominant lithology of the Athens Shale. In contrast to the uniform fine-grained lithology of lower beds of the Athens, lithofacies of the overlying Blountian succession vary along strike, as described below.

**4.5.2.1 Athens Shale and Chota Formation in section CI on the Tennessee embayment.** Strata overlying the lower calcareous black shale of the Athens Shale include at least seven coarsening-upward successions 15-60 m thick (Figure 4.8C). These coarsening-upward successions consist in the lower part of planar-laminated shale and siltstones, and wavy-, lenticular-, and ripple-laminated siltstones and very fine-grained sandstones. Laminae and thin beds of sandstone and bioturbation increase up section, and the top of each coarsening-upward succession consists of thick to medium bedded, fine- to medium-grained calcareous sandstones. Thick-bedded sandstones are dominantly massive, but thinner bedded sandstones and sandstones near the top of the Athens Shale have more ripples and cross-bedding structures, and wavy to planar contacts. Although siltstone-sandstone contacts are sharp, scour surfaces are not identified and rip-up clasts were observed only in very few beds.

The coarsening-upward trend of deposition continues in the Chota Formation. The fine-grained lithology is more silty and laminated than the calcareous shaly lithologies of the Athens Shale. Thin- to medium-bedded sandstones of the lower Chota Formation have sedimentary structures that change up section from ripple lamination in the lower part to hummocky and planar cross beds in the middle, and toward the top to planar and trough cross beds. Skeletal

fragments (bryozoans and crinoids) were identified in lower sandstones of the Chota Formation, and in bryozoan lenses in the middle part of the Chota Formation (Salisbury, 1961). Thick cross-bedded sandstones and horizontal-bedded, matrix-supported, cobble- to pebble-size conglomerates in the middle of the Chota Formation are the coarsest deposits found in section CI (Figure 4.8C). Caldwell (1992) reported herringbone cross bedding in sandstones of the Chota Formation in areas north of section CI. Overlying the conglomeratic sandstone interval are red and bioturbated sandy siltstones with slaty cleavage interbedded with argillaceous sandstones with scoured lower contacts and shale rip-up clasts, massive and planar cross-beds in sandstones, and a thin bed of quartzose conglomeratic sandstone at the top.

**4.5.2.2 Rockmart Slate in section RK.** Fine-grained lithologies are the dominant lithofacies in section RK on the accommodation zone, but sandstone and conglomerate interbeds are more common, coarser grained, and thicker to the southeast (Cressler, 1970; Sibley, 1983). Section RK was measured and described in one of the southeasternmost outcrops of the Rockmart Slate (Figure 4.9C), and the section is divided into two parts, as defined by the structure (Figure 4.9B). The lower structural part consists of at least six coarsening-upward successions. The lower part of each coarsening-upward succession consists of silty shale with thin interbeds of thin- to medium- bedded argillaceous and calcareous sandstones. Sandy siltstones and medium- to thick-bedded, massive, argillaceous sandstones are at the top of these successions. Primary sedimentary structures and nature of depositional contacts of the sandstone beds are obscured by foliation; however, normal and inverse grading, and gradational and planar contacts were observed. Interbedded with sandstones are cobble- to pebble-size conglomerates with flattened and elongated clasts parallel to the cleavage. The conglomerates are in medium to very thick lenticular beds, have sharp contacts with underlying and overlying sandstones, internally are massive and matrix-supported with sandy matrix. The upper structural part of the section makes the core of an overturned syncline (Figure 4.9B) and consists of fine-grained lithologies of calcareous and siliciclastic shales and silty shales with slaty cleavage (Figure 4.9C). A 4-cm-thick light green plastic claystone with isolated sand-size quartz grains and expandable clay (smectite) near the top may be an altered volcanic ash bed (or K-bentonite).

**4.5.2.3 Athens Shale in sections on the Alabama promontory and section FM.** The black shale and silty shale lithologies with varying intensity of slaty cleavage are the dominant

lithologies in section FM on the accommodation zone, and in sections LM, FC, CB, and HV on the Alabama promontory. Thin to medium beds of fine- to coarse-grained argillaceous sandstones interbedded with sandy siltstone and dark-colored silty shales with trace of fossils were observed in sections LM and HV on the Alabama promontory. These sandstone interbeds are in different structures from where graptolitic black shales have been reported (Figure 4.10). Sandstone beds are mostly massive, have sharp contacts with underlying and overlying beds, and few sandstones in section HV have internal gradations and planar laminations.

### **4.5.3 Composition of conglomerates and sandstones**

Conglomerate beds are distributed in three stratigraphic positions, and have a dominant population of limestone clasts. Thin and scattered conglomerates at the base of the Deaton Member in Rockmart (Plate 4.3) contain clasts mainly of dolomite, limestone, sandstones, and dark shales in a matrix of dolomite or feldspathic sandstone and siltstone (Cressler, 1970). In the lower part of the Rockmart Slate (middle Whiterockian, Figure 4.9C), the clast population (clast counting of 50 clasts after examinations of hand samples and one thin section) of conglomerates includes: dolomitized limestone and sandy dolomite (43%); limestones (micrite and calcarenites, 35%); black calcareous slate (20%); and chert, sandstones, and siltstones together (2 %). Cressler (1970) and Sibley (1983) reported the same order of composition of conglomerate clasts, in addition to quartzite fragments in trace amounts. The matrix of these conglomerates is subarkosic sandstones with calcareous cement. An olistolith (or exotic block) with a diameter of at least 15 m and enclosed by sandstones and slate has been reported by Sibley (1983) near section RK. The conglomerate clast population in the Chota Formation (early Mohawkian ? Figure 4.8C) reported by Kellberg and Grant (1956, point counting of 848 pebbles) and Caldwell (1992) includes: carbonates (80-87%); sandstones (5-10%); siltstones (2-4%); chert (2%); and quartzite, quartz veins, and pelites in trace amounts. The matrix of the conglomerates is sublitharenite with calcareous cement. Uppermost beds of the Chota Formation include a thin bed of quartzose conglomeratic sandstone with fragments identified in thin section of monocrystalline quartz, polycrystalline quartz, and chert; clay and oxides are in the matrix fraction.

Sandstones in the Athens Shale are arkosic, lithic arkoses, and subarkosic with 28 to 45% of matrix and cement, whereas sandstones in the Chota Formation are sublitharenites with a

range of matrix and cement from 30 to 52% (sandstone groups 1 to 8; Table 4.5, Figure 4.9D). In order of abundance, framework grains consist of monocrystalline quartz (33-88%), unidentified feldspar (includes albitized plagioclase and feldspar partly replaced by calcite, 1-30%), plagioclase (0-24%), sedimentary lithic fragments (0-19%), non-foliated polycrystalline quartz (0-10 %), potassium feldspar (0-9%), foliated polycrystalline quartz (0-4 %), metamorphic lithic fragments (0-3%), unidentified lithic fragments (0-3%), and chert (0-2%). Devitrified volcanic lithic fragments and plutonic rock fragments were identified in trace amounts.

The dominance of monocrystalline quartz and feldspars in the Athens Shale is illustrated by the group mean values in QFL and QmFLt diagrams (sandstone groups 1 to 6; Table 4.5, Figure 4.9D). Albitization is more common and pervasive than in middle foreland sandstones (Plate 4.2). Grains showing intergrowth of feldspars (perthite) and feldspar with quartz (myrmekite) were also observed (Plates 4.3 and 4.4). Sedimentary lithic grains are mainly sandy siltstones, siltstones, and shale fragments (Plate 4.4), whereas metamorphic lithic grains are mainly phyllite (foliated mica and quartz). Plutonic or coarse-grained metamorphic rock fragments are inferred from aggregates of feldspars and quartz. Micritic-carbonate-rock-fragment content varies from 0 to 14% in sandstones of the Athens Shale, and from 13 to 28% in the lower part of the Chota Formation. Carbonate rock fragments were not observed in upper beds of the Chota Formation. Interstitial constituents in sandstones of the proximal foreland are clay, oxides, micas, and more quartz and calcite cementation in sections RK and CI.

Composition of proximal foreland sandstones varies along strike and in the stratigraphic succession. Sandstones of the Athens Shale in sections that restore on the Alabama promontory and southern part of the accommodation zone (sections FM, LM, and HV) are arkosic to lithic arkosic (sandstone groups 1 and 2, Figure 4.9D), regardless of grain size or stratigraphic position. Sandstones of section RK on the accommodation zone are subarkosic (sandstone group 3, Figure 4.9D). The sandy matrix of the conglomerates is also subarkosic. Sandstone composition of the Athens Shale and lower Chota Formation in section CI on the Tennessee embayment varies from arkosic (sandstone groups 4 and 6, Figure 4.9D) to subarkosic in thick-bedded, massive medium- to coarse-grained sandstones. Composition of middle and upper sandstones of the Chota Formation is sublitharenitic (sandstone groups 7 and 8, Figure 4.9d),



with higher content of sedimentary lithic fragments (1-20%), non-foliated polycrystalline quartz, and chert than in underlying sandstones of the Athens Shale.

#### **4.6 MIDDLE AND PROXIMAL FORELAND STRATIGRAPHIC CORRELATION, AND INTERPRETATION OF DEPOSITIONAL ENVIRONMENTS**

Figures 4.6 and 4.7 show along-strike correlation of middle and middle-distal foreland strata based on the identification of 11 stratigraphic surfaces (Table 4.3). Surfaces 4, 7, 8, and 9 have the best spatial and chronostratigraphic constrains on the basis of conodont biostratigraphy in the distal foreland (Chapter 3). I use these surfaces, in addition to the lower and upper unconformities, to divide the Middle and Upper Ordovician succession into five stratigraphic intervals. This section gives a detailed description and interpretation of environment of deposition for strata in the lower three intervals; the description and interpretation for strata in intervals IV and V are given with more detail in Chapter 3.

##### **4.6.1 Strata and depositional systems of Interval I (upper Middle to lower Upper Ordovician)**

Interval I is bounded by the post-Knox unconformity and correlation surface 4. Lithofacies of basal beds of the Lenoir Limestone (i.e., Mosheim Member) in the proximal foreland vary both vertically and laterally, but all of them are suggestive of very shallow-marine to supratidal environments. Section HV on the Alabama promontory and parts of sections RK, CB, and FM on the accommodation zone do not record carbonate deposition at the base of the proximal Blountian succession (Figure 4.11A) (Cressler, 1970). Irregular and scattered distribution of chert and dolomite conglomerate beds overlying the post-Knox unconformity have been interpreted as the filling of karst topography (e.g., Drahovzal and Neathery, 1971; Chowns, 1977; Sibley, 1983). Benson (1986b) interpreted the dolomitic, fenestral, mud-rich limestone beds of the Mosheim Member as the record of peritidal environments; a similar interpretation is valid for basal reddish mudcracked mixed lithologies in section HM (e.g., Roberson, 1988). Intraclastic and skeletal wackestones to packstones and peloidal, intraclastic, algal packstones are more indicative of intertidal to very shallow subtidal environments (e.g., section AB; Benson, 1986b; Roberson, 1988). The wide variation in lithologies and depositional

environments may be an indication of the irregular topography associated with the post-Knox unconformity (e.g., Roberson, 1988).

Graptolite-bearing black shales overlying the basal carbonate unit or the post-Knox unconformity in the proximal foreland have been interpreted as pelagic deposition in a quiet-water, anoxic, deep marine environment (Figures 4.11A and B) (Shanmugam and Walker, 1978; Benson, 1986b). Lehmann et al. (1995) interpreted the Taconic black shales in the northern Appalachians as the pelitic tail of axial fan turbidite deposits. Calcareous black shales in sections RK and CI on the accommodation zone and Tennessee embayment, respectively, record a mixture of influx of mud carbonate particles from the carbonate ramp to the west and distal turbidite detritus from the east (Figure 4.11B) (Benson, 1986b). The massive aspect of thick-bedded sandstones, lack of shallow-water sedimentary structures, the sharp and non-erosive contacts between sandstone and siltstone beds, the presence of ripples and lenticular lenses in laminae and thin beds of sandstones, the feldspathic composition and matrix-rich fabric of sandstones, and the alternation of silt layers and pelagic shale, all suggest pelagic settling deposition intermittently interrupted by submarine turbidity current deposition. Shanmugam and Walker (1978) gave a similar interpretation of depositional environments for lower siliciclastic strata (Blockhouse and lower Sevier Formations) farther north in the Tennessee depocenter. In section RK, up section increase from laminae to thick beds of subarkosic and arkosic sandstones are interpreted as the approach of submarine turbiditic deposits. Interbeds of massive, wedge-shape conglomerates are interpreted as proximal debris-flow deposits, mixing with axial turbidity deposits (Figure 4.11B). Sibley (1983) interpreted the olistolith as a rock mass transported by submarine gravity sliding or slumpling.

K-bentonite beds and conodonts allow the correlation between deep-water siliciclastic strata to the southeast and shallow-water carbonates in the middle foreland on the Alabama promontory (Figures 4.11B, Plate 4.1). The main body of the Lenoir Limestone consists of argillaceous, peloidal, intraclastic wackestones to packstones with more diverse and abundant body fossils and algae than strata of the Mosheim Member. A restricted subtidal lagoonal environment has been interpreted for most of the Lenoir Limestone (Chapter 3) on the basis of abundance of algae, the restricted and few diverse body fossils, bioturbation, absence of shallow-water sedimentary structures, and abundance of micrite and argillaceous detritus. The upper beds of the Lenoir Limestone in sections CL and PF have an increase in open-marine skeletal

fragments (e.g., crinoids and bryozoans; Jones and Desrochers, 1992) and decrease of mud particles, green algae, and mollusk fragments, suggesting deposition in more high-energy, open-marine waters. These skeletal-rich beds pass upward at an abrupt transitional contact to skeletal-debris limestones and graptolite-bearing black shales, recording deposition on deep carbonate ramp settings (surface 3). Slump-folded strata in sections PF and AB, near surface 3, record platform instability in the deep carbonate ramp. Correlation using the boundary between *P. serra* and *P. anserinus* conodont zones indicates the lateral continuity of subtidal lagoonal (section AB), shallow to deep carbonate ramp (sections PF and CL), and basinal deposition (sections CL and EC) (Figure 4.11B, Plate 4.1). This southeast-dipping depositional profile is confirmed by deposition of siliciclastic shales in southern sections CL and EC. A deep carbonate ramp environment is recorded in section PF by calcareous graptolite-bearing calcareous shales with isolated hummocky cross beds that grade up section to calcareous mudstones.

Interval I thins abruptly in middle foreland sections near and on the accommodation zone (sections GS and HL) and on the Tennessee embayment (section HL). Lithofacies in these sections belong to the Mosheim Member, and are indicative of deposition in peritidal to very shallow-marine environments.

In general, Interval I records the early drowning of the Middle Ordovician carbonate platform in the proximal foreland and coeval peritidal to subtidal lagoonal limestone deposition in the middle foreland on the Alabama promontory (Figure 4.11A). Later drowning of the carbonate platform is documented in the middle foreland on the Alabama promontory, whereas a thin accumulation of peritidal carbonate deposits is recorded farther northeast on the Tennessee embayment (Figure 4.11B). On the proximal foreland, the thick siliciclastic succession consists of pelagic and submarine turbidity deposits, interbedded with local debris-flow conglomerates on the accommodation zone.

#### **4.6.2 Strata and depositional systems of Interval II (lower Upper Ordovician).**

Correlation of middle and proximal foreland strata on the Tennessee embayment (sections HM, RH, and CI) depends on regional lithostratigraphic correlation of stratigraphic correlation surfaces 4 and 7, which are defined by marine-flooding surfaces that affected middle and distal foreland settings (Table 4.3, Plate 4.1).

Surface 4 in section CI is located at the base of a thick interval of shales, silty shales, and siltstones that are interpreted to represent deepening of the basin floor. The up-section change in sedimentary structures from ripples to cross beds in sandstones in the lower part of interval II reflects an increase in energy of deposition. In addition, the coarsening-upward trend from fine-grained lithologies to interbedding of sandstones and siltstones suggests a shallowing trend in deposition on a clastic platform environment with influence of storm currents. In the upper part of interval II, interbedding of cross-bedded sandstones with horizontal-bedded limestone conglomerates documents an increase in energy of deposition and proximity to source areas (Figure 4.11C). Bioturbated red siltstones, argillaceous sublitharenites with scoured bases, and lenses of quartzose conglomerates in the uppermost beds of interval II indicate alternation of high-energy and low-energy regimes. The vertical coarsening-upward trend of sandy siltstones to conglomeratic sandstones followed by interbedding of sandstones and bioturbated siltstones is interpreted as the progradation of a tide-dominated delta, as illustrated by hypothetical prograding sand ridges and abandoned delta-plain vertical profiles of Dalrymple (1992).

In the middle foreland, deposition in interval II is recorded by a northeastward shallowing trend of carbonate depositional systems and influx of siliciclastic detritus from the east (Figure 4.11C). On the southern Alabama promontory (section PF), laminated argillaceous carbonate mudstones interbedded with calcareous shales are interpreted as deposition in deep-water carbonate ramp environments. Farther northeast on the northern Alabama promontory, dolomitic mudstones to packstones with peloids, intraclasts, algae, and sparse fauna in section GS are the record of subtidal lagoonal to peritidal deposition. Up-section decrease of faunal diversity, fenestral structures, and algal-laminated dolomitic mudstones toward the top of the Lenoir in section GS document dominance of low-energy supratidal to intertidal environments. The thin carbonate interval in section HL, a section that palinspastically restores inside the Birmingham graben and on the accommodation zone, records the low rates of creation of accommodation space associated with inversion of the graben structure (Chapter 3). Up-section dominance of coarse-grained algal and skeletal deposits in sections HM and RH on the Tennessee embayment suggest shallow subtidal environments with energy regimes higher than in the subtidal environment on the Alabama promontory. Cross-bedded, skeletal and quartz-rich, coarse-grained carbonates at the top in sections HM and RH on the Tennessee embayment indicate deposition continued in open, high-energy, shallow-ramp environments.

Termination of carbonate-platform deposition in the middle foreland and on the accommodation zone and Tennessee embayment (Figure 4.11C; sections HM, HL, and GS) is in shallower depths and in more oxidizing conditions than the earlier drowning of the carbonate platform (Interval I) in the middle foreland on the southern Alabama promontory. In sections HM, HL, and GS, the coarsening-upward trend of the lower siliciclastic succession from shales to siltstones and feldspathic sandstones, and the up-section increase of bioturbation and ripple laminations have been interpreted as shoaling cycles in a low-energy subtidal to shallow-shelf environment (Drahovzal and Neathery, 1971). Ripple laminated and cross-bedded sandstones in section GS and mudcracks in sections HM and HL suggest shallower subtidal depositional conditions on the Tennessee embayment (sections HM, RH) than on the Alabama promontory (section GS). Coarse interbeds of carbonate lithologies in sections HM and RH also indicate a close proximity of the carbonate platform to sections on the Tennessee embayment.

Proximal and middle foreland strata of Interval II record the filling of the proximal foredeep and initial progradation of the clastic wedge toward the carbonate ramp in the middle foreland. Patterns of proximal foreland clastic deposition are coarsening-upward and progradational with finer grained clastic platform deposits grading to coarser grained marginal deposits of tide-dominated deltas. Coeval depositional environments in the middle to distal foreland include a southwest-deepening carbonate ramp on the Alabama promontory and high-energy shallow-marine ramp on the Tennessee embayment. The east-to-northeastward shift from carbonate-ramp to low-energy clastic shelf deposition illustrates the process of termination of carbonate production in shallow environments by northeastward (along-strike) advance of the clastic wedge. Coarsening-upward siliciclastic successions in the middle foreland document shoaling of the clastic shelf and cratonward advance of the Blountian clastic wedge.

#### **4.6.3 Strata and depositional systems of Interval III (lower Upper Ordovician)**

Strata of Interval III are absent because of present level of erosion or by unconformable deposition of Devonian or Mississippian strata in sections of the proximal foreland. In the middle foreland, Interval III thickens northeastward (Figure 4.6); in the middle to distal foreland the thinnest record is in the middle of stratigraphic correlation DG-DM-BI (Figure 4.7). This interval is bounded at the base by the marine-flooding surface 7 constrained in distal foreland deposits (Table 4.3, Chapter 3) and at the top by the Millbrig or Deicke K-bentonite (Figure 4.6).

Skeletal and intraclastic debris beds and slump-folded strata in sections HM, RH, and GS are interpreted as the record of a marine transgression (i.e. transgressive lag deposit). Platform deepening is interpreted from carbonate platform instability and deposition of fine-grained, non-calcareous siliciclastic beds above the debris beds or shallow-water calcareous beds.

In sections HM, HL, and GS, intervals of only bioturbated sandy siltstones and coarsening-upward successions overlying surface 7 record depositional conditions shallower than those of the former clastic shelf. The coarsening-upward successions include bioturbated sandy siltstones and massive, cross-bedded, and bioturbated sandstones. In section RH, fine-grained mixed carbonate-siliciclastic beds interbedded with thin beds of calcareous mudstones dominate (Caldwell, 1992). The association of these lithologies may represent prograding sand ridges that accumulated in subtidal to intertidal environments of a tide-dominated delta (e.g., Dalrymple, 1992). The sharp basal contact and distribution of the Colvin Mountain Sandstone indicate an abrupt change in depositional conditions accompanied by an increase in coarse-grained sediment supply and accumulation of K-bentonites. Strata below the contact consist of bioturbated sandy siltstones and sandstones in sections HM, HL, and GS; these deposits represent shallow-water deposition in a low to moderate energy regime. In contrast, quartzarenites overlying the contact show planar and trough cross beds, have bimodal sand-size distribution in some beds, and texturally and compositionally are mature (Jenkins, 1984). Elongated vertical burrows in upper beds suggest a shallowing-upward trend of deposition in high-energy regimes in sections on the Alabama promontory and in the accommodation zone, whereas the thin accumulation of the Colvin Mountain Sandstone on the Tennessee embayment suggest the dominance of deposition in low to moderate energy regime.

The sharp change of depositional conditions between Greensport and Colvin Mountain units is diachronous and is younger in sections on the Tennessee embayment. The change is positioned below the Millbrig-Deicke K-bentonite interval in section GS, within the K-bentonite interval in section HL, and above the K-bentonite interval in section HM. In palinspastic maps, quartzarenites of the Colvin Mountain Sandstone form a narrow belt of shallow-marine sand bars that interfinger with subtidal siliciclastic deposition, and this belt is bounded by peritidal carbonate deposition on the northwest (Figure 4.12A). This belt of shallow-marine sand bars migrates northeastward from section GS on the Alabama promontory to section HL on the accommodation zone, and then to section HM where pinches out.

Interval III records a continuous shallowing trend of siliciclastic depositional systems from shallow clastic shelf to subtidal to intertidal environments in the middle foreland (Figure 4.12A). Diachronous northeastward migration of quartzose shallow-marine sand bars suggests an event of slight deepening and an oblique direction of dispersal of sediments in the middle foreland.

#### **4.6.4 Strata and depositional systems of Interval IV (lower-middle Upper Ordovician).**

Interval IV in the middle foreland thickens slightly northeastward and encompasses strata bounded by the Millbrig K-bentonite bed (surface 8) at the base and the regional marine-flooding surface 9 at the top (Figure 4.6). In section DG, where K-bentonite beds have not been reported, surface 8 is located at the base of a thick interval of red calcareous silty shales and siltstones that are interpreted to represent deepening of the basin floor (Figure 4.7). Stratigraphic sections that palinspastically restore farther to the northwest, but inside the Birmingham graben, show also the northeastward thickening of this interval (Figure 4.7).

In sections GS, HL (Figure 4.6), and DM (Figure 4.7), peritidal carbonate deposits and mudcracked fine-grained siliciclastic sediments prograded over shallow-marine sand bars and sandy siltstones. In sections GS and DM on the Alabama promontory, interbedding of fine-grained mixed lithologies with mudcracked dolomitic mudstones document the dominance of very shallow, peritidal deposits near the top of interval IV. Farther to the southwest in BI, equivalent strata correspond to shallow-marine carbonate beds of the upper Chickamauga Limestone (Figures 4.7 and 4.12B). In section HL, limited exposures of siltstones and thin beds of fine-grained sandstone suggest the dominance of low-energy regime of deposition. Farther northeast on the Tennessee embayment in section DG (Figure 4.7), the-up section change from laminated shales to bioturbated siltstones and fine arkosic sandstones with mudcracks document the shoaling of depositional conditions toward surface 9. Progradation of peritidal carbonate deposits over the clastic wedge was favored by variable low influx rates of sediment supply from the east. Consequently, the depocenter of siliciclastic deposition continued nearly in the same areas as for the upper deposits of interval III (Figure 4.12B).

#### **4.6.5 Strata and depositional systems of Interval V (strata between correlation surfaces 9 and the post-Ordovician unconformity, lower-middle Upper Ordovician).**

Interval V is bounded by the marine-flooding surface 9 and the post-Ordovician unconformity (surface 11 in Figures 4.6 and 4.7). Truncation at different levels of upper Ordovician strata at the post-Ordovician unconformity does not allow clear definition of thickness trends either in a northwest-southeast direction or in the middle foreland (Figure 4.6). Northeastward thickening of strata is more evident in the middle to distal foreland (Figure 4.7).

Strata between surfaces 9 and 11 show progradation of both carbonate and fine-grained mixed carbonate-siliciclastic deposits. In sections DM and GS on the Alabama promontory, progradation is indicated by the up-section decrease of reddish, bioturbated, fine-grained mixed lithofacies and increase of dolomitic limestone beds (Figures 4.6 and 4.7). In the DG section on the Tennessee embayment, the event of flooding at surface 9 is interpreted from calcareous shales and siltstones overlying a succession of mudcracked siltstones and fine-grained sandstones. In section DG and above the calcareous shales and siltstones, fine- and coarse-grained mixed carbonate lithologies are interbedded with siltstones in the middle part, and the succession grades to coarsening-upward successions of siltstones and cross-bedded quartzarenites in the upper part (Figure 4.7).

The lateral and vertical array of these lithofacies constitutes shoaling-upward successions with fine-grained subtidal to peritidal deposits at the bottom. However, depositional environment interpretation of the top of these shoaling-upward successions indicates northeast deepening of the basin floor (Figure 4.12C). Erosion of Upper Ordovician beds in section BI is documented by truncation by a skeletal limestone bed less than 1 meter thick of the Sequatchie Formation (Figure 4.7) (Benson and Stock, 1986), and by an angular discordance of 1.6 degree with a dip direction to the southeast between upper beds of the Ordovician and basal beds of the Silurian Red Mountain Formation (Thomas, 1986). Farther northeast in sections GS and DM on the Alabama promontory and in section HL on the accommodation zone, the dominance of dolomitic limestones and fine-grained siliciclastic deposits at the top of the succession record deposition in peritidal to intertidal environments. In section DG on the Tennessee embayment, coarser grained estuarine delta deposits suggest more subtidal environments with higher energy regimes (Rindsberg and Chowns, 1986; Martin, 1991). In this interval, the siliciclastic



depocenter migrated cratonward and mixed with carbonate deposits of the distal foreland (Chapter 3).

#### **4.7 PROVENANCE OF SANDSTONES AND CONGLOMERATES AND ISOTOPIC NEODYMIUM ANALYSIS**

Clastic deposits of the Blountian wedge have variations in grain size and composition both along and across strike of the foreland basin. In this section, I discuss the possible provenance of conglomerate and sandstones deposits, and include the results of Nd-isotopic composition of shales and siltstones.

##### **4.7.1 Conglomerates**

Conglomerate beds are distributed at both middle and proximal zones of the foreland, as well as at different stratigraphic levels, but they accumulated at different stages of the foreland and by distinct depositional processes. Karst-filling conglomerates overlying the post-Knox unconformity are oligomitic, but clast population is dominated either by carbonate clasts or by chert clasts. Chert-conglomerates of the Atalla Chert Conglomerate Member of the Chickamauga Limestone in the middle and middle to distal foreland are in sections that palinspastically restore inside the Birmingham graben (BI, DM, HL, DG; Figure 4.3, Plates 3.4 and 3.10). Dolomite conglomerates in sections RK and PF palinspastically restore southeast of the graben and are overlain by shales and carbonates, respectively, of stratigraphic Interval I (Plate 4.3). Abundance and compositional maturity of the conglomerates in sections restoring inside the graben suggest longer subaerial weathering and support the interpretation of inversion of the graben (Chapter 3); in contrast, earlier deposition on adjacent blocks and on proximal foreland settings allowed preservation of compositionally immature dolomite-clast conglomerates.

Conglomerates in the proximal foreland have a clast population dominated by carbonates, which have been identified as fragments of the Lenoir and older Paleozoic units of the Laurentian margin by Kellberg and Grant (1956) and Cressler (1970). Lenticular massive conglomerates in section RK, interpreted as debris-flow deposits, are interbedded with turbiditic sandstones and deep-water black shales of the lower part of Interval I. Calcareous black shales (20%) are the dominant subordinate clasts (Figures 4.9C), and the matrix is subarkosic. Fabric

and composition of these conglomerates suggest short distance of transport and proximity to uplifted areas in a deep-water system. This interpretation is further supported by the presence of a 15-m-diameter olistolith in section RK (Sibley, 1983). Horizontal-bedded conglomerates in section CI are part of coarsening-upward successions of prograding tide-dominated deltas at the top of Interval II. Subordinate clasts include sandstones and siltstones (7-14%) (Figure 4.8C), and the matrix is sublitharenite. Composition and depositional structures of conglomerates and interbedded cross-bedded sandstones in section CI suggest transport by high-energy, shallow-water currents, and possible mixing of carbonate clasts derived from extrabasinal and intrabasinal sources, as indicated by bryozoan fragments in sandstone beds. Therefore, conglomerate beds in sections RK and CI accumulated at different stages of the foreland evolution and by different sedimentary processes.

#### **4.7.2 Sandstones**

The Blountain clastic wedge has spatial and temporal variation in the composition of sandstones of Interval I and II (Athens Shale, Chota and Greensport Formations). On the Alabama promontory, sandstones are arkosic (sandstone groups 1 and 9), lithic arkosic (sandstone group 2), and subarkosic (sandstone groups 10 and 11) (Table 4.5; Figures 4.6B and 4.9D). Composition of sandstones on the accommodation zone and Tennessee embayment ranges between arkosic (sandstone groups 4 and 6), subarkosic (sandstone groups 3, 5, 13, and 14), sublitharenite (sandstone groups 7 and 8), and quartzarenite (sandstone group 12) (Table 4.5; Figures 4.6B and 4.9D). Albitization alteration makes the calculation of the initial relation between plagioclase and potassium feldspars difficult. However, potassium feldspar (orthoclase and microcline) is more easily identified (i.e., less albitized) in sandstones in section CI on the Tennessee embayment (e.g., sandstone group 5; Table 4.5) than in sandstones in sections on the Alabama promontory and accommodation zone. Similarly, potassium feldspars are more evident in sandstones of the Greensport and Sequatchie Formations in the middle to distal foreland (e.g., sandstone groups 11, 14, 19, and 20; Table 4.5). Micritic carbonate rock fragments are very common in sandstones of the Tennessee embayment (section CI). Along-strike variations in petrofacies suggest more feldspathic sandstones on the Alabama promontory than farther north, more compositionally mature sandstones (i.e., more quartzose) on the accommodation zone,

more albitization in proximal sandstones on the Alabama promontory and accommodation zone, and more carbonate fragments on the Tennessee embayment.

Mack's (1985) interpretation of coarse-grained plutonic or gneissic rocks with a sedimentary cover as the main rock types in source areas is additionally supported in this study by the identification of (1) high content of both plagioclase and potassium feldspars, (2) feldspar aggregates, (3) myrmekite structures, (4) feldspar-quartz aggregates, and (5) higher and more diverse population of sedimentary lithic fragments than low-grade metamorphic components (quartzite and metamorphic lithics) (Table 4.5). The higher concentration of feldspar on the Alabama promontory, and the higher content of quartzose, sedimentary lithic, and carbonate rock fragments on the Tennessee embayment suggest either deeper erosion in source areas supplying sediments to the Alabama promontory or less transportation and less weathering of sediments accumulated on the Tennessee embayment. Supply of carbonate fragments from intrabasinal sources (i.e., carbonate platform to the northwest) should be also considered by the record of well-preserved bryozoan fragments and bioclastic debris beds in sections CI and PF (Salisbury, 1961; Finney, 1977; Caldwell, 1992).

The subarkosic-arkosic composition of Blountian foreland sandstones and the irregular location of detrital modes in provenance diagrams of Dickinson (1985) (Figures 4.6B and 4.9D) further support the interpretation of sandstone provenance from basement-cored uplifts with a sedimentary cover dominated by chemically-unstable rocks. The Cambrian-Lower Ordovician sedimentary cover of the outer margin of Laurentia margin includes >60% of carbonate and evaporite rocks on the Alabama promontory, whereas on the Tennessee embayment the siliciclastic units are >75% of the Precambrian-Lower Ordovician sedimentary succession (estimates from figures 3 and 4 of Thomas, 1991). Here, I propose that the southern Blountian highlands involved basement and outer-margin stratigraphy of the Alabama promontory, and orogenic uplifts were more chemically-weathered on the southern part than on the northern part (record of carbonate detritus increase northeastward).

The abrupt increase of non-metamorphic quartz and sedimentary lithic fragments at the top of interval II, as documented in sandstones and conglomerates of the upper Chota Formation, influenced the up-section increase of compositional maturity of coeval and younger middle foreland strata (Figures 4.11C and 4.12A). In section RH, the influx of quartz is recorded in quartz-rich laminae of cross-bedded skeletal grainstones of the Holston Limestone (Interval II).

Farther southwest, quartzarenites of the Colvin Mountain (Interval III) mark an abrupt change in the mechanical and compositional maturity of sandstones in the middle foreland (Table 4.5, sandstone groups 16 and 17). The increasing influx of quartzose detritus is documented in subarkoses and quartzarenites of the Sequatchie Formation in section DG, and at the uppermost beds of Interval V in sections HL, DM, and in section BR in the distal foreland (Chapter 3).

#### **4.7.3 Shales and siltstones (Nd-isotopic analysis)**

Nd-isotopic composition of shales and siltstones from the Athens Shale, Lenoir Limestone, Greensport Formation, Colvin Mountain Sandstone, and Sequatchie Formation (Table 4.6) show an up-section increase of  $\epsilon_{Nd}$  values. These results reinforce the regional trend reported previously in Middle and Upper Ordovician rocks of the southern Appalachians and Ouachita Mountains (Gleason et al., 1995b; Andersen and Samson, 1995; Gleason et al., 2002).

Figure 4.13 and Table 4.6 show Nd-isotopic compositions from rocks of the Blountian clastic wedge on the Alabama promontory, Tennessee embayment, and Virginia promontory. Temporal and spatial comparisons of these data suggest: (1) in synorogenic deposits,  $\epsilon_{Nd}$  increases to less negative values more uniformly on the Alabama promontory than on Tennessee embayment; (2)  $\epsilon_{Nd}$  of basal Blountian black shales is less negative to the northeast; (3) the trend toward less negative values in the Tennessee embayment has an abrupt fall at 456 Ma (post-Tellico deposition); (4) the less negative  $\epsilon_{Nd}$  is in the Virginia promontory; and (5)  $\epsilon_{Nd}$  variations in strata younger than 454 Ma are poorly constrained.

Along-strike comparison of  $\epsilon_{Nd}$  within the Blountian clastic wedge may give an independent constraint on temporal and spatial variation in supply of juvenile material, under the assumption that supply of juvenile sediment yields less negative  $\epsilon_{Nd}$ . Andersen and Samson (1995) and Gleason et al. (2002) suggested that Grenville rocks were the most likely source of juvenile sediments for the Ordovician synorogenic deposits. Therefore, stripping of the sedimentary cover should yield more negative  $\epsilon_{Nd}$  values because siliciclastic rocks of the southern Laurentian passive-margin succession were supplied from the craton interior (i.e., Archean and Grenville crust) (Mack, 1980). As uplift and erosion in the Blountian highlands exposed Grenville basement rocks, supply of juvenile sediments to the foreland basin increased. Therefore, an uniform increase to less negative values of  $\epsilon_{Nd}$  would be expected in foreland sediments recording unroofing of the basement-cored uplifts.

## 4.8 TECTONIC SUBSIDENCE

Curves of total and tectonic subsidence for sections restoring in middle and distal foreland illustrate different along-strike behaviors of the top of basement during Middle and Late Ordovician deposition. Figure 4.14 shows representative curves of total and tectonic subsidence for sections restoring on the Alabama promontory, accommodation zone, and Tennessee embayment. Total subsidence curves may be divided into four segments. The first segment has a negative slope and corresponds to the last stage of post-rift thermal subsidence and accumulation of the Knox Group along the southern margin of Laurentia (Thomas and Astini, 1999). The second segment is flat and corresponds to the post-Knox unconformity. The third segment also has a negative slope and is between the post-Knox unconformity and the Millbrig and Deicke K-bentonite beds (surface 8). The total subsidence curve of section GS has the fourth segment that is between the K-bentonite beds and the top of the Silurian with a gentle negative slope to flat trend. Tectonic subsidence curves show a different geometry than total subsidence curves, and a total of five segments (segments a to e, Figure 3.11) is recognized after the segment of thermal subsidence of the Knox Group and before Silurian.

Tectonic subsidence curves in the middle foreland (sections HM, GS, and AB in Figure 4.14A) include the local effects of inversion of the Birmingham graben (Chapter 3) and flexure by loading at the plate margin. The minimal amount of erosion of upper Knox strata is represented by segment a in sections AB and GS. In section AB on the Alabama promontory, the inflection after initiation of Middle Ordovician deposition is divided into a gentle and large downslope and a steep and short downslope (segments c and d, respectively, Figure 4.14A). The former segment is better explained by inversion of the Birmingham graben that created accommodation space in inverted downthrown blocks, and the latter reflects the later advance of the flexural wave that placed the platform in deep-water settings. After a longer interval of exposure of the passive-margin strata in section GS than in section AB (segment a), the tectonic subsidence curve in section GS includes a gentle downslope trend followed by a flat-to-upslope trend (segments d and e, Figure 4.14A). These two segments have been observed in other sections in the middle and distal foreland (Chapter 3, Appendix C) and have been interpreted as distal effects of flexural subsidence (segment d) followed by a rise of the top of basement related to migration of the flexural wave toward the thrust belt (segment e; Chapter 3). Low tectonic subsidence, flexural uplift, and regional rise of sea level favored shallow-water carbonate and

clastic deposition in section GS. In section HM on the Tennessee embayment, deep truncation of Knox strata may be the record of inversion uplift of the Randolph-Heard graben (Figure 4.3; segment b in Figure 4.14A). After initiation of Blountian deposition, the steep slope of the tectonic subsidence curve in section HM is the result of lithosphere flexure. Farther to the east in section RH, the preserved record of upper units of the Knox Group and early record of the Lenoir Limestone (Cressler, 1974) suggest that inversion uplift did not affect this area, but flexural subsidence caused the initiation of carbonate deposition.

Tectonic subsidence curves in the proximal foreland sections CI and RK reflect rapid drowning of the carbonate platform (segment d) after initiation of Blountian deposition (Figure 4.14B). The steepest slope in section RK on the accommodation zone documents the stronger influence of flexural subsidence in this section that restores nearest the zone of collision (Figure 4.11A). The slope of the curve is less in section CI that restores farther cratonward on the Tennessee embayment. Because thickness and biostratigraphic control in section HV are not constrained, the tectonic subsidence curve for section CL is shown to illustrate subsidence on the Alabama promontory (Figure 4.14B). The downslope curve in section CL is divided into two segments. Segment c has a gentle downslope that may correspond to distal effects of subsidence in inverted downthrown blocks (Chapter 3) and flexural uplift (i.e., forebulge?) related to tectonic loading along the plate margin. The subsequent segment d has a steeper slope than segment c and documents the rapid drowning of the platform to deep-water settings as result of migration of the flexural wave.

## **4.9 DISCUSSION**

Stratigraphic, sedimentologic, compositional, and tectonic subsidence data of the Blountian clastic wedge in the southern Appalachians of Georgia and Alabama allow the establishment of some considerations on how the pre-existing rift-related configuration affected the along-strike evolution of the middle and proximal foreland basin and orogenic belt.

### **4.9.1 Relationship between Blountian foreland basin evolution and the inherited configuration of the plate margin**

The identification of coeval carbonate ramp, basal shales, and submarine sandstone turbidites units of an underfilled foreland basin (Sinclair, 1997) during the earliest stages may

give a good approximation of the initial flexural profile for water-filled foredeeps. Therefore, the examination of how these three (or trinity) underfilled units evolve across and along strike of the foreland may give an approximation of the early migration of the early Blountian flexural wave. Lower strata of stratigraphic Interval I include the underfilled trinity units (Figure 4.11A). The highest rates of deposition are toward the deepest part of the Blountian foreland basin and in intraplate settings (Chapter 3), as documented by coeval deposition of the Lenoir Limestone and Athens Shales at both extremes. In the distal foreland, carbonate deposition at depths < 100 m is favored by the low influx of clastic sediments (Walker et al., 1983; Dorobek, 1995), and subsidence related to inversion of the Birmingham graben (Figure 4.15C, profile a) (Chapter 3). Toward the hinterland, coarse-grained axial submarine fan deposits in the deepest part of the basin record the influx of sediments from the tectonic loads (Walker et al., 1983; Sinclair, 1997). In the middle of the foreland, thin accumulations of carbonate and siliciclastic mud record the drowning of the platform to deep-water settings with low influx of mud particles from axial fan turbidites and the carbonate platform.

Distribution of sedimentary environments in the Blountian foreland basin for strata underlying stratigraphic surface of correlation 1 shows a belt of carbonate deposition that thins toward the accommodation zone and south-to-southeastward deepening of the basin (Figure 4.11A). The earliest event of flexure is recorded in section HV on the Alabama promontory, where deep-water graptolitic shales rest over the youngest Knox strata. Farther northwest across strike and northeast along strike, coeval peritidal to very-shallow carbonate deposition was occurring in the middle foreland on the Alabama promontory and in wide areas on the Tennessee embayment (Figure 4.11A). The early and wide record of peritidal carbonate deposition may correspond to (1) fluctuations of sea level; (2) lateral effects of tectonic loads centered on the Alabama promontory; or (3) local subsidence effects of basement fault reactivation. Middle Ordovician sea-level fluctuations are recorded in plate-marginal sections of Laurentia (Figure 4.4; Ross and Ross, 1995); however, those fluctuations do not explain the presence of intraplate uplifts in the distal foreland (Figures 4.15A and B). The variation in area of carbonate deposition (31-78 km, calculated from Figure 4.15) and areas of exposure in the distal foreland (10-40 km, calculated from Figure 4.15) can not be explained either by flexural models. Models of flexural subsidence indicate that optimal carbonate deposition (0-100 m) occurs in platforms 5 to 40 km wide, and that the platform migrates together with the peripheral bulge in early foreland stages

(Dorobek, 1995). The varying magnitude of exposed areas in the middle to distal foreland and the wide peritidal to very shallow-marine platform in the Tennessee embayment (Mosheim Member beds) may reflect both local effects of fault reactivation (Chapter 3) and marginal-scale flooding related to sea-level fluctuations.

Along-strike comparison of the evolution of initial flexural profiles (Interval I, Figure 4.15B) shows a wider carbonate platform with less area of exposure on the Tennessee embayment than on the Alabama promontory, and a steeper slope of the foredeep on the Alabama promontory than on the Tennessee embayment. The flexural wave migrated first northeastward to sections RK and CI (drowning at surfaces 1 and 2, respectively), and later continued northwestward to sections EC, AA', CL, PF, and AB (drowning at surface 3) (Figures 4.11B and 4.15C). In the distal foreland, deposition on the wide carbonate platform was affected by inversion of the Birmingham graben on the Alabama promontory (Chapter 3), and by backstepping of the carbonate ramp (Walker et al., 1983) and marginal-scale sea-level fluctuations on the Tennessee embayment (Steinhauff and Walker, 1995). The transition from optimal carbonate deposition in ramps (< 100m, Dorobek, 1995) to dominantly shale deposition (>300 m, Benedict and Walker, 1978) spreads across ~ 10 km in the foredeep on the Alabama promontory, and in ~ 18-23 km in the foredeep on the Tennessee embayment (Figure 4.15B).

The pre-existing configuration of the Laurentia margin continued to influence basin geometry and deposition in later stages of the Blountian foreland, where the foredeep widens and the fill thickens toward the Tennessee embayment. Progradation of shallow-water siliciclastic deposition is recorded in section CI of the proximal foreland (Interval II, Figure 4.11C), and in the middle and distal foreland (Intervals II to V, Figure 4.12). Northeastward and northwestward dispersal of synorogenic detritus is documented by dominantly carbonate deposition in southwestern section PF, mixed siliciclastic and carbonate deposition in section GS, and by northeastward thickening and coarsening of red siliciclastic deposits of the Greensport and Sequatchie Formations (e.g., section DG and HM). Northwestward dispersal of synorogenic sediments on the Alabama promontory was controlled by the inversion of the Birmingham graben in the distal foreland (Chapter 3), and by northeast migration of orogenic loads (Figures 4.11 and 4.12). In contrast, the northeastward migration of the Blountian orogenic belt and siliciclastic depocenter rapidly filled the less steep foredeep on the Tennessee embayment, which also widened with time (Figures 4.12 and 4.16).



#### **4.9.2 Reactivation of pre-existing intraplate structures**

Besides of inversion of the Birmingham graben, as documented in Chapter 3, and of the western fault system of the Randolph-Heard graben, as documented by deep erosion in section HM, flexural deformation may trigger the reactivation of other basement faults in the middle and proximal foreland. Flexural normal reactivation of basement faults adds to lithospheric flexure and may contribute to the abrupt change from limestone to shales in underfilled foreland basins, as documented in the Taconic foreland basin in New York and Ontario (Bradley and Kidd, 1991; Lehmann et al., 1995).

The along-strike differences in flexural profiles between the narrow foredeep on the Alabama promontory and wider foredeep on the Tennessee embayment may be accommodated by reactivation of cross-strike structures in the accommodation zone. Castle (2001) proposed this type of reactivation in a distal foreland basin to accommodate along-strike variations in subsidence patterns, which coincided with the boundaries of promontories and embayments. Normal flexural extension and cross-strike reactivation may create intra-foredeep uplifts, which may be the source areas of the olistolith, conglomeratic debris flows interbedded with turbiditic sandstones and black shales in section RK (Figure 4.11B).

#### **4.9.3 Identification and trace of the foredeep side of the forebulge**

During the early stages of flexural wave migration, the overall geometry of the shallow portion of the flexural wave is obscured by reactivation of basement faults in the distal foreland (Chapter 3) and flexural normal fault reactivation in the proximal and middle foreland. Intraplate flexure associated with inversion of the Birmingham graben creates a fixed small-scale structure and local flexural wave superimposed on to the plate-marginal scale migration of the Blountian flexural wave (e.g., Figure 4.15C, profile a). The local effects of the inversion would be diminished as the foredeep side of the Blountian flexural wave passes across the inverted downthrown block. Therefore, the clearer picture of the Blountian flexural wave is observed where the platform deepens uniformly southeastward.

The trace of the foredeep side of the forebulge at the time of stratigraphic surface of correlation 3 does not follow the same strike of facies belts (Figure 4.15A) because of the inversion of the Birmingham graben. On the Alabama promontory, the approximate trace of the foredeep side of the forebulge is located near section PF. The top of the Lenoir Limestone in

section PF contains shallow-water skeletal grainstones that grade southeastward in section CL to deep-water calcareous shales and debris-like, argillaceous skeletal beds (Lenoir Limestone-Athens Shale contact). Farther northwest in section AB, mud-rich carbonate lithologies (upper Lenoir Limestone) indicate northwestward deepening to subtidal lagoonal conditions caused by local effects of the inversion. On the Tennessee embayment, the carbonate profile east of section HM deepens uniformly southeastward, suggesting that the Blountian flexural wave masks the effects of graben inversion in this area. Farther northeast in Tennessee, Roberson (1994) and Steinhauff and Walker (1995) recognized the forebulge as the narrow area with no record of Middle Ordovician deposition within the carbonate platform (i.e., area between sections DE and P in Figure 4.15B).

In stratigraphic intervals III to V, identification of the foredeep side of the forebulge in the middle and distal foreland is on the basis of profiles of carbonate-siliciclastic depositional systems, tectonic subsidence curves, and truncation of upper Ordovician strata. The evolution of the depositional profile of Upper Ordovician Blountian deposits records the position and migration of a submerged to partly exposed forebulge (Figures 4.16A and B). Before the time of deposition of the Deicke and Millbrig K-bentonite beds, the depositional profile has the shallowest part at section DM (Figure 4.16B), where peritidal deposition of the carbonate platform dominated on the northwest and subtidal siliciclastic deposition dominated on the southeast. The position of the foredeep side of the forebulge is inferred to be at this location or farther northwest because of the thin accumulation at section DM (Figure 4.7) with several beds showing mudcracks, an indicator of subaerial exposure. Latest effects of inversion of the Birmingham graben preclude the determination of the position of maximum flexural uplift at this time (Chapter 3). The transition between carbonate and siliciclastic deposition, nearly parallel to the trace of the forebulge but more toward the foredeep zone, had the maximum extent of progradation on the northern part of the Alabama promontory (~ 61 km, Figure 4.16A).

Rise of the top of basement in middle and distal foreland sections during deposition of upperbeds of Interval II, Interval IV and lower part of Interval V is interpreted as result of migration of the forebulge toward the orogenic belt (Chapter 3). The rise of the top of basement in section GS (Alabama promontory, Figure 4.14A) is also observed, but in less magnitude, in other sections restoring as far as 90 km to the northwest of section GS (e.g., sections BR, GU, Appendix C) and in other middle and distal foreland sections restoring on the Tennessee

embayment (e.g., sections DG, RI). Lack of sedimentary record of Intervals III to V in sections southeast of GS does not permit the determination of the distance of hinterland migration, and if the migration was associated to a period of quiescence (e.g., Quinlan and Beamont, 1984) or thrusting (e.g., Flemings and Jordan, 1990). The regional coeval cratonwide rise of sea level after the time of Millbrig-Deicke K-bentonites (Figure 4.14A, Bond and Kominz, 1991) and hinterland migration of the flexural wave created the conditions for the wide expanse of shallow-water carbonate and siliciclastic deposits in the distal and middle foreland.

For the latest Ordovician, the shallowest part of the depositional profile adjacent to the foredeep migrated farther northwestward onto the carbonate platform, as indicated by exposure surfaces and meteoric water cements in cross-bedded skeletal and phosphatic rich limestones on the Tennessee embayment (northwest of sections CH and RI, Figure 4.16D, Martin, 1991; Kher, 1996), and by meteoric water cements and truncation of Upper Ordovician strata and thin deposition of skeletal limestones in the Birmingham section (Figure 4.7) (Benson and Stock, 1986; Thomas, 1986; Tobin and Walker, 1994). The tectonic subsidence curve in the northeasternmost section DG indicates an event of flexural subsidence during the early Silurian (Chapter 3, Figure 3.11A). This event of flexure may be related to the last migration of the flexural wave in the latest Ordovician. In the upper part of Interval V, the foredeep side of the forebulge advanced farther cratonward on the Tennessee embayment (~ 73 km) than on the Alabama promontory (~ 11 km) (Figure 4.16C). Overall, the greatest migration of the forebulge and siliciclastic depocenter was on the accommodation zone (Figures 4.16A to C), indicating that, on the plate margin, the transition between the Alabama promontory and Tennessee embayment was loaded most of the time during the Middle and Late Ordovician.

#### **4.9.4 Migration of the flexural wave**

Flexural wave migration in a homogenous foreland lithosphere may be kinematically linked to the rates of propagation of orogenic belts and of convergence in the collisional margin (DeCelles and DeCelles, 2001). In the depocenter of the Blountian foreland basin in the Tennessee embayment (northeastern Tennessee) an average rate of migration of 13 mm/yr (ranging in time from 40 mm/yr to 9 mm/yr) was calculated using the difference in age of the stratigraphic base of the black shale succession of two sections located in the proximal foreland area (Finney et al., 1996). This average rate corresponds to flexural wave migration across the

deep part of the foredeep (initiation of black shales deposition) in the first 3.8 m.y and on the Tennessee embayment. On the Alabama promontory, a rate of  $\sim 8$  mm/yr is calculated using the difference in age and palinspastic distance between the basal Athens Shale in section HV (stratigraphic surface 1) and in section CL (stratigraphic surface 3) (50 km/6 m.y.; Figures 4.3 and 4.4). Farther northwest, a rate of  $\sim 11$  mm/yr is calculated using the difference in age and palinspastic distance between sections CL and PF (stratigraphic surface 3 in both sections; 13 km/1.2 m.y; Figures 4.3 and 4.4).

Comparison of migration rates of the flexural wave indicate that the Blountian thrust belt propagated faster on the Tennessee embayment than on the Alabama promontory, under the assumptions of a uniform foreland lithosphere, an instantaneous response of the lithosphere to applied loads, and rate of plate convergence was the same along strike. Slow movement of the flexural wave may also document the presence of weak zones in the Alabama foreland lithosphere (e.g., the Birmingham graben, Chapter 3) (Waschbusch and Royden, 1992). Besides in differences on lithosphere configuration, the rates of flexural wave migration are measured using different sources of palinspastic maps (see Figure 4.3 for the Alabama promontory and Finney et al., 1996, for the Tennessee embayment), although the time constraint is the same and based on graptolite determinations of Finney et al. (1996).

Using the trace of the foredeep side of the forebulge on the accommodation zone, the average rate of flexural wave migration between stratigraphic surfaces 3 and 8 is  $\sim 15$  mm/yr (61 km/4 m.y.; Figure 4.16A), and between stratigraphic surfaces 8 and 11 is  $\sim 5$  mm/yr (55 km/10 m.y.; Figure 4.16A). Comparison of flexural wave migration on the accommodation zone and the Alabama promontory over the time span of the Blountian orogen indicate an overall deceleration in migration of the flexural wave from the earliest stages of foreland development (8 to 15 mm/yr) to the latest stage in the Late Ordovician (5 mm/yr). Deceleration of foreland migration can be expected either by the northeastward migration of the orogenic loads (Figures 4.11 and 4.12), a decrease in rate of propagation of orogenic wedges with time (DeCelles and DeCelles, 2001), and passage of the flexural wave above a weak zone of the lithosphere (Waschbusch and Royden, 1992).

#### **4.9.5 Interaction between Blountian hinterland and the inherited configuration of the plate margin**

Along-strike differences in composition of siliciclastic detritus and irregular distribution of conglomerates in the proximal foredeep may be also related to the pre-existing configuration of the plate margin. According to the provenance interpretation from sandstones and conglomerates, Blountian highlands supplying detritus to the clastic wedge had Grenville basement and sedimentary cover rocks of the Laurentian margin (Figure 4.17). Up-section increase of sedimentary lithic grains and quartzose fragments at the time of deposition of the Chota Formation and younger beds (ca 457 Ma, stratigraphic surface of correlation 6) suggest exposure of a new sedimentary cover as result of break-forward thrusting of the Blountian thrust belt (Figure 4.17). Abundant K-bentonite beds and a few volcanic rock fragments in upper sandstones of the Blountian clastic wedge are the only indication of magmatic activity in the orogenic belt. The greater abundance of feldspars and the more uniform rate of change to less negative  $\epsilon_{Nd}$  on the Alabama promontory than on the Tennessee embayment may suggest increasing supply of juvenile sediments because of more exposure of Grenville basement rocks. The increased influx of quartzose and sedimentary-cover sediments and the record of coarse-grained tidal-influenced marginal facies on the Tennessee embayment (e.g., top of Chota Formation in section CI and top of Sequatchie Formation in section DG) may reflect less exposure of basement rocks and the farther cratonward advance of the orogenic belt.

The along-strike change in foredeep width supports the interpretation of along-strike variation of deformation in the orogenic belt (Figures 4.12 and 4.16). In the recess-salient model of orogenic belts (Figure 4.1), high deformation in the recess brings to surface older rocks in the orogenic belt and creates a narrow and steep foreland basin. In the salients of the orogenic belt, the orogenic belt is less shortened and advances farther cratonward. The wider foredeep and higher content of quartzose sedimentary lithic fragments on the Tennessee embayment than on the Alabama promontory suggest the presence of a salient curve of the Blountian thrust belt at the position of the Tennessee embayment. Farther southeast along strike, the higher content of feldspars grains, less negative  $\epsilon_{Nd}$  values, and the narrow and steep foredeep on the Alabama promontory support the curved geometry of the Blountian thrust belt.

#### 4.10 CONCLUSIONS

Stratigraphy, sediment composition, and tectonic subsidence patterns of the proximal and middle strata of the Blountian foreland basin document along-strike variations genetically related to the rifted-margin configuration of southern Laurentia. The Blountian foredeep, as depicted by change in depositional depth of coeval Middle Ordovician carbonate and black shale strata, was narrower and had steeper slope in the Alabama promontory than in the Tennessee embayment. Flexural reactivation of basement normal faults in the foredeep may have contributed to the rapid drowning of the carbonate platform. Deposition of the wide carbonate platform on the distal foreland and on the Alabama promontory was controlled primarily by uplift and subsidence related to the inversion of the Birmingham graben, whereas flexural subsidence and eustasy controlled distal foreland carbonate deposition on the Tennessee embayment. Differential flexural subsidence along the Blountian foredeep may be accommodated by reactivation of transverse basement faults on the accommodation zone.

Northeastward and northwestward migration of marginal sediment and tectonic loads, as indicated by diachronous drowning of the Middle Ordovician platform in the proximal foreland, controlled the migration of the clastic wedge depocenter and forebulge in middle and distal foreland. Up-section coarsening and shoaling of proximal and middle foredeep strata on the Tennessee embayment documents: (1) up section increase in influx of terrigenous detritus throughout the section, (2) an abrupt increase of quartz and sedimentary lithic fragments in coarse deltaic deposits toward the top, (3) cratonward progradation of shallow clastic platform to marginal environments, and (4) cratonward advance of a salient in the Blountian orogenic belt. In contrast, the low influx of terrigenous detritus to the narrow foredeep on the Alabama promontory favored the establishment of a carbonate ramp in the southwestern part, whereas shallow-water carbonate and siliciclastic deposition interfingered in the foredeep on the Alabama promontory and the accommodation zone.

The flexural wave initially migrated farther cratonward on the Alabama promontory, but as the tectonic loads moved northeastward, the forebulge migrated rapidly cratonward on the Tennessee embayment. In the early stages of foreland evolution, the rate of flexural wave migration is higher on the Tennessee embayment (9-40 mm/yr) than on the Alabama promontory (8-11 mm/yr) and accommodation zone (15 mm/yr). If flexural rigidity (or elastic thickness) of the lithosphere is uniform, propagation rates of tectonic/sediment loads on the Tennessee

embayment are inferred to be higher than those on the Alabama promontory; however, weak zones on the Alabama promontory lithosphere may explain the relative slow propagation of the flexural wave on the promontory. On the accommodation zone, rates of migration of the flexural wave decelerate through time from 15 mm/yr to 5 mm/yr. The largest migration of the forebulge on the accommodation zone may suggest that this zone was loaded most of the time during the Middle and Late Ordovician.

Intrabasinal uplifts and differential deformation in the Blountian orogenic belt are recorded by along-strike changes in the composition of the Blountian clastic wedge. Local conglomerates interbedded with turbiditic feldspar-bearing sandstones in the underfilled stratigraphy of the Blountian foredeep suggest the mixing of sediments transported by axial submarine fan deposits and debris flows derived from intrabasinal uplifts. Petrographic and Nd-isotopic data indicate a source area composed of Grenville basement and a sedimentary cover with a Laurentian-margin stratigraphy. The uniform increase of Nd-isotopes, the higher percentages of feldspars in the clastic wedge on the Alabama promontory, and the more abundant quartzose and sedimentary lithic fragments in the clastic wedge on the Tennessee embayment, suggest that the Blountian tectonic load was more deeply eroded in areas supplying sediments to the promontory, and the sedimentary cover was more exposed in areas supplying the embayment. This pattern of deformation is similar to the gradients of deformation documented in curved thrust belts, a geometry that is primarily controlled by the rifted configuration of the older margin.

In short, this chapter relates the along-strike change from a promontory to an embayment configuration of the Laurentian margin with (1) evolution of the depositional profile of the Blountian foredeep, (2) differential subsidence history and migration rates of the Blountian foredeep, and (3) intensity in deformation of the Blountian orogenic belt. Therefore, geodynamic modeling of the Blountian foreland basin needs to consider along-strike variations in the geometry of tectonic loads and reactivation of different basement structures.

**Table 4.1** Explanation of lithofacies codes and lithofacies interpretations for carbonate and mixed carbonate and siliciclastic deposits.

		<b>Lithology code</b>	<b>Rock name (Dunham, 1962)</b>	<b>Energy, Water depth</b>	<b>Environment of deposition. Dominant framework grains. Structures</b>
<b>CARBONATES</b> <i>L= Limestone D= Dolomite</i>	Lm, LDm, Dm = micrite-dominant constituents	Lmm, LDmm Dmm	Mudstone to wackestone	Low < 4 m	Supratidal to intratidal. Peloids, intraclasts, algae, restricted fauna. Fenestral, ripple and horizontal laminated, mudcracks, bioturbated.
		Lmms, LDmms Dmms	Mudstone to wackestone	Generally low < 16 m	Supratidal to subtidal (lagoon). Restricted fauna fragments of conglomerate size. Massive, fenestral.
		Lmo, LDmo	Wackestone to grainstone	Low to high < 16 m	Supratidal to shallow subtidal. Algae, oncoids, peloids, intraclasts, minor skeletal (mixed fauna). Massive, fenestral, ripple lamination, stylonodular.
		Lmi, LDmi	Wackestone to packstone	Moderate to high < 64 m	Intratidal to shallow subtidal with restricted circulation (lagoon). Intraclasts dominantly of Lmo lithologies. Massive, bioturbated, stylonodular, poor sorting.
		Lmr, LDmr	Wackestone to packstone	Low to moderate < 16 m	Shallow to intermediate subtidal, ramp or lagoon. Mixed restricted and open-water skeletal fragments, minor algae and peloids. Massive, stylonodular, fenestral.
		Lms	Wackestone to grainstone	Moderate to low < 64 m	Subtidal, open-marine circulation (shallow ramp). Open-marine fossils, trace of algae, intraclasts and peloids.
		Lml	Mudstone to wackestone	Generally low < 256 m	Massive, laminated, cross beds, stylonodular, bioherms. Intermediate to deep ramp. Thin horizontal lamination, internal grading and thin beds of Lss and Sb.
	Ls, Ds = sparry, calcarenite, rudite	Dsm	Coarse-crystalline dolomite		Non-skeletal. Massive. Original components must have been destroyed during dolomitization.
		Lso	Grainstone	Moderate to high < 16 m	Shallow ramp, shoals, tidal bars. Ooids, algae, trace of skeletal fragments, quartz. Cross beds, normal grading, lamination.
		Lss	Packstone to grainstone	Moderate to high < 16 m	Shallow ramp, shoals, tidal bars. Open-marine skeletal fragments, sand-size quartz. Massive, cross beds, good sorting.
		Lsp	Packstone to grainstone	Moderate to low < 16 m	Very shallow, intratidal to subtidal. Peloids and intraclasts, rare skeletal grains. Lamination, cross beds, good sorting.
		Lsi, Dsi	Packstone to grainstone	Moderate to high < 16 m	Very shallow, intratidal to subtidal. Intraclasts and open-marine skeletal grains, sand-size quartz. Massive, horizontal- and cross-bedded, good to moderate sorting.
					restricted-water skeletal fragments: ostracods, trilobites, mollusks, brachiopods, coral <i>Tetradium</i> , crinoids, green algae, oncoids open-marine skeletal fragments: brachiopods, trilobites, crinoids, bryozoans, corals, red algae
<b>MIXED LITHOLOGIES</b> LS (carbonate dominant); SL (siliciclastic dominant)		<b>Lithology code</b>	<b>Dominant carbonate and siliciclastic lithologies</b>	<b>Energy, Water depth</b>	<b>Environment of deposition. Dominant framework grains. Structures</b>
		LSbs, SLbs	Lml, Lms, Lss, Sb	Low < 1024 m	Deep-water ramp, distal carbonate turbidites. Graptolites. Horizontal lamination, soft-sediment deformation.
		LSf, SLf	LDmm, Ldmo, Lml, Sfsm, Sfm, calcisiltite	Generally low < 16 m	Intertidal, subtidal lagoon. Trace of skeletal grains. Mottled, diverse degree of bioturbation, massive, ripples and horizontal lamination, cross beds, mudcracks.
		LSci, SLci	Lmi, Lms, Ssm, Sgcg conglomerate	High < 64 m	Subtidal, debris-flow deposit. Massive, cross-bedded, matrix- to clast-supported, bioturbated, argillaceous, matrix of LSf, Sfsm, Ssm.
		LSes, SLcs	Lss, Lms, Sst, Ssp, Ssm, Sgcg conglomerate	High < 16 m	Very shallow ramp, shoals, tidal bars. Open-marine skeletal fragments, trace of peloids and intraclasts. Cross beds, cuneiform and lenticular beds, clast-supported.



**Table 4.1** (previous page) Explanation of lithofacies codes and lithofacies interpretations for carbonate and mixed carbonate and siliciclastic deposits. The codes have uppercase letters to indicate which is the dominant composition of each lithofacies (L=limestone, D=dolomite, S=siliciclastic (see Table 3.2)). Mixed lithofacies have two uppercase letters (LD=dolomitized limestone; LS=carbonate-siliciclastic). In only carbonates lithofacies, the first lowercase letter indicates either micritic (m) or sparry (s) lithologies. The second and third lowercase letter(s) denote important components or structures of the lithofacies: p =peloidal, i =intraclastic, o =non-skeletal allochems, r = association of skeletal fragments indicates restricted-water environments (ostracods, trilobites, mollusks, brachiopods, *Tetradium*, crinoids, green algae, oncoids), s = association of skeletal fragments indicates open-marine environments (brachiopods, trilobites, crinoids, bryozoans, corals, red algae), l =laminated, m=massive. In mixed lithologies, the lowercase letters indicate: bs = interbedding with black shales, f = fine-grained lithologies, ci = coarse-grained intraclastic, cs = coarse-grained skeletal.

**Table 4.2** Explanation of lithofacies codes and lithofacies interpretations for siliciclastic deposits. The code uses the uppercase letter “S” to identify the lithofacies as siliciclastic. The first lowercase letter denotes the grain size: g = gravel-size deposits, s = sand-size deposits, f = silt-size deposits, b = shale deposits. The second and/or third lowercase letters denote an important structure, as described in the table, and allow the identification of each lithofacies.

<b>Lithology code</b>	<b>Dominant grain size</b>	<b>Structures</b>	<b>Interpretation. Range of depositional environments</b>
Sgmm	Gravel, matrix-supported	Massive to weak grading	Plastic debris flow. Subaerial to submarine fans
Sgmg	Gravel, matrix-supported	Inverse to normal grading	Pseudoplastic debris flow. Subaerial to submarine fans
Sgmh	Gravel, matrix-supported	Crude horizontal bedding	Hyperconcentrated flow. Subaerial to submarine fans
Sgcg	Gravel, clast-supported	Normal grading	Hyperconcentrated flow. Subaerial to fan deltas
Sgcm	Gravel, clast-supported	Massive to crude horizontal bedding	Clast-rich debris flow, pseudoplastic debris flow, hyperconcentrated flow. Fan deltas
Sgh	Gravel, clast-supported	Crudely- to horizontally bedded, Imbrication	Longitudinal bedforms; lag or sieve deposits. Subaerial unconfined water flows
Sgt	Gravel, stratified	Trough cross-beds	Transverse bedforms, channel fill. Fluvial to fan deltas
Sgp	Gravel, stratified	Planar cross-beds	Transverse bedforms, deltaic growths from older bar remnants. Fluvial to fan deltas
Sst	Sand, fine to very coarse, locally pebbly. (i= bimodal grain size distribution)	Solitary or grouped trough cross-beds	Sinuuous-crested and linguoid 3-D dunes.
Ssti			Fluvial, subtidal, longshore bars
Ssp	Sand, fine to very coarse, locally pebbly. (i= bimodal grain size distribution)	Solitary or grouped planar cross-beds	Transverse and linguoid 2-D dunes. Fluvial, subtidal, longshore bars
Sspi			
Sse	Sand to pebble	Sigmoidal or ellipsoidal bedding	Lateral accretion. Fluvial to subtidal bars
Ssr	Sand, fine to coarse	Ripple cross-lamination (current or oscillatory)	Ripples (lower flow regime). Fluvial to deep-water turbidites
Ssh	Sand, fine to very coarse, locally pebbly. (i= bimodal grain size distribution)	Horizontal lamination with parting or streaming lineation	Plane-bed flow (critical flow). Fluvial to deep-water turbidites
Sshi			
Ssl	Sand, fine to very coarse, locally pebbly	Low-angle (<15°) cross-beds	Scour fills, humpback or washed-out dunes, antidunes. Fluvial
Sss	Sand to pebble	Broad, shallow scours	Scour fill. Fluvial, subtidal, longshore bars
Ssm	Sand, fine to coarse	Massive, or faint lamination	Sediment-gravity flow deposits. Fluvial to deep-water turbidites
Ssw	Sand, fine to coarse	Wave ripples and planar cross-beds	Sand dunes reworked by wave-dominated currents. Intratidal to shallow shelf
Ssb	Sand, fine	Hummocky cross-beds	Wave-dominated currents (storm currents). Shallow shelf
Sshe	Sand, mud	Heterolithic lamination, lenticular lamination	Continuing change from suspension to lower flow regime. Intratidal to shallow shelf
Ssfl	Sand, mud	Flaser or thin horizontal lamination	Deposition and/or erosion of mud laminae. Fluvial, intratidal, shallow shelf

**Table 4.2 (continued).**

Sfl	Sand, mud, slightly calcareous	Fine lamination, very thin lenses of sandstones, ripples, rare skeletal fragments (mollusks, brachiopods, bryozoans)	Overbank, abandoned channel, or waning flood deposits, intermediate-water suspension. Fluvial to deep-water turbidites
Sfsm	Sand, mud	Massive, leached carbonate, mottled by bioturbation, thin lenses of Ssm, Sss	Suspension in intermediate waters. Fluvial to intratidal
Sfm	Mud	Massive, faint lamination, dolomitic, desiccation cracks	Suspension in intermediate waters; overbank, abandoned channel, or drape deposits. Fluvial to intratidal
Sb	Black shale	Fissil, organic, calcareous and non-calcareous, graptolites	Suspension in deep water. Offshore and slope suspension; distal tail of submarine fans

**Table 4.3** Explanation of key stratigraphic surfaces.

	Age	Significance of the event in carbonate and mixed lithologies successions (sections restoring in the middle to distal foreland)	Significance of the event in siliciclastic successions (sections restoring in the proximal to middle foreland)
11		<b>Post-Ordovician unconformity. Total to partial drowning</b> of the Ordovician platform. Deposition of basal shales of the Red Mountain Formation with thin interbeds of fine-grained sandstones with hummocky cross beds.	<b>Post-Ordovician unconformity. Regional onset of shale deposition</b> of the Red Mountain Formation with thin interbeds of fine-grained sandstones with hummocky cross beds in section GS.
10	late Late Ordovician (Cincinnatian, ca 446)	<b>Marine flooding</b> and shoaling with deposition of coarser-grained, phosphatic, skeletal carbonates (section BR and BI), mixed lithologies (sections BR and RI), and quartzarenites (sections DM, HL, DG) ( <i>A. ordovicicus</i> zone).	
9	middle Late Ordovician (Mohawkian – Cincinnatian, ca. 451)	<b>Limited subaerial exposure followed by regional marine flooding</b> above surface 8 in carbonate lithologies at section BR, in mixed lithologies at GS ( <i>P. tenuis</i> to <i>B. confluens</i> ), and in siliciclastic lithologies in section DG.	<b>Regional marine flooding</b> in mixed lithologies in section GS ( <i>P. tenuis</i> to <i>B. confluens</i> )
8	ca 454 Ma	<b>Millbrig and Deicke K-bentonite interval</b> in dolomitic limestones in section BR and BI.	<b>Millbrig and Deicke K-bentonite interval</b> in red siltstones in section HM, at the base of quartzarenite deposits in sections HL and DM, and toward the top of the quartzarenite interval in GS.
7	early Late Ordovician (middle Mohawkian, ca 456)	<b>Subaerial exposure followed by regional marine flooding</b> below surface 8 in sections BR and BI (upper <i>E. quadridactylus</i> to lower <i>B. compressa</i> zones).	<b>Subaerial exposure followed by regional marine flooding</b> below surface 8 in sections HM, HL, DM, GS and PF ( <i>C. bicornis</i> zone). Resurgence of limestone deposition in section RH.
6	Late Ordovician (early Mohawkian)	Marine flooding in southern sections BR and BI ( <i>E. quadridactylus</i> zone).	Coarsening-upward, shallowing, and <b>termination of carbonate deposition</b> . Onset of fine-grained siliciclastic deposition in northern sections HM and RH ( <i>P. gerdae</i> zone).
5	Late Ordovician (early Mohawkian)	Marine flooding in section BI ( <i>P. aculeata</i> zone) and onset of carbonate deposition in section BR (older than <i>E. quadridactylus</i> zone). Inferred latest onset of deposition in sections DG and DM.	Shoaling, <b>termination of carbonate deposition</b> , and onset of fine-grained siliciclastic deposition in section GS (younger than <i>P. Sweetii</i> conodont zone).
4	Middle-Late Ordovician (ca. 458)	<b>Subaerial exposure followed by regional marine flooding</b> in section BI (upper <i>C. Sweetii</i> to lower <i>P. aculeata</i> zones).	<b>Regional marine flooding</b> in southern section PF ( <i>N. gracilis</i> to <i>C. bicornis</i> zones).
3	Middle-Late Ordovician (ca. 458)	<b>Onset of carbonate deposition</b> in section BI ( <i>C. sweetii</i> zone) and inferred for GS ( <i>P. serra</i> zone).	<b>Drowning</b> of the carbonate platform. Graptolitic, black shales deposition in sections AB and CL; slight shoaling and <b>drowning</b> at PF (top of <i>G. teretiusculus</i> to <i>N. gracilis</i> zones; Finney et al., 1996). The drowning in section CL occurred 1.2 m.y. earlier than in section PF (Finney et al., 1996).
2	late Middle Ordovician (late Whiterockian, ca. 463)	<b>Onset of carbonate deposition</b> at RH ( <i>P. serra</i> zone) and uncertain for HM. Marine flooding events may have been recorded in the carbonate interval in sections CH, RI, PF, AB, and CL.	<b>Drowning</b> of the carbonate platform on the Tennessee embayment. Graptolitic, calcareous shales deposition ( <i>D. teretiusculus</i> zone) at CI (Finney et al., 1996).
1	late Middle Ordovician (middle Whiterockian, ca 466-464 Ma)	<b>Localized onset of carbonate deposition</b> in section PF ( <i>C. friendsvillensis</i> zone), and uncertain in sections CH, RI, AB, and CL.	<b>Drowning</b> of the carbonate platform on the accommodation zone and Alabama promontory. Graptolitic shales deposition ( <i>D. murchisoni</i> zone) at RK, LM, FC, and HV (Finney et al., 1996).
		<b>Post-Knox unconformity</b> . This surface incorporates surfaces 1, 2, 3, 4, or 5 due to the diachronous onset of carbonate deposition in the distal foreland.	<b>Post-Knox unconformity</b> . This surface corresponds to surface 1 in section HV (Alabama promontory). In sections FC, FM, and RK (accommodation zone) peritidal carbonates < 38 m thick overlie the unconformity and underlie surface 1.

**Table 4.4** Parameters for sandstone point counts

Symbol	Grain category	Recalculated parameters
Qm	Monocrystalline quartz	<b>Q+F+L:</b>
Qpf	Foliated polycrystalline quartz	$Q = Qm + Qpf + Qpo + Ch$
Qpo	Non-foliated polycrystalline quartz	$F = P + K + Fu$
Ch	Chert	$L = Ls + Lv + Lm + Lu$
P	Plagioclase feldspar	
K	Potassium feldspar, microcline	<b>Qm+F+Lt:</b>
Fu	Unidentified feldspar, albitized feldspar	$Qm = Qm$
Ls	Sedimentary lithic fragments	$F = P + K + Fu$
Lm	Metamorphic lithic fragments	$Lt = Ls + Lv + Lm + Lu +$
Lv	Volcanic (devitrified) lithic fragments	$Qpf + Qpo + Ch$
Lu	Unidentified lithic fragments	
Lp	Plutonic rock fragments (0.0 indicate presence)	
Rc	Carbonate rock fragments (excluding skeletal fragments)	

Inters. = Interstitial (matrix-cement) points (n) / framework points (300) + n

**Table 4.5** Raw point-count data and recalculated modal point-count data for sandstones of the Blountian clastic wedge. Stratigraphic levels of samples are shown in Figures 4.8 to 4.10 for proximal foreland sandstones and in Figures 4.6 and 4.7 for middle to distal foreland sandstones. For each sandstone group, a mean and standard deviation is calculated and plotted in Ternary diagrams in Figures 6B and 9D. See Table 4.4 for explanation of codes and recalculated parameters

Sandstone Group	Sample	Inter s.	QUARTZ				FELDSPAR				LITHICS				QFL			QmFLt			
			Qm	Qpf	Qpo	Ch	P	K	Fu	Ls	Lm	Lv	Lu	Lp	Rc	Q	F	L	Qm	F	Lt
Group 1. Athens Shale, sections FM, LM, CL.	S2-2216	7.7	54.3	0.6	8.6	0.0	3.3	3.3	25.3	3.6	0.6					63.8	32.0	4.2	54.5	32.0	13.5
	I4-0601	57.6	46.0	1.6	6.6	4.3	9.6	9.0	13.6	3.6	2.3			3.0		58.7	32.3	8.9	46.2	32.3	21.5
	O4-0401s	29.4	58.6	1.0	6.3	1.3	14.3	3.0	5.3	5.6	3.0	0.3	1.0			67.4	22.7	9.9	58.8	22.7	18.6
	O4-0403	46.2	39.6	1.0	6.3		23.3	2.0	23.6	1.3	2.6					47.0	49.0	3.9	39.7	49.0	11.2
Group 2. Athens Shale, section HV	R3-0401	29.6	65.0	3.6	2.6	2.0	9.6	1.3	9.3	3.6			2.3	0.0		73.7	20.3	5.9	65.5	20.3	14.2
	R3-0801	29.6	70.0	1.6	3.3	1.3	4.3	1.6	8.0	8.6	0.3		0.6	0.0		76.5	14.0	9.5	70.3	14.0	15.8
	R3-0803	31.8	54.3	3.3	7.0	2.3	5.6	5.3	9.3	8.3	2.6		1.6			67.2	20.3	12.6	54.5	20.3	25.2
	R3-0806	51.5	49.6	1.3	6.3	1.0	16.3	6.3	11.3	4.6	1.3		1.6			58.4	34.0	7.5	49.8	34.0	16.2
Group 3. Rockmart Slate, section RK.	H3-1007	45.8	73.0	2.0	4.3	0.3	8.6	0.0	8.6	0.3	0.6			0.0	2.0	81.5	17.6	0.9	74.7	17.6	7.7
	H3-1008	47.2	73.5	3.5	4.5	0.0	13.5	0.0	4.0	1.0						81.5	17.5	1.0	73.5	17.5	9.0
	H3-1009	39.0	75.0	1.6	6.0	4.6	4.0	0.0	7.6	0.0	1.0					87.4	11.6	1.0	75.2	11.6	13.2
	H3-1012	45.4	76.0	1.6	5.3	1.6	9.6	0.0	4.0	0.6	1.0					84.8	13.6	1.6	76.2	13.6	10.1
	H3-1013	38.8	82.3	1.0	6.0	0.6	2.6	0.0	7.3							90.1	9.9	0.0	82.5	9.9	7.6
	H3-1301	49.4	81.0	0.5	10.0	0.0	3.5	0.0	5.0							91.5	8.5	0.0	81.0	8.5	10.5
	H3-1303	45.7	87.0	1.5	3.0	2.0	3.5	0.0	2.0				1.0			93.5	5.5	1.0	87.0	5.5	7.5
Group 4. Athens Shale, section CI.	E3-1904	34.8	49.6	0.0	3.3	0.0	14.3	2.6	18.0	3.0	1.6			0.0	7.3	57.3	37.8	5.0	53.7	37.8	8.5
	E3-2101	48.5	33.0	0.0	2.5		17.0	5.5	29.5	3.0	2.0			0.0	7.5	38.4	56.2	5.4	35.7	56.2	8.1
	E3-2106	49.5	35.5		0.5	0.0	18.5	5.0	22.5	3.0	1.0			0.0	14.0	41.9	53.5	4.7	41.3	53.5	5.2
Group 5. Athens Shale, section CI.	E3-2102	20.6	74.0	0.5	5.0	0.5	2.0	7.5	8.5	2.0				0.0		80.0	18.0	2.0	74.0	18.0	8.0
	E3-2103	32.4	70.6	0.3	3.0	0.6	9.3	8.3	5.6	1.6	0.3			0.0		74.8	23.3	1.9	70.9	23.3	5.8
	E3-2104	33.3	72.6	0.0	1.6	0.3	5.0	1.3	11.0	3.0				0.0	5.0	78.6	18.2	3.2	76.6	18.2	5.2
	E3-2105	26.2	86.5	1.0	2.5	0.5	0.5	4.5	3.5	1.0						90.5	8.5	1.0	86.5	8.5	5.0
Group 6. Chota Formation, section CI.	E3-2202	61.1	40.0		2.0	0.0	24.5	0.5	8.0	11.0	0.5				13.5	48.6	38.2	13.3	46.2	38.2	15.6
	E3-2201	59.8	43.0	0.0	1.5	0.5	17.0	0.5	6.0	2.5	0.5				28.5	62.9	32.9	4.2	60.1	32.9	7.0
	E3-2203	36.6	50.3	0.3	0.6	0.0	5.3	3.3	6.6	1.6	0.3				31.3	75.0	22.3	2.8	73.6	22.3	4.1
Group 7. Chota Formation, section CI.	E3-2204	29.7	67.6	0.6	2.0	3.0			0.6	10.0	0.3				15.6	87.0	0.7	12.2	80.4	0.7	18.9
	E3-2205	31.5	61.6	1.0	2.6	0.6			0.3	16.0	1.0				16.6	79.2	0.4	20.5	74.1	0.4	25.5
	E4-2901	28.4	77.0	0.6	4.0	1.3			0.3	15.6	1.0					83.1	0.3	16.6	77.2	0.3	22.5
	E4-2902	33.3	79.3	0.3	4.0	0.6			2.6	12.3	0.3		0.3			84.5	2.6	12.9	79.5	2.6	17.9
	E4-2903	42.9	72.0	0.0	2.5	3.0			3.0	19.1	0.5					77.4	3.0	19.6	71.9	3.0	25.1
Group 8. Chota Formation, section CI.	E3-2207	32.0	78.0	3.5	5.5	3.0			1.0	9.0						90.0	1.0	9.0	78.0	1.0	21.0
	E3-2206	28.7	88.3	2.6	1.0	6.0			0.6	1.3						98.1	0.6	1.3	88.5	0.6	10.9

0.0 denotes trace amounts of that fragment in the sample



**Table 4.6** Sm-Nd isotopic data for Middle and Upper Ordovician strata from the Blountain clastic wedge. Samples are distributed in three areas, which are from south to north, the Alabama promontory, the Tennessee embayment, and the Virginia promontory.

Sample	Location	Unit	Rock type	Biostratigraphy (1)		Sm ppm	Nd ppm	$^{147}\text{Sm}/^{144}\text{Nd}$	$^{143}\text{Nd}/^{144}\text{Nd}$	$\epsilon_{\text{Nd}}$	$\epsilon_{\text{Nd}}$	$T_{\text{DM}}$ (Ga)	reference
				graptolite	Ma			(3)	(4)	present	initial		
				conodont	(2)			(3)	(4)	(5)	(5,6)	(7)	
<b>Alabama promontory</b>													
R3-0504	Harpersville	Athens	shale	<i>D. murchisoni</i>	463			0.1305	0.511902 ± 11	-14.4	-10.6		this study
duplicate													
V-1	Vincent	Athens	shale	<i>D. murchisoni</i>	463	4.09	21.30	0.1162	0.511896 ± 9	-14.5	-9.9	1.79	Gleason et al., 2002
S2-2406	Calera	Lenoir	bentonitic shale	<i>P. serra</i>	460			0.1587	0.512022 ± 10	-12.0	-9.9		this study
Duplicate (7)													
S2-2502	Calera	Lenoir	calcareous shale	<i>P. serra</i>	460			0.1469	0.512015 ± 10	-12.2	-9.4		this study
17-2	Calera	Athens	shale	<i>G. teretiusculus</i>	458	5.23	27.71	0.1141	0.511939 ± 9	-13.6	-8.9	1.69	Gleason et al., 2002
26/28	Calera	Athens	shale	<i>G. teretiusculus</i>	458	4.67	24.26	0.1163	0.511932 ± 7	-13.8	-9.2	1.74	Gleason et al., 2002
84/3	Calera	Athens	shale	<i>N. gracilis</i>	457	5.16	27.38	0.1139	0.511921 ± 11	-14.0	-9.2	1.71	Gleason et al., 2002
106-1	Calera	Athens	shale	<i>N. gracilis</i>	457	6.20	33.08	0.1134	0.511941 ± 22	-13.6	-8.8	1.67	Gleason et al., 2002
M3-2305	Greensport	Greensport	dolomitic shale	<i>P. sweeti</i>	455			0.1151	0.511951 ± 10	-13.4	-8.8		this study
M3-2203	Greensport	Colvin Mountain	siltstone	<i>B. compressa</i>	454			0.0974	0.511929 ± 8	-13.8	-8.2		this study
K3-2906	Big Ridge	Sequatchie	shale	<i>A. ordovicicus</i>	446			0.0944	0.511965 ± 11	-13.1	-7.3		this study
<b>Tennessee embayment</b>													
M-1	Mosheim	Blockhouse	shale	<i>G. tere.-N. gracilis</i>	458	5.86	31.30	0.1132	0.511876 ± 5	-14.9	-10.0		Andersen and Samson, 1995
M-2	Mosheim	Blockhouse	shale	<i>G. tere.-N. gracilis</i>	458	6.10	33.30	0.1108	0.511899 ± 6	-14.4	-9.4		Andersen and Samson, 1995
SHD-8-3	Holston dam	Blockhouse	sandstone	<i>N. gracilis</i>	457	7.27	34.20	0.1318	0.512045 ± 6	-11.6	-7.8		Andersen and Samson, 1995
SHD-6-2	Holston dam	Blockhouse	shale	<i>N. gracilis</i>	457	10.10	48.50	0.1254	0.512031 ± 8	-11.8	-7.7		Andersen and Samson, 1995
HOL-1	E. Tennessee	Tellico	shale		457	9.21	49.35	0.1127	0.512001 ± 8	-12.4	-7.5	1.57	Gleason et al. 1995
HOL-2	E. Tennessee	Tellico	lithic sandstone		457	6.30	33.43	0.1139	0.512028 ± 5	-11.9	-7.0	1.55	Gleason et al. 1995
SHD-3-6	Holston dam	Tellico	shale	<i>N. gracilis</i>	456	7.86	41.20	0.1154	0.512031 ± 5	-11.8	-7.1		Andersen and Samson, 1995
SHD-3-4	Holston dam	Tellico	shale	<i>N. gracilis</i>	456	8.23	40.80	0.1218	0.512010 ± 7	-12.2	-7.9		Andersen and Samson, 1995
TH-2	E. Tennessee	Mantirsburg	lithic sandstone		450	6.30	28.12	0.1355	0.512000 ± 7	-12.4	-8.9	2.03	Gleason et al. 1995
TH-1	E. Tennessee	Juniata	lithic sandstone		445	9.17	41.45	0.1337	0.512095 ± 5	-10.6	-7.0	1.80	Gleason et al. 1995
TH-3	E. Tennessee	Clinch	quartzose sandstone		440	3.45	16.40	0.1272	0.512044 ± 7	-11.6	-7.7	1.76	Gleason et al. 1995
<b>Virginia promontory</b>													
C-5	Chilhowie	Rich Valley	shale	<i>N. gra.-C. bicornis</i>	457	6.30	34.60	0.1100	0.511878 ± 4	-14.8	-9.7		Andersen and Samson, 1995
311-2	Blacksburg	Bays	sandstone		454	7.80	35.30	0.1333	0.512131 ± 5	-9.9	-6.2		Andersen and Samson, 1995

(1) conodont zones from Hall et al. (1986); graptolite zones from Finney et al (1996).

(2) Sample M3-2203 is few meters below the Millbrig K-bentonite and a 454 Ma is assigned. Assignment of ages for other samples is relative and accommodates the samples in an older-to-younger order, as depicted in Figure 13 and using the time framework of Figure 4.4 Ages of samples TH-1, TH-2, and TH-5 from Gleason et al. (1995).

(3) two-sigma error better than 1% for data of this study; better than 0.5% for Gleason et al. (2002)

(4) measured ratio, normalized to  $^{146}\text{Nd}/^{144}\text{Nd} = 0.7219$ . Uncertainties are  $\pm 2$  s (Anderson and Samson, 1995); are  $\pm 2$  s of the mean on 105 ratios, and reflect in-run precision for the other data.

(5) this study follows Gleason et al (2002) calculations; for other samples, see original papers

$$\epsilon_{\text{Nd}} = 10^4 \left[ \frac{^{143}\text{Nd}/^{144}\text{Nd}_{(\text{SAMPLE})}}{^{143}\text{Nd}/^{144}\text{Nd}_{(\text{CHUR})}} - 1 \right]; \quad ^{143}\text{Nd}/^{144}\text{Nd}_{(\text{CHUR})} = 0.512638$$

(6) calculated for 450 Ma in data from Gleason et al. (2002) and this study

(7) Nd isotopic ratio only was calculated



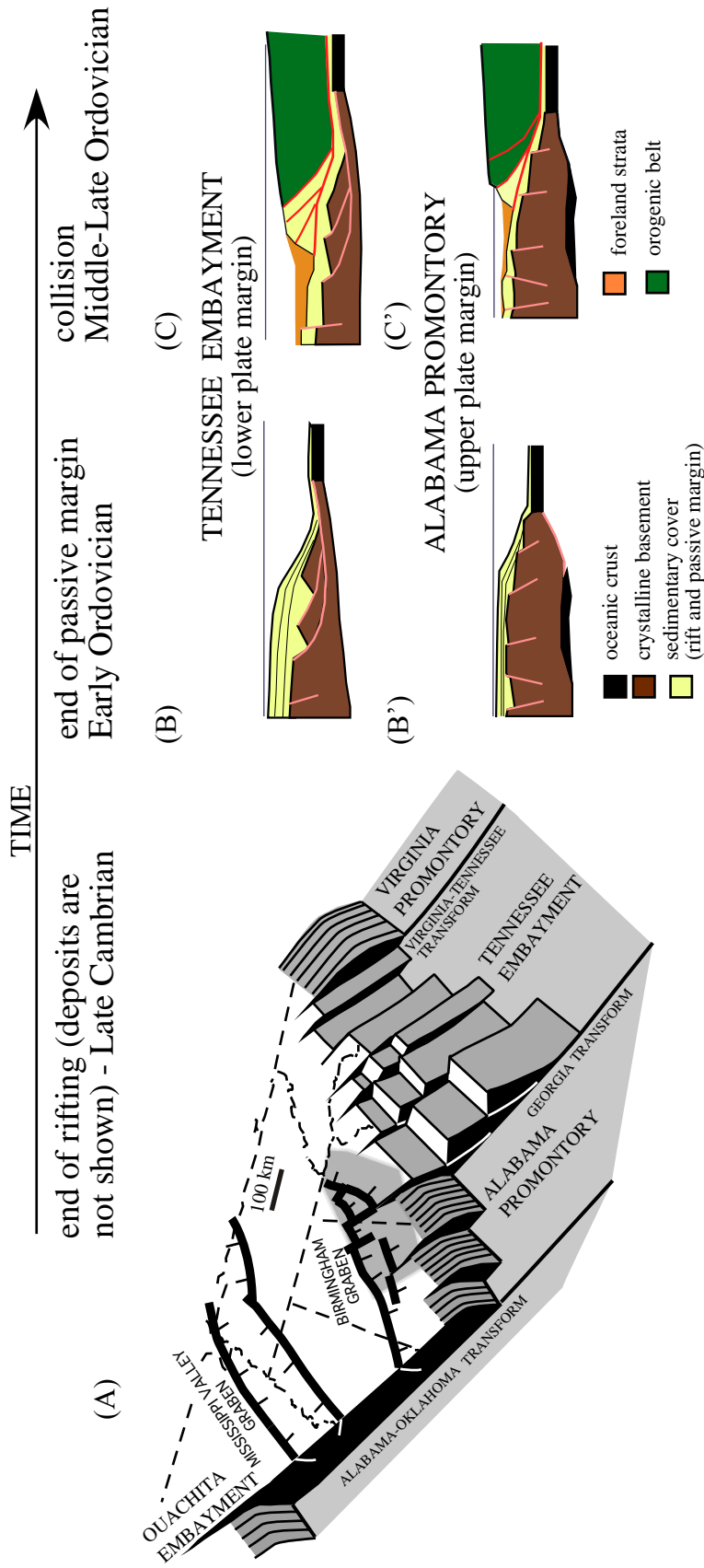


**Figure 4.1** (A) Three-dimensional block diagram illustrates the marginal and intraplate basement structural configuration of southern Laurentia after Cambrian rifting (Thomas, 1993). The study area (shaded polygon southeast of the Birmingham graben) encompasses the northern part of the Alabama promontory, an accommodation or transfer zone that may connect with the Georgia transform, and the southern part of the Tennessee embayment. The Birmingham graben bounds the study area on the northwest (trace of basement faults from Chapter 2). The three-dimensional block shows only the northwest boundary fault systems (short tick on the downthrown side) of the Birmingham graben and another graben system to the southeast. (B) and (B') Schematic structural profiles showing basement structures and overlying rift and passive-margin sedimentary cover for the Alabama promontory and Tennessee embayment. The synrift and passive-margin succession on the Tennessee embayment is thicker than the sedimentary cover on the Alabama promontory. (C) and (C') Schematic structural profiles across the foreland-orogenic belt. Note the difference in deformation of the orogenic belt and thickness of foreland strata between the profile at the promontory and the profile at the embayment.

**Figure 4.2**

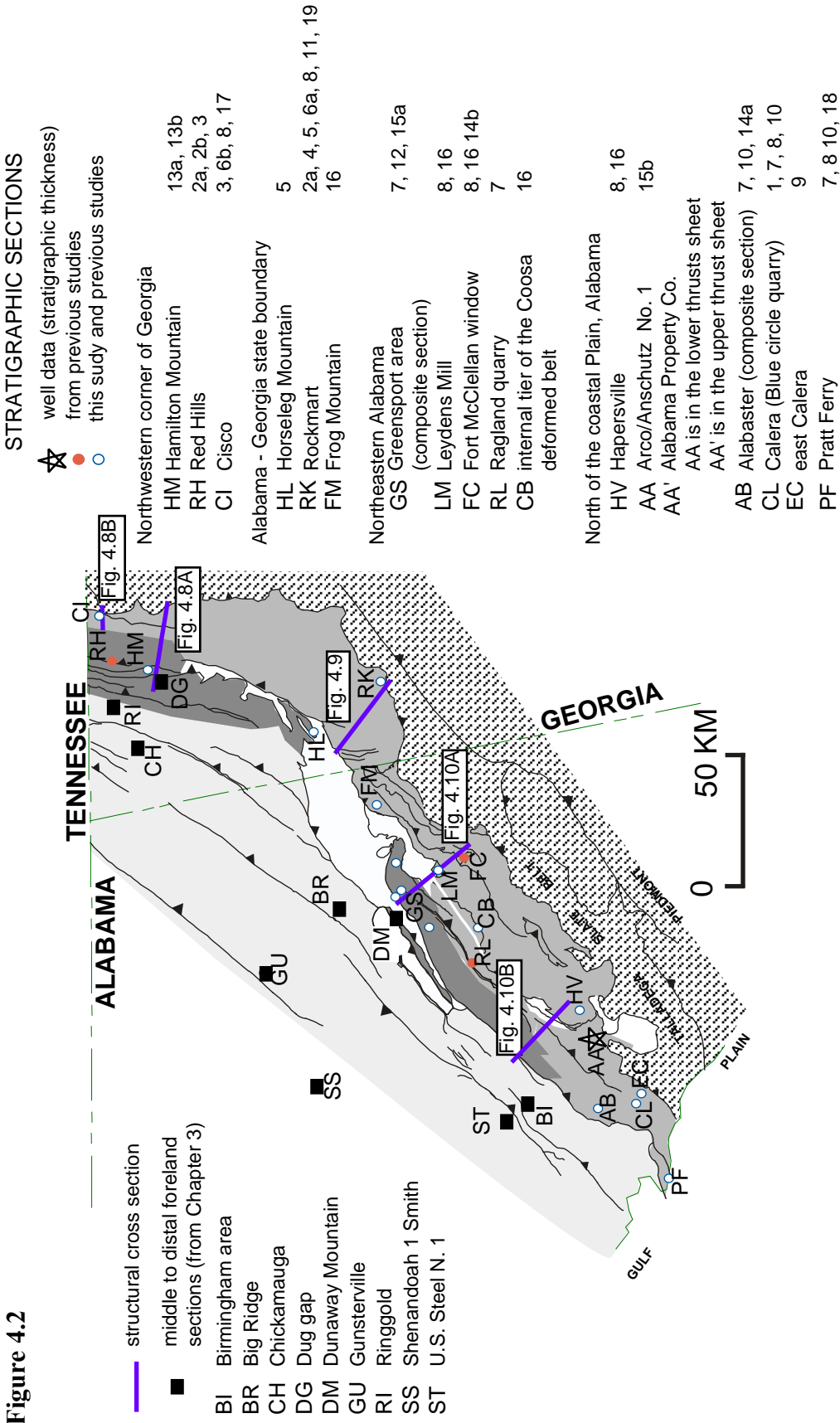


**Figure 4.2** (previous page) Location of study sections and distribution of lithofacies belts of the Middle and Upper Ordovician strata in the Appalachian thrust belt of Georgia and Alabama. References to sources of stratigraphic sections are listed in alphabetic order: 1) Bearce, 1999; 2a) Bergström, 1973; 2b) Bergström 1977; 3) Caldwell, 1992; 4) Chowns, 1977; 5) Chowns and Carter, 1983; 6a) Cressler, 1970; 6b) Cressler, 1974; 7) Drahovzal and Neathery, 1971; 8) Finney et al., 1996; 9) Guthrie, 1994; 10) Hall et al., 1986; 11) Higgins et al., 1988; 12) Jenkins, 1984; 13a) Kath et al., 1994; 13b) Randal L. Kath, written communication, 2001; 14a) Osborne, 1996; 14b) Ed Osborne, written communication, 2001; 15a) Raymond, 1973; 15b) Raymond, 1991; 16) Thomas and Drahovzal in prep; 17) Salisbury, 1961; 18) Shaw et al., 1989; 19) Sibley, 1983. See Chapter 3 for a complete list of references to sources of stratigraphic sections and a more detailed description of sections in the middle to distal foreland.

Figure 4.3

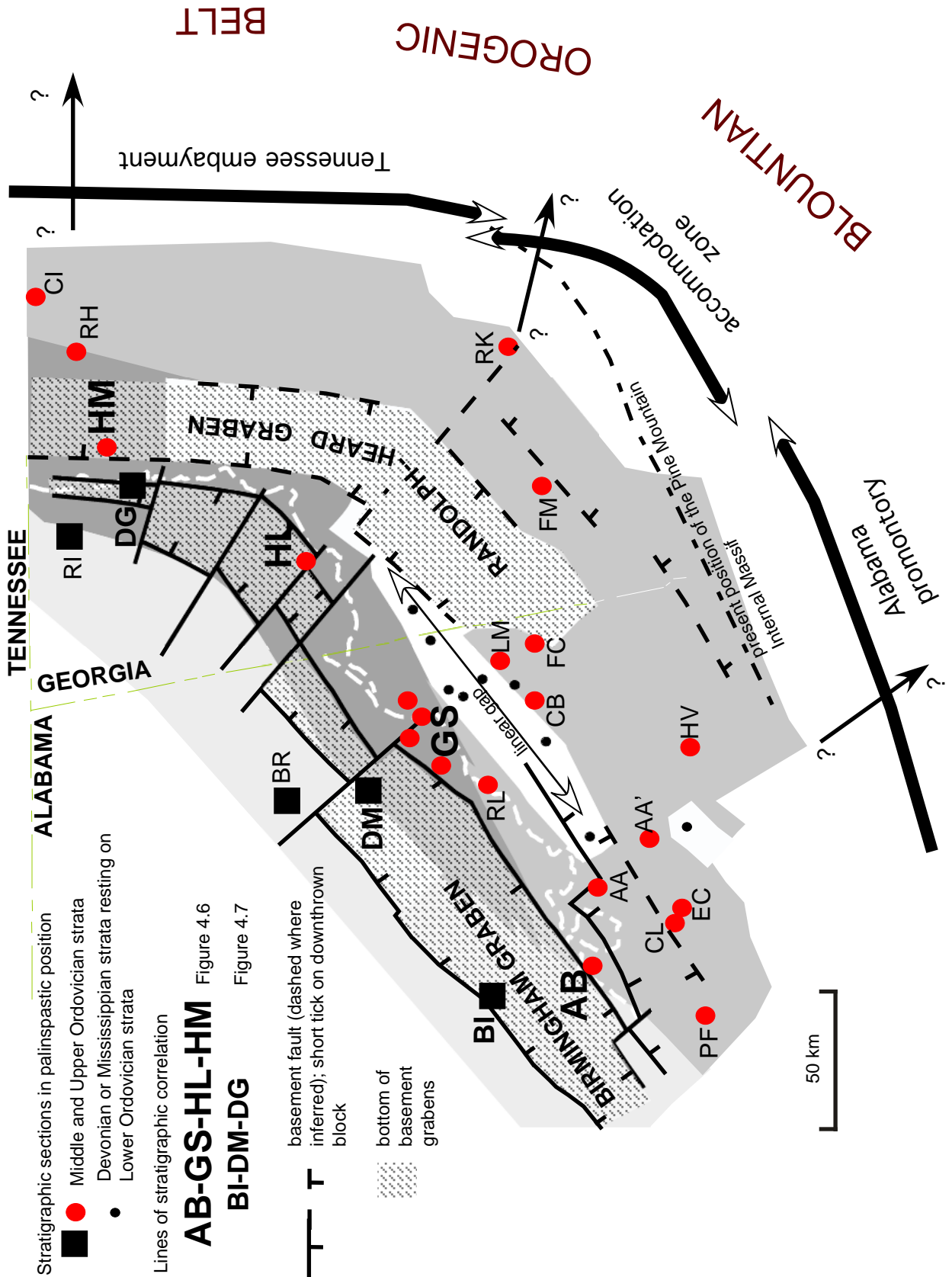


**Figure 4.3** (previous page) Palinspastic map showing location of study sections, lines of stratigraphic correlation, and lithofacies belts. See Figure 4.2 for explanation of lithofacies belts. The leading trace of the Appalachian metamorphic thrust belt (white dash line) is shown in present location for reference. Eastern boundary of the southeastern lithofacies belt corresponds to the trailing edge of unmetamorphosed Paleozoic rocks. See Chapter 2 for details on the construction of the palinspastic map. This Figure 4.3 also shows the distribution of study sections and lithofacies belts in relation to subsurface basement faults and the configuration of the rifted-margin of Laurentia (from Thomas, 1993). Note the concentration of cross-strike structures in the accommodation zone, which is parallel to the Georgia transform at the plate margin (Figure 4.1). Question marks between the southeasternmost sections and the orogenic belt indicate no constraint on the palinspastic distance to the leading edge of the Blountian orogenic belt. Black dash line shows the present location of the leading edge of the Pine Mountain internal basement massif (Osborne et al., 1988).

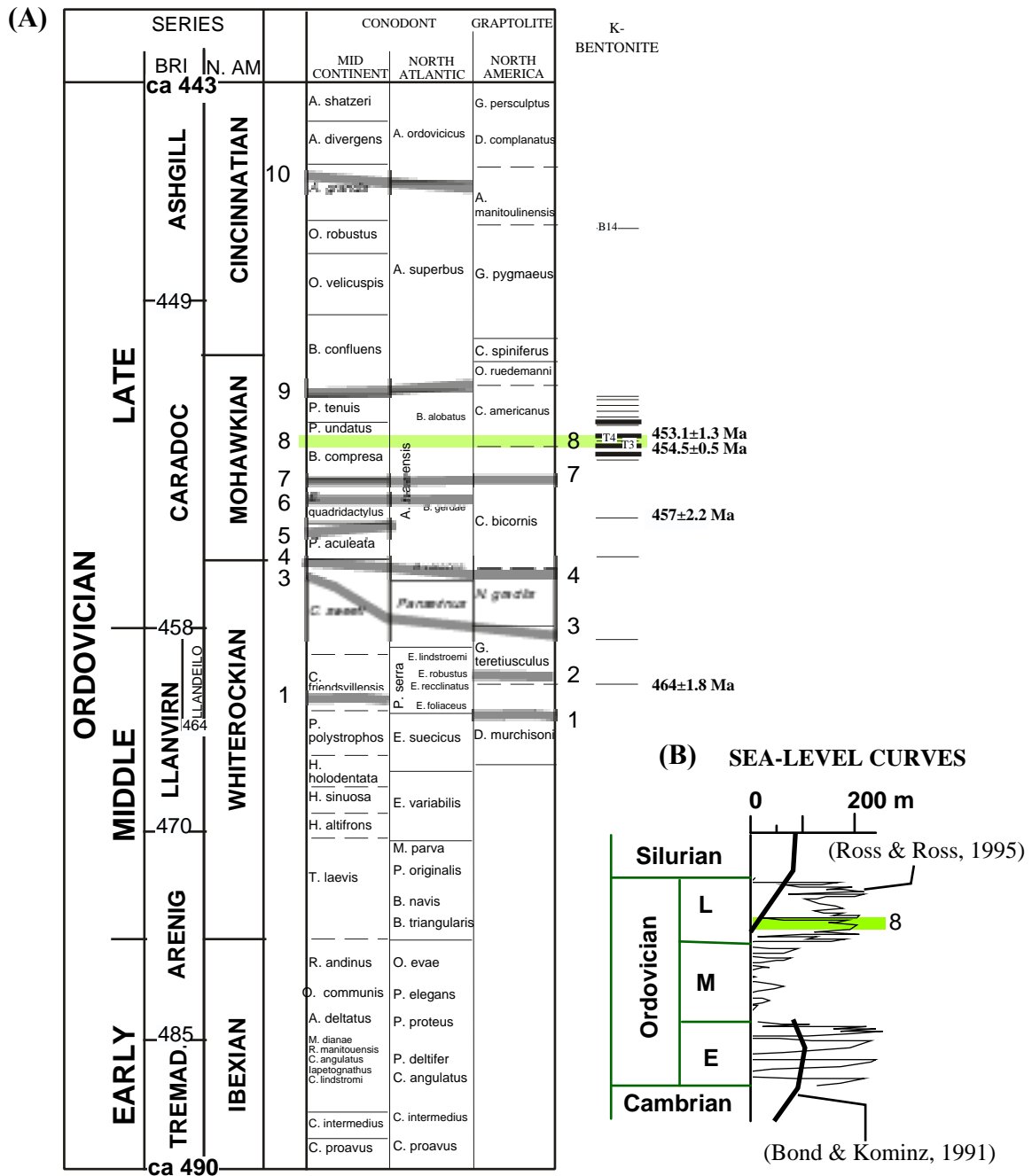
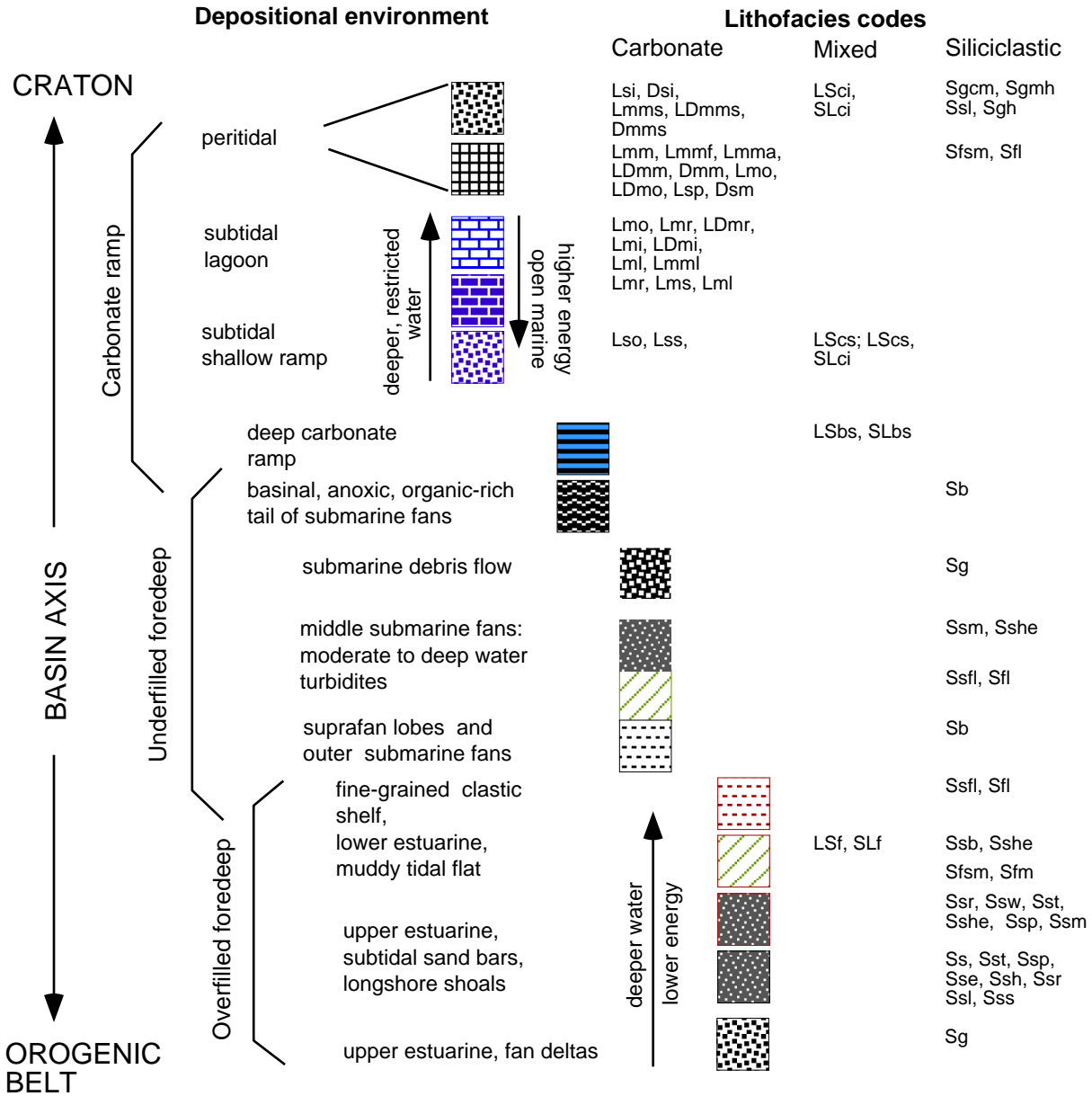


Figure 4.4

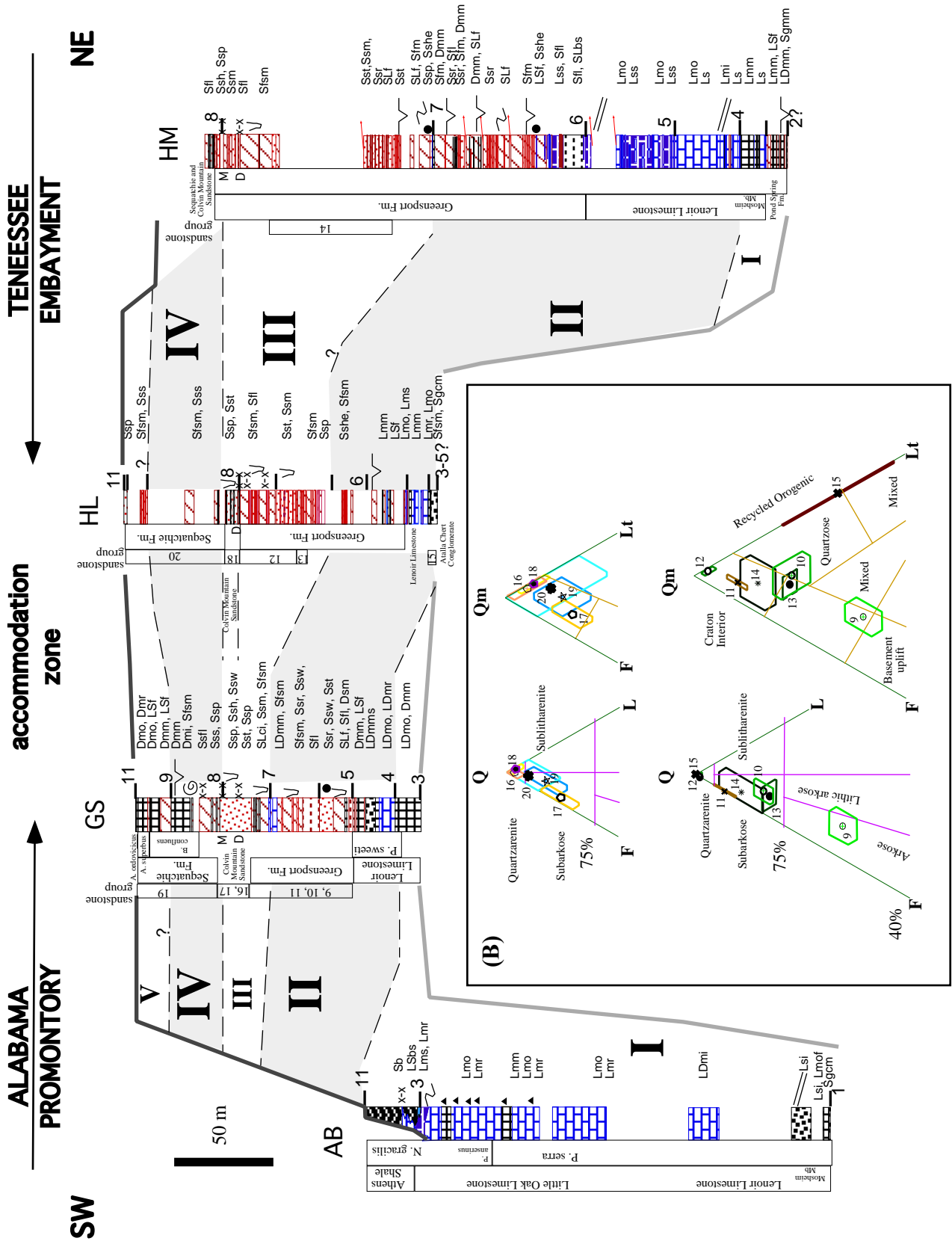
**Figure 4.4** (previous page) (A) Ordovician series (from Webby, 1998) and correlation of conodont zones, graptolite zones, and K-bentonite beds (modified from Kolata et al., 1996); radiometric ages of Mohawkian K-bentonites from Kolata et al. (1996, 1998), and of older K-bentonites from correlations made by Finney et al. (1996). Also are shown the positions of the stratigraphic surfaces discussed in the text (numbers 1 to 10, see Table 4.3 for definition of each of these surfaces). (B) Proposed Ordovician sea-level curves. Ross and Ross (1995) curve is based on third-order stratigraphic sequences from several key sections in North America. Bond and Kominz (1991) curve is relative to a section in the stable craton. The latter curve was used in constructing tectonic subsidence curves. The stratigraphic position of surface 8 is shown for reference.



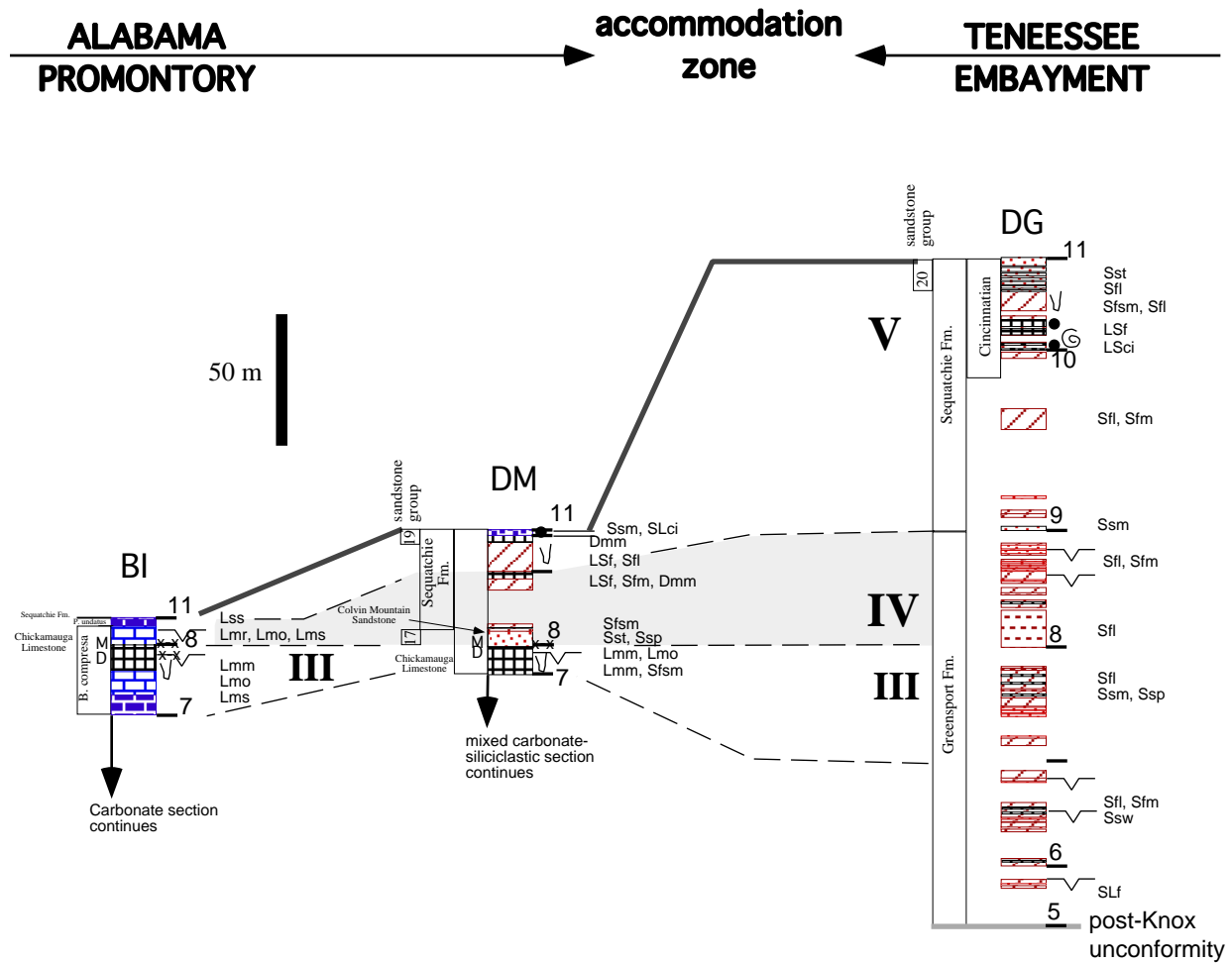
**Figure 4.5** Key to facies for stratigraphic columns in Figures 4.6 to 4.10. Explanation of lithofacies codes is given in Tables 4.1 and 4.2.



Figure 4.6



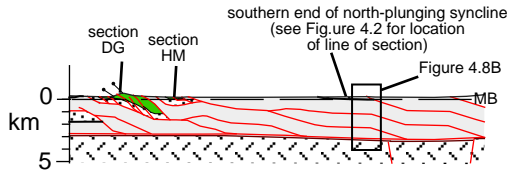
**Figure 4.6** (previous page) (A) Along-strike stratigraphic correlation of the middle Blountian foreland showing stratigraphic units, biostratigraphic data, lithofacies, stratigraphic correlation surfaces (numbered 1 to 11), and stratigraphic intervals (numbers I to V). Sections AB and GS palinspastically restore on the Alabama promontory and southeast of the Birmingham graben; section HL restores inside the graben and on the accommodation zone; and section HM restores on the Tennessee embayment and inside the Randolph-Heard graben (Figure 4.3). Datum of correlation is the Deicke and Millbrig K-bentonite beds (surface 8). Note the early record of thick carbonates and thin black shales in the southwestern section AB, the thinner but most complete stratigraphic record of section GS, and the northeastward thickening of red siliciclastic deposits. See Figure 4.3 for location of sections, and Figure 4.5 and Tables 4.1 and 4.2 for facies codes. (B) Ternary diagrams for middle Blountian foreland sandstones. See left column in stratigraphic sections and Table 4.5 for identification of sandstone groups; mean and standard deviations (polygons) of each group are plotted.



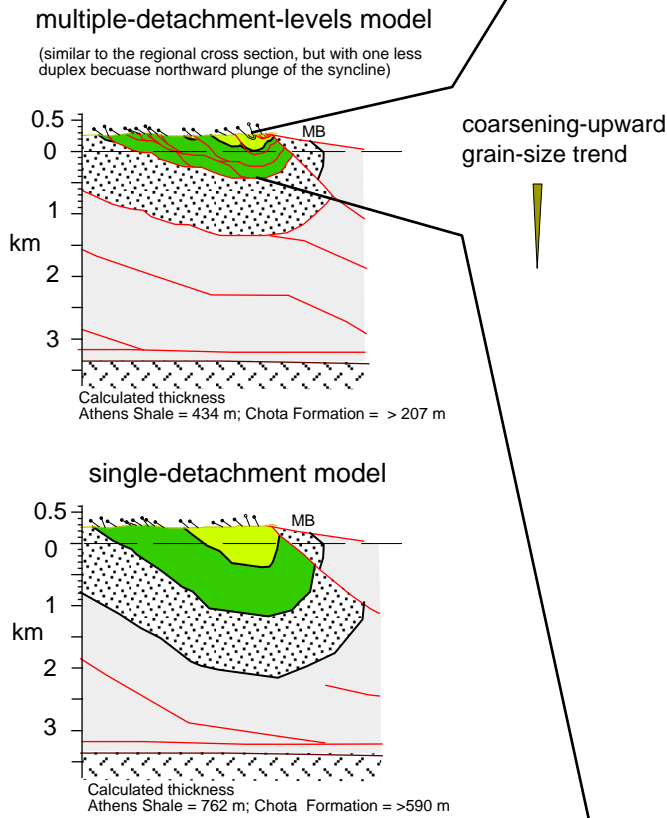
**Figure 4.7** Along-strike stratigraphic correlation of middle to distal foreland strata between stratigraphic surfaces of correlation 7 and 11. Sections show stratigraphic units, biostratigraphic data, lithofacies, stratigraphic correlation surfaces (numbered 5 to 11), and stratigraphic intervals (numbers III to V). All three sections palinspastically restore inside the Birmingham graben (Figure 4.3). This diagram shows thinning of the clastic wedge in Interval III toward section DM, and northeastward thickening of the clastic wedge in Intervals IV and V (datum of correlation is the Deicke and Millbrig K-bentonite beds, surface 8). See Chapter 3 for details of the stratigraphy in sections BI and DM below surface 7. See Figure 4.3 for location of sections, and Figure 4.5 and Tables 4.1 and 4.2 for facies codes. Provenance data of sandstone groups are in Figure 4.6B.

**Figure 4.8**

**(A) Regional cross section (25 km south of section C1)**



**(B) Local cross section (section C1; Cisco, Georgia)**



**LEGEND FOR CROSS SECTIONS**

- Chota Formation
- Athens Shale (Middle Ordovician to Lower Mississippian units for the regional cross section)
- Upper Cambrian - Lower Ordovician (Knox Group)
- Lower-Middle Cambrian
- Crystalline basement
- MB Metamorphic belt
- fault      ——— contact
- ∞ dip of beds at surface (open circle = overturned beds)

**(C) Stratigraphic column (section C; Cisco, Georgia)**

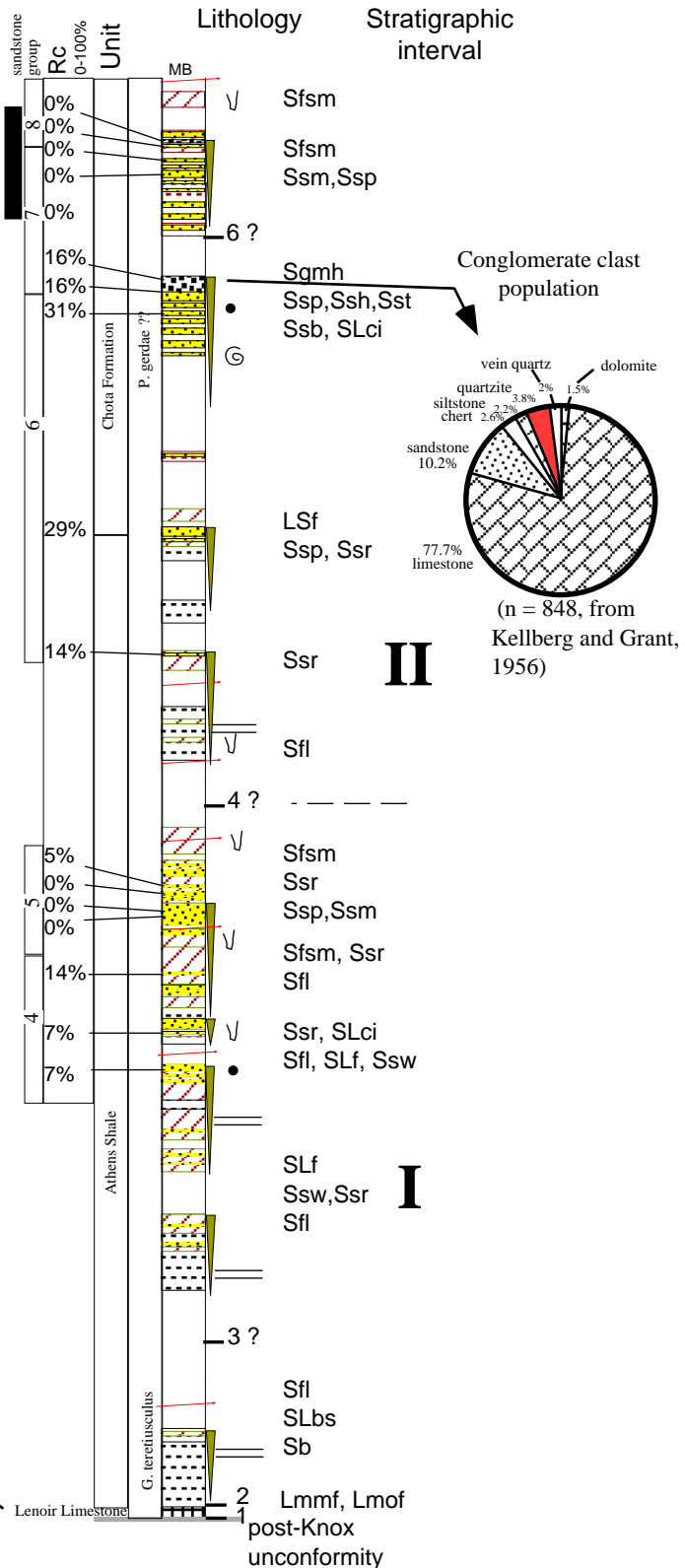
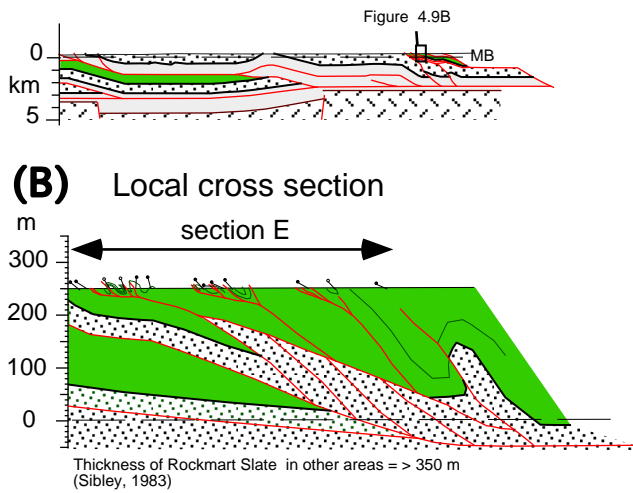


**Figure 4.8** (previous page) (A) regional structural cross section across stratigraphic sections DG and HM and at the southern end of the north-plunging syncline that includes stratigraphic section CI; (B) local structural cross section across stratigraphic section CI (see Figure 4.2 for location of cross sections). Interpretation of stratigraphic order and thickness depends on the structural model. I prefer the multiple-detachment-levels model because it honors the changes in dip domains and fits the regional duplex style of deformation in trailing structures of the Appalachian thrust belt in Georgia (Chapter 2). The single-detachment model is shown for comparison of the structure and calculated thickness of the Athens Shale and Chota Formation. (C) Stratigraphic column for section CI showing stratigraphic units, biostratigraphic data, lithofacies, stratigraphic correlation surfaces (numbered 1 to 6), stratigraphic intervals (numbers I to II), and conglomerate clast population for conglomeratic levels of the Chota Formation. Section CI palinspastically restores on the Tennessee embayment and includes the most complete record of proximal Blountian foreland stratigraphy. Sandstone beds in the middle of the Athens and conglomerate beds in the middle of the Chota Formation are in the tops of coarsening-upward successions that record the filling of the foredeep, the shoaling of depositional environments, and propagation of marginal deposits. Note the variable content of carbonate rock fragments (Rc) along the section. Provenance data of sandstone groups are in Figure 4.9D. See Figure 4.3 for location of section CI, and Figure 4.5 and Tables 4.1 and 4.2 for facies codes.

**Figure 4.9**

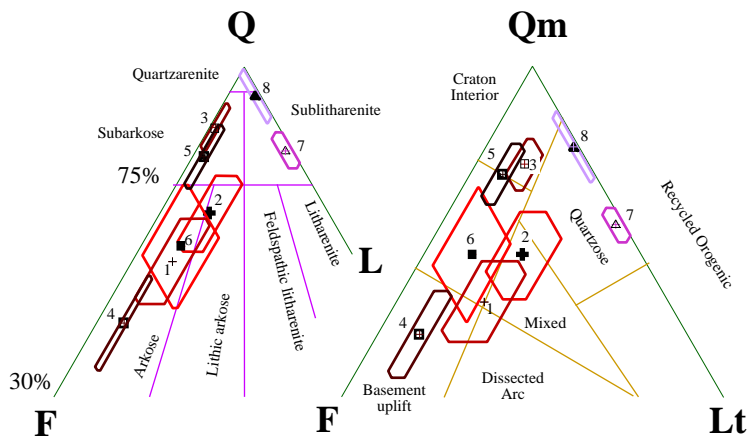
**(A)** Regional cross section  
(3 km west of section RK, Rockmart)



**LEGEND FOR CROSS SECTIONS**

- Lenoir Limestone and Rockmart Slate (Middle Ordovician to Lower Mississippian units for the regional cross section)
- Upper Cambrian - lower Ordovician (Knox Group)
- Lower-Middle Cambrian
- Crystalline basement
- MB Metamorphic belt
- fault      — contact
- ∩ dip of beds at surface (open circle = overturned beds)

**(D)** Ternary diagrams



**(C)** Stratigraphic column  
(section E; Rockmart, Georgia)

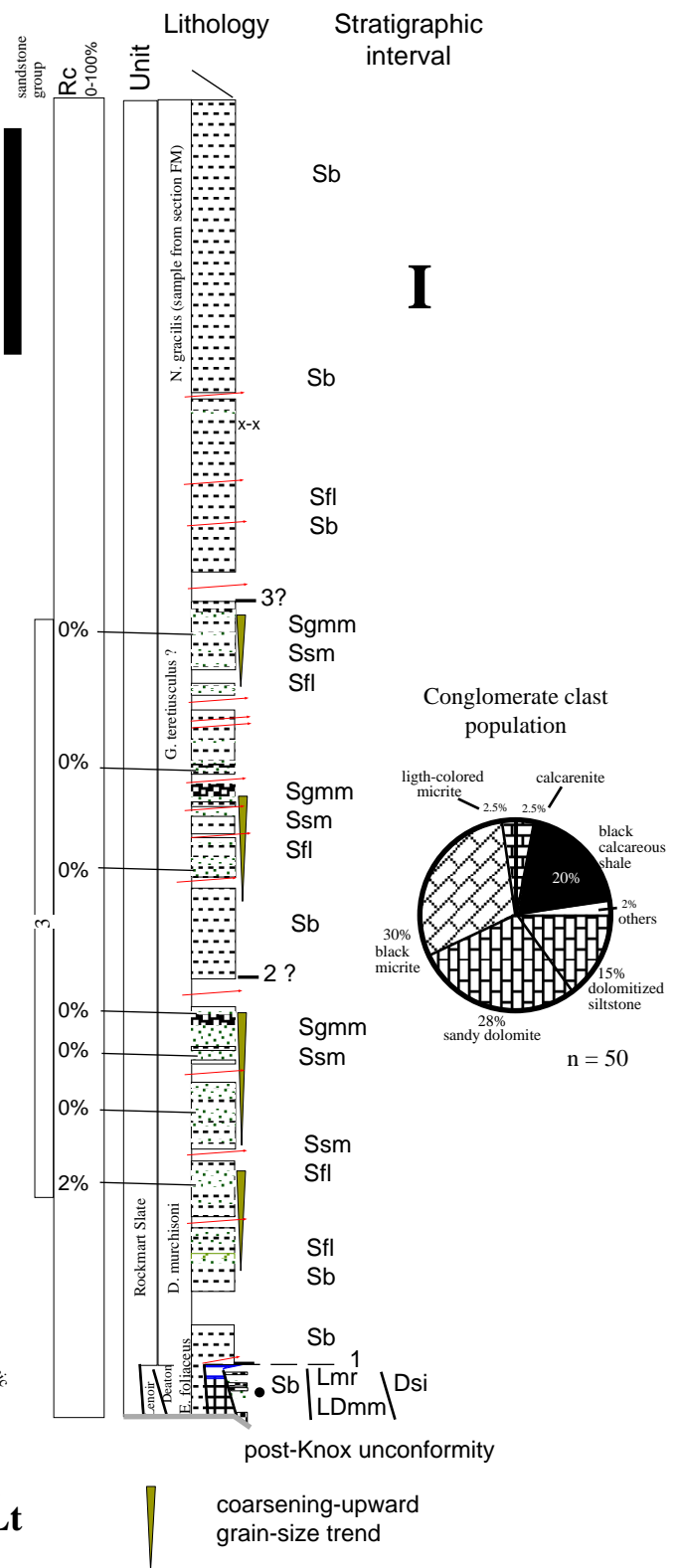
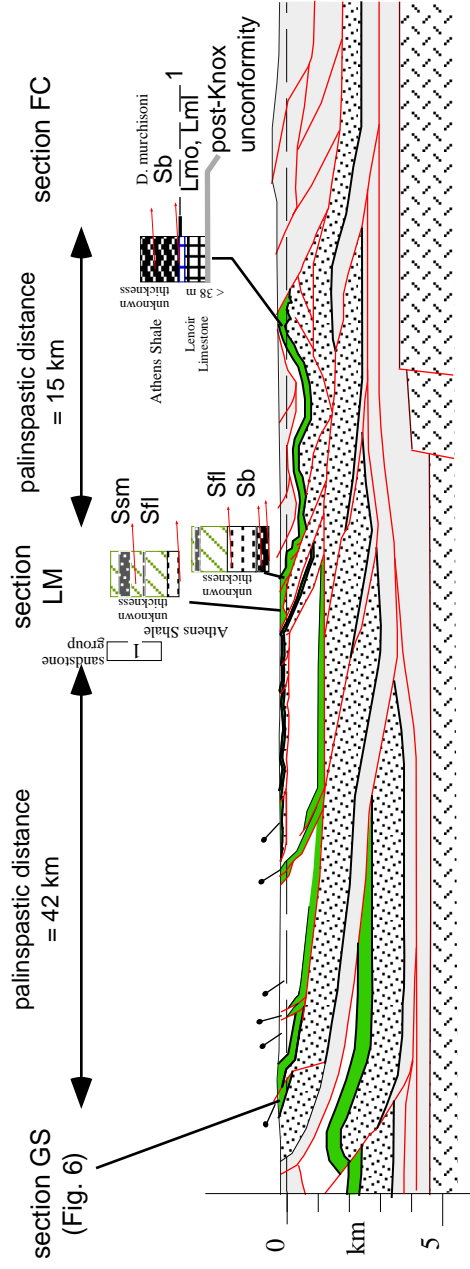


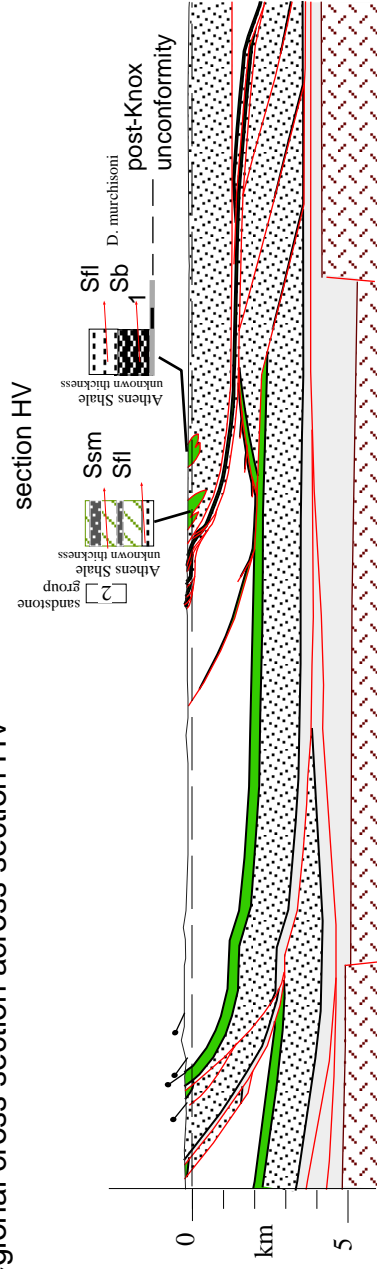
**Figure 4.9** (previous page) (A) and (B) are regional and local structural cross sections, respectively, near stratigraphic section RK (see Figure 4.2 for location of section). Interpretation of structural stacking of strata (deformation and lack of fossils preclude construction of a continuous stratigraphic column) depends on the structural model. We follow the model of overturned folds of Sibley (1983), and Alleghanian deformation followed multiple levels of detachment in upper units of the Knox Group and in the Athens Shale (similar structural style of the multiple-detachment-levels in Figure 4.8B). Other models of deformation considered structural fabrics of the Rockmart slate and the faulted contact with the Knox Group as pre-Alleghanian structures (e.g., Higgins et al., 1988). (C) Stratigraphic column for section RK showing biostratigraphic data, lithofacies, stratigraphic correlation surfaces (numbered 1 to 3), and conglomerate clast population. Section RK palinspastically restores on the accommodation zone and contains the most proximal record of the Blountian foreland. Note the heterogeneity of lithofacies in basal beds, the interbedding of conglomerate with sandstones in the lower half of the section, the dominance of fine-grained deposits in the upper half, and the very low content of carbonate rock fragments (Rc). See Figure 4.3 for location of section RK, and Figure 4.5 and Tables 4.1 and 4.2 for facies codes. (D) Ternary diagrams for proximal Blountian foreland sandstones. See left column in stratigraphic sections in Figures 4.8 to 4.10 and Table 4.5 for identification of sandstone groups; only the mean and respective standard deviations (polygons) of each group are plotted.

**Figure 4.10**

**(A) Regional cross section across sections GS, LM, and FC**



**(B) Regional cross section across section HV**



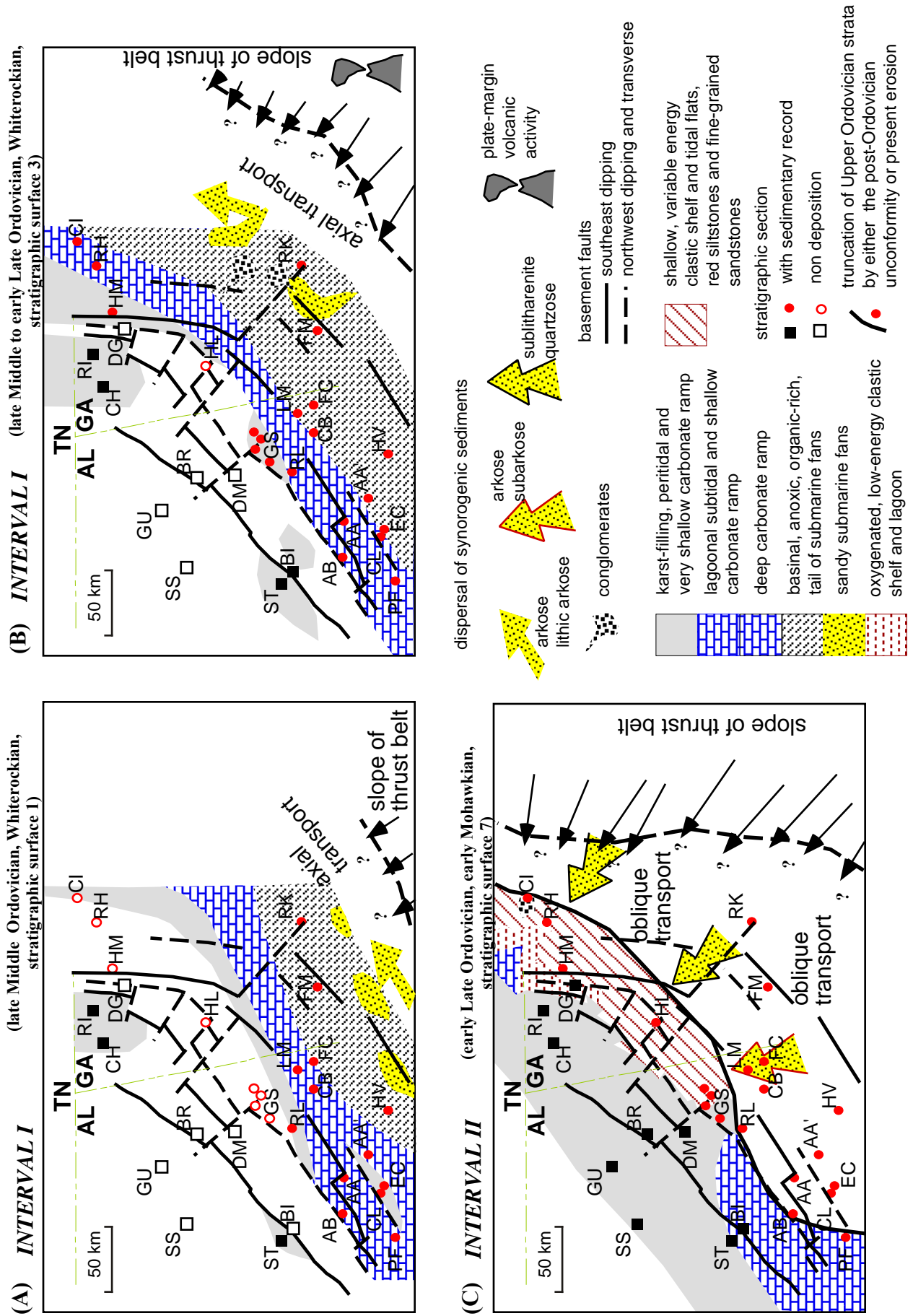
**LEGEND FOR CROSS SECTIONS**

- Upper Mississippian - Pennsylvanian
- Middle Ordovician - Lower Mississippian
- Lower-Middle Cambrian
- Crystalline basement
- Upper Cambrian - lower Ordovician (Knox Group)
- fault
- contact
- dip of beds at surface



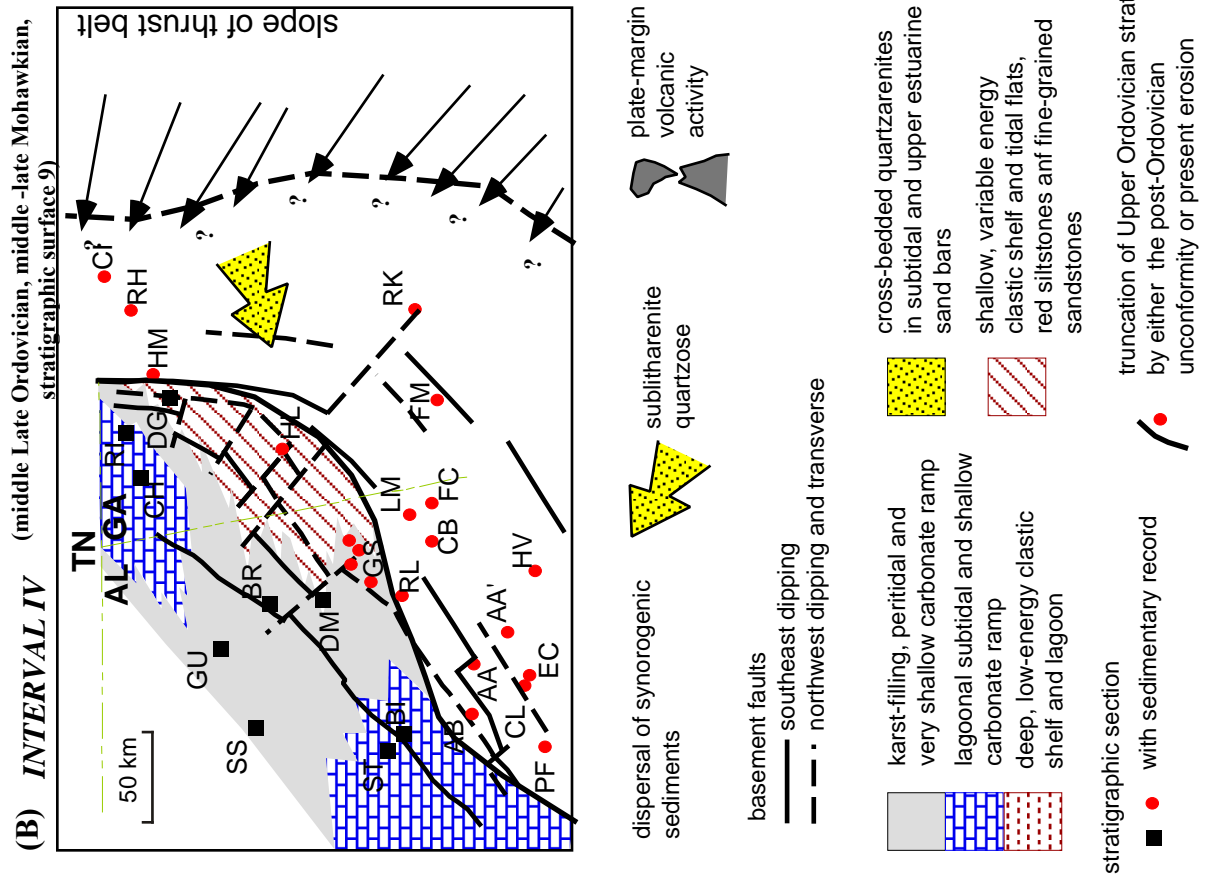
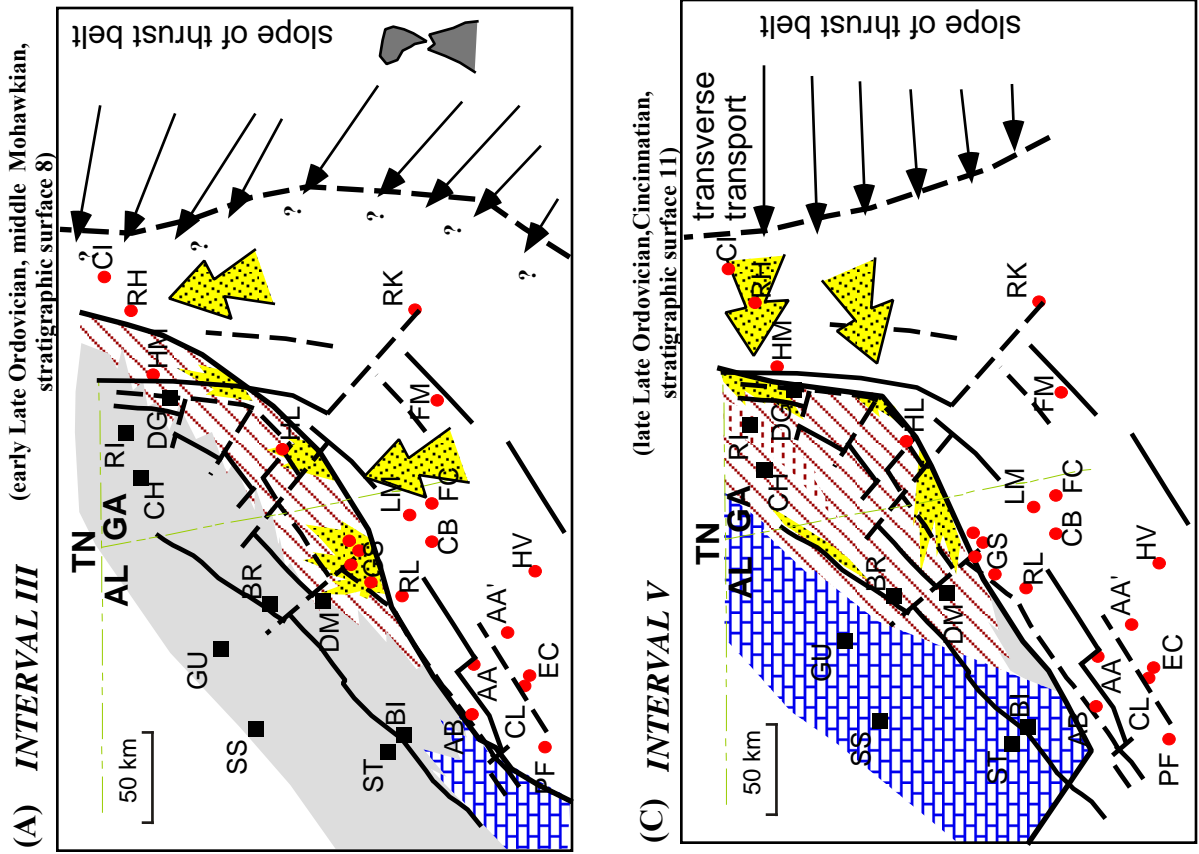
**Figure 4.10** (previous page) (A) and (B) are regional structural cross sections across sections GS, LM, FC (on Figure 10.A), and HV, which contain proximal foreland stratigraphy and restore on the Alabama promontory (see Figure 4.2 for location of sections). Poor exposures and intense deformation preclude construction of continuous stratigraphic columns and a calculation of stratigraphic thickness. Instead, vertical and lateral lithostratigraphic relations are defined in the present structural position (see stratigraphic column for each section), but following the stratigraphic trend observed in sections CI and RK (Figures 4.8 and 4.9, respectively). Biostratigraphic data are also shown in each section. In these proximal sections on the Alabama promontory, graptolitic black shales (comparable to the lower beds in sections CI and RK) are in different structures than the turbiditic sandstones (comparable to intermediate beds in sections CI and RK). Note that surface of correlation 1 is at the post-Knox unconformity in section HV; other proximal foreland sections farther northeast (e.g. sections FC and RK) have a thin succession of peritidal carbonates between the post-Knox unconformity and stratigraphic surface of correlation 1. See Figure 4.3 for location of sections, and Figure 4.5 and Tables 4.1 and 4.2 for facies codes. Provenance data of sandstone groups are in Figure 4.9D.

Figure 4.11

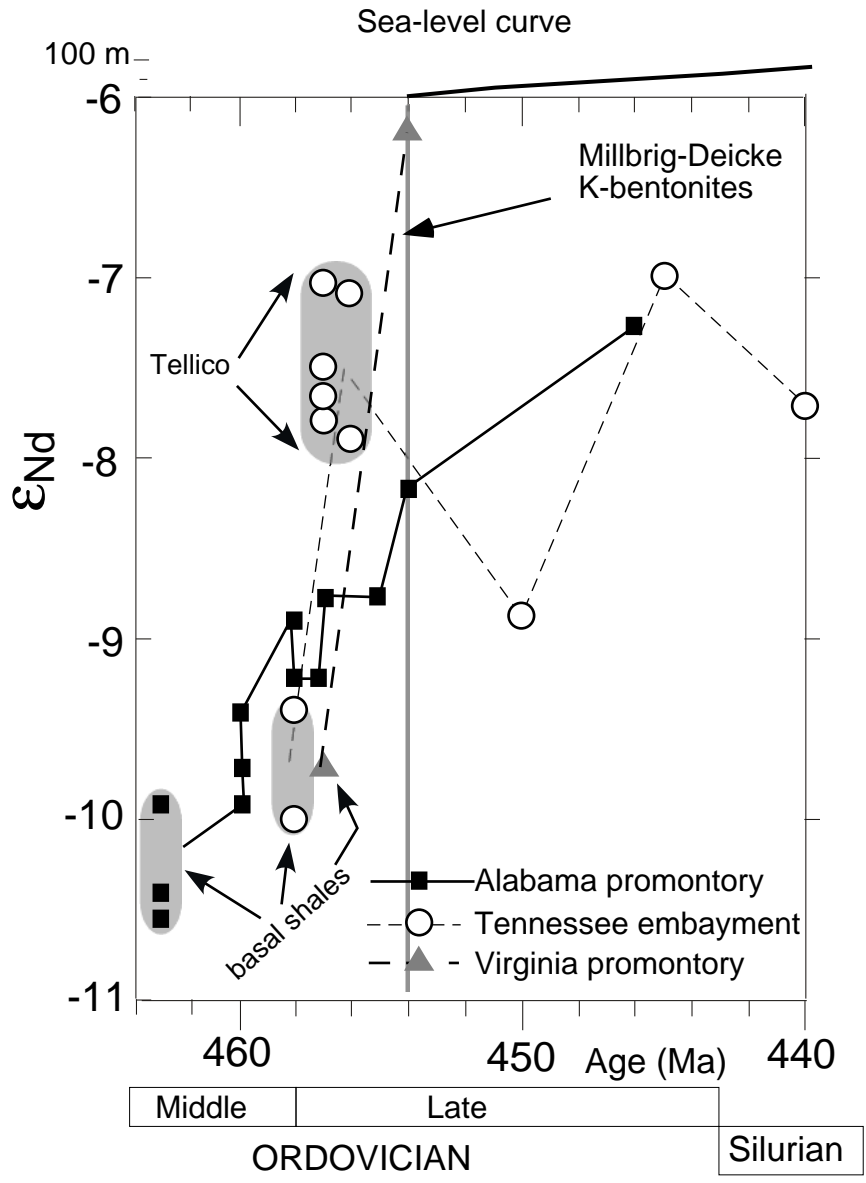


**Figure 4.11** (previous page) Paleogeographic maps showing the evolution of the underfilled stage of the Blountian foreland basin through the Middle Ordovician to early Late Ordovician. Each map represents the time of deposition for deposits underlying the stratigraphic surface indicated. Location of source areas for synorogenic detritus is shown tentatively on the east side of each diagram. Note the northeastward and northwestward migration of basinal black-shale deposition and drowning of the carbonate platform, and the diachronous and irregular onset of carbonate deposition on middle to distal foreland areas. See Figure 4.2 for key code of sections.

Figure 4.12

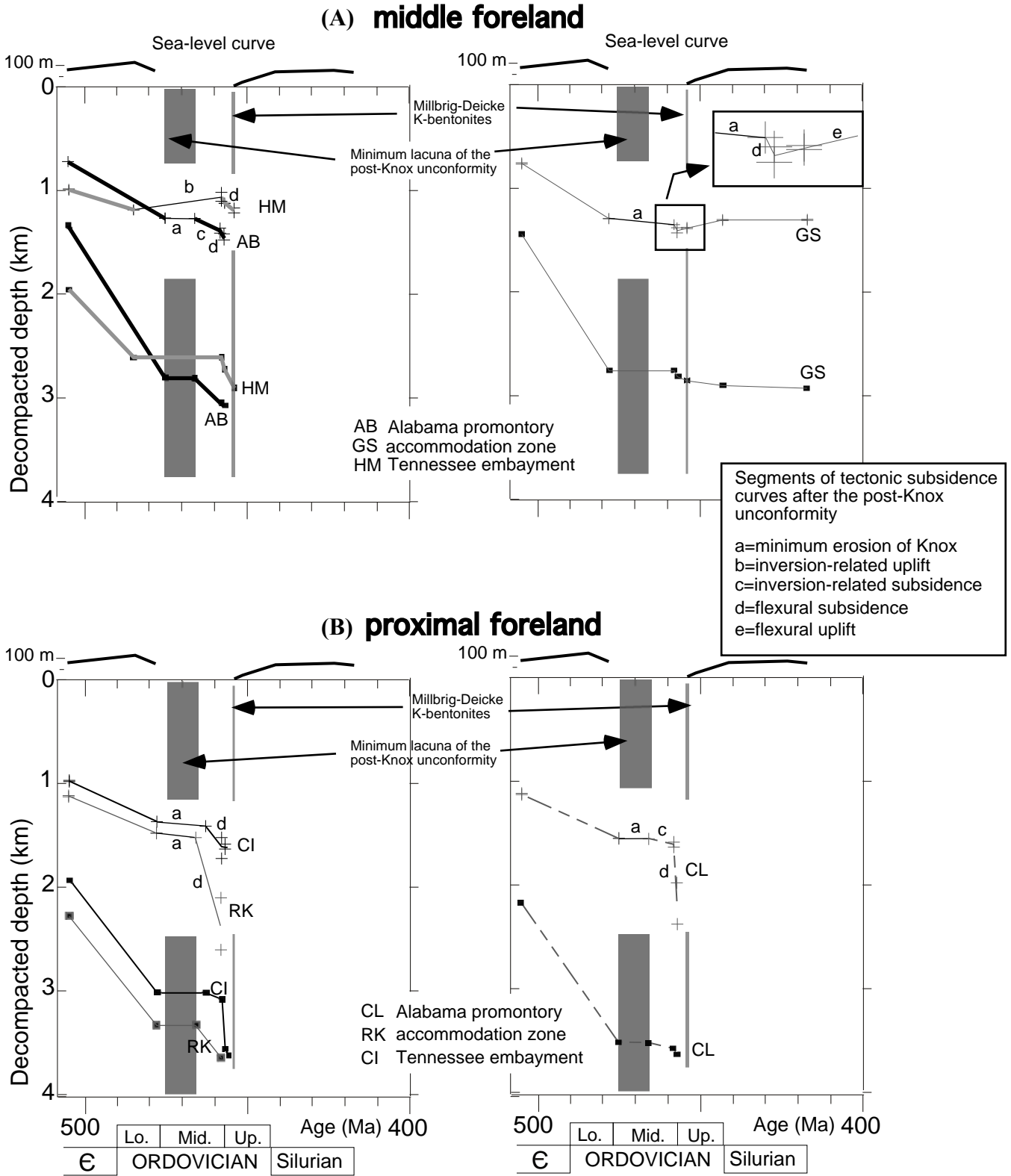


**Figure 4.12** Paleogeographic maps showing the evolution of the Blountian foreland basin through the Late Ordovician. Each map represents the time of deposition for deposits underlying the stratigraphic surface indicated. Location of source areas for synorogenic detritus is shown tentatively on the east side of each diagram. Note the northeastward migration of siliciclastic depocenters and dominance of carbonate deposition to the southwest, indicating that source areas supplying synorogenic detritus and direction of dispersal of those sediments into the basin changed through time. See Figure 4.2 for key code of sections.



**Figure 4.13** Temporal and lateral variation of Nd-isotopic compositions of the Blountain clastic wedge on the Alabama promontory, Tennessee embayment, and Virginia promontory. Sea-level curve at the top from Bond and Kominz (1991). See Table 4.6 for stratigraphic units and locations of each sample, and text for discussion of data.

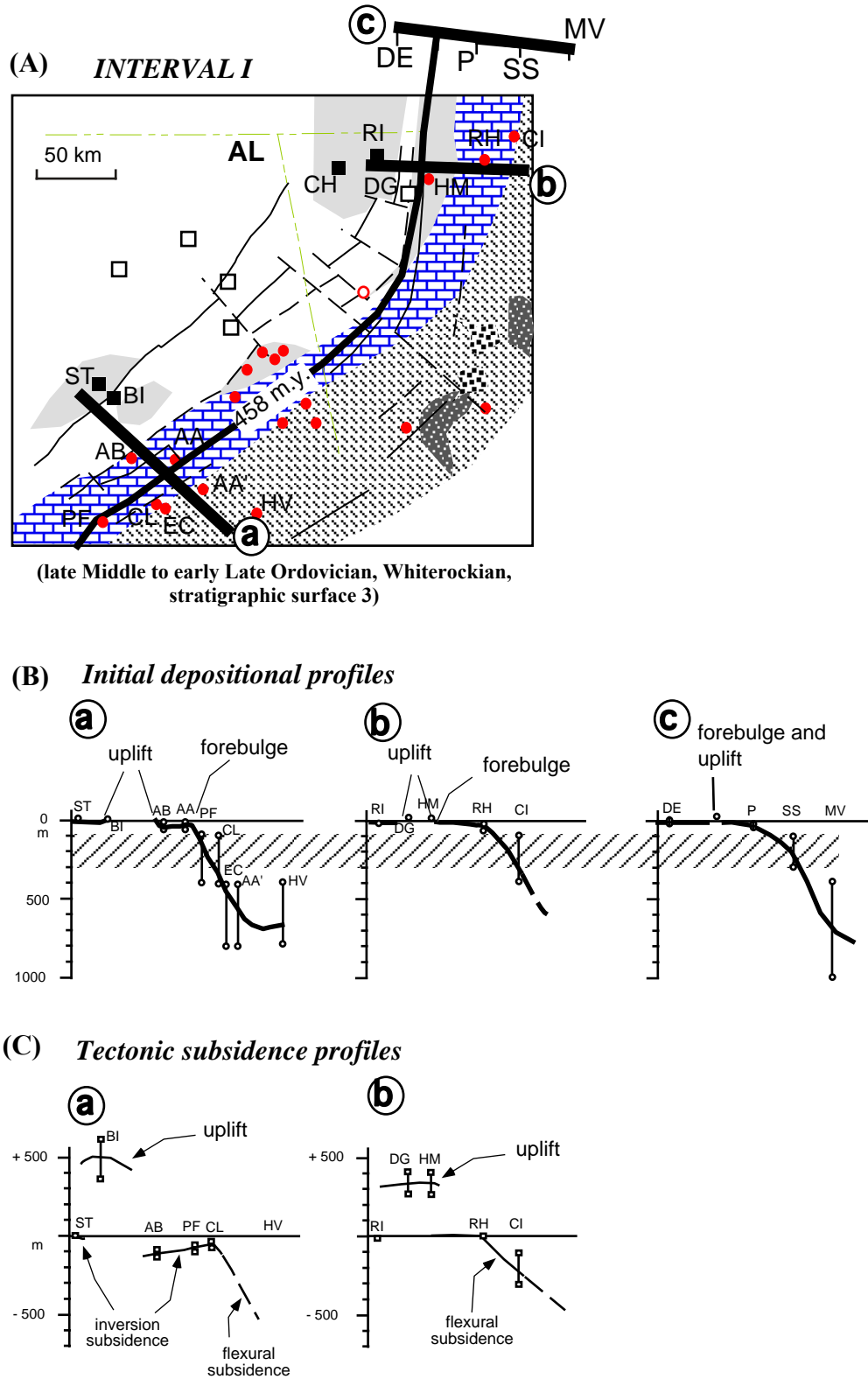
Figure 4.14



**Figure 4.14** (previous page) Total and tectonic subsidence curves (lower and upper curves, respectively) for representative sections in the middle (A) and proximal (B) foreland, and with sections on the Alabama promontory, accommodation zone, and Tennessee embayment. Cross symbols in tectonic subsidence curves correspond to the error in determination of water depth for the upper strata of each interval. Definitions of water-depth criteria are from Steinhauff and Walker (1996). Correction for sea-level fluctuations uses the sea-level curve relative to the Iowa craton (Bond and Kominz, 1991) in order to give a minimum estimate of relative sea-level fluctuation along the plate margin. However, Ross and Ross (1995) reported minor fluctuations of sea level (Figure 4.4B) that probably affected sections restoring near the plate margin.



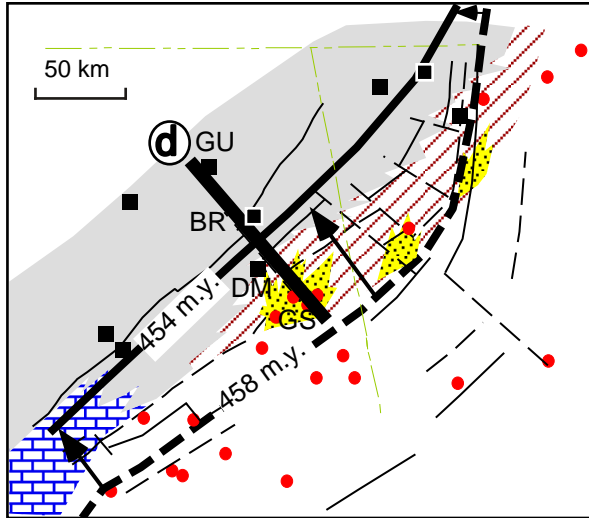
Figure 4.15



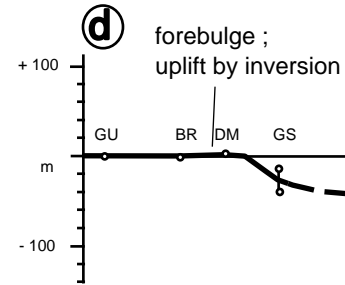
**Figure 4.15** (previous page) (A) Estimated position of the foredeep side of the forebulge at stratigraphic surface of correlation 3 (Interval I, same as Figure 4.11B). The trace (thick black line) follows the axis from where the carbonate platform deepens uniformly southeastward (i.e., no uplifts). (B) Initial depositional profiles a (Alabama promontory), and b and c (Tennessee embayment) give a good approximation of along-strike changes of the downwarped Blountian foredeep, position of the forebulge, and intraplate uplifts. On the Alabama promontory, uplifted areas are wider, the carbonate ramp southeast of the uplift is wider, and the foredeep is steeper than the profiles on the Tennessee embayment. Depositional profile c in the Tennessee embayment uses the strata along surface of correlation 1 of Walker et al. (1983). Location of sections DE, the uplifted portion between DE and P, P, SS, and MV are in palinspastic position and to scale of the map. See Walker (1977) and Benedict and Walker (1978) for the names and descriptions of sections. Slope is calculated using the interpreted profiles and between 100 m and 300 m depths. (C) Tectonic subsidence profiles a and b illustrate subsidence related to the inversion of the Birmingham graben in the distal foreland and subsidence related to flexure in the most proximal zones.

Figure 4.16

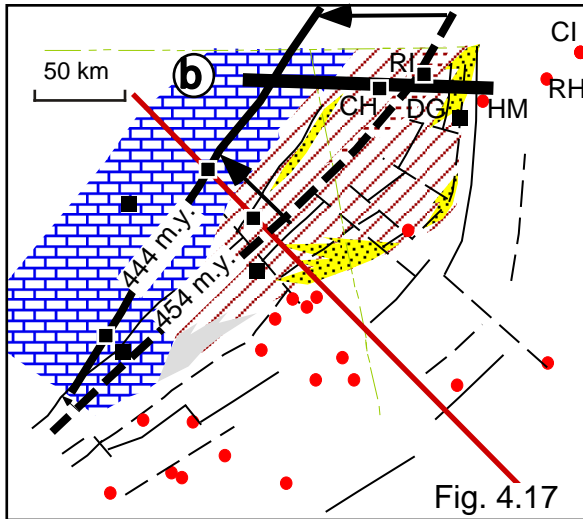
(A) *INTERVAL III* (early Late Ordovician, middle Mohawkian, stratigraphic surface 8)



(B) *depositional profile*



(C) *INTERVAL V* (late Late Ordovician, Cincinnati, stratigraphic surface 11)



(D) *depositional profile*

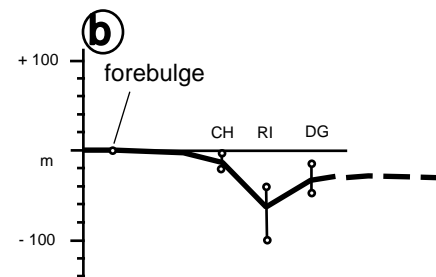
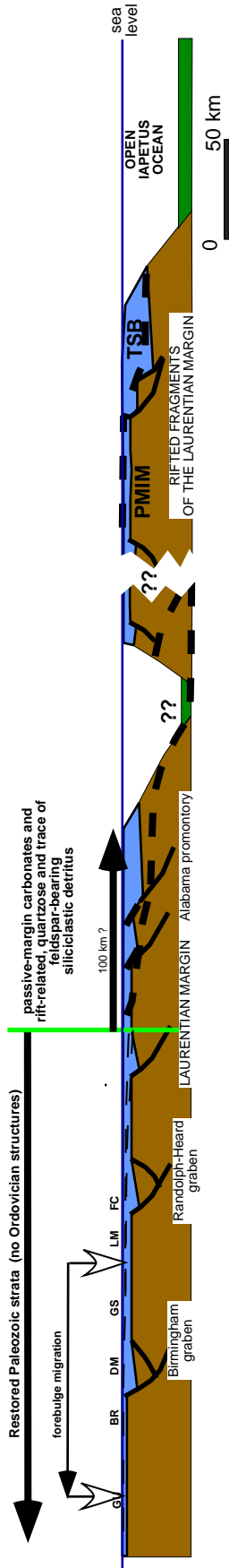


**Figure 4.16** (previous page) (A) Estimated position of the foredeep side of the forebulge at stratigraphic surface of correlation 8 (Interval III, same as Figure 4.12A). The trace of the foredeep side of the forebulge (thick black line) is defined where peritidal carbonate successions have common indicators of subaerial exposure and strata to the southeast grade to subtidal mixed carbonates and red siliciclastic deposits. Inversion of the Birmingham graben obscures the precise location of the crest of the bulge. (B) Depositional profile d showing the position of the forebulge and southeastward deepening of the basin floor to subtidal environments. (C) Estimated position of the foredeep side of the forebulge at stratigraphic surface of correlation 11 (Interval V). The position of the forebulge is defined where open-water, high-energy carbonate successions with indicators of subaerial exposure grade eastward to subtidal mixed carbonates and red siliciclastic deposits or deep lagoonal successions. Cratonward advance of the forebulge is shown by arrows between successive positions shown on maps A and C. Note that the foredeep side of the forebulge advanced farther on the Alabama promontory than in the Tennessee embayment between intervals I and III (466 to 454 Ma), whereas between intervals III and V (454 to 443 Ma), the forebulge advanced farther in the Tennessee embayment than in the Alabama promontory. However, the maximum total advance occurred in the accommodation zone. Map C shows the location of cross section in Figure 4.17. (D) Depositional profile b showing the position of the forebulge on the carbonate platform and southeastward deepening of the basin floor to deep lagoonal and subtidal environments.

**(A) End of passive-margin deposition (early Middle Ordovician (ca 477))**



**(B) Blountian orogeny (Latest Ordovician (ca 443))**

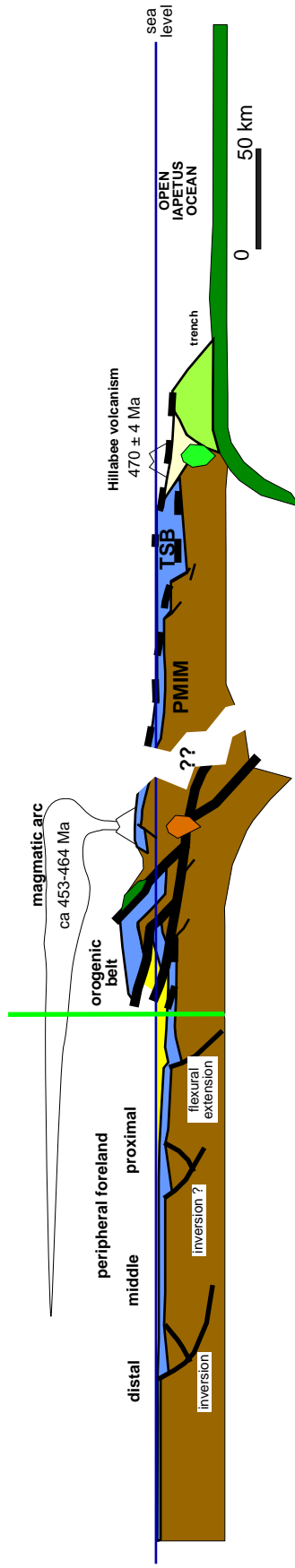


**Figure 4.17** Two-dimensional tectonic evolution of the Laurentia margin during the Blountian orogeny (see location of cross section in Figure 4.16C). (A) Configuration of the rifted Laurentian margin at the end of passive-margin deposition (ca 477 Ma). The cross section uses the palinspastic restoration of passive-margin and intraplate rift strata across the northern part of the Alabama promontory (strata northwest of the vertical gray line; line of cross section is the same as the restored cross section 8 in Plate 2.1). A simplified sketch of basement graben structures is also shown in their post-rift stage in the early Middle Ordovician. Thin dashed lines in restored pre-Middle Ordovician strata show the trace of the initial and final flexural profiles for the top of the passive-margin strata. White arrows point to successive locations of the forebulge (distance of forebulge migration from Figure 4.16). The outer part of the Laurentian margin (right of the gray line) is not constrained, but depicts the suggested location of tectonic loads and source of Blountian synorogenic detritus in palinspastic position. Thick dashed line indicates the trajectory of the detachment level. Although the Pine Mountain internal basement massif (PMIM) and Talladega slate belt stratigraphy (TSB) may have been transported from an uncertain palinspastic position during the Alleghanian orogeny (e.g., Steltenpohl and Tull, 2002), we infer that the microplate colliding with the southern corner of Laurentia in the Middle Ordovician had a similar configuration (Grenville basement and Laurentian-type sedimentary cover). Oceanic crust or thinned Laurentian crust may separate the microplate and the Laurentian margin.

(B) Collision of the microplate with the Alabama promontory. The diagram illustrates from west to east: (1) erosion of the passive-margin succession from the allochthon block and thin accumulation of the clastic wedge in the distal foreland associated with the inversion of the Birmingham graben; (2) slight variations of the southeast thickening trend of the Blountian clastic wedge because of reactivation of other inferred basement structures; (3) basement-cored uplifts with a Laurentian-margin sedimentary cover as source area for Blountian detritus; (4) eastward-dipping subduction and continental volcanism; (5) relative position of Pine Mountain internal massif, the Talladega slate belt, and Ordovician bimodal volcanism; and (6) west-dipping subduction along the eastern margin of the microplate. A similar tectonic setting of microcontinent-continent collision has been proposed recently for the northern Appalachians (Waldron and Staal, 2001).

## CHAPTER FIVE

### SUMMARY OF CONCLUSIONS

#### **5.1 CONSTRUCTION OF THE PALINSPASTIC MAP AND A MAP OF SUBSURFACE BASEMENT FAULTS: INSIGHTS TO THE REGIONAL GEOMETRY AND KINEMATICS OF THE APPALACHIAN THRUST BELT IN ALABAMA AND GEORGIA**

As a fundamental step for the analysis of Blountian strata, it was necessary to determine the palinspastic location of Blountian deposits previous to the late Paleozoic Alleghanian orogeny. In addition, subsurface mapping of basement structures beneath the Appalachian thrust belt of Georgia and Alabama allows the establishment of a spatial relation of the palinspastic position of each stratigraphic section with the seismically constrained Birmingham graben and the stratigraphically and structurally constrained Randolph-Heard graben. As discussed in the next sections, the knowledge of the spatial relation between stratigraphic sections and basement structures is fundamental to the analysis of proximal to distal Blountian foreland strata. The following conclusions are derived from the integrated analysis of structural cross sections and the effects of some sub-décollement basement structures in the evolution of the Alleghanian thrust belt.

Geometry and kinematics of structural styles in the thin-skinned and unmetamorphosed Appalachian thrust belt of Alabama and Georgia may be directly and indirectly related to sub-décollement basement structures and the pre-deformational stratal architecture of the unit that hosts the regional décollement. In the leading and intermediate imbricates of Georgia and the leading imbricates in Alabama, low-amplitude fault-related anticlines form where depth to basement is shallow. In the intermediate imbricates in Alabama, high-amplitude fault-related anticlines form where the regional décollement is deep within the Birmingham graben; detachment folds nucleate above down-to-southeast basement faults with moderate vertical separation; and a mushwad evolves above a broad graben bounded by basement faults with large vertical separation and containing a large volume of weak strata (i.e., shale).

Small-scale curvatures of the thrust belt are also related to changes in basement elevation across basement transverse faults. Small-scale salients or convex-to-the-foreland curvatures of the Helena fault and Gadsden mushroom are very abrupt, and they are related to a transverse basement fault that separates a narrow Birmingham graben on the northeast from a wider and deeper graben on the southwest. We use this direct observation to suggest that a transverse basement fault primarily controlled the salient geometry of the Rome, eastern Coosa, and Talladega faults. Abrupt curvatures are confined in transverse zones suggesting that distribution of northwest-striking basement faults and related changes in elevation of the top of basement played a primary role in the location of transverse structures in the thrust belt.

Vertical and horizontal gradients of deformation were partially controlled both by differences in elevation of the top of basement and pre-deformational basin architecture. Shallow basement promontories bounded by intersections of northeast-striking and transverse basement faults acted as stress concentrators that favored strain partitioning and differences in the style of deformation within the advancing thin-skinned thrust belt. These promontories contribute to the nucleation of thin-skinned transverse structures and the different transverse zones recognized in the thrust belt in Alabama and Georgia. The regional décollement is dominantly within weak layers of the Rome and Conasauga Formations, but thick shale beds in intermediate levels of the sedimentary wedge contributed to the generation of upper levels of detachment and the vertical differentiation of deformation into duplexes and imbricate-fan systems.

## **5.2 INTERACTION OF BIRMINGHAM GRABEN INVERSION AND FLEXURAL DEFORMATION AT DISTAL TO MIDDLE BLOUNTIAN FORELAND SETTINGS**

Patterns of carbonate, mixed, and siliciclastic deposition in the distal Blountian foreland basin and during Middle and Late Ordovician time were controlled by the interaction of basement-fault inversion, fluctuated migration of the Blountian flexural wave, and rise of sea level. Each of these factors dominated at different stages of the foreland evolution, and they are identified from the local, plate-margin, or cratonwide effects on foreland deposition. The inversion of the Birmingham graben created a topography in the distal foreland that consisted of inverted upthrown blocks (former Birmingham graben) and inverted downthrown blocks (former shoulders of the Birmingham graben) (Figure 5.1).



Late Middle Ordovician inversion of the northeast-striking Birmingham graben enhanced erosion of Knox strata in inverted upthrown blocks and controlled the initiation of carbonate deposition in adjacent inverted downthrown blocks. The greatest magnitude of the lacuna is observed in sections that restore inside the Birmingham graben. Thin Knox intervals imaged in seismic reflection profiles also restore palinspastically inside the graben. Tectonic inversion of the graben explains the relief to cause the deep truncation of Knox strata and the late onset of deposition in sections restoring on the inverted upthrown block. The inversion model also explains the preservation of the youngest units of the Knox Group and the earlier Blountian carbonate deposition in inverted downthrown blocks. The thick and mappable record of karst-filling chert conglomerates in sections restoring inside the graben indicates longer exposure and weathering of inverted upthrown blocks; in contrast, limestone-conglomerate clasts in sections at inverted downthrown blocks indicate short time of exposure below the basal conglomerates. Inverted upthrown blocks supply coarse-grained chert and quartz grains and recharge of meteoric waters to aquifers in carbonate depocenters in inverted downthrown blocks.

Local bending effects of inverted upthrown blocks triggered carbonate deposition in areas adjacent to the active inverted faults. Tectonic subsidence curves of lower carbonate deposits of the Chickamauga and Lenoir beds (Interval I) in sections restoring in both the northwestern (section CH-RI) and southeastern (sections PF, AB) inverted downthrown blocks document the development of the earliest carbonate depocenters in the distal foreland. Stacking patterns of deposition are dominantly aggradational, suggesting that the rate of carbonate production kept pace with creation of accommodation space in inverted downthrown blocks. This irregular pattern of carbonate deposition in the distal foreland is explained using a flexural model of deformation of a continuous elastic plate and considering the inverted block as the tectonic load. Inversion loading bends the elastic plate and two asymmetrical basins are formed (e.g., Tucotte and Schubert, 1982). As this model predicts, thicker and deeper water deposition occurs in sections adjacent to the inverted structure (e.g., section AB, PF) than in sections farther away from the inverted load (e.g., section CL, southeast of sections AB and PF), disturbing the marginal-scale flexural deformation associated with loading at the plate margin. Tectonic subsidence curves in sections adjacent to inverted upthrown blocks indicate that subsidence related to local flexural effects occurred earlier than flexural subsidence related to loading at the plate margin. This geodynamic model of inversion corroborates the link between intraplate

uplift and deposition, and together with stratigraphic and provenance analyses allow to reject the model of flexural uplift as the solely mechanism to create the post-Knox unconformity in southernmost Laurentia.

Flexural subsidence related to loading along the plate margin and influx of siliciclastic detritus strongly contributed to the diachronous termination of carbonate platform deposition in the southeastern inverted downthrown block. Drowning of the carbonate platform in the southeastern part of the southeastern inverted downthrown block occurred at the Middle-Late Ordovician boundary (e.g., section CL). Termination of carbonate deposition by combined effects of deepening and influx of terrigenous clastic detritus occurred in early Late Ordovician at the northeastern end of the southeastern inverted downthrown block (e.g., section RH), and in sections adjacent to the inverted structure (e.g., section GS). The inverted upthrown block restricted the cratonward advance of the synorogenic clastic wedge during early and middle Late Ordovician. As a consequence, carbonate-platform deposition in the northwestern downthrown block dominated during the early and middle Late Ordovician, and termination of carbonate-platform deposition did not occur until the latest Ordovician as a result of cratonward progradation of synorogenic siliciclastic deposits.

The early signature of basin inversion in the distal foreland was subdued gradually by flexural subsidence/uplift and fluctuations of sea level. After initiation of fine-grained siliciclastic deposition in low-energy and oxygenated environments, and during a cratonwide rise of sea level, siliciclastic and carbonate deposits in the middle and distal foreland record episodes of shoaling and hinterland progradation of shallow-water to peritidal carbonates over the siliciclastic depocenter. Tectonic subsidence curves indicate an event of rise of the top of basement during the middle to late Late Ordovician that is related to the migration of the flexural wave toward the hinterland and was accompanied initially by deposition of volcanic ash material. Therefore, the combined effects of cratonwide sea-level rise and forebulge migration created the conditions for continuous shallow-water deposition and the record of shoaling-upward successions forming third-order depositional cycles in both siliciclastic and carbonate depocenters.

### **5.3 ROLE OF THE RIFTED-MARGIN CONFIGURATION OF LAURENTIA IN THE ARCHITECTURE AND COMPOSITION OF MIDDLE TO PROXIMAL BLOUNTIAN FORELAND STRATA**

Along-strike variations in the stratigraphy, sediment composition, and tectonic subsidence patterns of the proximal and middle strata of the Blountian foreland basin are partly related to the along-strike change in configuration of the rifted margin of eastern Laurentia from the Alabama promontory on the southwest, to the accommodation zone, and to the Tennessee embayment on the northeast.

The Blountian foredeep, as depicted by change in depositional depth of coeval Middle Ordovician carbonate and black shale strata, was narrower and had steeper slope in the Alabama promontory than in the Tennessee embayment (Figure 5.1). Normal flexural reactivation of basement faults in the foredeep may have contributed to the rapid drowning of the carbonate platform, as documented by the abrupt contact between carbonate beds of the Lenoir Limestone and graptolitic shales of the Athens Shale. Deposition of the wide carbonate platform on the distal foreland and on the Alabama promontory was controlled primarily by uplift and subsidence related to the inversion of the Birmingham graben, whereas flexural subsidence and eustasy controlled distal foreland carbonate deposition on the Tennessee embayment. Differential flexural subsidence along strike of the Blountian foredeep may be accommodated by reactivation of transverse basement faults on the accommodation zone.

The sedimentary filling of the Blountian foreland basin also changes along strike. Up-section coarsening and shoaling of proximal and middle foredeep strata on the Tennessee embayment documents: (1) up section increase in influx of terrigenous detritus throughout the section, (2) an abrupt increase of quartz and sedimentary lithic fragments in coarse deltaic deposits toward the top, (3) cratonward progradation of shallow clastic platform to marginal environments, and (4) cratonward advance of a salient in the Blountian orogenic belt. In contrast, the low influx of terrigenous detritus to the narrow foredeep on the Alabama promontory favored the establishment of a carbonate ramp in the southwestern part (e.g., section PF), whereas shallow-water carbonate and siliciclastic deposition interfingered in the foredeep on the Alabama promontory (section GS) and the accommodation zone (section HL).

Intrabasinal uplifts and differential deformation in the Blountian orogenic belt are recorded by along-strike changes in the composition of the Blountian clastic wedge. Olistoliths

and local conglomerates interbedded with turbiditic feldspar-bearing sandstones and black slates in the underfilled stratigraphy of the Blountian foredeep suggest the mixing of sediments transported by axial submarine fan deposits and debris flows derived from intrabasinal uplifts. Petrographic and Nd-isotopic ( $\epsilon_{Nd}$ ) data of sandstones and mudstones, respectively, indicate a source area composed of Grenville basement and a sedimentary cover with a Laurentian-margin stratigraphy. The mostly uniform increase of  $\epsilon_{Nd}$ , the higher percentages of feldspars in the clastic wedge on the Alabama promontory, and the more abundant quartzose and sedimentary lithic fragments in the clastic wedge on the Tennessee embayment, suggest that the Blountian tectonic load was more deeply eroded in areas supplying sediments to the promontory, and the sedimentary cover was more exposed in areas supplying sediment to the embayment. This pattern of deformation is similar to the gradients of deformation documented in salient and recess geometry of the Georgia and Alabama thrust belt, respectively, a geometry that is primarily controlled by the zig-zag configuration of the older Laurentian rifted margin.

#### **5.4 MIGRATION OF THE BLOUNTIAN FLEXURAL WAVE**

Finney et al. (1996) documented a diachronous northeastward and northwestward migration of the Blountian flexural wave on the basis of determination of the age of initiation of graptolitic black shales in the proximal foreland. This dissertation documents the migration of the foredeep side of the forebulge in middle and distal foreland because the inversion of the Birmingham graben obscures the identification of the maximum flexural uplift in the distal foreland.

In the distal foreland, deposition in inverted downthrown and upthrown blocks was primarily controlled by basement fault inversion; however, the northeastward migration of the Blountian foredeep and tectonic loads also played an important role in what type of sediments accumulated in the distal foreland. Lowermost deposits above the post-Knox unconformity in inverted upthrown blocks are older and calcareous to the southwest (e.g., lower Chickamauga Limestone in sections BI and BR), in contrast to younger and siliciclastic to the northeast (e.g., Greensport Formation in sections HL and DG). In the southeastern inverted downthrown block, termination of carbonate deposition and accumulation of deep-water black shales is older to the southeast (Athens Shale in section CL) than in the northwest (sections AB and PF). In the middle foreland, termination of carbonate deposition and accumulation of dark-colored to red

shales is also younger to the northwest and northeast (Greensport Formation in sections GS, HM, and RH).

Although basement inversion and normal-fault reactivation might have disrupted the geometry of the flexural wave, the migration of the shallow part of the foredeep side of the forebulge was identified using profiles of carbonate-siliciclastic depositional systems, tectonic subsidence curves, and truncation of upper Ordovician strata in the middle and distal foreland. At the Middle-Late Ordovician time boundary, the foredeep side of the forebulge was marked by a carbonate platform profile uniformly deepening southeastward to basinal settings. In early Late Ordovician and before the time of deposition of the Deicke and Millbrig K-bentonite beds, the depositional profile indicates an area of subaerial exposure and thin accumulation in section DM (Figure 4.16B) that separates peritidal deposition of the carbonate platform on the northwest from subtidal siliciclastic deposition on the southeast. Effects of inversion of the Birmingham graben preclude the determination of the position of maximum flexural uplift at these two intervals of time.

During the middle to late Late Ordovician, tectonic subsidence curves indicate a rise of the top of basement that is interpreted as the migration of the flexural wave toward the thrust belt. This interpretation is additionally supported by (1) shoaling of siliciclastic depocenters favoring deposition of shallow-marine sandy shoals of the Colvin Mountain Sandstone; (2) later southeastward progradation of shallow-water to peritidal carbonates over siliciclastic deposits; and (3) aggradational to retrogradational carbonate deposition in section CH-RI to the northwest. The migration of the flexural wave toward the orogenic belt was initially accompanied by accumulation of K-bentonite beds and high influx of sand-sized quartzose detritus followed by a decrease in influx of siliciclastic detritus to the distal foreland. Cratonwide sea-level rise of ~80 m (Bond and Kominz, 1991) created the conditions for the record of a submerged southeastward migration of the flexural wave, the thick and widespread record of deposition of volcanic ash beds, and the thicker and aggradational to retrogradational pattern of deposition in section CH-RI.

For the latest Ordovician, the shallowest part of the depositional profile adjacent to the foredeep migrated farther northwestward onto the carbonate platform, as indicated by exposure surfaces and meteoric water cements in cross-bedded skeletal and phosphatic rich limestones on the Tennessee embayment (Figure 4.16D), and by meteoric water cements and truncation of

Upper Ordovician strata and thin deposition of skeletal limestones in section BI (Figure 4.7). The tectonic subsidence curve in the northeasternmost section DG indicates an event of flexural subsidence during the early Silurian. This event of flexure may be related to the last migration of the flexural wave in the latest Ordovician.

The flexural wave initially migrated farther cratonward on the Alabama promontory, but as the tectonic loads moved northeastward, the forebulge migrated rapidly cratonward on the Tennessee embayment. In the early stages of foreland evolution, the rate of flexural wave migration is higher on the Tennessee embayment (9 to 40 mm/yr) than on the Alabama promontory (8 to 11 mm/yr) and at the accommodation zone (15 mm/yr). If flexural rigidity (or elastic thickness) of the lithosphere is uniform along strike and the response of the lithosphere to applied loads is instantaneous, propagation rates of tectonic/sediment loads on the Tennessee embayment are inferred to be higher than those on the Alabama promontory. Slow movement of the flexural wave may also document the presence of weak zones in the Alabama foreland lithosphere (e.g., the Birmingham graben, Chapter 3) (Waschbusch and Royden, 1992). On the accommodation zone, rates of migration of the flexural wave decelerated through time from 15 mm/yr to 5 mm/yr. The largest migration of the forebulge on the accommodation zone may suggest that this zone was loaded most of the time during the Middle and Late Ordovician.

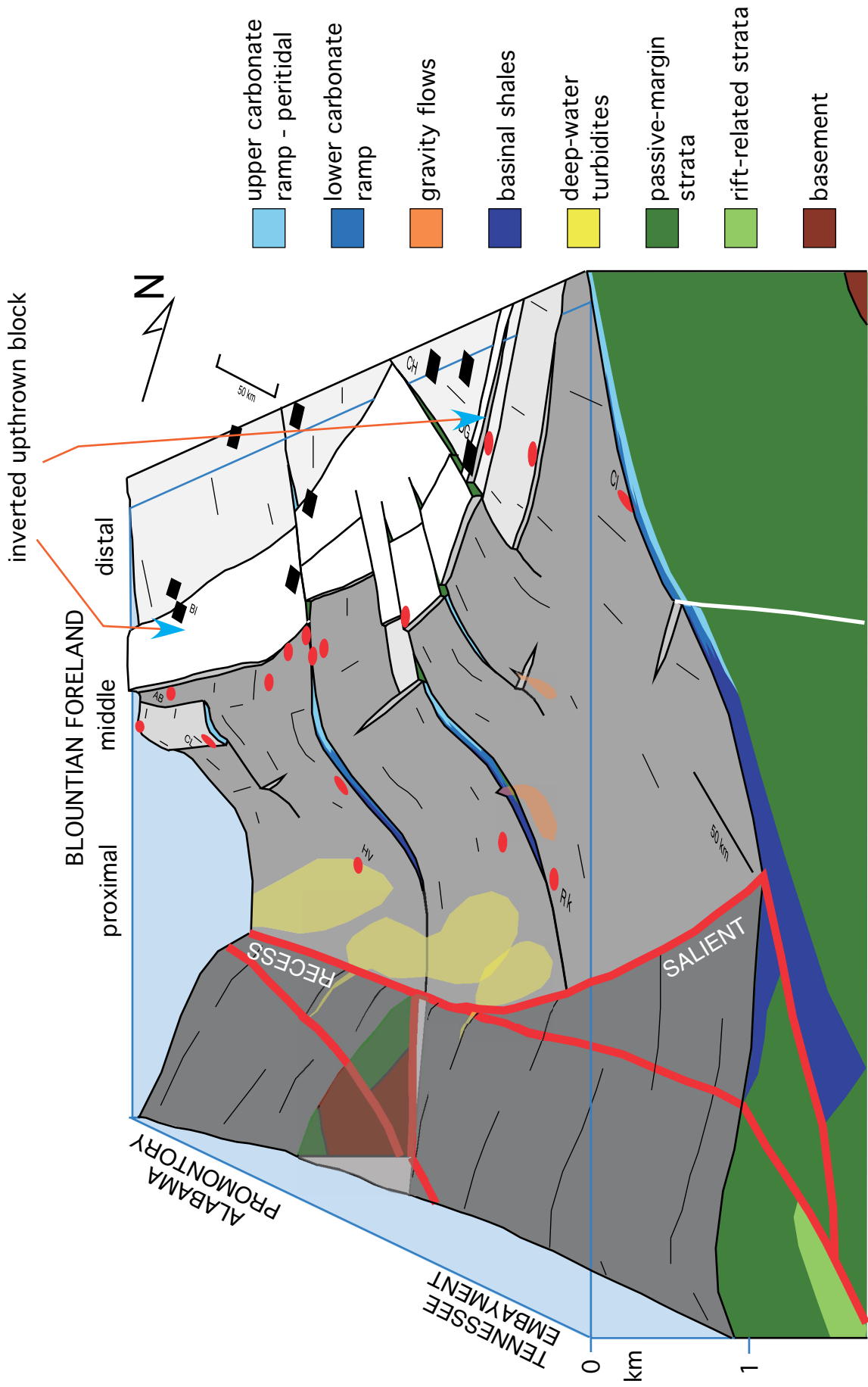


**Figure 5.1.** This diagram illustrates the role of different rift-related structures on the early geometry of the Blountian foredeep (late Middle to early Late Ordovician, Whiterockian, stratigraphic surface 3) distribution of depositional environments at different settings of the foreland, and deformation of tectonic loads. Evolution of the Blountian foreland basin and deformation of the Blountian orogenic belt were primarily controlled by the pre-existing configuration of the Laurentian margin and reactivation of intraplate basement structures.

## APPENDIX A

### IDENTIFICATION OF K-BENTONITES

Identification of K-bentonite beds has been essential for stratigraphic correlation of Ordovician strata in the southern Appalachians as well as for constraining interpretations of tectonic settings for the Taconic orogeny (Haynes, 1994; Kolata et al., 1996). Phenocrystal and XRD analyses were carried out in 17 samples from the Middle and Upper Ordovician succession of Alabama in order to establish if they are bentonite beds and how they correlate with other reported K-bentonite beds in the Alabama Appalachians. The methods of phenocrystal separation and XRD analysis are the same as described by Haynes (1994); identification of mixed-layer illite/smectite is based on the interpretation of XRD patterns of air versus ethylene glycol-solvated samples, and comparison with the XRD patterns of a calcareous black shale of the Lenoir Limestone and red siltstone of the Greensport Formation. The analyses were carried out at the University of Cincinnati and the University of Kentucky. These 17 samples are grouped into two different sets.

One set of samples comes from the Middle Ordovician Lenoir Limestone and Athens Shale in Calera (section CL, Figure 4.2), and one bentonite bed in the Rockmart Slate. This study documents at least three K-bentonites in three different stratigraphic levels in section CL. The lower level is in the Lenoir Limestone. The intermediate level is in lower beds of the Athens Shale, which has been inferred as a bentonite layer (Drahovzal and Neathery, 1971). The upper level is at the top of the Athens Shale. From this set of K-bentonites, only one K-bentonite bed has been reported in section RL (Drahovzal and Neathery, 1971; Haynes, 1994), and this study documents one K-bentonite bed in the upper Rockmart Slate in section RK.

Another set of samples comes from the Upper Ordovician Greensport Formation, Colvin Mountain Sandstone, Sequatchie Formation, and Inman Formation. This set of samples is in a stratigraphic position similar to the widespread Deicke and Millbrig K-bentonite beds (Haynes, 1994), but at least 12 K-bentonite beds have been reported in the early Late Ordovician (middle Mohawkian) in the southern Appalachians (Figure 4.4) (Kolata et al., 1996). The K-bentonite beds of this set reported in this study are from sections GS, DM, GU, HL, and HM.



Phenocrystal association and clay mineralogy of the two sets of samples are very different. The results of this study indicate that altered micas (biotite?), and gypsum dominates the phenocrystal fraction of the lower set (Middle Ordovician), with trace heavy minerals (oxides?) and quartz (K-bentonite in section RK). Expandable clay minerals in the lower set are inferred from changes in the backslope of peak 10 Å, and they may be better identified as bentonitic shales. Biotite and quartz are the common phenocrystal association of the Upper Ordovician set. Mixed-layer illite/smectite is the predominant clay mineral and permit the identification of these beds as K-bentonites (Haynes, 1994). Bentonitic shales and K-bentonites reported here contribute to the tectonic and stratigraphic analyses of the Middle and Upper Ordovician succession of Alabama and Georgia. The record of volcanic material in shale beds of the Lenoir Limestone may be used to identify the switch between passive-margin and collisional deposition in southern Laurentia.

Table A.1 gives a detailed description of the 17 samples analyzed in this study. Figure A.1 shows the XRD patterns of some samples.

**Table A.1** Description of K-bentonite beds

Olol= Lenoir-Little Oak Limestone; Ol= Lenoir Limestone; Oa= Athens shale; Og= Greensport Fm; Ocm= Colvin Mtn SS; Os = Sequatchie Fm; Dfm= Frog Mountain Formation..

Sample	Thickn ess (cm)	Section	Stratigraphic position	General remarks	Description of phenocrystals	Clay mineralogy
S2-2406	4	CL CALERA (Blue circle)	40 m below Ol-Oa contact	Reddish, fissil, calcareous shale with micas (muscovite? biotite)	-Black oxides, gypsum, micas (altered biotite?), one flake of biotite. Trace of quartz grains coated with yelsh oxides -shale-like fragments have yellow color.	Bentonitic shale: trace of expandable clay component (mixed layer I/S?) documented by peak 14.03 Å in the ethylene-glycol-solveted sample
S2-2502	5	CL CALERA (Blue circle)	36 m below Ol-Oa contact	fissil, calcareous shale		Illite + chlorite (huff, pers. commun, 2000.) No expandable clay.
S2-2207	8	CL CALERA (Blue circle)	9 m above Ol-Oa contact	Lower Bentonite bed. Highly altered, calcareous, light green claystone. breaks like flakes.	Oxides, gypsum, pyrite?, reworked quartz, trace of biotite. -clay color is light brownish gray.	Illite + chlorite-kaolinite. No clear signature of expandable components.
S2-2213	4.5	CL CALERA (Blue circle)	47 m above Ol-Oa contact	Upper bentonite bed. Highly altered, light green to gray, alters to yellowish color, claystone, abundant oxides.	Gypsum, trace of quartz, red oxides, black & shiny heavy minerals. Trace of micas. -clay color is yellow	Bentonitic shale: trace of expandable clay component (mixed layer I/S?) documented by peaks 17.29 and 13.83 Å in the ethylene-glycol-solveted sample
S2-2806	3	CL CALERA (Vulcan quarry)	9 m above Oa-Ol contact. The total thickness of the lower bed is 9 cm	Lower layer of the lower bentonite bed. Light gray, rich in veins of calcite; fibrous clay (volcanicblack grains may be shale fragments. It is 3 cm thick, but the basal 0,5 cm looks like the upper layer.	Light brown to yellow, translucent flakes of biotite; gypsum. Granular-shape, shinny and black heavy? Minerals. Trace of quartz. -Clay has a medium to light gray-brown color	Bentonitic shale: expandable (mixed-layer I/S) clay documented by peak 18.01 Å in the ethylene-glycol-solveted sample. Chlorite-kaolinite clay is inferred by the peak 7.08 Å
S2-2808	2	CL CALERA (Vulcan quarry)	9 m above Oa-Ol contact	Upper layer of the Lower bentonite bed. Here consists of light gray, thin laminated, with black grains (biotite?) and platty grains (muscovite?) in a fibrous gray matrix (ash ?)	Abundant light brown to yellow, translucent flakes of altered biotite; gypsum; trace of quartz. Clay color is white to very light brown.	K-bentonite: mixed-layer I/S clay documented by peak 17.16 Å in the ethylene-glycol-solveted sample. Chlorite-kaolinite clay is inferred by the peak 7.55 Å and feldspar by peak 3.18 Å
M3-2313	6	GS GREENSPORT (Alexander gap)	4.7 m above Ocm-Os contact	Blue greenish clay with abundant flakes of mica and feldspar	Abundant flakes of biotite. Reddish, blocky fragments may be oxides (hematie?), trace of black heavy minerals. -Clay color is light orange.	K-bentonite: mixed-layer I/S clay (order R3) documented by peaks 18.01 and 16.53 Å in the ethylene-glycol-solveted sample.
L4-0106	0-30	DM DUNAWAY MOUNTAIN	Og-Ocm contact	Bluish to greenish, matrix-supported, bentonic sandstone (Qz=95%-cht+biotite=5%)	Reworked Qz; oxides are coating some grains. Light yellow to brown flakes of biotite; shiny, granular and black heavy minerals. Clay color is light to medium brown.	K-bentonite: mixed-layer I/S clay (order R2-R3) documented by peaks 11.70 and 9.74 Å in the ethylene-glycol-solveted sample.
L4-0505	0-10	DM DUNAWAY MOUNTAIN	1.5 m above Og-Ocm contact	Greenish, micaceous bentonite	Green and brown flakes of biotite, minor amount of quartz, some quartz grains are coated by oxides. -clay color is light grayish-blue, but in suspension is dark orange.	K-bentonite: mixed-layer I/S clay (order R3) documented by peaks 11.77 and 10.10 Å in the ethylene-glycol-solveted sample.
J4-0807	7 cm	GU GUNTERSVILLE	8.5 m below of the top of Inman Fm (Drah&Neat., 1971).	Greenish, micaceous? Bentonite?	Biotite flakes, dark gray to black color. Clay color is light green, and milky to light brown in suspension	K-bentonite: mixed-layer I/S clay (order R3-R2) documented by peaks 11.29 and 9.90 Å in the ethylene-glycol-solveted sample.

**Table A.1** (continued)

Olol= Lenoir-Little Oak Limestone; Ol= Lenoir Limestone; Oa= Athens shale; Og= Greensport Fm; Ocm= Colvin Mtn SS; Os = Sequatchie Fm; Dfm= Frog Mountain Formation.

Sample	Thickness (cm)	Section	Stratigraphic position	General remarks	Description of phenocrystals	Clay mineralogy
G11-1006 (top) G11-1007 (bottom)	116 cm	HL HORSELEG MOUNTAIN Radio Spring road Livingstone quad. N 34° 13'25" W 85° 15'01"	It marks the contact between the Greensport and Colvin Mountain Sandstone Formations	Top: collected along the Mount Alto road. Light greenish, plastic and massive claystone. Bottom: collected along the Radio Spring road where it is not altered as in the Mount Alto road. Light greenish, plastic (but with more blocky fracture than the other sample) and massive claystone with vf sand-sized black flakes of biotite and white angular crystals (feldspars?)	Top: trace of hyaline quartz,; yellow, translucent micas (biotite); and black, angular, blocky, (heavy) minerals  Bottom: dominates yellow, translucent micas (biotite); trace of black, angular, blocky, (heavy) minerals; and pink, white quartz	K-bentonite: mixed-layer I/S clay (order R3) documented by peaks 11.7 and 9.90 Å in the ethylene-glycol-solvated sample.
G11-1009	Up 3 cm	HL HORSELEG MOUNTAIN Radio Spring road Livingstone quad. N 34° 13'25" W 85° 15'01"	12.6 m below Og-Ocm contact	Yellowish to greenish, massive and silty claystone in elongated, flat, thin lenses; It is not as plastic as G11-1006. This claystone interfingers in an interval of 1.4 m with massive and mottled reddish siltstone.	- dominates coarse-silt to fine sand-size quartz; trace of yellow, translucent micas (biotite); only a few grains of black, angular, blocky, (heavy) minerals were observed. Red siltstones may be derived from interlayered laminae.	K-bentonite: mixed-layer I/S clay (order R3) documented by peaks 13.8, 11.7 and 9.90 Å in the ethylene-glycol-solvated sample. Chlorite-kaolinite clay is inferred by the peak 7.1 Å
D3-1607	30 cm	HM HAMILTON MOUNTAIN 501 Reed road Dalton N. quad. N 34° 48'09" W 84° 58'25"	Deicke (?) bentonite; sample collected at 15 m below Og-Ocm contact.	Light green, massive, plastic, and gummy with water. thin interbeds of reddish shale.	Poor recovery of phenocrystals: trace of quartz,; yellow, translucent micas (biotite); and black, angular, blocky, (heavy) minerals	K-bentonite: mixed-layer I/S clay (order R1-2)
D3-1608	50 cm (upp); 50 cm (mid); 70 cm (low)	HM HAMILTON MOUNTAIN 501 Reed road Dalton N. quad. N 34° 48'09" W 84° 58'25"	The Millbrig (?) bentonite is divided into three beds. Sample D3-1608 is from the lower bed, at 6 m below the Og-Ocm contact. Sample D3-1609 is from the middle bed. Upper bed is similar to the lower bed.	Reddish, medium-sand grained, biotite rich K-bentonite. Medium to thin laminae interbeds; micas give an aspect of lamination. Phenocrystals are 30-40%	Dominates yellow-brown, translucent micas (biotite); traces of very fine to fine quartz and black or red, angular, blocky, (heavy) minerals	K-bentonite: mixed-layer I/S clay (order R2)
D3-1609	50 cm (mid)	HM HAMILTON MOUNTAIN 501 Reed road Dalton N. quad. N 34° 48'09" W 84° 58'25"	Middle bed of the Millbrig (?) bentonite. Sample located at 5 m below Og-Ocm contact.	Light green, massive bentonite with less than 10% of phenocrystals	Quartz dominates the phenocrystal components; yellow-brown, translucent micas (biotite) are very common.	K-bentonite: mixed-layer I/S clay (order R1-2); kaolinite
H3-1304	4 cm	RK ROCKMART Rockmart S. quad. N 33° 58'34" W 85° 02'16"	Near the axial plane of an overturned syncline (structural upper part of the Rockmart Slate, according to the map of Sibley (1983)).	Light green, sandy, plastic and gummy in contact with water, bentonite (?); slate cleavage observed in several fragments	-Quartz with very irregular shapes; trace of black, angular, blocky, (heavy) minerals. Identification of micas is questionable by micas development along slate cleavage planes	K-bentonite: mixed-layer I/S clay (order R0); kaolinite

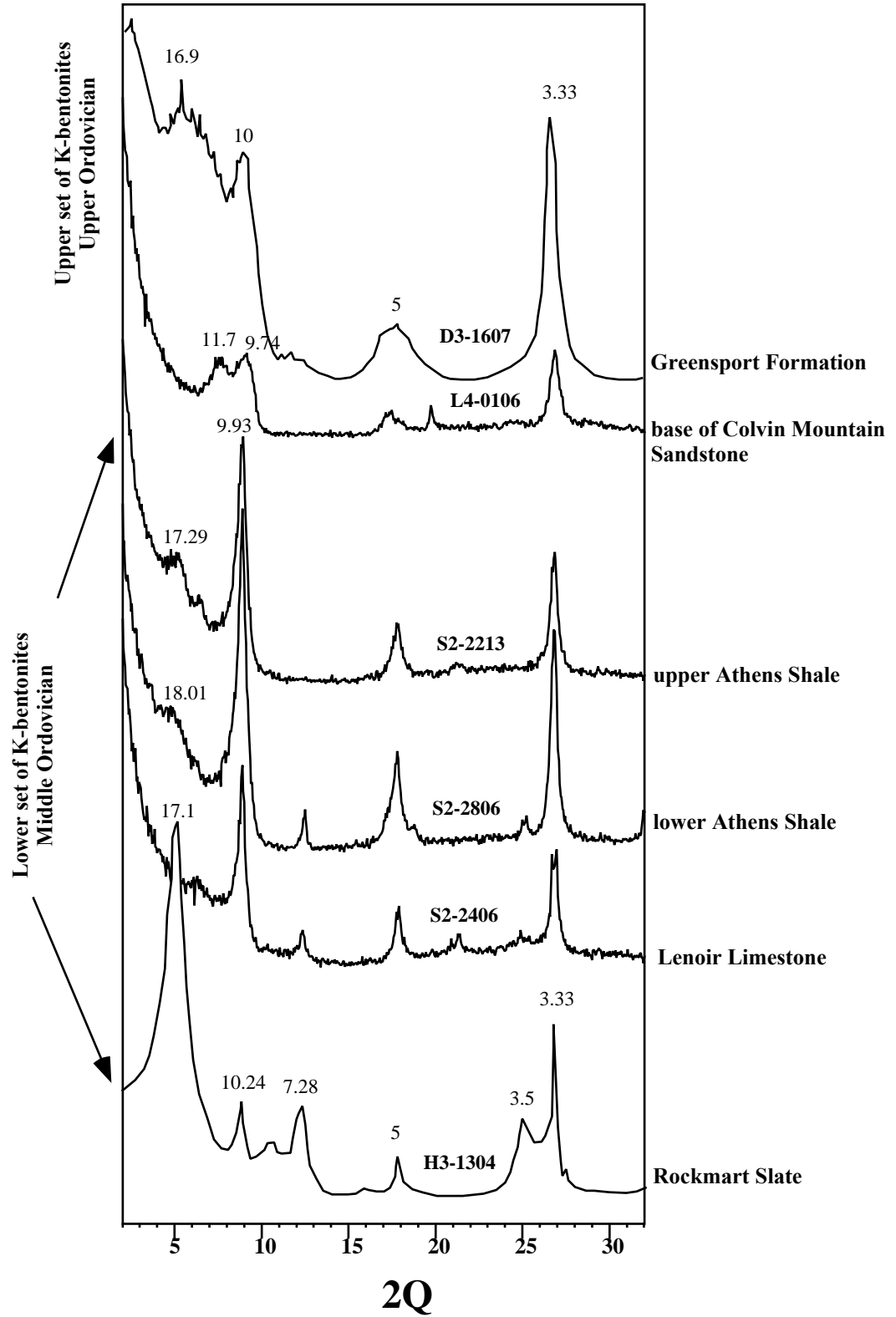


**Figure A.1** Selected X-ray diffraction (XRD) patterns of the clay fraction of the Middle and Upper Ordovician K-bentonites. Samples are saturated with ethylene glycol.

## APPENDIX B

### IDENTIFICATION OF GRAPTOLITES

By Stanley Finney  
 Department of Geological Sciences  
 California State University - Long Beach  
 Lithologic description and collection of samples by Germán Bayona

**Table B.1** Identification of graptolites

Olo= Lenoir-Little Oak Limestone; Ol= Lenoir Limestone; Oa= Athens Shale; Dfm= Frog Mountain Formation

Sample	Location	Stratigraphic position	General remarks	Graptolites (by Stanley Finney)	Remarks (by Stanley Finney)
T2-2601	PF PRATT FERRY SW1/4 NE1/4 sec 33 T24N R10E West Blocton East quad.	7 m above Ol-Oa contact	Soft-sediment deformation. Locality #2 of Finney et al., 1996	<i>Didymograptus sp.</i> <i>Reteograptus geinitzianus</i> <i>Cryptograptus tricornis</i> <i>Glossograptus ciliatus</i> <i>Dicellograptus gurleyi</i> <i>Dicellograptus sextans</i> <i>Glyptograptus sp.</i>	Correlation: <i>Nemagraptus gracilis</i> Zone
S2-2203	CL CALERA (Blue circle) SW1/4 sec 19 T22S R2W Montevallo quad.	5 m above Ol-Oa contact	Lowermost graptolites in section CL; interval with shale rich in skeletal grains and medium beds of dark gray skeletal limestone. Locality #3 of Finney et al., 1996	<i>Pseudoclimacograptus angulatus</i>	Correlation: This species ranges through the <i>Glyptograptus teretiusculus</i> and <i>Nemagraptus gracilis</i> Zones. The level at which it occurs in the Calera section has been correlated by Finney et al. (1996, fig. 7) with the top of the <i>G. teretiusculus</i> Zone.
S2-2206	CL CALERA (Blue circle)	8-9 m above Ol-Oa contact	Below the lower bentonite bed (S2-2207 in Appendix B)..	<i>Didymograptus sp.</i> <i>Cryptograptus tricornis</i> <i>Glossograptus ciliatus</i> <i>Pseudoclimacograptus angulatus</i> <i>Pseudoclimacograptus modestus</i> <i>Climacograptus meridionalis</i> <i>Glyptograptus teretiusculus</i> <i>Glyptograptus euglyphus</i>	Correlation: <i>Nemagraptus gracilis</i> Zone, probably very low level in that zone given its stratigraphic level
S2-2208	CL CALERA (Blue circle)	9-10 m above Ol-Oa contact	Above lower bentonite bed (S2-2207 in Appendix B)	<i>Reteograptus geinitzianus</i> <i>Cryptograptus tricornis</i> <i>Glossograptus ciliatus</i> <i>Pseudoclimacograptus angulatus</i> <i>Pseudoclimacograptus modestus</i> <i>Glyptograptus teretiusculus</i>	Correlation: <i>Nemagraptus gracilis</i> Zone, probably very low level in that zone given its stratigraphic level.
S2-2212	CL CALERA (Blue circle)	46-47 m above Ol-Oa contact	Below upper bentonite bed (S2-2213 in Appendix B)	<i>Cryptograptus tricornis</i> <i>Pseudoclimacograptus angulatus</i> <i>Pseudoclimacograptus modestus</i> <i>Glyptograptus teretiusculus</i> <i>Dicellograptus gurleyi</i> <i>Dicellograptus sextans</i>	Correlation: <i>Nemagraptus gracilis</i> Zone
S2-2214	CL CALERA (Blue circle)	47-48 m above Ol-Oa contact	Above upper bentonite bed (S2-2213 in Appendix B)	<i>Didymograptus sp.</i> <i>Pseudoclimacograptus modestus</i> <i>Climacograptus meridionalis</i> <i>Glyptograptus teretiusculus</i> <i>Glyptograptus euglyphus</i> <i>Dicellograptus sextans</i> <i>Dicellograptus alabamensis</i> <i>Nemagraptus gracilis</i>	Correlation: <i>Nemagraptus gracilis</i> Zone
S2-2219	CL CALERA (Blue circle)	1 m beneath Oa-Dfm contact	Graptolites in the uppermost black shale lithofacies	<i>Didymograptus sp.</i> <i>Cryptograptus tricornis</i> <i>Glyptograptus teretiusculus</i> <i>Glyptograptus euglyphus</i> <i>Dicellograptus gurleyi</i> <i>Dicellograptus sextans</i> <i>Dicellograptus alabamensis</i> <i>Leptograptus trentonensis</i>	Correlation: upper part of <i>Nemagraptus gracilis</i> Zone

**Table B.1 (continued)**

Sample	Location	Stratigraphic position	General remarks	Graptolites (by Stanley Finney)	Remarks (by Stanley Finney)
S2-2220	CL CALERA (Blue circle)	0.3 m beneath Oa-Dfm contact	Graptolites in green silty shale lithofacies overlying sandstone beds of the Athens Shale; however, graptolites disappear abruptly in a few centimeters above.	<i>Glyptograptus euglyphus</i> <i>Pseudoclimacograptus modestus</i> <i>Dicellograptus sp.</i>	Correlation: <i>Nemagraptus gracilis</i> Zone. Too few species to determine level within zone.
S2-2506	EC EAST CALERA SE1/4 SW1/4 sec 16 T22S R2W Ozan quad.	3-5 m above Ol-Oa contact	Here the section is only 15 m thick	<i>Thamnograptus sp.</i> <i>Didymograptus superstes</i> <i>Reteograptus geinitzianus</i> <i>Cryptograptus tricornis</i> <i>Glyptograptus teretiusculus</i> <i>?Nemagraptus gracilis</i>	Correlation: <i>Nemagraptus gracilis</i> Zone. Too few species to determine level within zone.
S2-2805	CL CALERA (Vulcan quarry)	10 m above Oa-Ol contact	Graptolites below and above bentonite bed (S2-2806 and S2-2807)	<i>Didymograptus sp.</i> <i>?Glossograptus sp.</i> <i>Pseudoclimacograptus angulatus</i> <i>Glyptograptus euglyphus</i>	Correlation: Many specimens, but most are too heavily carbonized to identify. Those identified range from the <i>G. teretiusculus</i> Zone through the <i>N. gracilis</i> Zone.
Q3-0201	AB ALABASTER NE1/4 SW1/4 sec. 25 T20S R3W Helena quad.	3-5 m above Olol-Oa contact.	The Oa is only 10 m thick and pinches out (?) northward	<i>?Nemagraptus sp.</i> <i>Pseudoclimacograptus sp.</i> <i>Climacograptus sp.</i>	Correlation: Nemagraptid identification is uncertain. Can only state with some uncertainty that this collection correlates with a level somewhere within the <i>G. teretiusculus</i> and <i>N. gracilis</i> Zones.
Q3-0303	AB ALABASTER (junction 31-119 roads) SW1/4 NE1/4 sec. 2 T21S R3W Alabaster quad.	6 m above Ol-Oa contact	The Oa is 27 m thick	<i>?Glyptograptus</i>	
Q3-0304	AB ALABASTER (junction 31-119 roads) SW1/4 NE1/4 SEC. 2 T21S R3W Alabaster quad.	23-25 m above Ol-Oa contact	The Oa is 27 m thick	<i>Didymograptus sp.</i> <i>Cryptograptus sp.</i> <i>Pseudoclimacograptus angulatus?</i> <i>Pseudoclimacograptus modestus?</i> <i>Climacograptus meridionalis?</i> <i>Glyptograptus sp.</i> <i>Glyptograptus euglyphus?</i> <i>Dicellograptus alabamensis</i>	Correlation: specimens are tectonically deformed and very poorly preserved, making identifications of species difficult. Nevertheless, this collection can be correlated with the <i>Nemagraptus gracilis</i> Zone.
R3-0702	HV HARPERSVILLE (junction 79-76) NE1/4 NE1/4 sec 14 T20S R2E Harpersville quad.	Lower Athens Shale?	Structurally is located in the eastern belt that corresponds to black shales with graptolites	<i>biseriate graptolite?</i>	but further identification not possible. Several specimens are very faint molds in very friable mudstone. I wonder if they are even graptolites. Correlation: middle to upper Ordovician if specimens are graptolites
R3-0703	HV HARPERSVILLE (junction 79-76) NE1/4 NE1/4 sec 14 T20S R2E Harpersville quad.	Lower Athens Shale?	Structurally is located 40 m to the east of sample R3-0702	<i>Climacograptus sp.</i> <i>Pseudoclimacograptus angulatus</i> <i>Glyptograptus sp.</i>	Correlation: <i>murchisoni</i> , <i>teretiusculus</i> , or <i>gracilis</i> zone; can't be more precise.
R3-0807	HV HARPERSVILLE NW 1/4 sec 23 T19S R2E Harpersville quad.	Lower Athens Shale?	Structurally is located to the east, in the black shale belt with graptolites. Locality #5 of Finney et al., 1996. 1 sample.	<i>Cryptograptus tricornis</i> <i>Pseudoclimacograptus sp.</i> <i>Glyptograptus teretiusculus</i>	Correlation: <i>murchisoni</i> , <i>teretiusculus</i> , or <i>gracilis</i> zone; probably one of the first two.
O4-0406	LM Leydens Mill NE1/4 NE1/4 sec 19 T14S R8E Jacsonville West quad.	Athens shale	Greenish silty shale interbedded with sandstones		Couple of unidentifiable, questionable graptolites
I4-0601	FM FROG MOUNTAIN NE1/4 SW1/4 sec 16 T12S R10E Piedmont quad.	Athens Shale	Greenish silty shale interbedded with sandstones	<i>Dicellograptus sp.</i> <i>Glyptograptus sp. (probably G. teretiusculus)</i>	Correlation: somewhere in <i>N. gracilis</i> Zone.

## APPENDIX C

### TECTONIC SUBSIDENCE DATA

Tectonic subsidence analysis was carried out in each section assuming that the top of Ordovician was ultimately buried to a depth of at least 4 km (from an estimate of the thickest post-Ordovician succession in the Cahaba synclinorium in the southern Appalachians, cross section 16, Plate 2.1). I used backstripping techniques (e.g., Slater and Christie, 1980; Allen and Allen, 1992) to decompact the measured stratigraphic thickness; this technique assumes a lithology-dependent exponential decrease of porosity with depth, a fully saturated column of sediments, and local compensation (Airy isostasy) of sedimentary loads. Initial porosities and porosity-depth coefficients (values from Slater and Christie, 1980) were averaged according to the percentage of each lithology in each stratigraphic interval (Plates 3.1 to 3.10 and Plates 4.2 to 4.3). Tectonic subsidence analysis for each section was carried out using MatLab programs written by Nestor Cardozo at Cornell University. The tectonic subsidence program uses the assumptions specified above.

The Paleozoic strata were divided into the following intervals: Rome Formation and older units; Conasauga Formation; Conasauga Formation and older units (if data of the Rome Formation or older units are not available); Knox Group; post-Knox unconformity; the Middle and Upper Ordovician strata are divided using the stratigraphic surfaces of correlation; Silurian strata; Devonian strata; Carboniferous strata; model= stratigraphic thickness needed to bury the top of Ordovician to a depth of 4 km. Calculation of thickness of post-Ordovician strata is from the literature and cross sections in Plate 2.1.

Figure C.1 explains how I interpreted the behaviour of the top of basement through the post-Knox unconformity. For calculation of the amount of basement uplift in sections BI, DG, HL, HM, and RH, I calculated the difference of decompacted (maximum) and compacted (minimum) thickness of the Knox Group between adjacent sections (e.g., difference in thickness of the Knox Group between sections BI and ST). This calculation assumes that the pre-Middle Ordovician thickness of the Knox Group was the same in sections BI and ST, thermal subsidence had the same slope until 475 Ma (Figure C.1), and the top of basement was fixed during the shortest chronostratigraphic gap of the post-Knox unconformity.

The following table includes the parameters used for each interval in the calculation of tectonic subsidence. From left to right are: top and base of units, ages of the top and base, density= average dry density, c= coefficient determining the slope of the porosity-depth curve, porosity= average initial porosity, minimum and maximum estimate of water depth for the top of the interval, and sea level position relative to present. Figures C.1 and C.18 include, for each section, one plot of decompacted depth versus time, and another plot showing total thickness, total decompacted thickness, total decompacted thickness corrected for the weight of sediments, and tectonic subsidence versus time



section AB ALABASTER

INTERVAL	top	base	top	base	density	c	porosity	water depth (km)		Sea level
	(km)	(km)	(Ma)	(Ma)	(kgr m-3)	(km-1)		minimum	maximum	(km)
Rome Fm. and older	5.923	6.228	517	544	2680	0.39	0.56	0.004	0.004	0.03
Conasauga Fm.	5.49	5.923	505	517	2710	0.71	0.7	0.004	0.016	0.07
Knox Group	4.256	5.49	475	505	2710	0.71	0.7	0	0.004	0.08
post-Knox unconformity	4.256	4.256	466	475	0	0	0	0	0	0
1-3	4.027	4.256	458	466	2710	0.71	0.7	0.016	0.064	0
3-6	4	4.027	457	458	2720	0.51	0.63	0.064	0.125	0
post-Ordovician unconformity	4	4	417	457	0	0	0	0	0	0.07
Devonian	3.999	4	354	417	2650	0.27	0.49	0.016	0.016	0.15
Carboniferous	1.966	3.999	290	354	2680	0.39	0.56	0.016	0.016	0.15
model	0	1.966	270	290	2680	0.39	0.56	0.016	0.016	0.15

section BR BIG RIDGE

INTERVAL	top	base	top	base	density	c	porosity	water depth (km)		Sea level
	(km)	(km)	(Ma)	(Ma)	(kgr m-3)	(km-1)		minimum	maximum	(km)
Rome Fm. and older	5.872	6.116	517	544	2680	0.39	0.56	0.004	0.004	0.03
Conasauga Fm.	5.238	5.872	505	517	2710	0.71	0.7	0.004	0.016	0.07
Knox Group	4.165	5.238	483	505	2710	0.71	0.7	0	0.004	0.1
post-Knox unconformity	4.165	4.165	458	483	0	0	0	0	0	0
5-6	4.15	4.165	457	458	2710	0.71	0.7	0.004	0.016	0
6-8	4.092	4.15	454	457	2710	0.71	0.7	0	0.004	0
8-11	4	4.092	443	454	2710	0.62	0.67	0.016	0.064	0.065
Silurian	3.86	4	417	443	2680	0.39	0.56	0.004	0.016	0.07
Devonian	3.852	3.86	354	417	2720	0.51	0.63	0.016	0.016	0.15
Carboniferous	3.398	3.852	290	354	2685	0.5	0.61	0.016	0.016	0.15
model	0	3.398	270	290	2680	0.39	0.56	0.016	0.016	0.15

section BI BIRMINGHAM

INTERVAL	top	base	top	base	density	c	porosity	water depth (km)		Sea level
	(km)	(km)	(Ma)	(Ma)	(kgr m-3)	(km-1)		minimum	maximum	(km)
Rome Fm. and older	5.602	7.571	517	544	2680	0.39	0.56	0.004	0.004	0.03
Conasauga Fm.	4.858	5.602	505	517	2710	0.71	0.7	0.004	0.016	0.07
Knox Group	4.096	4.858	490	505	2710	0.71	0.7	0	0.004	0.09
post-Knox unconformity	4.096	4.096	458	490	0	0	0	0	0	0
3-6	4.067	4.096	457	458	2710	0.71	0.7	0.004	0.016	0
6-8.1	4.011	4.067	454	457	2710	0.71	0.7	0	0.004	0
8.1-11	4	4.011	443	454	2710	0.71	0.7	0.016	0.064	0.065
Silurian	3.922	4	417	443	2680	0.39	0.56	0.016	0.064	0.07
Devonian	3.89	3.922	354	417	2720	0.51	0.63	0.016	0.016	0.15
Carboniferous	2.79	3.89	290	354	2685	0.5	0.61	0.016	0.016	0.15
model	0	2.79	270	290	2680	0.39	0.56	0.016	0.016	0.15

section CL CALERA

INTERVAL	top	base	top	base	density	c	porosity	water depth (km)		Sea level
	(km)	(km)	(Ma)	(Ma)	(kgr m-3)	(km-1)		minimum	maximum	(km)
Rome Fm. and older	5.732	6.723	517	544	2680	0.39	0.56	0.004	0.004	0.03
Conasauga Fm.	5.358	5.732	505	517	2710	0.71	0.7	0.004	0.016	0.07
Knox Group	4.124	5.358	475	505	2710	0.71	0.7	0	0.004	0.08
post-Knox unconformity	4.124	4.124	466	475	0	0	0	0	0	0
1-3	4.065	4.124	458	466	2710	0.71	0.7	0.016	0.064	0
3-6	4	4.065	457	458	2720	0.51	0.63	0.4	0.8	0
post-Ordovician unconformity	4	4	417	457	0	0	0	0	0.004	0.07
Devonian	3.998	4	354	417	2650	0.27	0.49	0.016	0.016	0.15
Carboniferous	1.965	3.998	290	354	2680	0.39	0.56	0.016	0.016	0.15
model	0	1.965	270	290	2680	0.39	0.56	0.016	0.016	0.15

section CH-RI CHICKAMAUGA-RINGGOLD

INTERVAL	top	base	top	base	density	c	porosity	water depth (km)		Sea level
	(km)	(km)	(Ma)	(Ma)	(kgr m-3)	(km-1)		minimum	maximum	(km)
Rome Fm. and older	6.399	6.459	517	544	2680	0.39	0.56	0.004	0.016	0.03
Conasauga Fm.	5.236	6.399	505	517	2713	0.65	0.68	0.004	0.016	0.07
Knox Group	4.504	5.236	478	505	2710	0.71	0.7	0	0.004	0.085
post-Knox unconformity	4.504	4.504	466	478	0	0	0	0	0	0
1-5	4.457	4.504	458	466	2710	0.71	0.7	0.004	0.016	0
5-6	4.399	4.457	457	458	2710	0.71	0.7	0.004	0.016	0
6-8	4.19	4.399	454	457	2710	0.71	0.7	0	0.004	0
8-11	4	4.19	443	454	2705	0.65	0.67	0.016	0.064	0.065
Silurian	3.855	4	417	443	2680	0.39	0.56	0.016	0.016	0.07
Devonian	3.85	3.855	354	417	2720	0.51	0.63	0.016	0.016	0.15
Carboniferous	3.02	3.85	290	354	2689	0.49	0.6	0.016	0.016	0.15
model	0	3.02	270	290	2680	0.39	0.56	0.016	0.016	0.15

section CI CISCO

INTERVAL	top	base	top	base	density	c	porosity	water depth (km)		Sea level
	(km)	(km)	(Ma)	(Ma)	(kgr m-3)	(km-1)		minimum	maximum	(km)
Conasauga Fm. and older	5.548	6.758	505	544	2696	0.5	0.61	0.004	0.016	0.07
Knox Group	4.634	5.548	478	505	2710	0.71	0.7	0	0	0.085
post-Knox unconformity	4.634	4.634	463	478	0	0	0	0	0	0
2-3	4.562	4.634	458	463	2720	0.51	0.63	0.1	0.3	0
3-6	4.068	4.562	457	458	2712	0.49	0.62	0.016	0.064	0
6-7	4	4.068	456	457	2704	0.46	0.6	0.004	0.016	0
model	0	4	270	456	2680	0.39	0.56	0.016	0.016	0.15

section DG DUG GAP

INTERVAL	top	base	top	base	density	c	porosity	water depth (km)		Sea level
	(km)	(km)	(Ma)	(Ma)	(kgr m-3)	(km-1)		minimum	maximum	(km)
Rome Fm. and older	5.225	6.08	517	544	2713	0.49	0.62	0.004	0.016	0.03
Conasauga Fm.	4.725	5.225	505	517	2715	0.61	0.67	0.004	0.016	0.07
Knox Group	4.268	4.725	490	505	2710	0.71	0.7	0	0.004	0.09
post-Knox unconformity	4.268	4.268	458	490	0	0	0	0	0	0
5-6	4.244	4.268	457	458	2710	0.71	0.7	0	0.004	0
6-8	4.157	4.244	454	457	2705	0.46	0.6	0.004	0.016	0
8-11	4	4.157	443	454	2701	0.45	0.6	0.004	0.016	0.065
Silurian	3.63	4	417	443	2680	0.39	0.56	0.016	0.016	0.07
Devonian	3.603	3.63	354	417	2664	0.67	0.69	0.016	0.016	0.15
Carboniferous	2.433	3.603	290	354	2689	0.49	0.6	0.016	0.016	0.15
model	0	2.433	270	290	2680	0.39	0.56	0.016	0.016	0.15

section DM DUNAWAY MOUNTAIN

INTERVAL	top	base	top	base	density	c	porosity	water depth (km)		Sea level
	(km)	(km)	(Ma)	(Ma)	(kgr m-3)	(km-1)		minimum	maximum	(km)
Rome Fm. and older	5.625	7.277	517	544	2680	0.39	0.56	0.004	0.004	0.03
Conasauga Fm.	4.991	5.625	505	517	2715	0.61	0.67	0.004	0.016	0.07
Knox Group	4.077	4.991	483	505	2710	0.71	0.7	0	0.004	0.1
post-Knox unconformity	4.077	4.077	458	483	0	0	0	0	0	0
5-6	4.059	4.077	457	458	2711	0.69	0.69	0	0.004	0
6-8	4.047	4.059	454	457	2712	0.68	0.69	0	0.004	0
8-11	4	4.047	443	454	2704	0.54	0.63	0.016	0.064	0.065
Silurian	3.86	4	417	443	2680	0.39	0.56	0.004	0.016	0.07
Devonian	3.852	3.86	354	417	2720	0.51	0.63	0.016	0.016	0.15
Carboniferous	3.398	3.852	290	354	2685	0.5	0.61	0.016	0.016	0.15
model	0	3.398	270	290	2680	0.39	0.56	0.016	0.016	0.15

section GS GREENSPORT

INTERVAL	top	base	top	base	density	c	porosity	water depth (km)		Sea level
	(km)	(km)	(Ma)	(Ma)	(kgr m-3)	(km-1)		minimum	maximum	(km)
Rome Fm. and older	5.299	6.051	517	544	2680	0.39	0.56	0.004	0.004	0.03
Conasauga Fm.	5.189	5.299	505	517	2720	0.51	0.63	0.004	0.016	0.07
Knox Group	4.153	5.189	478	505	2710	0.71	0.7	0	0.004	0.085
post-Knox unconformity	4.153	4.153	458	478	0	0	0	0	0	0
3-6	4.098	4.153	457	458	2709	0.65	0.68	0.016	0.064	0
6-8	4.047	4.098	454	457	2698	0.45	0.59	0.004	0.016	0
8-11	4	4.047	443	454	2707	0.6	0.65	0.004	0.016	0.065
Silurian	3.967	4	417	443	2680	0.39	0.56	0.004	0.016	0.07
Devonian	3.962	3.967	354	417	2680	0.39	0.56	0.016	0.016	0.15
Carboniferous	3.086	3.962	290	354	2685	0.5	0.61	0.016	0.016	0.15
model	0	3.086	270	290	2680	0.39	0.56	0.016	0.016	0.15

section GU GUNSTERVILLE

INTERVAL	top	base	top	base	density	c	porosity	water depth (km)		Sea level
	(km)	(km)	(Ma)	(Ma)	(kgr m-3)	(km-1)		minimum	maximum	(km)
Rome Fm. and older	5.921	6.11	517	544	2680	0.39	0.56	0.004	0.004	0.03
Conasauga Fm.	5.287	5.921	505	517	2710	0.71	0.7	0.004	0.016	0.07
Knox Group	4.296	5.287	485	505	2710	0.71	0.7	0	0.004	0.11
post-Knox unconformity	4.296	4.296	458	485	0	0	0	0	0	0
5-8	4.056	4.296	454	458	2710	0.71	0.7	0	0.004	0
8-11	4	4.056	443	454	2710	0.62	0.67	0.016	0.064	0.065
Silurian	3.942	4	417	443	2680	0.39	0.56	0	0.004	0.07
Devonian	3.927	3.942	354	417	2720	0.51	0.63	0.016	0.016	0.15
Carboniferous	3.482	3.927	290	354	2685	0.5	0.61	0.016	0.016	0.15
model	0	3.482	270	290	2680	0.39	0.56	0.016	0.016	0.15

section HM HAMILTON MOUNTAIN

INTERVAL	top	base	top	base	density	c	porosity	water depth (km)		Sea level
	(km)	(km)	(Ma)	(Ma)	(kgr m-3)	(km-1)		minimum	maximum	(km)
Rome Fm. and older	5.361	6.081	517	544	2713	0.49	0.62	0.004	0.016	0.03
Conasauga Fm.	4.861	5.361	505	517	2712	0.59	0.65	0.004	0.016	0.07
Knox Group	4.311	4.861	485	505	2710	0.71	0.7	0	0.004	0.11
post-Knox unconformity	4.311	4.311	458	485	0	0	0	0	0	0
3-6	4.203	4.311	457	458	2710	0.71	0.7	0.004	0.016	0
6-8	4.004	4.203	454	457	2712	0.5	0.62	0.016	0.064	0
8-9	4	4.004	451	454	2700	0.45	0.6	0.016	0.016	0.023
model	0	4	270	451	2680	0.39	0.56	0.016	0.016	0.15

section HL HORSELEG MOUNTAIN

INTERVAL	top	base	top	base	density	c	porosity	water depth (km)		Sea level
	(km)	(km)	(Ma)	(Ma)	(kgr m-3)	(km-1)		minimum	maximum	(km)
Conasauga Fm. and older	4.819	5.794	505	544	2705	0.51	0.62	0.004	0.016	0.07
Knox Group	4.209	4.819	490	505	2710	0.71	0.7	0	0.004	0.09
post-Knox unconformity	4.209	4.209	458	490	0	0	0	0	0	0
3-6	4.172	4.209	457	458	2699	0.57	0.65	0	0.004	0
6-8	4.063	4.172	454	457	2704	0.46	0.6	0.004	0.016	0
8-11	4	4.063	443	454	2704	0.46	0.6	0.016	0.064	0.065
Silurian	3.63	4	417	443	2680	0.39	0.56	0.016	0.016	0.07
Devonian	3.603	3.63	354	417	2664	0.67	0.69	0.016	0.016	0.15
Carboniferous	2.433	3.603	290	354	2689	0.49	0.6	0.016	0.016	0.15
model	0	2.433	270	290	2680	0.39	0.56	0.016	0.016	0.15

section LM LEYENDS MILL

INTERVAL	top	base	top	base	density	c	porosity	water depth (km)		Sea level
	(km)	(km)	(Ma)	(Ma)	(kgr m-3)	(km-1)		minimum	maximum	(km)
Conasauga Fm. and older	5.679	6.541	505	544	2696	0.5	0.61	0.004	0.016	0.07
Knox Group	4.643	5.679	478	505	2710	0.71	0.7	0	0.004	0.085
post-Knox unconformity	4.643	4.643	466	478	0	0	0	0	0	0
1-3	4	4.643	458	466	2714	0.5	0.62	0.4	0.8	0
post-Ordovician unconformity	4	4	354	458	0	0	0	0.016	0.016	0.15
model	0	4	270	354	2680	0.39	0.56	0.016	0.016	0.15

section PF PRATT FERRY

INTERVAL	top	base	top	base	density	c	porosity	water depth (km)		Sea level
	(km)	(km)	(Ma)	(Ma)	(kgr m-3)	(km-1)		minimum	maximum	(km)
Rome Fm. and older	5.887	6.878	517	544	2680	0.39	0.56	0.004	0.004	0.03
Conasauga Fm.	5.513	5.887	505	517	2710	0.71	0.7	0.004	0.016	0.07
Knox Group	4.279	5.513	478	505	2710	0.71	0.7	0	0.004	0.085
post-Knox unconformity	4.279	4.279	466	478	0	0	0	0	0	0
1-3	4.122	4.279	458	466	2710	0.71	0.7	0.016	0.064	0
3-6	4.017	4.122	457	458	2715	0.61	0.67	0.064	0.125	0
6-8.1	4	4.017	443	457	2710	0.71	0.7	0.064	0.125	0
post-Ordovician unconformity	4	4	417	443	0	0	0	0	0	0.07
Devonian	3.991	4	354	417	2650	0.27	0.49	0.016	0.016	0.15
Carboniferous	3.965	3.991	290	354	2680	0.39	0.56	0.016	0.016	0.15
model	0	3.965	270	290	2680	0.39	0.56	0.016	0.016	0.15

section RH RED HILL

INTERVAL	top	base	top	base	density	c	porosity	water depth (km)		Sea level
	(km)	(km)	(Ma)	(Ma)	(kgr m-3)	(km-1)		minimum	maximum	(km)
Conasauga Fm. and older	4.771	5.991	505	544	2696	0.5	0.61	0.004	0.016	0.07
Knox Group	4.161	4.771	485	505	2710	0.71	0.7	0	0.004	0.11
post-Knox unconformity	4.161	4.161	458	485	0	0	0	0	0	0
3-6	4.07	4.161	457	458	2710	0.71	0.7	0.004	0.016	0
6-7	4	4.07	456	457	2708	0.53	0.63	0.016	0.016	0
model	0	4	270	456	2680	0.39	0.56	0.016	0.016	0.15

section RK ROCKMART

INTERVAL	top	base	top	base	density	c	porosity	water depth (km)		Sea level
	(km)	(km)	(Ma)	(Ma)	(kgr m-3)	(km-1)		minimum	maximum	(km)
Conasauga Fm. and older	5.265	6.765	505	544	2696	0.5	0.61	0.07	0.016	0.07
Knox Group	4.35	5.265	478	505	2710	0.71	0.7	0.085	0.004	0.085
post-Knox unconformity	4.35	4.35	466	478	0	0	0	0	0	0
1-3	4	4.35	458	466	2714	0.5	0.62	0	1	0
post-Ordovician unconformity	4	4	417	458	0	0	0	0.07	0	0.07
Devonian	3.91	4	354	417	2650	0.27	0.49	0.15	0.016	0.15
model	0	3.91	270	354	2680	0.39	0.56	0.15	0.016	0.15

section SS SHENANDOAH 1 SMITH well

INTERVAL	top	base	top	base	density	c	porosity	water depth (km)		Sea level
	(km)	(km)	(Ma)	(Ma)	(kgr m-3)	(km-1)		minimum	maximum	(km)
Rome Fm. and older	5.958	6.046	517	544	2680	0.39	0.56	0.004	0.004	0.03
Conasauga Fm.	5.299	5.958	505	517	2710	0.71	0.7	0.004	0.016	0.07
Knox Group	4.308	5.299	485	505	2710	0.71	0.7	0	0.004	0.11
post-Knox unconformity	4.308	4.308	458	485	0	0	0	0	0	0
5-8	4.062	4.308	454	458	2710	0.71	0.7	0	0.004	0
8-11	4	4.062	443	454	2710	0.62	0.67	0.016	0.064	0.065
Silurian	3.991	4	417	443	2680	0.39	0.56	0	0.004	0.07
Devonian	3.985	3.991	354	417	2720	0.51	0.63	0.016	0.016	0.15
Carboniferous	3.549	3.985	290	354	2685	0.5	0.61	0.016	0.016	0.15
model	0	3.549	270	290	2680	0.39	0.56	0.016	0.016	0.15

section ST U.S. 1 STEEL well

INTERVAL	top	base	top	base	density	c	porosity	water depth (km)		Sea level
	(km)	(km)	(Ma)	(Ma)	(kgr m-3)	km-1		minimum	maximum	(km)
Rome Fm. and older	6.106	6.124	517	544	2680	0.39	0.56	0.004	0.004	0.03
Conasauga Fm.	5.362	6.106	505	517	2710	0.71	0.7	0.004	0.016	0.07
Knox Group	4.234	5.362	485	505	2710	0.71	0.7	0	0.004	0.11
post-Knox unconformity	4.234	4.234	458	485	0	0	0	0	0	0
3-8	4.028	4.234	454	458	2710	0.71	0.7	0	0.004	0
8-11	4	4.028	443	454	2710	0.62	0.67	0.016	0.064	0.065
Silurian	3.845	4	417	443	2680	0.39	0.56	0.004	0.016	0.07
Devonian	3.84	3.845	354	417	2720	0.51	0.63	0.016	0.016	0.15
Carboniferous	2.74	3.84	290	354	2685	0.5	0.61	0.016	0.016	0.15
model	0	2.74	270	290	2680	0.39	0.56	0.016	0.016	0.15

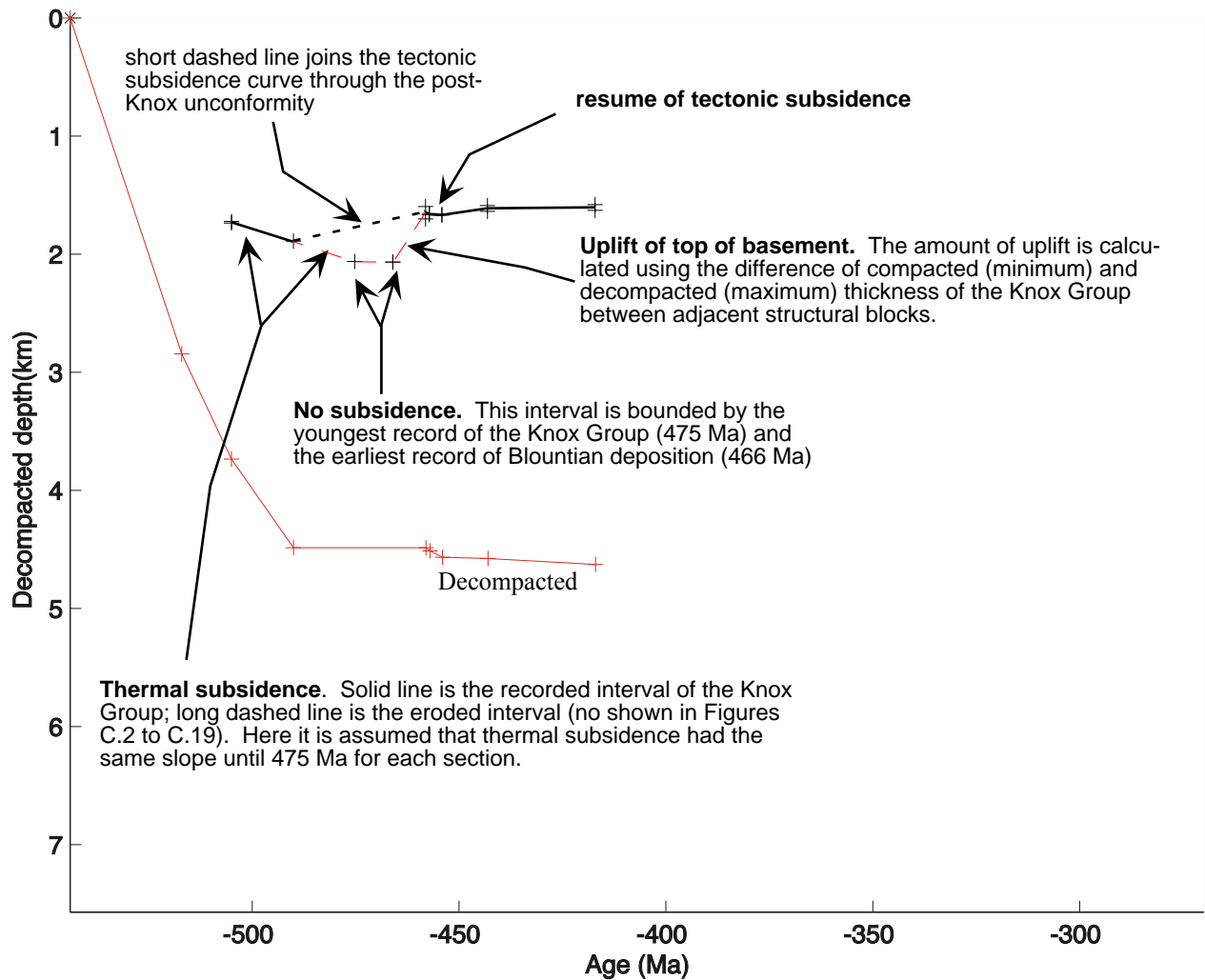


**Figure C.1** Explanation of the trace of the tectonic subsidence curve through the post-Knox unconformity (short dashed line shown in Figures C.2 to C.19). The long dashed line illustrates the behaviour of the top of basement through the post-Knox unconformity in a section that restores inside the Birmingham graben (e.g., section BI, Figure C.3). This approach assumes that passive-margin deposition was continuous until 475 Ma, the top of basement was stable during the shortest chronostratigraphic gap of the post-Knox unconformity, and the inversion of the Birmingham graben caused the uplift of the top of basement. The short dashed line joins the tectonic subsidence curve of the recorded interval of the Knox and the calculated position of the top of basement at the time of initiation of Blountian deposition. Figure C.2 (section AB) shows a section that restores outside of the graben, has the shortest chronostratigraphic gap of the post-Knox unconformity, and subsides because of the inversion of the Birmingham graben. Figure C.10 (section GS) shows a section with a longer chronostratigraphic gap of the post-Knox unconformity and a late initiation of subsidence. For simplicity, the long dashed line is not shown in Figures C.2 to C.19.

Figure C.2 Section AB - Alabaster

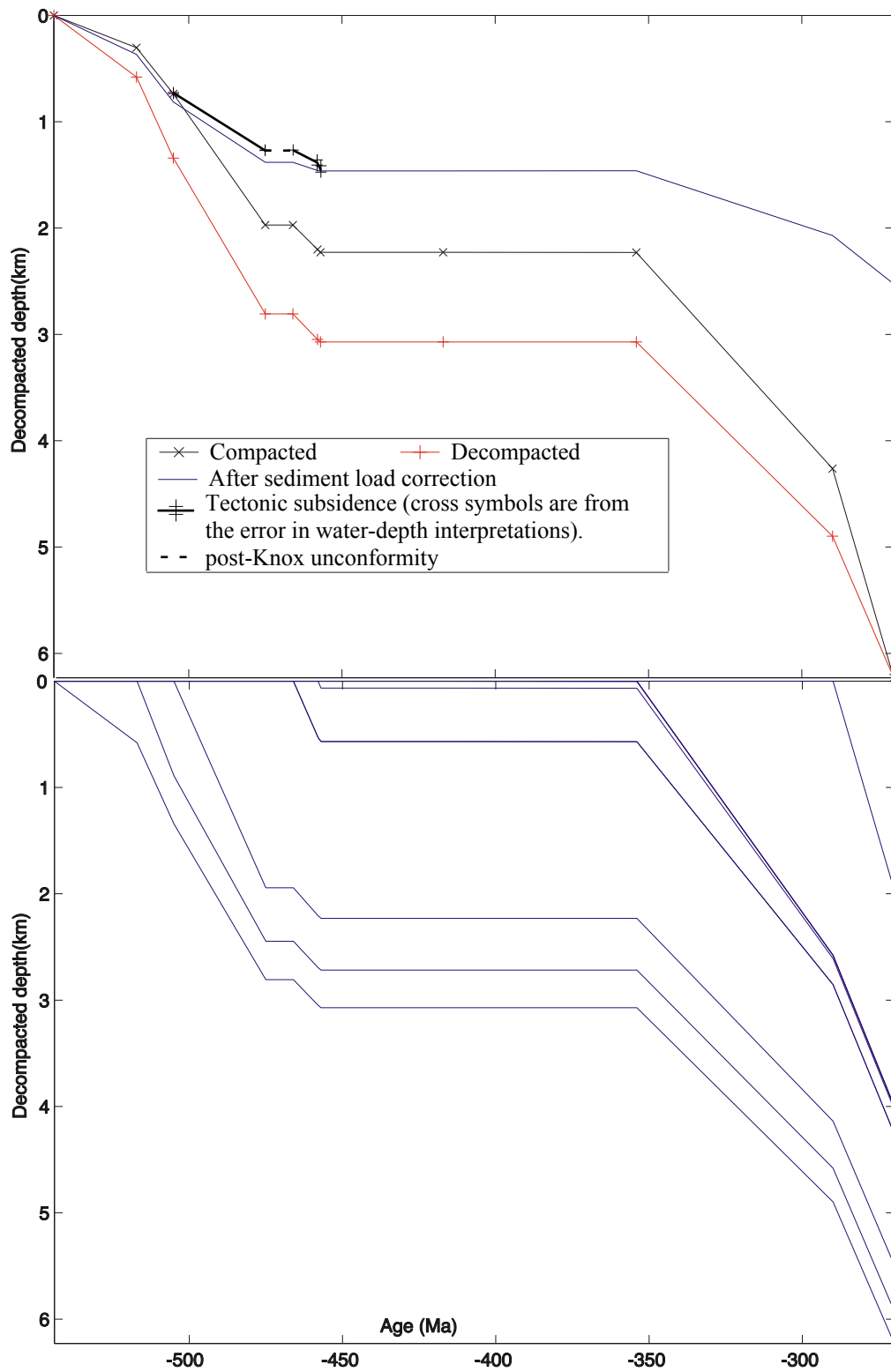


Figure C.3 Section BR - Big Ridge

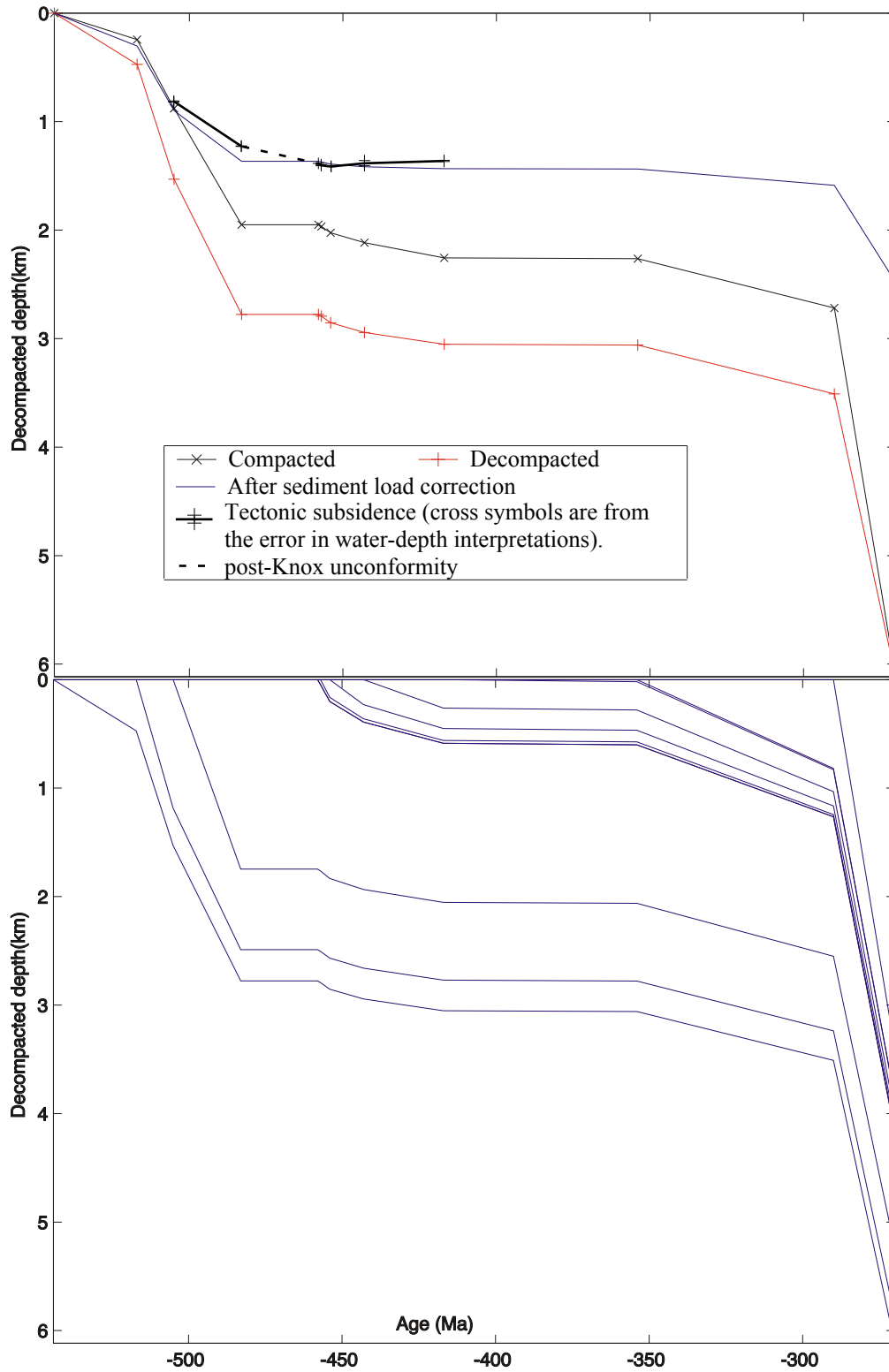




Figure C.4 Section BI - Birmingham

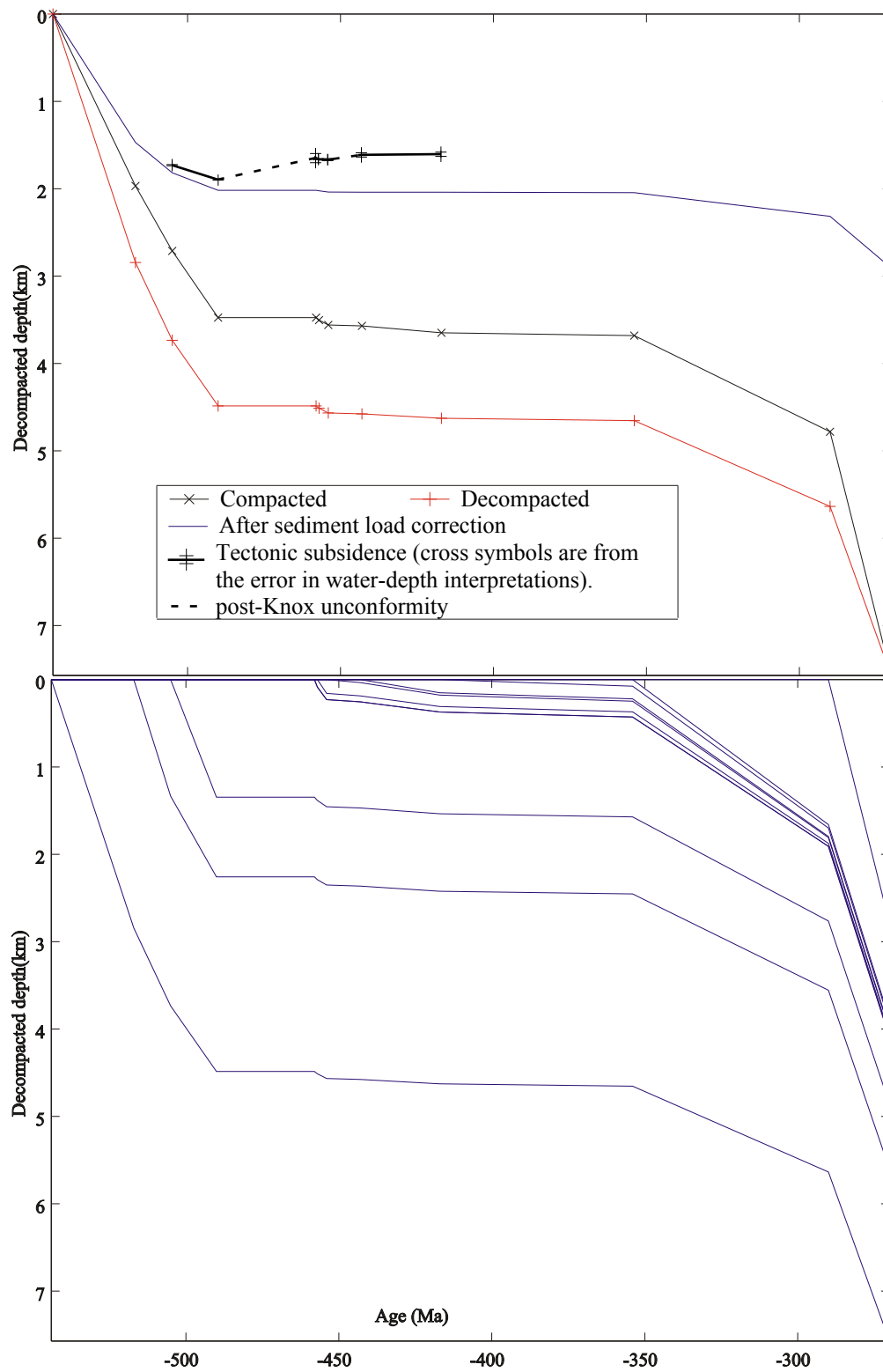


Figure C.5 Section CL - Calera

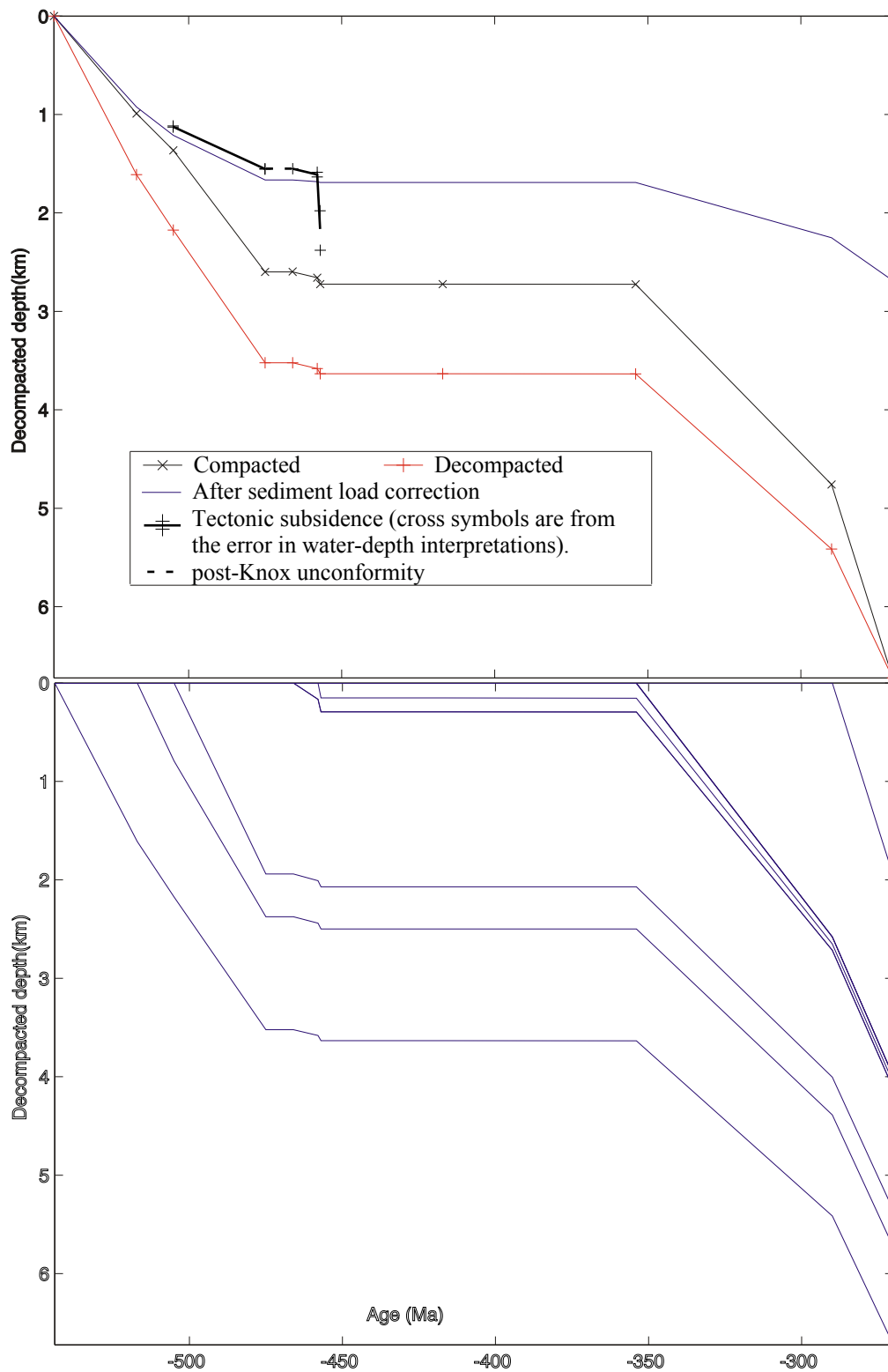


Figure C.6 Section CH-RI - Chickamauga - Ringgold

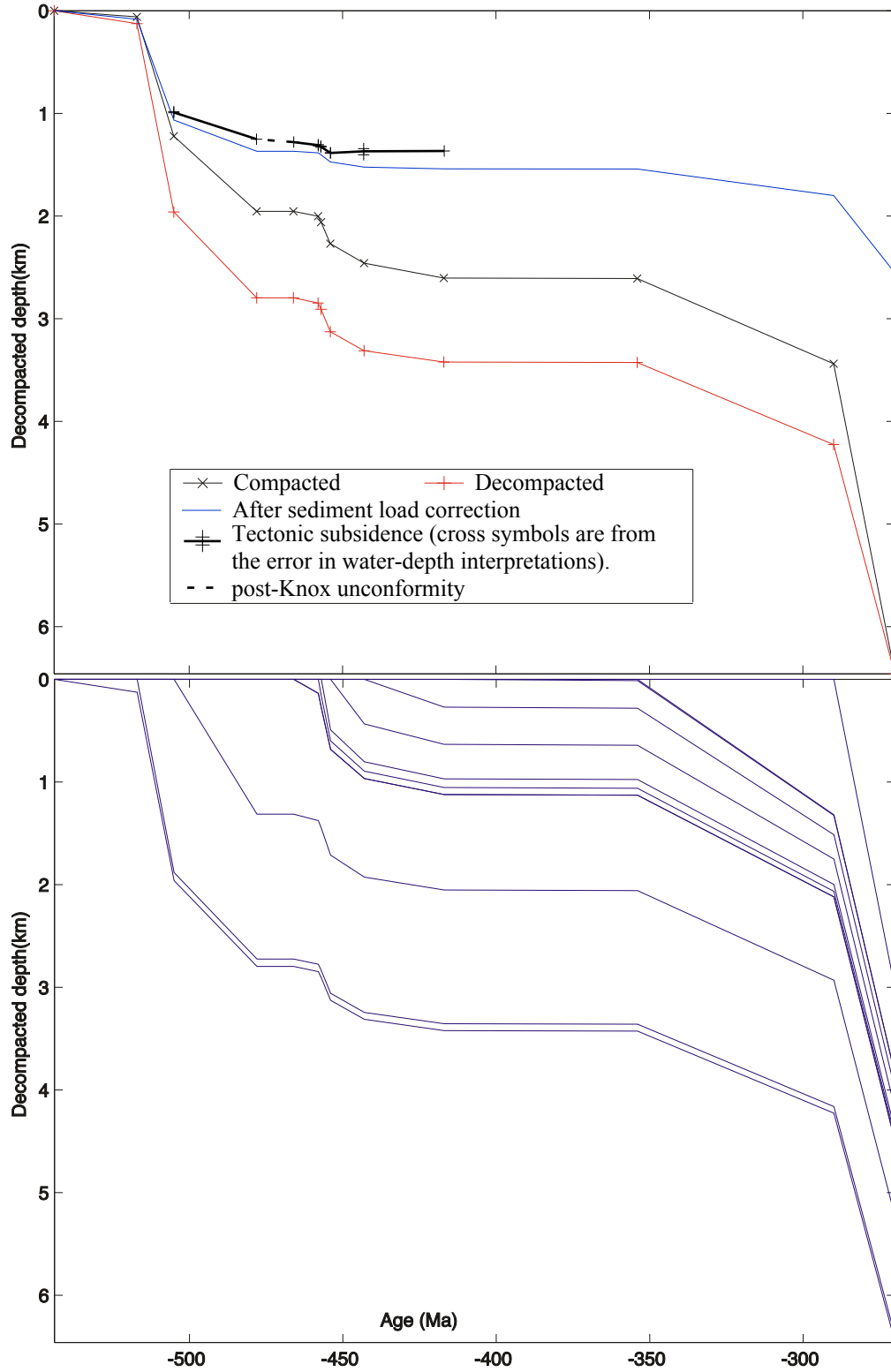
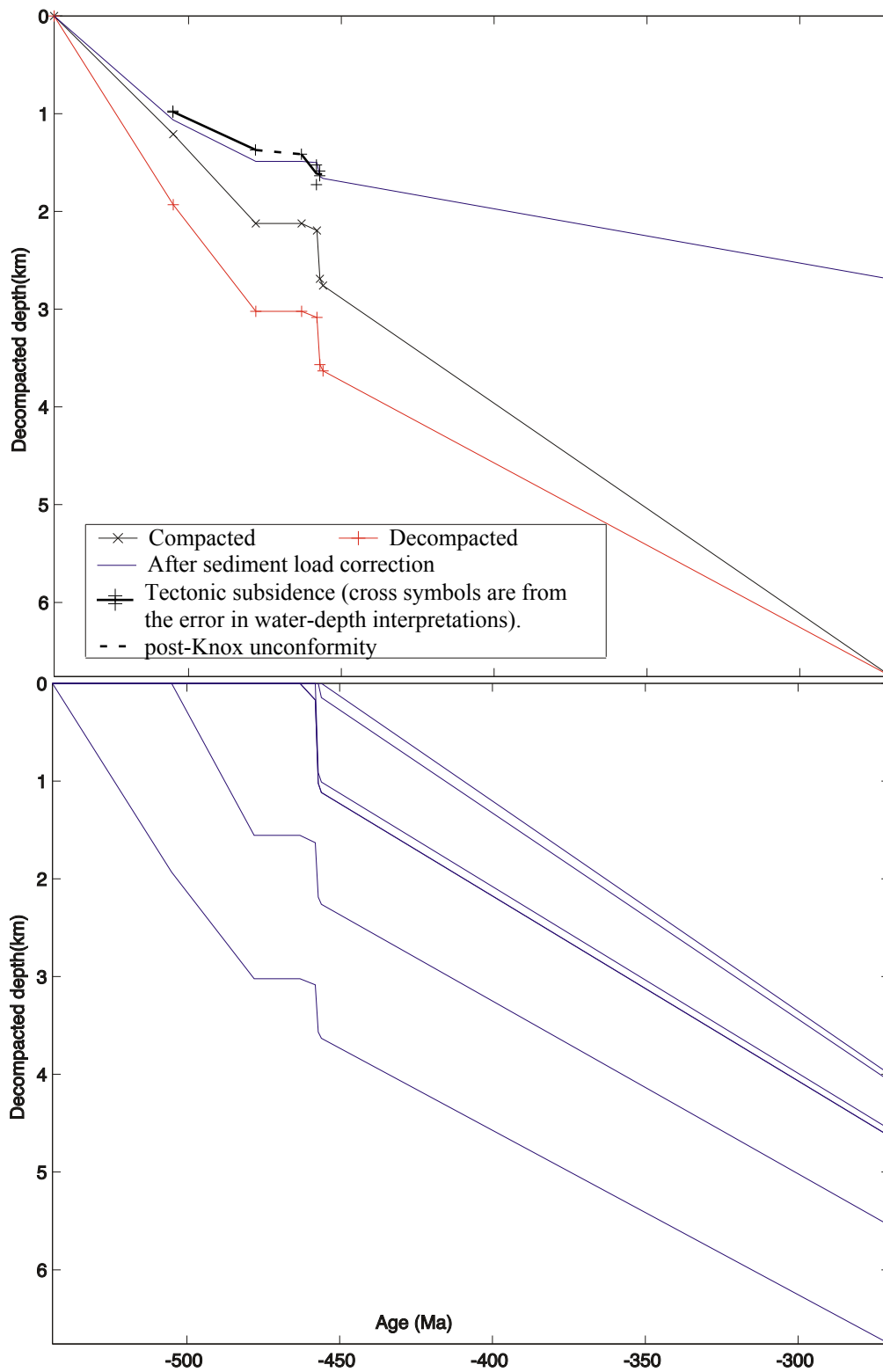
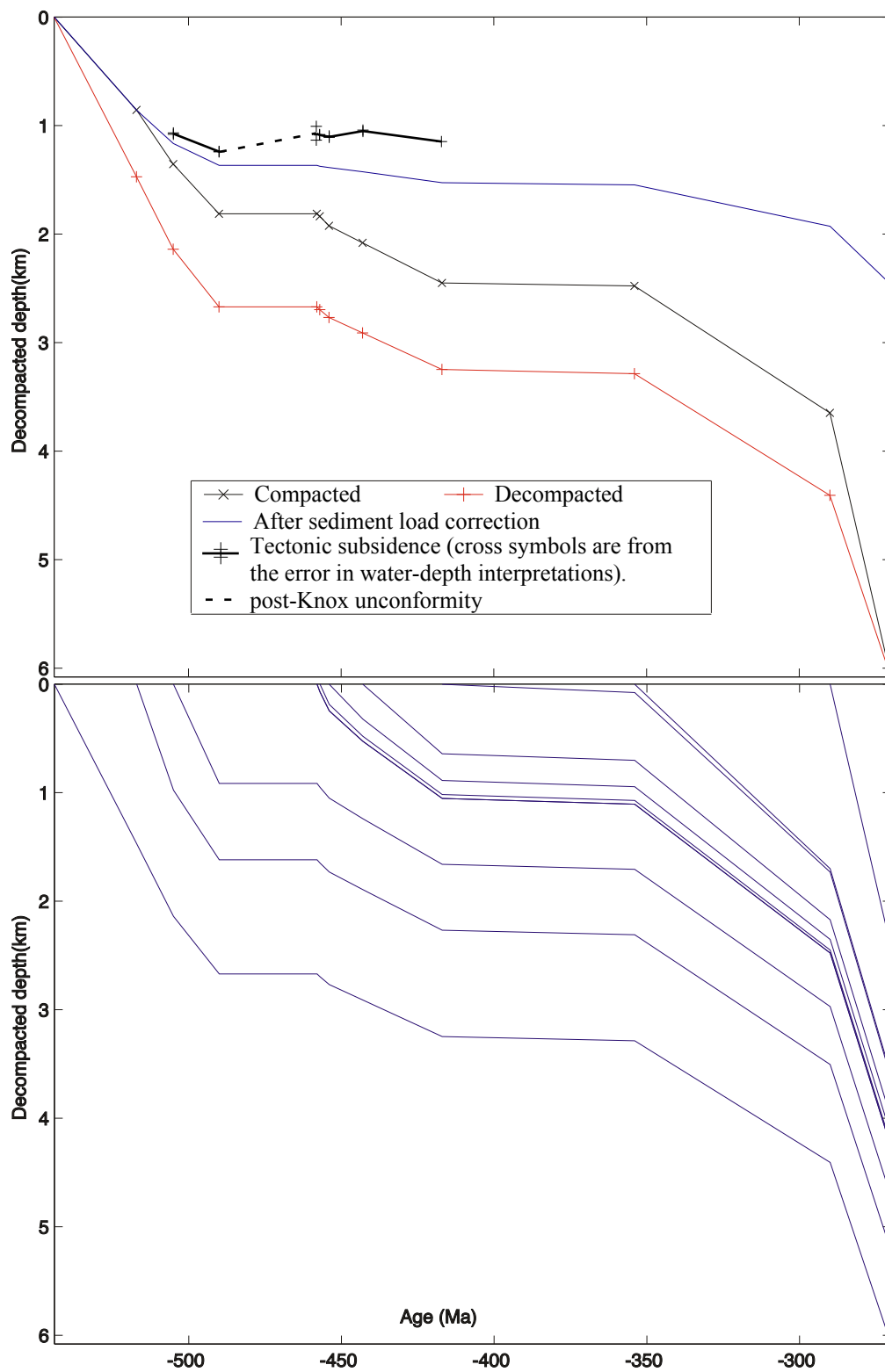


Figure C.7 Section CI - Cisco



**Figure C.8** Section DG - Dug Gap



**Figure C.9** Section DM - Dunaway Mountain

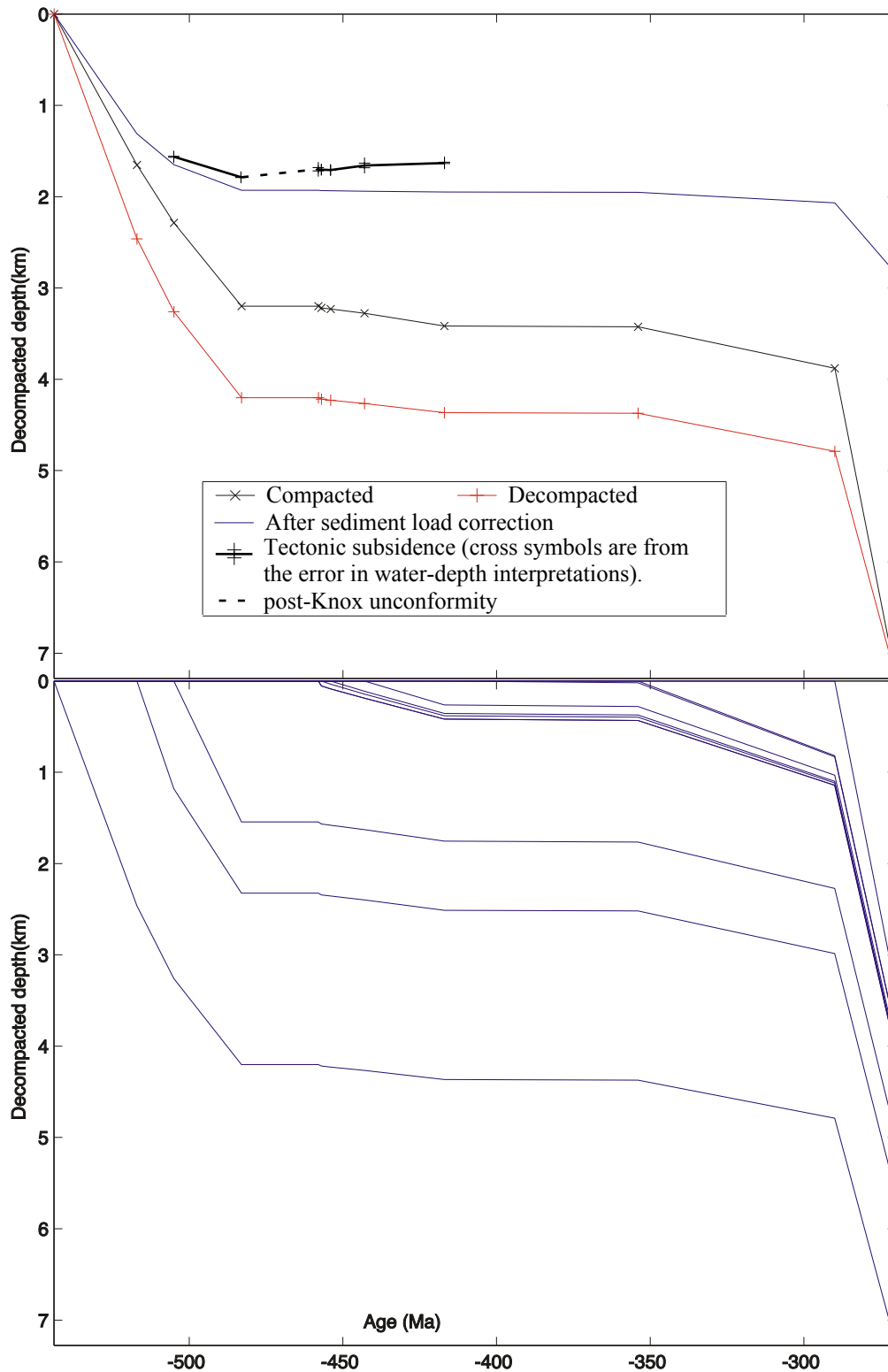


Figure C.10 Section GS - Greensport

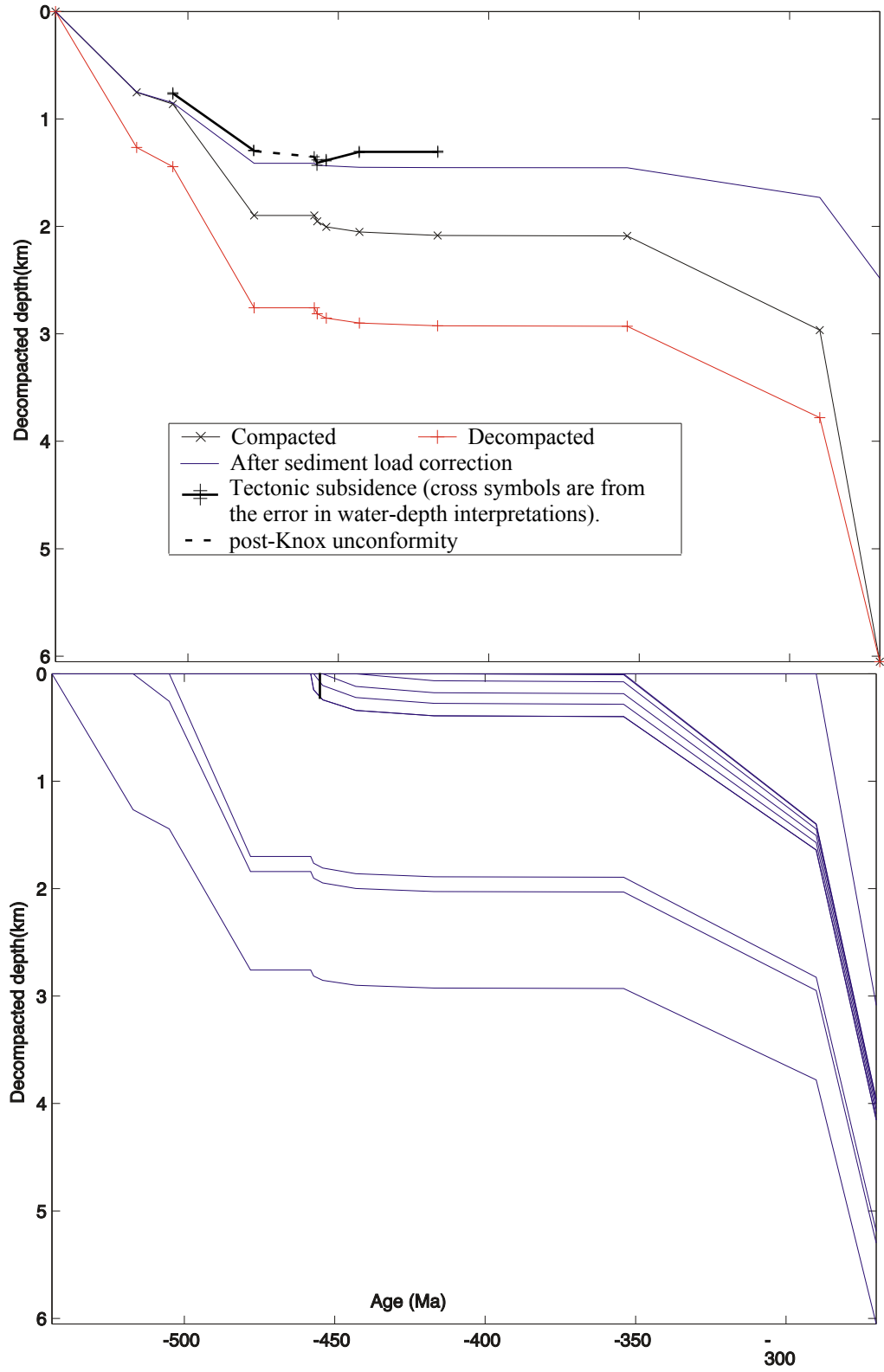
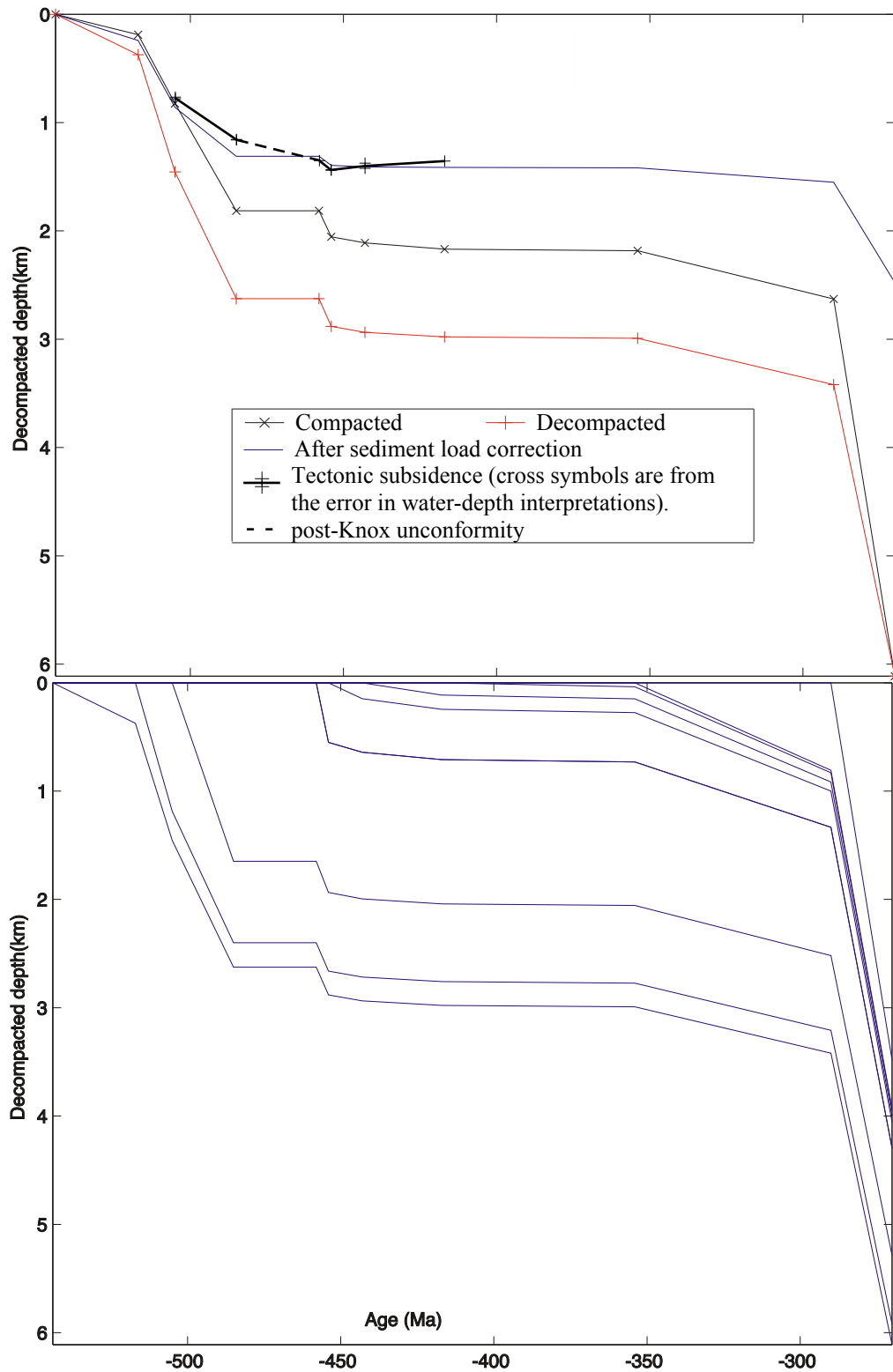
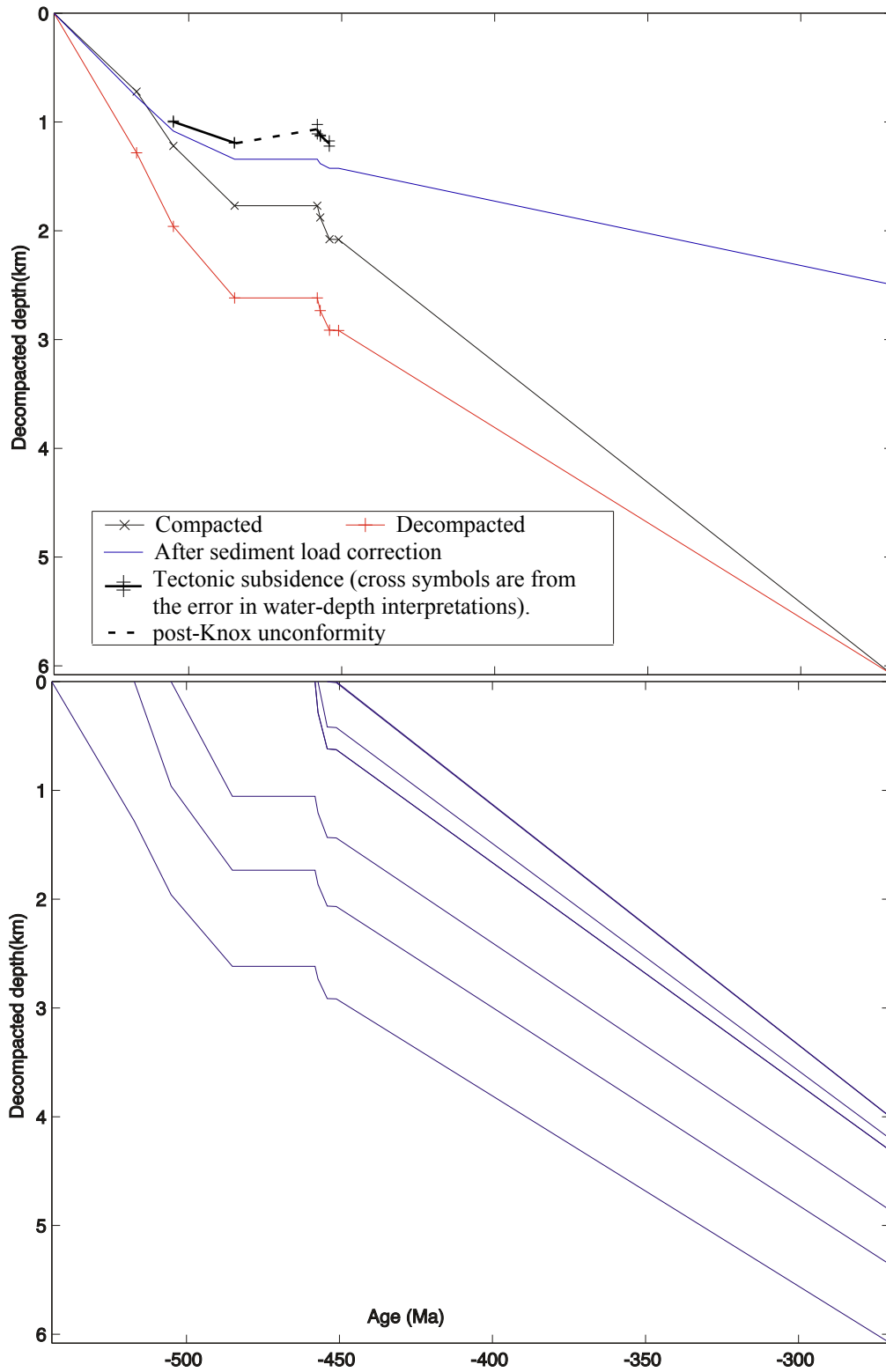


Figure C.11 Section GU - Gunsterville





**Figure C.12** Section HM - Hamilton Mountain



**Figure C.13** Section HL - Horseleg Mountain

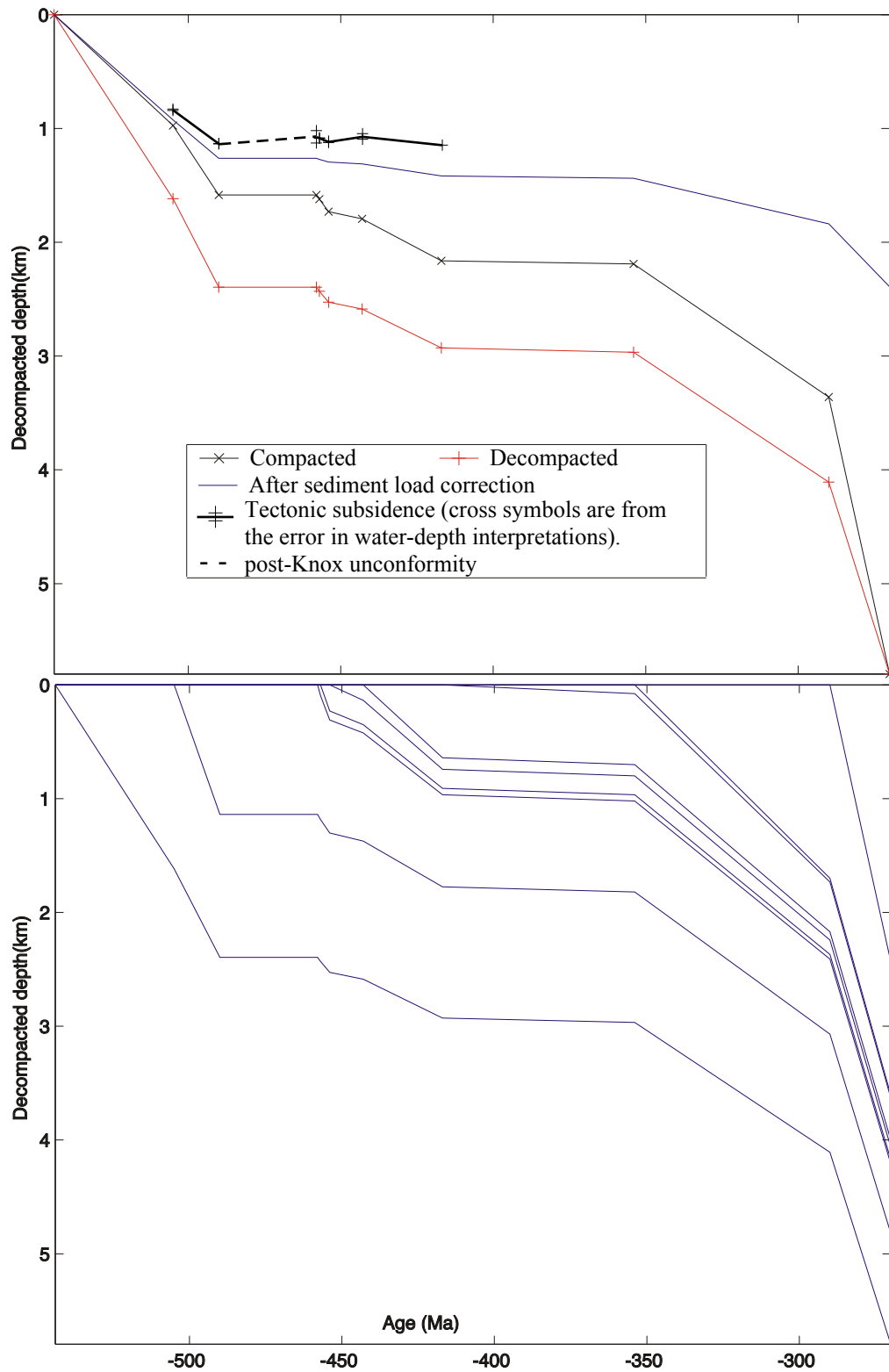


**Figure C.14** Section LM - Leyends Mill

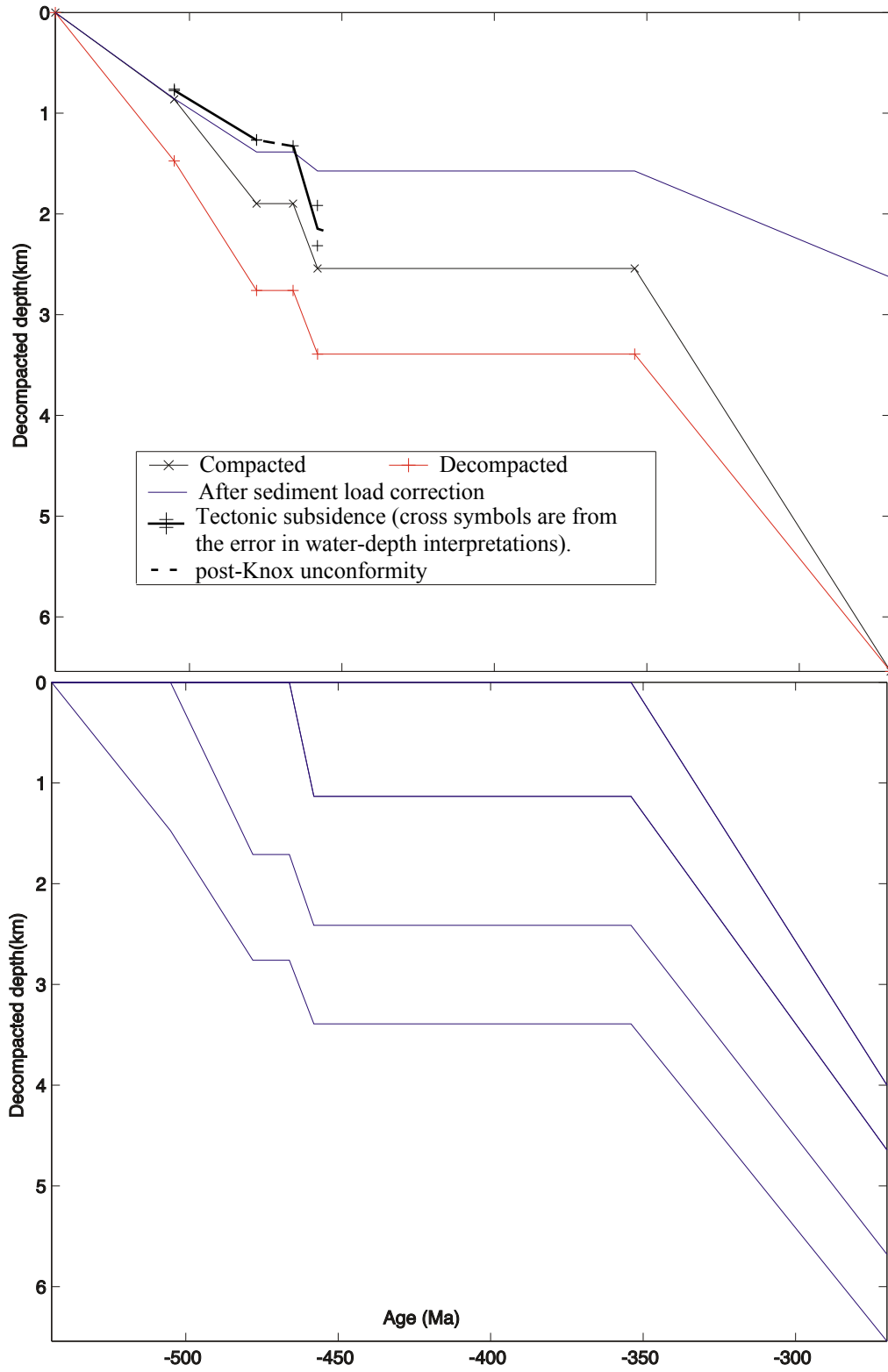


**Figure C.15** Section PF - Pratt Ferry

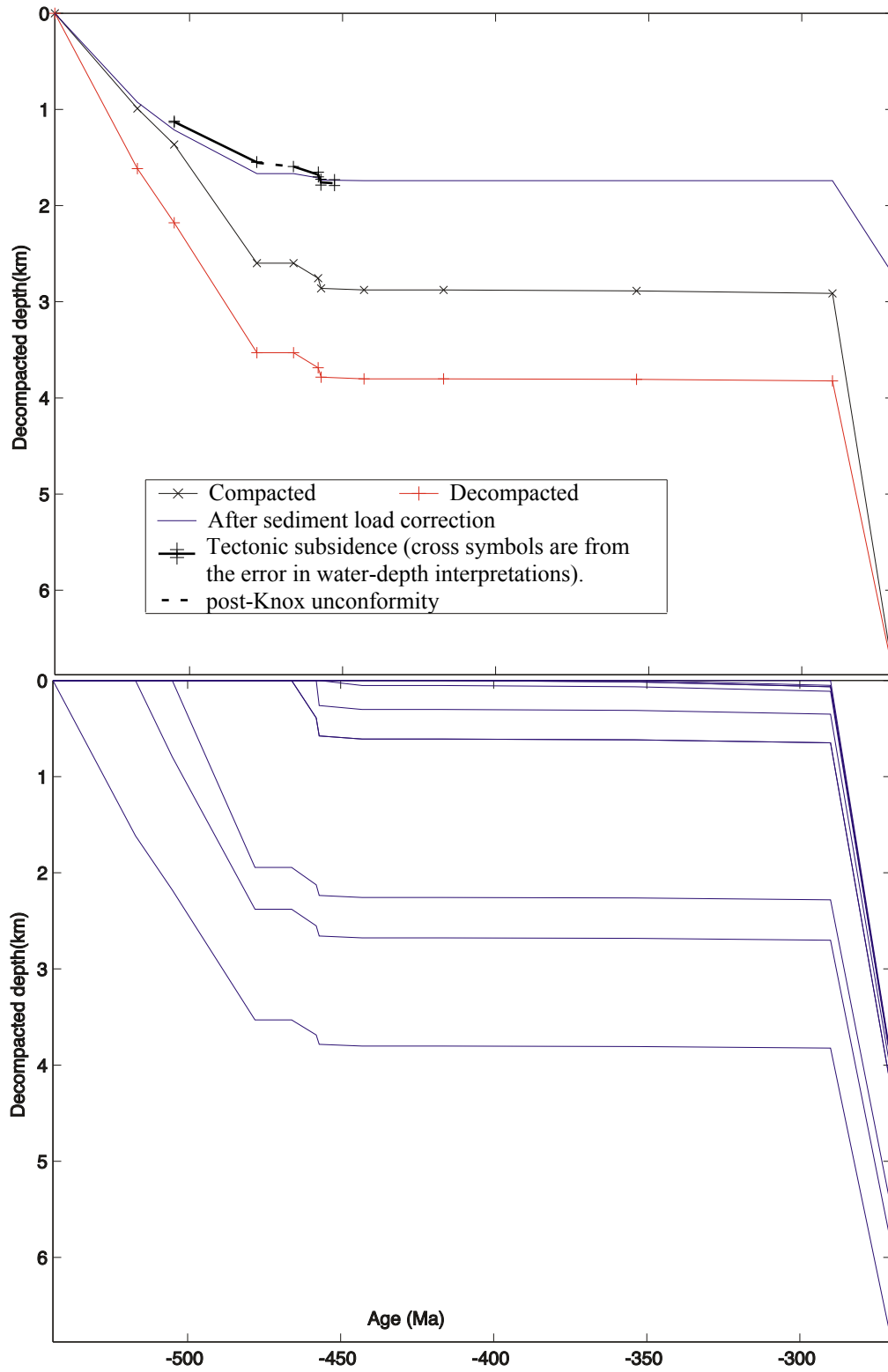


Figure C.16 Section RH - Red Hill

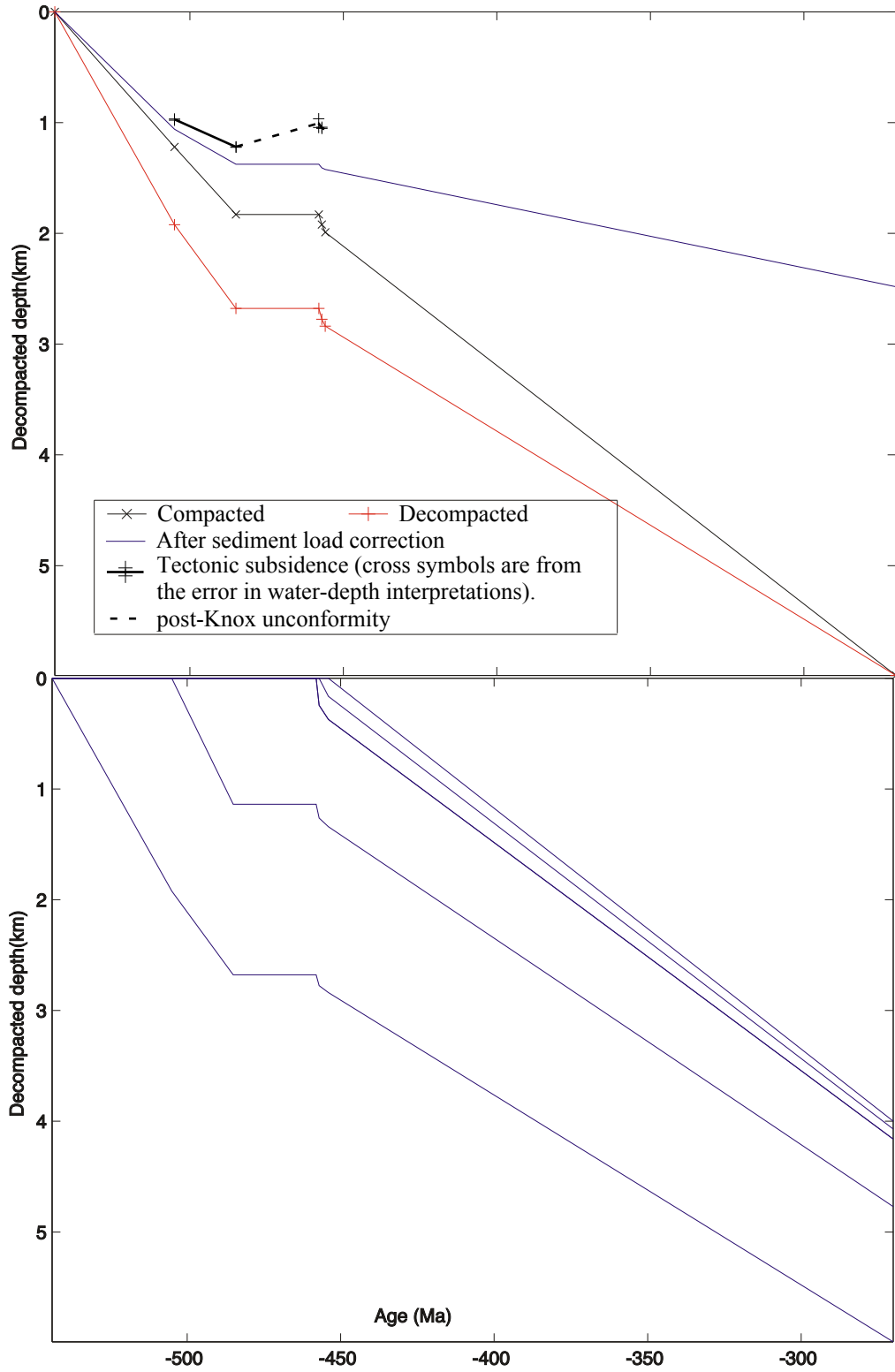
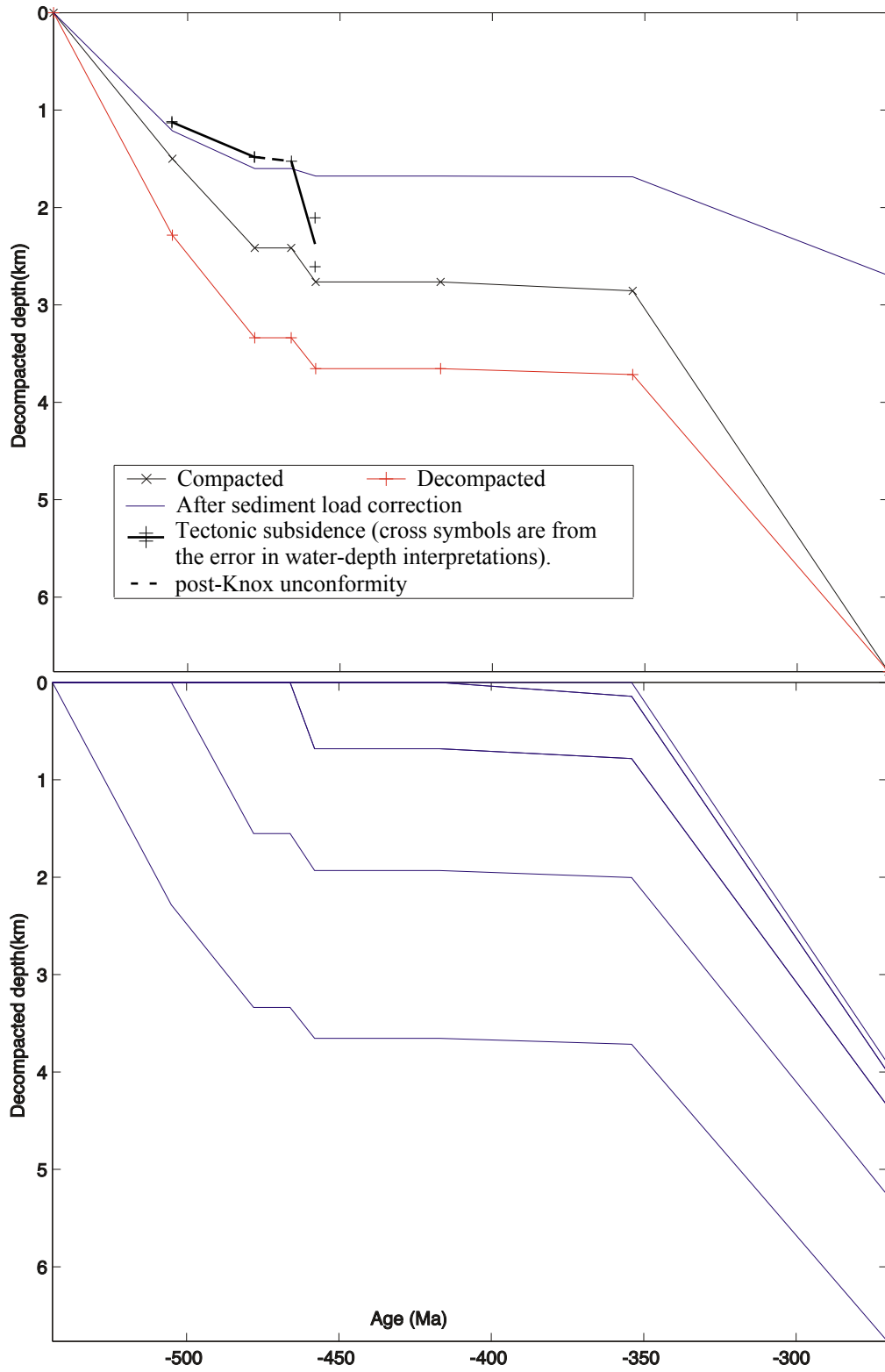
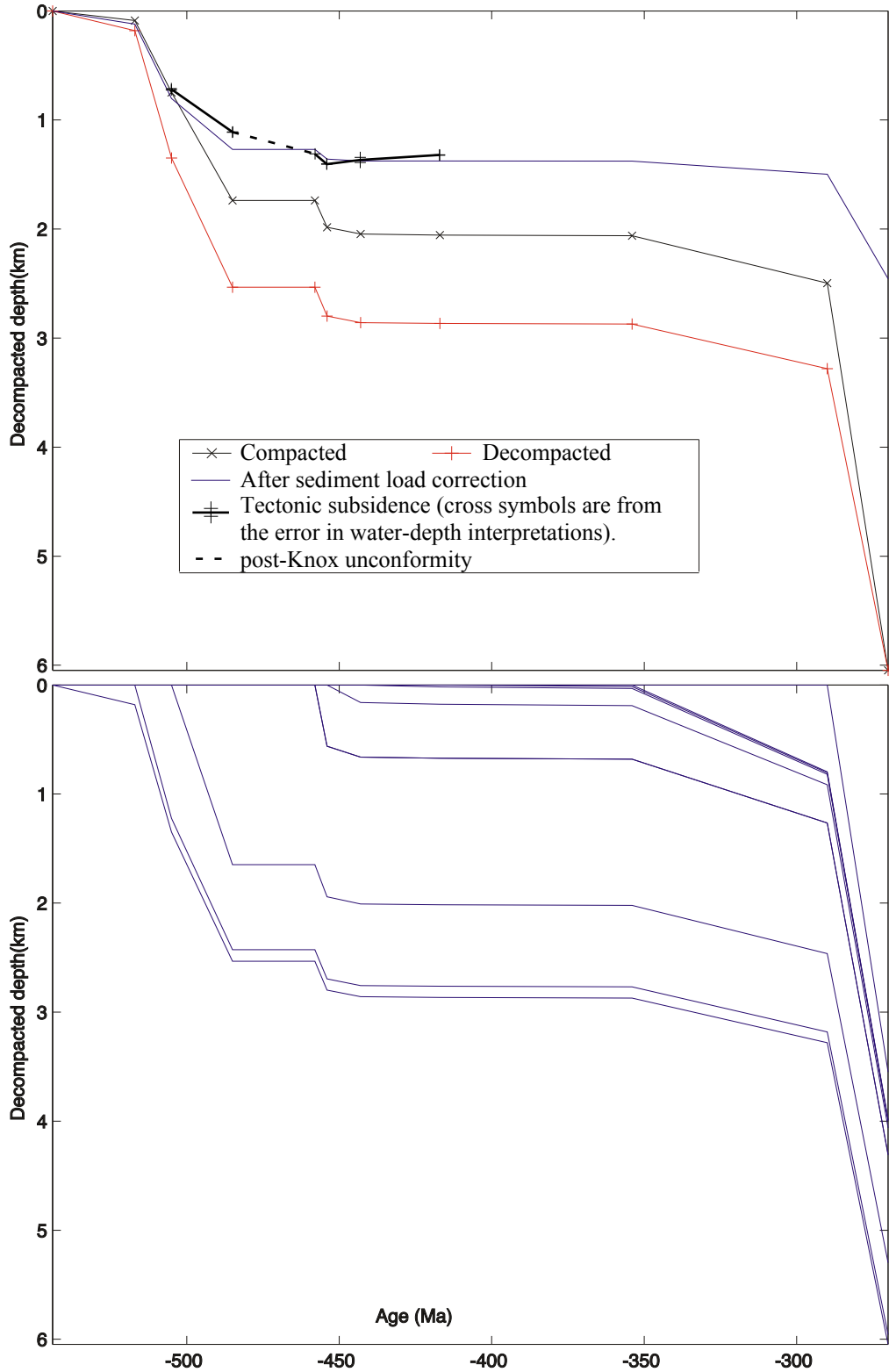


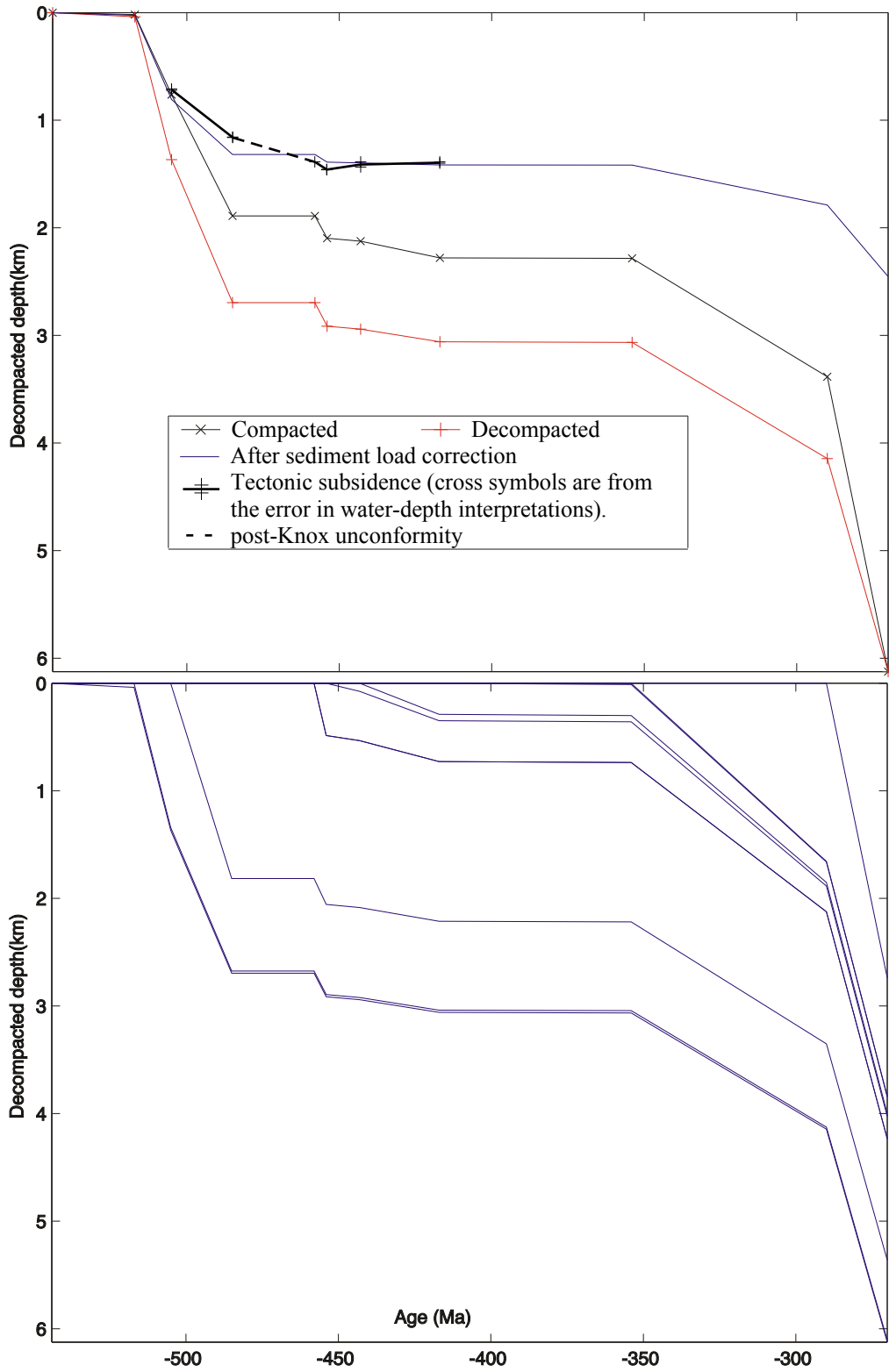
Figure C.17 Section RK - Rockmart



**Figure C.18** Section SS - Shenandoah 1 Smith well



**Figure C.19** Section ST - U.S. 1 Steel well





## APPENDIX D

### DESCRIPTION OF THIN SECTIONS AND HAND SAMPLES

Table D.1 summarizes the description of some hand samples and thin sections (marked with @ on the left side of the table). Samples are listed by sections. For stratigraphic location of samples see the correspondent plate. Abbreviations are as follow:

**Units:** Dfm= Frog Mountain Formation; Oa= Athens Shale; Och= Chickamauga Limestone; Oca= Atalla Chert Conglomerate Member of the Chickamauga Limestone; Ocho; Chota Formation; Ocm= Colvin Mountain Sandstone; Og= Greensport Formation; Ol= Lenoir Limestone; Olol= Little Oak-Lenoir Limestone; Olo1= Little Oak Limestone; On= Newala Limestone; Oo= Odenville Limestone; Or= Rockmart Slate; Os= Sequatchie Formation; Srm= Red Mountain Formation.

**Name:** For carbonates: A= algal; I= intraclasts; S= skeletal; P= peloidal; argil.= argillaceous; P wackestone/I packstone = peloidal wackestone interbedded with intraclastic packstone; mixed = mixed carbonate and siliciclastic lithologies.

Sandstones and conglomerates:

Grain size: cgl= conglomerate; m= medium sand; bimodal = two grain sizes

Composition: Q, F, and L are modal composition (see Table 4.4)

**Non Skeletal:** I= population of intraclasts

**Skeletal:** brach.= brachiopod; bryo.= bryozoan; echinod.= echinoderms, crinoids; ostrac.=ostracods; pelecyp.= pelecypods.

**Q, F, L** = see Table 4.4 for explanation of codes

**Matrix/cement:** qz= quartz; mi= micrite; dol= dolomite; cal= calcareous; ox= oxides; pmtx= pseudomatrix

**Other:** bt= biotite; chl.= chlorite; glauc.= glauconite; hn= hornblende; musc.= muscovite; phosp.= phosphates; py= pyrite; zr= zircon

**Structures/fabric:** dol= dolomitization; mod.= moderate; styl= stylonodular

**Table D.1** Description of thin sections (@) and some hand samples

sample unit	rock name	non skeletal carbonates	algae	skeletal	Q, F	L/ conglomerates clast	matrix/cement	other	structures/fabrics
PF Pratt Ferry									
@ T2-1901	OI IPS wackestone	peloids; intraclast with girnavella	calcisphere, coated grains	ostrac., mollusk	Q		mi		
@ T2-1902	OI P1A packstone	peloids (silt-fine sand size), intraclasts	calcisphere, coated grains, oncolithes	ostrac., mollusk	Q		mi, spar		
T2-1903	OI PS packstone	peloids		brach., mollusk, ostrac., trilobite			mi, clay		
@ T2-2604	OI AS packstone/SA wackestone	intraclast	calcisphere, oncolithes, nuia, dasycladids	echinod., brach., mollusk, trilobite	Q		mi, dol		mod. sorted
@ T2-2603	OI IPS packstone	PS intraclasts, peloids	calcisphere	echinod., trace of trilobite			equigranular spar		well sorted
@ T2-2602	OI S grainstone			ostrac., mollusk	Q, Ch, albitized P		mi, ox		laminated
@ T2-2601	Oa mixed mudstone			ostrac., mollusk	Q		mi, microspar		
@ T2-1701	Oa S wackestone to mudstone	silt-size peloids	calcisphere?	ostrac., trilobite, mollusk	Q				
CL Calera, Blue circle quarry									
S2-2400a	Oo PAJ packstone to grainstone	peloids, intraclast	algae	ostrac., brach.?, trilobite?			spar		burrows
S2-2400	Oo PA packstone to grainstone	peloids	algae	ostrac.	Q		mi		fenestral, styl
S2-2401	Oo I wackestone	intraclast					mi		dol
S2-2402	Oo P1A grainstone	peloids, intraclasts	algae				mi		burrows
S2-2607	Oo AIP grainstone	peloids, intraclasts	algae				mi		burrows
@ S2-2608	Oo S1 wackestone	intraclasts	nuia	echinod., mollusk, brach.	Q, F?		dol, spar		dol
@ S2-2403	Oo IS-wackestone	peloids (up .25 mm); I= LDmo	coated grains	trilobite, echinod.			dol, mi		
@ S2-2609	OI IS packstone	I= S wackestone					dol, mi, clay	py	debris-like, styl, dol
@ S2-2404	OI IS-wackestone	I= AS wackestones			Q		dol, mi		debris-like fabric
@ S2-2405	OI IA-wackestone	I=meritic	nuia, girnavella	brach., bryoz.?			mi, dol		styl, dol
@ S2-2501	OI S wackestone	intraclast	algae	echinod., brach., trilobite	Q, F?		mi, dol, clay		styl
@ S2-2503	OI AS-wackestone	intraclast	calcisphere, nuia	trilobite, echinod., ostrac.			mi, spar		burrows
@ S2-2504	OI A1-packstone	intraclast	oncoids, nuia	trilobite, brach.			mi, dol		styl
S2-2201	OI S1 wackestone to mudstone	intraclast		echinod., brach., trilobite			mi, clay		styl
S2-2202	Oo argil. S wackestone to packstone			echinod., brach., trilobite, bryoz.			mi, clay		thin bedded
S2-2203	Oo argil. S wackestone			echinod., brach., trilobite, bryoz.			mi, clay		massive, debris-like
@ S2-2204	Oo argil. S mudstone to S grainstone			echinod., brach., trilobite			microspar, silica, ox		laminated, normal grading
S2-2205	Oo argil. S wackestone to S grainstone			echinod., brach., trilobite			mi, clay		thin bedded
@ S2-2209	Oa mixed mudstone			ostrac.	Q		micro spar, clay		laminated
S2-2210	Oa calcareous shale								
@ S2-2216	Oa fine; Q64F32 L4				Qm>>Op, altered+albitized F?	silstone, claystone	clay, pmix	bt, hn	well sorted
S2-2215	Oa fine-very coarse, Q95 L+F 5				Op=sandstone, altered F?	grpy, plastic claystone clast	clay		mod-poor sorted
S2-2221	Oa fine-very coarse, Q87 F8 L5				Qm>>Op, altered+albitized P	sandstone, rip-up clasts	clay, pmix		mod-poor sorted
@ S2-2217	Oa fine; Q87 F3 L 10				Qm>>Op, altered+albitized P	silstone, claystone, vf sandstone	clay, pmix		well-mod. sorted
@ S2-2218	Dfm fine-c; Q95 F+L 5				Qm>>Op, altered+albitized P	silstone, claystone	clay; ox		floating fabric
CL Calera, Vulcan quarry									
@ S2-2801	OI SA wackestone/argil. I wackestone	I= SA wackestone	nuia	trilobite, brach., echinod., ostrac.			clay, mi		styl, debris
@ S2-2803	OI S packstone	I= SA wackestone	nuia, dasycladids	echinod., brach., trilobite	Q		dol, mi		massive, styl
@ S2-2804	OI- S wackestone-packstone	I= S wackestone		echinod., brach., trilobite, bryoz.	Q, F?		clay, mi		thin bedded

sample unit	rock name	non skeletal carbonates	algae	skeletal	Q, F	L/ conglomerates clast	matrix/cement	other	structures/fabrics
EC East Calera									
S2-2505	Ol S wackestone to packstone			echinod., trilobite, brach.	Qm>Qp>cht; Qpf; less altered F	silty clst; slst; egl=fossil, slst, Qp	mi, clay		styl
@ S2-2507	Dfm m-coarse; Q85 F5 L10				Qm>>cht<Qp; P, K (microcline)	silty clast, phyllite?	clay coating grains	phosp., hn	mod-poor sorted well-mod. sorted
@ S2-2508	Dfm fine-coarse; Q78 F21 L1								
AB Alabaster, Stop Q2									
@ Q2-2901	Ol IS grainstone	I= mud-dominated		echinod., brach., bryoz., ostrac.	Q-Ch, up 2mm		spar and microspar		
Q2-2604	Ol SI grainstone	I= mud-dominated and dolomite		echinod., brach., bryoz., trilobite	Q-Ch, up 10 mm		spar		
@ Q2-2605	Ol SI grainstone	I= mud-dominated		echinod.>>brach., bryoz.	Qm+Qp+Ch		microspar, qz	phosp.	cross bedded
Q2-2606	Ol IS grainstone	reddish intraclasts		echinod.>>brach., gastropods	pebble Ch				
AB Alabaster, Stops Q3 and Q4									
@ Q2-2602	Oo? I packstone to wackestone	I= AP wackestone		mollusk, trilobite, brach., echinod.	Q		mi, partly dolomitized	py	
@ Q2-2601	Olm fenestral, PIS grainstone	Peloids; I= mud-dominated		peleypods, mollusk, ostrac.	Q		spar		fenestral
@ Q2-2603	Olot PAS packstone/mudstone	peloids	nuia, girnavella	mollusk, trilobite, ostrac., echinod.	Q		clay, microspar,	py	styl; burrows
@ Q3-0101	Olot ISAP wackestone to packstone	peloids; I= mud-dominated	algal, nuia	brach., echinod., trilobite	Q		clay, dol		burrows, styl
@ Q3-0102	Olot PSAI packstone/argil. I mudstone	peloids	nuia, dasytylids	echinod., trilobite, bryoz.	Q and F		dol, mi, spar		styl
Q3-0103	Olot P grainstone/subarkose	peloids		ostrac., brach.					
Dfm				silicified fossil fragments	Ch>>Qpf, albitized P	silty shale	clay coating grains, ox	hn	poor sorted
@ Q3-0104	Dfm course-pebble; Q94 F3-5								
AB Alabaster, Stop Q9									
@ Q3-0202	Olot PS packstone/dolomitic S mudstone	peloids	calcisphere	echinod., trilobite, ostrac., peleyp.	Q<1%		mi		laminated
@ Q3-0203	Olot calcareous mudstone/fine-m Q>>F			echinod.	Q, F?		dol, mi		
@ Q3-0204	Dfm fine-ni, isolated pebble; Q87F10L2			echinod.	Ch>Qp; unaltered P, microcline	silty shale	cal, clay, mi	phosp., glauc., zr	well sorted, thin bedded
@ Q3-0205	Olot S grainstone/wackestone			bryoz., echinod., brach.	Q		mi		
AB Alabaster, Stop Q12									
Q3-0301	Ol S grainstone			echinod., trilobite, brach.			clay, mi		
@ Q3-0302	Ol- PS grainstone/S Oa grainstone/mudstone	peloids		echinod., trilobite, brach.			mi, clay		well sorted, thin bedded
HV Harpersville, Stop R2									
R3-0400	Omp? S wackestone/PS grainstone	peloids?		ostrac., trilobite, echinod., brach.			mi		foliated, dol
HV Harpersville, Stop R3, 4									
@ R3-0401	Oa fine to isolated coarse; Q74F20L6				Qm>>Qp+Ch, albitized and twinned P	subarkose siltstone, shale, F+Q aggregate	clay	zr, hn	floating text., mod to poor sorted
R3-0501	Oa fine to very coarse, lithic arkose				Qm>>Qp, twinned, perthitic F	Qp+F aggregates, siltstones	qz overgrowth		fractured
@ R3-0502	Oa m to coarse; Q80F10L10				Qm>>Qp+Ch; twinned P >>K	Shale, subarkose, phyllite?			fractured
@ R3-0503	Oa argil., fine; Q50F45L5				albitized P, antiperthites	Ls>>Q+F aggregates; devitrified Lv?	clay		mod to poor sorted
@ 441	Oa m-coarse; lithic arkose								

sample unit	rock name	non skeletal carbonates	algae	skeletal	Q, F	L / conglomerates clast	matrix/cement	other	structures/fabrics
HV Harpersville, Stop R13									
@ R3-0801	On m-coarse grained; Q77F14L10				rounded F? albitized P	shale, siltstone >> Q+F aggregate	clay	zr, musc.	normal grading
@ R3-0803	On m-coarse; Q67F20L13				deformed Qm, albitized P, perthite	shale, arkosic siltstone >> Lm+Lp; Lv?	clay	musc.	
@ 431	On lithic arkose				On embayment; twinned P, albitized P	shale, siltstone, schist; Q+F aggregate	clay		
HV Harpersville, Stop R14-15									
R3-0805	Oo? PS packstone to grainstone	peloids		ostrac., pelecyp., echinod., brach.	Qm >> Qp+Ch; twinned+albitized P	shale, siltstone; phyllite; Lv?	micritic clay		styl
@ R3-0806	On m-fine; Q58F34L8				isolated Qm; altered F		ox		matrix-supported laminated
@ R3-0807	On sandy siltstone								
FM Frog Mountain, Stop II., 4									
@ J4-0601	On fine; Q59F32L9				Qm embayments, Qpo, Ch	siltstone, phyllite, Lv?	clay	micas	matrix supported
LM Leydens Mill, Stop O3, 6, 10									
@ O4,	On fine-m; Q67F10L23				Qm embay., Qm >> Qp+Ch; albitized and wormed F	sandy siltstone > Lm+Lv?	clay, micas, pmix	zr, musc.	matrix supported
@ O4-0403	On fine; Q47F49L4				anperthite, albitization?		clay, ox	zr, bt, musc.	matrix supported
@ O4-0405	On fine-course; Q40L35F25					siltstone > Lm+Lv?			matrix supported
GS Greensport, Greensport gap									
M3-1601	On P grainstone	peloids; F micritic					dol		burrows
@ M3-1501	OI SA packstone	pebble intraclast	mita, Girvanella, solonopora	bryoz>echinod., brachiop., trilobite	Q		dolomitized mi		dol
M3-1502	OI SI wackestone	intraclast?		trilobite, ostrac.					burrows
M3-1602	Og calcareous sandy siltstone				Qm >> Qp+Ch; P>K	Lm=micaceous schist	dol	bt, musc., zr	well sorted
@ M3-2108	Og very fine; subarkose				Qm >> Qp+Ch; P>K	Lm and Ls	cal, clay, ox	hn	immature sandstone
@ M3-1705	Og very fine; Q77F19L4				Qm >> Qp+Ch; P>K		cal, ox	glauc., zr, chl.	bioturbated
@ M3-2110	Og very fine; Q59F40L1				Qm >> Qp+Ch; P>K		cal, ox		
M3-2109	Og very fine-fine; arkose to subarkose				Qm >> Qp+Ch; P>K		clay, ox	glauc., zr, bt, chl.	
@ M3-1704	Og very fine-fine; Q52F40L8				subarkose siltstone	Lm	spar, dol, clay	glauc., zr, hn	burrows
@ M3-1708	Og mixed P packstone, siltstone	peloids	red & green algae	trilobite, ostrac., echinod., bryoz.	Q, microcline		mi, dol		normal grading
@ M3-1707	Og IAS packstone								bioturbated
M3-1706	Og sandy siltstone, subarkose							glauc.	ripple laminated
M3-1703	Og sandy siltstone								
M3-1702	Og- argil. fine quartzose siltstone				Q	black L, oxides, rip up clasts			
@ M3-1701	Oc- bimodal; Q98L2				Qm >> Qp+Ch+F, very altered F?	Lm ?	clay	glauc., zr, oxides	
@ M3-1804	Oc- coarse; Q100						sand and silt	zr	cross bedded
@ M3-1803	Oc- m-coarse; Q100				Qm >> Qp+cht		sand, silt, clay, ox	zr	laminated
@ M3-1805	Oc- m; Q100				Qm >> Qp+cht	recycling quartzarenites	silica	zr	cross bedded
@ M3-1801	Oc- fine-course; Q100				Fk?		silt matx, clay and	zr, hn	cross bedded
@ M3-1901	Os very fine-fine; Q85F10L6			echinod., bryoz.	altered F? P>K		silica cmr		cross bedded
@ M3-1903	Os mudstone						clay and ox	glauc., zr, hn, musc.	
@ M3-2107	Os mixed mudstone				Q>F; P>K		dol		burrows, dol
@ M3-1902	Os mixed mudstone; Q80F20				Q80F20; Qm, Op, P, gl>Fk		spar, dol,	glauc., zr	ripples, burrows
M3-2106	mixed mudstone				silt-grained clastics		dol in biotul / clay		ripples, burrows
@ M3-2105	Os mudstone				silt-grained clastics		dol		laminated
							dol		massive, dol

sample unit	rock name	non skeletal carbonates	algae	skeletal	Q, F	L/ conglomerates clast	matrix/cement	other	structures/fabrics
@ M3-2104	Os mudstone			pelecyp., echinod.	silt-grained Q, F on laminae		dol	zr	dol
@ M3-2103	Os S wackestone				Q		dol	phosp.	dol
M3-2102	Srm calcareous subarkosic siltstone				Q		dol	hn	burrows, hummocky
@ M3-2101	Srm mixed mudstone				Q, Ch, P, K			glauc.	
GS Greensport, Alexander gap									
@ M3-2309	Oc bimodal; Q93F4L3				Qpf, Ch, altered F		clay	zr, hn	cross bedded
@ M3-2310a	Oc m-coarse; Q100				F?		silica, clay	hn	irregularly laminated
M3-2312	m m-coarse; Q100					green rip-up clasts= bentonite?			
GS Greensport, Glencoe									
@ M3-2404	On P packstone			ostrac., echinod., bryoz.		ostrac., echin., bryoz.			
@ M3-2403	OI PSA grainstone		nutia, dusyclads	mollusk, ostrac., brach., trilobite			dol		styl
@ M3-2402	OI PS packstone/dolomitic mudstone		nutia, encrusting algae	trilobite, brach., echinod., sponge	Q	ostrac., gastrop., ostrac., brachiopod, trilobite	isolated dol		
@ M3-2401	OI PS packstone			Tetradium, gastropod, ostrac., trilobite, echinod.		sponge	partly dolomitized		
@ M3-2301	OI S wackestone/P packstone		encrusting algae	gastropods, trilobite, sponges?	Q	gastrop., ostrac., trilobite, sponges?	dol		burrows
@ M3-2302	OI A wackestone-packstone			pelecyp., gastropods, ostrac., trilobite, echinod.		pelec., gastrop., ostrac., trilobite, echinod.	mi		intense burrowing
@ M3-2303	OI A dolestone		algal lamination?				dol		
@ M3-2306	Og very fine-fine; Q83F13L4				Ch?, Qp, P>>K, perthite		dol, ox	zr, hn	
@ M3-2307	Og fine; subarkose				Qpf, altered F		dol, ox	hn	
GS Greensport, Canon gap									
@ M3-2510	OI S packstone-wackestone			bryoz., echinod., brach.	Q		dol, ox		debris-like
@ M3-2509	OI/ IS wackestone-mudstone			bryoz.	Q		zoned dol		
@ M3-2508	Og mixed silty subarkose/ S mudstone			echinod., trilobite			dol, ox	phosp.	flaser
@ M3-2507	Og fine-n grained, Q84F9L7				Qp, Ch, altered F		cal, ox, silica	zr, glauc.	ripples
@ M3-2506	Og v. fine-f, calc. Q80F11L9				Qp, Ch, microcline		cal, clay, silica, ox	zr, hn, glauc.	cross bedded
@ Og									
@ M3-2505	Og v. fine-fine-grained Q73F25L2				Qpf, altered and fresh P, K				ripples
@ M3-2504	Og v. fine-fine-grained Q61F29L10				Ch, perthites, altered F		clay, ox	zr, glauc., bt	burrows, ripples
@ M3-2503	Og fine-grained, Q63F31L6				microcline, P>K, altered F		clay, silica	hn, glauc., bt	
@ M3-2502	Og fine, Q80F17L4				Qm, Qpf, Ch, microcline, albitization, P>K		clay, ox, pmtx	zr, hn, musc.	horizontal lamination
@ M3-2501	Og v. fine-grained Q59F28L13				Qm, Ch, K = P		clay, ox, pmtx	zr, glauc., bt, musc.	cross bedded
GS Greensport, U.S. 231									
@ M3-2206	Og fine; Q56F36L8				P>K, microcline		clay, ox	hn, glauc.	
@ M3-2205	Og very fine-fine, subarkose				P>>K		dol, clay	glauc.	burrows
@ M3-2204	Oc bimodal, Q89F11L0				trace Op, dissolved F		silice, clay, ox		matrix supported
@ M3-2201	Oc fine, Q85F12L3				Qp+Ch; P>K		clay, ox	zr, hn	matrix supported
mO									
s									
GS Greensport, county road 26									
M3-2207	Srm calcareous mudstone								
@ M3-2208	Og very fine-fine, subarkose		unidentified skeletal fragments		Ch=tr; P>>K		cal, ox	glauc., phos.	hummocky cross beds

sample unit	rock name	non skeletal carbonates	algae	skeletal	Q, F	L/ conglomerates clast	matrix/cement	other	structures/fabrics
DM Dunaway Mountain, Stop L10									
@ L3-3102	Oca mud-supported pebble conglomerate	peloids; intraclasts up 1 cm	algae laminae?		Qm from silt to up .6 mm		dol		laminated, burrows
@ L4-0105	Os calcareous siltstone			bryoz up 17 mm	Q, P>K		microspar, dol		
L4-01....	Os m-coarse, quartzarenite, skeletal			bryoz.	Q				
@ L4-0104	Os m-coarse, subarkose			echinod.	Ch=tr, microcline	Lv=microlithic, Ls=shale	spar, dol, ox, clay	phosp., zr	
L4-0103	coarse, quartzose, skeletal			skeletal grains	Ch		dol, ox	phosp., zr	
@ L4-0102	Os m, Q90P9L1				Qm>>Qp+Ch, microcline, albtrized P	Lv=microlithic			
@ L4-0102s	Os				P>>K, microcline	phyllite	clay, cal, ox	zr, glauc., chl	
@ L4-0101	Srm very fine-fine, subarkose								
DM Dunaway Mountain, Stop L17									
@ L4-0501	Oca argil., Q93.5F6L0.5				Qm>>Qp+Ch; P=K; microcline		limonite, clay, qz	glauc., hn, phosp., zr	bimodal grain size
@ L4-0502	Oca calcareous, fine, Q95F5				altered P and K, microcline	rip-up clasts	dol, ox, qz, clay	hn, phosp.	cross bedded, burrows
@ L4-0503	Oca calcareous, fine, Q89F11				P, K, microcline		dol, qz, limonite	hn, zr, phosp.	laminated
@ L4-0504	Oca PS mudstone/SP packstone	peloids	algae	pelecyp., ostrac., brach., echinod.	Qm, Ch, microcline		micritic		burrows
@ L4-0506	Oca argil., fine, Q79F19L2				Qm>>Qp+Ch; K>P; microcline	shale	limonite, qz		irregularly laminated
	in- Os								
GU Gunsterville									
@ J4-0805	Os S-grainstone	I= dolomitic		echinod., bryoz., trilobite, brach.	Ch		spar		well sorted
BR Big Ridge, Stop K3-3									
@ K3-3002	Oca pebble chert egl; matrix= Q99F1				autogenic Q, chalcodony, Ch; perthite, sand-size: Qm68.3Qp46H26.5F1		limonite		
@ K3-3003	Oca SI packstone	intraclast, peloids		pelecyp.	autogenic Q, Ch		microspar	phosp.	grading of skeletal grains
@ K3-3004	Oca egl, fine-course chert sandstone				autogenic Q, chalcodony, Ch		calcareous, clay	phosp.	
@ BR Big Ridge, Interstate I 59									
@ K3-2908	Srm argillaceous, very fine-silt subarkose						clay, ox	hn	hummocky cross beds
BI Birmingham, Argo section									
@ P3-1200	Oca m-coarse, Q40Ch60				Qm detrital and autogenic	several types of Ch	qz, limonite		
@ P3-1206	Oca m-coarse to pebble chert conglomerate				Qm and Qp dominates fine-m sand		qz, limonite		crude horizontal lamination
@ P3-1207	Oca sandy pebble chert conglomerate				Qm detrital and autogenic		qz		matrix-supported
@ P3-1205	Oca sandy chert conglomerate				Qm and Qp dominates fine-m sand	Ch and trace of Ls=sandy claystone	qz		
@ P3-1203	Oca calcareous chert conglomerate	I= micritic		ostrac., brach.	Qm detrital and autogenic		dol, qz	phosp., glauc	
@ P3-1202a	Oca SPI wackestone to packstone			skeletal concentrated on laminae	Ch up 15 mm		qz	phosp.	clastics on laminae
@ P3-1202b	Oca I packstone /mudstone	I= dolomitic mudstone		ostrac., pelecyp.	isolated Ch conglomerate grains		spar, qz		irregularly laminated
@ P3-1202c	Oca PISA packstone	I= dolomitic and micritic mudstone		mollusk, trilobites, ostrac., brach., echin., bryoz.	isolated Ch conglomerate grains		qz, dol		massive, matrix-supported
@ P3-1208	Oca ISP grainstone	I= micritic	algae	mollusk, brach., echinod., bryoz.	Q and Ch		qz	phosp.	
@ P3-1209	Oca IS grainstone	I= micritic		pelecyp., mollusk, ostrac.	Q and Ch		qz		low-angle cross bedded
@ P3-1201	Oca PS packstone	I= dolomitic and micritic mudstone							

sample unit	rock name	non skeletal carbonates	algae	skeletal	Q, F	L/ conglomerates clast	matrix/cement	other	structures/fabrics
BR Big Ridge, Interstate I 59									
@ K3-2703	Och P grainstone	I=micrite to biomicrite		pelecyp., trilobite, brach.	Q and F		qz	bt	debris-flow like
@ K3-2707	Och IPS packstone-biostrone	I=micrite dominates		pelecyp., trilobite, tetraridium, sponges			gradational spar		laminated
@ K3-2705	Och SP packstone to wackestone	peloids dominate in some layers		pelecyp., trace of ostrac.s			dol		
@ K3-2706	Os P grainstone	I=dolomitic		pelecyp., trace of ostrac.s	Q and F		single spar		ripple laminated
@ K3-2801	Os IP packstone	I=dolomitic		ostrac.			dol, ox		poor sorted
@ K3-2802	Os m-coarse, S packstone	I=micrite	oncolite	brach.s, echinod., bryoz.			drusy cement		sand dunes
@ K3-2804	Os S grainstone			crinoid, bryoz.	Q and F		poikilitic spar, ox	glauc.	
@ K3-2907	Os fine-n, Q83F13L4			silicified skeletal grains	Qn, Qpf, Ch, P, microcline, perthite	arkosic sandstone, siltstone (volc?), igneous	ox, clay	phosp.	
@ K3-2909	Os S grainstone to feldspathic litharenite			trilobite, brach., echinod., bryoz.	Qn, Qp, microcline	Ls phosphatic matrix	feruginous spar		well rounded and sorted
@ K3-2904	Os m-very coarse, Q96F2L2			brach., bryozoon	Qp, Ch, microcline	Ls arkosic with phosphatic matrix	qz, cal, ox	phosp.	well rounded, mod-poor sorted
@ K3-2903	Os S grainstone	I=dolomitic S-elastic mudstone		trilobite, brach., echinod., bryoz.	Ch		qz	glauc., phosp.	mod.- well sorted
@ K3-2905	Os clay, phosphate sublitharenite			skeletal grains	Qp, microcline, P, perthite		clay, ferruginous	hn, phosp.	
@ K3-2902	Os c-very coarse, Q95F0.3L47		red algae	bryoz.	Qn with chlorite, Qpf, Ch	siltstone to very fine sandstone	qz, cal, ox	phosp.	
@ K3-2901	Os very fine to fine, Q82F12L6				Qpf, Ch, microcline, P	Ls=massive shale, Lm=phyllite	clay, ferruginous	hn, glauc., phosphate	
HL Horseleg Mountain									
@ G11-1001	Os bimodal, Q98F1L1				Qm>> Qpf	Ls=shale, included in the matrix; Lm	qz, pmtx	hn, zr	
@ G11-1002	Os argil., very fine, Q79F12L9				Ch, K, microcline	Ls=sd slst, Lm=phyllite	clay, ox, pmtx	hn, zr, bt	laminated
@ G11-1003	Os m, Q99F0L1				Ch, trace of F	Ls=siltstone	ox, qz, clay	dissolved fragments	cross bedded
@ G11-1004	Oc fine-very coarse, Q99.5L0.5				Qm>> Qpf, Ch	isolated granules of qz	clay, ox	hn, zr	horizontal bedded
@ G11-1005	Oc fine-n, Q99F1				Qm>> Qpf, trace microcline	Ls=part of pseudomatrix	qz, pmtx	zr	
@ G111009	Og argil., vfine-f, Q99F1				Qm>> Qpf, Qp, Ch		clay, ox, pmtx	hn, zr	
A	Og argil., quartzarenite				Qm> Qp, Ch	Qn up 5mm	clay, ox, pmtx		transgressive lag
@ G11-1008	Og mod. bimodal, Q99.5F0.5				Qm>> Qp, Ch		qz, clay	hn, zr	
@ G11-1010	Og Bimodal Q98.5F1.5				Qm>> Qp, Ch		clay	hn	
@ G11-1020	Og argil., f, Q99F1				Qm>> Qp, Ch		clay	hn, zr	heterolithic lamination
@ G11-1021	Og m-c, Q99F1				Qm>> Qpf		qz, clay		
@ G11-1011	Og fine-grained, Q81F18L1				kaolinite replacing F? microcline	Lm=reddish, phyllite	qz, clay	zr	cross bedded
@ G11-1019	Og vfine-f grained, Q77F14L9				kaolinite replacing F	Lm=reddish, phyllite	qz, clay	musc.	horizontal laminated
@ G11-1012	O1 ISA packstone	I=micrite	red and green algae	pelecyp., trilobite, brach., echinod.	Qn, Qp, Ch		clay, equant spar		
@ G11-1016	O1 S1 grainstone	I=micrite	algae	trilobite, ostrac., brach., echinod.			clay, equant spar		transgressive lag
@ G11-1018	O1 IS packstone	I=micrite	algae	pelecyp., mollusk, ostrac., echinod., bryoz.			clay, equant spar		fenestral
@ G11-1018									
RK Rockmart, Portland quarry									
H3-0800	On P grainstone								
@ H3-0801	O1 foliated, S wackestone	I=dominantly micrite		echinod., ostrac., pelecyp.; recrystallized			spar, clay, qz		fenestral voids slightly deformed
@ H3-0802	O1 foliated S mudstone	I=micrite		echinod., trilobite; recrystallized			microspar		clay in laminae
@ H3-0803	O1 foliated, S wackestone	I=coarse microspar		flattened shell, echinod.			equant spar in voids		burrows

sample unit	rock name	non skeletal carbonates	algae	skeletal	Q, F	L/ conglomerates clast	matrix/cement	other	structures/fabrics
RK Rockmart, Vulcan quarry									
H3-0901 Oo	S wackestone-packstone						microspar		burrows styl, burrows, dol
@ H3-0902 OI	mudstone	dolomite filling bioturbation		tribolite, echinod.	Q rounded Qm				
H3-0903 On	Quartzose P grainstone								
RK Rockmart, Stop H4									
@ H3-0904	SIP packstone to wackestone	peloids; F= micritic		tribolite, echinod.			microspar, qz in voids		
RK Rockmart, Deaton Mine									
@ H3-1001 OI	Pebble l wackestone	F= micritic to microspar, skeletal		tribolite, echinod.			course dol		clay coating rhombs, dol
@ H3-1002 OI	Pebble l packstone	F= dolomitic		phosphatic shell fragments			dol, limonite	chamosite, phosp.	
@ H3-1003 OI	Ferruginous limestone		algae? replaced by oxides	skeletal fragments replaced by oxides			dol?		
@ H3-1004 OI	conglomeratic IS wackestone	F= dolomitic		brach., trilobite, mollusk?			ox	chamosite, phosp.	
@ H3-1005 OI	S wackestone / mudstone			brach. replaced by phosphates			dolomitic, ox	chamosite, phosp. laminated	
RK Rockmart, section in Figure 4-9									
@ H3-1006c	Or fine-grained subarkose				grains of Qp hard to identify; albitization		pressure Qp, ox	hn, micae, illite, chl.	laminated
@ H3-1007 Or	fine-course, Q81F18L1				Qp, Ch replacing dolostone		pressure Qp, ox, cal	zr	poor sorted
@ H3-1008 Or	argillaceous, fine-m; Q82F18L1				Qp, Ch replacing dolostone, albitization	Ln, Q-F aggregates, carbonate grains Ls=siltstones	pressure Qp, ox	zr	poor sorted
@ H3-1009 Or	m-course; Q87F12L1				Qp, Ch replacing dolostone (up 2mm) foliated, matrix-supported	isolated granules		hn, zr	poor sorted
@ H3-1010 Or	Limestone conglomerate	F= quartz-rich micritic intraclasts				5 types limestones, 1 type of Ch, silt oxidized 1st clasts	cal subarkose		
H3-1011 Or	Limestone conglomerate								
@ H3-1012 Or	very fine-m; Q85F14L2	chert replacing dolostones			Qp, Ch replacing dolostone		micas, qz, Qp	micas	poor sorted
@ H3-1013 Or	fine-very coarse, Q90F10L0				Myrmekite, Qp, Ch, albitization		qz	micas	poor sorted
@ H3-1014 Or	clay, fine-course, subarkose				Qp, Ch replacing dolostone; albitization	F aggregates	ox, pressure Qp	micas	laminated, mod. to poor sorted
@ H3-1015 Or	fine-course, subarkose				Qp, Ch; albitization		ox, pressure Qp, clay	hn	mod. to poor sorted
H3-1201 Or	Pebble conglomerate					Clst are dissolved, shered, dolomitic?	clay, subarkose		matrix-supported
H3-1202 Or	Pebble conglomerate					Clst are dissolved, shered, dolomitic?	clay, subarkose		matrix- to clast-supported
H3-1203 Or	Pebble conglomerate					black mudstone, gray-pink, oxidized limestones	clay, cal subarkose		matrix-supported
@ H3-1301 Or	fine-e, Q92F9				Qp (rotation and recovery), albitization	siltified P grainstone	cal, qz	hn, zr	horizontal bedded
@ H3-1303 Or	fine-very coarse, Q94F6L1				Qp (rotation and recovery), albitization		Qp, ox	micas, zr	
DG Dug gap, Stop C1-C12									
@ C3-1401 Og	calcareous, very fine subarkose				Qm>>Qp, Ch, albitization	Ln=schist	cal, ox	bt	ripple laminated.
@ C3-1402 Og	subarkose	peloids			Qm; albitization		cal, ox	micas	ripple laminated, burrows
@ C3-1403 Og	fine; Q81F19				Qp, Ch; K>P; albitization, microcline	subarkose siltstone, Q+F aggregate	qz, ox	zr, hn, bt	horizontal laminated, burrows
DG Dug gap, Stop C17									
@ C3-1501 Oe	conglomeratic quartzarenite				Qm, Qp up pebble size				clast supported
DG Dug gap, Stop C19a-21									
@ C3-1504 Os	very fine-fine, Q100				recovery Qp, trace of Ch		qz, ox	phosp.	
@ C3-1506 Os	Bimodal, Q92F7.9			brach, s	Qm>>Qp, Ch; P, K, microcline		qz, ox	zr, hn	



sample unit	rock name	non skeletal carbonates	algae	skeletal	Q, F	L/ conglomerates clast	matrix/cement	other	structures/fabrics
Hamilton Mountain, Step D1									
@ D3-1601	Ol	SI granistone	I= micritic	echinod., bryoz., brach., ostrac.	Q in matrix and intraclasts		spar, drusy spar		
@ D3-1602	Ol	S granistone	I= micritic	echinod., bryoz., brach., pelecyp.	Q		spar		
@ D3-1603	Og	subarkosic wackestone	I= micritic	echinod., brach., pelecyp.	Qm, Qp, P, K	Ls, Lv	qz, spar	phosp., glauc.	
@ D3-1604	Og	mixed mudstone	I= micritic	bryoz., echinod., trilobite	Qm, P	Lm-slate	cal, ox	glauc., phosp., zr	ripple lamination debris-like
@ D3-1605	Og	conglomeratic S packstone	I= micritic		Qm->Qp, Ch, K>P		qz, ox	hn, zr, micas	
@ D3-1606	Og	fine-m, Q91F9			recovery Qp, altered F	Ls=shally with oxides; Ls or Lv silicified Lv= devitrified with oxides	qz, ox, pmx	hn, bt	cross bedded
@ D3-1608	Mill brng	vincr-crystalline Lapilli-tuff			Qn clean; Qm cloudy		devitrified glass, ox	bt	
@ D3-1610	Oc	conglomeratic, Q95.5L4.5			Qm, Qp recovery, Qp, Ch	Ls= sandy siltstones	pmx, qz, clay	zr, phosp.	cross bedded
CI Cisco, Figure 4.8									
@ E3-1903	Op	P1 granistone	peloids, I=micritic	trilobite, ostrac.			mi, spar	isolated dolomite	massive, fenestral
@ E3-1904	On	argil., very fine-m, Q57F38L5	I=micritic, P packstone	trilobite	F=clay+carbonate+albitization, microcline	siltstone; schist; Q+F aggregate	clay, cal	micas, zr; hn, phosp.	
@ E3-2101	On	calcareous very fine-m, Q38F56L5	I=microspar	echinod.	F=clay+carb + albitization; microcline	siltstone; schist; Q+F aggregate	clay, cal	zr, hn, bt	burrows
@ E3-2102	On	fine-course, Q80F18L2			K>P, albitization	siltstone; schist; Q+F aggregate	clay, ox, qz, pmx	dissolved carbonates	cross bedded
@ E3-2103	On	fine-m, Q75F23L2	I=microspar and dolomite		albitization, microcline	shale; phyllite; Q+F aggregate	cal, qz, ox	hn, chl	massive
@ E3-2104	On	fine-m, Q79F18L3	I=micritic, microspar, P wackestone	dissolved fragments	F= clay+carbonate+albitization, microcline mymekite; K>P	sandy siltstone	spar		burrows
@ E3-2105	On	fine-m, Q91F9L1	I=micritic		albitization, P>K	sandy siltstone	qz, ox	micas, hn	
@ E3-2106	On	calcareous very fine- fine-Q42F53L5	I=micritic, P wackestone	trilobite	P>K, albitization	foliated shale; Q+F aggregate	cal	chl., bt	
@ E3-2202	On	very fine-fine, Q49F38L13	I=micritic		P>K, albitization	shale	cal, pmx	zr, hn, bt	ripple
@ E3-2201	On	very fine-fine, Q63F33L4	I=micritic		P>K, albitization	shale; slate	cal	zr, hn, bt, glauc., musc.	ripple
@ E3-2203	On	fine-course, Q75F22L3	I= P wackestone	bryoz., trilobite, echinod., conodont	P, albitization, microcline	shale	spar	phosp., musc., chl., zr	cross bedded
@ E3-2204	Och	m-very coarse, Q87F11L2	I=micritic, P packstone, dolomitic mudstone		F= albitization + carbonate	shale, siltstone, calcareous sandstone; slate	qz, spar		
@ E3-2205	Och	m-course, Q79L20	I=micritic, P packstone, dolomitic mudstone		fractured Q, Qm>>Qp+Ch, albitization	shales; sandstone, silicified carbonate	cal		
@ E4-2901	Och	fine-course, Q83L17			face of F? Qm>>Qp+Ch	shale	clay, qz, pmx, ox	hn, oxides	cross bedded
@ E4-2902	Och	fine-m, Q84F3L13			F altered to clay, Qm>>Qp+cht	shale	clay, ox, qz, pmx	zr, hn,	
@ E4-2903	Och	m-course/siltstone, Q77F3L20			Ch	foliated sandy siltstone, silicified carbonate	ox	zr	
@ E4-2207	Och	argil., fine-s, Q90F1L9			very altered F	quartzarenite, massive shale	clay, ox, pmx		
@ E3-2206	Och	fine to conglomeratic, Q98F1L1				conglomeratic clasts of Ch, Qp, and Qm	qz, clay, ox	zr	

## REFERENCES

- Allen, P., and Allen, J., 1992, Basin analysis, Principles and Applications: London, Blackwell Scientific Publications, 451 p.
- Allen, P.A., Burgess, P.M., Galewsky, J., and Sinclair, H.D., 2001, Flexural-eustatic numerical model for drowning of the Eocene perialpine carbonate ramp and implications for Alpine geodynamics: Geological Society of America Bulletin, v. 113, p. 1052-1066.
- Andersen, C.B., 1995, Provenance of mudstones from two Ordovician foreland basins in the Appalachians, *in* Dorobek, S.L, and Ross, G.M., eds., Foreland basin stratigraphy: Society of Economic Paleontologists and Mineralogists Special Publication 52, p. 53-63.
- Andersen, C.B., and Samson, S.D., 1995, Temporal changes in Nd isotopic composition of sedimentary rocks in the Sevier and Taconic foreland basins: Increasing influence of juvenile sources: *Geology*, v. 23, p. 983-986.
- Bayona, G., Van der Voo, R., and Thomas, W.A., in press, Kinematics of thrust sheets within transverse zones: a structural and paleomagnetic investigation in the Appalachian thrust belt of Georgia and Alabama: *Journal of Structural Geology*
- Bearce, D.N., 1978, Structure of the eastern Coosa valley, Alabama: *American journal of Science*, v. 278, p. 461-476.
- Bearce, D.N., 1999, Geology of the Blue Circle limestone quarry, Calera, Alabama: Alabama Geological Society, Winter Fieldtrip Guidebook, no page numbers.
- Beaumont, C., 1981, Foreland basins: *Royal Astronomical Society Geophysical Journal*, v. 65, p. 291-329.
- Beaumont, C., Quinlan, G., and Hamilton, J., 1988, Orogeny and stratigraphy: Numerical models of the Paleozoic in the Eastern interior of North America: *Tectonics*, v. 7, p. 389-416
- Benedict, G.L., and Walker, K.R., 1978, Paleobathymetric analysis in Paleozoic sequences and its geodynamic significance: *American Journal of Science*, v. 278, p. 579-607.
- Benson, D.J., 1986a, Stratigraphic setting of the Middle Ordovician of the Alabama Appalachians, *in* Benson, D.J., and Stock, C.W., eds., Depositional history of the Middle Ordovician of the Alabama Appalachians: Alabama Geological Society, Guidebook, 23<sup>rd</sup> Annual Field Trip, p. 3-14.

- Benson, D.J., 1986b, Depositional setting and history of the Middle Ordovician of the Alabama Appalachians, *in* Benson, D.J., and Stock, C.W., eds., Depositional history of the Middle Ordovician of the Alabama Appalachians: Alabama Geological Society, Guidebook, 23<sup>rd</sup> Annual Field Trip, p. 15-31.
- Benson, D.J., 1992, Tectonic Vs. Eustatic controls on Ordovician deposition in the Alabama Appalachians: Geological Society of America Abstracts with Programs, v. 24, n. 7, p. 141.
- Benson, J.D., and Stock, C.W., 1986, Depositional history of the Middle Ordovician of the Alabama Appalachians: Alabama Geological Society, Guidebook, 23<sup>rd</sup> Annual Field Trip, Stop 6, p. 110-112.
- Bergström, S.M., 1973, Biostratigraphy and facies relationships in the lower Middle Ordovician of easternmost Tennessee: American Journal of Science, v. 273-A, p. 261-293.
- Bergström, S.M., 1977, Notes on the conodont biostratigraphy of the Alcoa highway section, *in* Ruppel, S.C., and Walker, K.R., eds., The ecostratigraphy of the Middle Ordovician of the southern Appalachians (Kentucky, Tennessee, and Virginia), U.S.A.: A field excursion: Knoxville, University of Tennessee Department of Geological Sciences Studies in Geology 1, p. 74-76.
- Bond, G.C., and Kominz, M.A., 1991, Disentangling Middle Paleozoic sea level and tectonics events in cratonic margins and cratonic basins of North America: Journal of Geophysical Research, v. 96, B4, p. 6619-6639
- Boyer, S.E., and Elliott, D., 1982, Thrust systems: American Association of Petroleum Geologists Bulletin, v. 66, p. 1196-1230.
- Bradley, D.C., 1989, Taconic plate kinematics as revealed by foredeep stratigraphy, Appalachian orogen: Tectonics, v. 8, p. 1037-1049.
- Bradley, D.C., and Kidd, W.S., 1991, Flexural extension of the upper continental crust in collisional foredeeps: Geological Society of America Bulletin, v. 103, p. 1416-1438.
- Caldwell, B. E., 1992, The lithostratigraphy, petrology, and depositional environments of Middle Ordovician rocks of the Red Hills and Sand Mountain belts, Whitfield and Murray counties, Georgia (M.S. thesis): Tallahassee, Florida, The Florida State University, 404 p.
- Cardozo, N., and Jordan, T., 2001, Causes of spatially variable tectonic subsidence in the Miocene Bermejo foreland basin, Argentina: Basin Research, v. 13, p. 335-357.

- Carter, B.D., and Chowns, T.M., 1986, Stratigraphical and environmental relationships of Middle and Upper Ordovician rocks in northwestern Georgia and northeastern Alabama, *in* Benson, D.J., and Stock, C.W., eds., Depositional history of the Middle Ordovician of the Alabama Appalachians: Alabama Geological Society, Guidebook, 23<sup>rd</sup> Annual Field Trip, p. 33-50.
- Castle, J. W., 2001, Foreland-basin sequence response to collisional tectonism: Geological Society of America Bulletin, v. 113, p. 801-812.
- Chapple, W.M., 1978, Mechanics of thin-skinned fold- and-thrust belts. Geological Society of America Bulletin, v. 89, p. 1189-1198.
- Chowns, T.M., 1972, Depositional environments in the Upper Ordovician of northwest Georgia and southeast Tennessee, *in* Chowns, T.M., ed., Sedimentary environments in the Paleozoic rocks of northwest Georgia: Georgia Geological Society, Guidebook 11, p. 3-12.
- Chowns, T.M., 1989, Stratigraphy and major thrust sheets in the Appalachian thrust belt of Georgia, *in* Fritz, W.J., ed., Excursions in Georgia Geology: Georgia Geological Society Guidebooks, v. 9, n.1, p. 211-238.
- Chowns, T.M., and McKinney, F.K, 1980, Depositional facies in Middle-Upper Ordovician and Silurian rocks of Alabama and Georgia, *in* Frey, R.W., and Neathery, T.L., eds, Excursions in southeastern Geology, Geological Society of America, 1980 Field Trip n. 16, Guidebook, p. 323-348.
- Chowns, T.M., and Carter, B.D., 1983, Middle Ordovician section along Mount Alto Road at southwest end of Horseleg Mountain, *in* Chowns, T.M., ed., Geology of Paleozoic rocks in the vicinity of Rome, Georgia: Georgia Geological Society, Guidebook, 18<sup>th</sup> Annual Field Trip, p. 70-73.
- Chowns, T. M., Sanders, R. P., Connell, D. A., O'Connor, B. J., and Friddell, M. S., 1992, Stratigraphy and Sedimentology of the Knox Group at Graysville gap, Catoosa county, Georgia: *in* Chowns, T. M and O'Connor, B. J, eds., Cambro-Ordovician strata in Northwest Georgia and Southeast Tennessee; the Knox Group and the Sequatchie Formation, Georgia Geological Society Guidebook, v. 12, n. 1, p. 5-38.
- Coleman, J. L., Jr., 1988, Geology of the Anniston CSD: Alabama Geological Society Guidebook, 25th Annual Field Trip, p. 41-43.

- Cook, B.S., 2001, Structural response of the Pell City thrust sheet to an oblique lateral ramp in the footwall, Appalachian thrust belt, Alabama (M. S. thesis): Lexington, Kentucky, University of Kentucky, 80 p.
- Crampton, S.L., and Allen, P.A., 1995, Recognition of forebulge unconformities associated with early stage foreland basin development: Example from the North Alpine foreland basin: *American Association of Petroleum Geologists*, v. 79, p. 1495-1514.
- Cressler, C.W., 1970, Geology and ground-water resources of Floyd and Polk Counties, Georgia: *Georgia Geological Survey Information Circular 39*, 95 p.
- Cressler, C.W., 1974, Geology and ground-water resources of Gordon, Whitfield, and Murray Counties, Georgia: *Georgia Geological Survey Information Circular 47*, 56 p.
- Cummings, D., 1965, Stratigraphy and heavy minerals of the Bays Formation, Bays Mountain synclinorium, northeast Tennessee: *Geological Society of America Bulletin*, v. 76, p. 591-600.
- Dalrymple, R.W., 1992, Tidal depositional systems: *in* Walker, R.G., and James, N.P., eds., *Facies models: Response to sea-level change*: Geological Association of Canada, 195-218 p.
- Davis, D., Suppe, J., and Dahlen, F.A., 1983, Mechanics of fold-and-thrust belts and accretionary wedges: *Journal of Geophysical Research*, v. 88, p. 1153-1172.
- Dahlstrom, C.D.A., 1969, Balanced cross sections: *Canadian Journal of Earth Sciences* v. 6, p. 743-757.
- DeCelles, P.G., and DeCelles, P.C., 2001, Rates of shortening, propagation, underthrusting, and flexural wave migration in continental orogenic systems: *Geology*, v. 29, p. 135-138.
- DeCelles, P.G., and Giles, K.A., 1996, Foreland basin systems: *Basin Research*, v. 8, p. 105-123.
- DeCelles, P.G., and Mitra, G., 1995, History of the Sevier orogenic wedge in terms of critical taper models, northeast Utah and southwest Wyoming: *Geological Society of America Bulletin*, v. 107, p. 454-462.
- Dickinson, W.R., 1985, Interpreting provenance relations from detrital modes of sandstones, *in* Zuffa, G.G., ed., *Provenance of arenites*: Dordrecht-Boston, Reidel, NATO, ASI Series, v. 148, p. 333-361.

- Diecchio, R. J., 1991, Taconian sedimentary basins of the Appalachians, *in* Barnes, C. R., and Williams, S. H., eds., *Advances in Ordovician geology: Geological Survey of Canada Paper 90-9*, p. 225-234.
- Diecchio, R. J., 1993, Stratigraphic interpretation of the Ordovician of the Appalachian basin and implications for Taconian flexural modeling: *Tectonics*, v. 12, p. 1410-1419.
- Dorobek, S.L., 1995, Synorogenic carbonate platforms and reefs in foreland basins: controls on stratigraphic evolution and platform/reef morphology, *in* Dorobek, S.L., and Ross, G.M., eds, *Stratigraphic evolution of foreland basins: Society for Sedimentary Geology Special Publication 52*, p. 127-147.
- Drahovzal, J.A., 1975, Studies along the Anniston lineament complex, Northeast Alabama, *in* Neathery, T.L., Self, D.M., Copeland, C.W., Drahovzal, J.A., and Deininger, R.W., eds., *Studies on Recent faulting criteria in Alabama: Alabama Geological Survey*, p. 334-358.
- Drahovzal, J.A., and Neathery, T.L., 1971, Middle and Upper Ordovician stratigraphy of the Alabama Appalachians, *in* Drahovzal, J.A., and Neathery, T.L., eds., *The Middle and Upper Ordovician of the Alabama Appalachians: Alabama Geological Society, Guidebook, 9<sup>th</sup> Annual Field Trip*, p. 1-62.
- Drake, A.A., Sinha, A.K., Laird, J., and Guy, R.E., 1989, The Taconic orogen, *in* Hatcher, R.D., Jr., Thomas, W.A., and Viele, G.W., eds., *The Appalachian-Ouachita Orogen in the United States: Boulder, Colorado, Geological Society of America, The Geology of North America*, v. F-2, p. 101-178.
- Eldredge, S., and Van der Voo, R., 1988, Paleomagnetic study of thrust sheet rotations in the Helena and Wyoming salients of the northern Rocky Mountains, *in* Schmidt, C., and Perry, W., eds., *Interaction of the Rocky Mountains Foreland and the Cordilleran thrust belt: Geological society of America Memoir 171*, p. 319-332.
- Ettensohn, F.R., 1991, Flexural interpretation of relationships between Ordovician tectonism and stratigraphic sequences, central and southern Appalachians, U.S.A., *in* Barnes, C.R., and Williams, S.H., eds, *Advances in Ordovician Geology: Geological Survey of Canada, Paper 90-9*, p. 213-224.
- Ferrill, B.A., 1989, Middle Cambrian to Lower Mississippian synsedimentary structures in the Appalachian fold-thrust belt in Alabama and Georgia (Ph. D. dissertation): Tuscaloosa, Alabama, The University of Alabama, 270 p.

- Finney, S.C., 1977, Graptolites of the Middle Ordovician Athens Shale, Alabama (Ph. D. dissertation): Columbus, Ohio, The Ohio State University, 585 p.
- Finney, S.C., Grubb, B.J., and Hatcher, R.D., Jr., 1996, Graphic correlation of Middle Ordovician graptolite shale, southern Appalachians: An approach for examining the subsidence and migration of a Taconic foreland basin: Geological Society of America Bulletin, v. 108, p. 355-371.
- Flemings, P.B., and Jordan, T.E., 1990, Stratigraphic modelling of foreland basins: Interpreting thrust deformation and lithosphere rheology: Geology, v.18, p. 430-434.
- Flemings, P.B., and Nelson, S.N., 1991, Paleogeographic evolution of the latest Cretaceous and Paleocene Wind River basin: Mountain Geologists, v. 28, p. 37-52.
- Garry, W.B., 2001, Stratigraphy and structure of the Dunaway Mountain thrust sheet revealed through geologic mapping and interpretation of the Ashville 7.5 minute quadrangle, Alabama (M.S. thesis): Lexington, Kentucky, University of Kentucky, 201 p.
- Gleason, J.D., Patchett, P.J., Dickinson, W.R., Ruiz, J., 1994, Nd isotopes link Ouachita turbidites to Appalachian sources: Geology, v. 22, p. 347-350.
- Gleason, J.D., Patchett, P.J., Dickinson, W.R., Ruiz, J., 1995a, Nd isotopes link Ouachita turbidites to Appalachian sources, Reply to comment by W. A. Thomas: Geology, v. 23, p. 93-95.
- Gleason, J.D., Patchett, P.J., Dickinson, W.R., Ruiz, J., 1995b, Nd isotopic constraints on sediment sources of the Ouachita-Marathon fold belt: Geological Society of America Bulletin, v. 107, p. 1192-1210.
- Gleason, J.D., Patchett, P.J., Dickinson, W.R., Ruiz, J., 1997, Nd isotopic constraints on sediment sources of the Ouachita-Marathon fold belt, Reply to alternative interpretation by W. A. Thomas: Geological Society of America Bulletin, v. 109, p. 779-787.
- Gleason, J.D., Finney, S.C., and Gehrels, G.E., 2002, Paleotectonic implications of a Mid- to Late-Ordovician provenance shift, as recorded in sedimentary strata of the Ouachita and southern Appalachian Mountains: The Journal of Geology, v. 110, p. 291-304.
- Graham, G.B., 1999, Geometry and kinematics of two juxtaposed lateral ramps, southern Appalachian thrust belt in northeastern Alabama (M.S. thesis): Lexington, Kentucky, University of Kentucky, 70 p.

- Grubbs, K.L., and Van der Voo, R., 1976, Structural deformation of the Idaho-Wyoming overthrust belt (USA), as determined by Triassic paleomagnetism: *Tectonophysics*, v. 33, p. 321-336.
- Guinn, S.A., and Long, L.T., 1978, A gravity survey of the Dalton area, Georgia area: *Georgia Geological Survey Bulletin*, v. 93, p. 78-82.
- Gupta, S., and Allen, P.A., 2000, Implications of foreland paleotopography for stratigraphic development in the Eocene distal Alpine foreland basin: *Geological Society of America Bulletin*, v. 112, p. 515-530.
- Gurnis, M., 1992, Rapid continental subsidence following the initiation and evolution of subduction: *Science*, v. 255, p. 1556-1558.
- Guthrie, G.M., 1994, Geology of the Columbiana area, Chilton, Coosa, and Shelby counties, Alabama: *Geological Survey of Alabama Bulletin* 151, 80 p.
- Hall, J.C., 1986, Conodonts and conodont biostratigraphy of the Middle Ordovician in the western overthrust region and Sequatchie Valley of the southern Appalachians, (Ph. D. dissertation): Columbus, Ohio, The Ohio State University, 346 p.
- Hall, J.C., Bergström, S.M., and Schmidt, M.A., 1986, Conodont biostratigraphy of the Middle Ordovician Chickamauga Group and related strata of the Alabama Appalachians, *in* Benson, D.J., and Stock, C.W., eds., *Depositional history of the Middle Ordovician of the Alabama Appalachians: Alabama Geological Society, Guidebook, 23<sup>rd</sup> Annual Field Trip*, p. 61-80.
- Harris A.G., and Repetski, J.E., 1982, Conodonts revise the Lower-Middle Ordovician boundary and timing of miogeoclinal events in the east-central Appalachians: *Geological Society of America Abstracts with Programs*, v. 14, p. 261.
- Harris, P.T., Pattiaratchi, C.B., Keene, J. B., Dalrymple, R.W., Gardner, J.V, Baker, E.K., Cole, A.R., Mitchell, D., Gibbs, P., and Schroeder, W.W., 1996, Late Quaternary deltaic and carbonate sedimentation in the Gulf of Papua Foreland basin: Response to sea-level change, *Journal of Sedimentary Research*, v. 66, p. 801-819.
- Hatcher, R.D., Jr., 1989, Tectonic synthesis of the U.S. Appalachians, *in* Hatcher, R.D., Jr., Thomas, W.A., and Viele, G.W., eds., *The Appalachian-Ouachita Orogen in the United States: Boulder, Colorado, Geological Society of America, The Geology of North America*, v. F-2, p. 511-535.



- Hatcher, R.D., Jr., 1999, Crust-forming processes, *in* Sinha, A.K., ed., Basement tectonics, v. 13: Kluwer Academic Publishers, The Netherlands, p. 88-118.
- Hatcher, R.D., Jr., Osberg, P.H., Drake, A.A., Robinson, P., and Thomas, W.A., 1989, Tectonic map of the U.S. Appalachians, *in* Hatcher, R.D., Jr., Thomas, W.A., and Viele, G.W., eds., The Appalachian-Ouachita Orogen in the United States: Boulder, Colorado, Geological Society of America, The Geology of North America, v. F-2, plate 1.
- Haynes, J.T., 1994, The Ordovician Deicke and Millbrig K-Bentonite beds of the Cincinnati Arch and the southern Valley and Ridge province: Geological Society of America Special Paper 290, 80 p.
- Hayward, A.B., and Graham, R.H., 1989, Some geometric characteristics of inversion, *in* Cooper, M., and Williams, G., eds, Inversion tectonics: Geological Society of London Special Publication 44, p. 17-40.
- Hibbard, J., 2000, Docking Carolina: Mid-Paleozoic accretion in the southern Appalachians: *Geology*, v. 28, p. 127-130.
- Higgins, M.W., Atkins, R.L., Crawford, T.J., Crawford, R.F., III., Brooks, R., and Cook, R.B., 1988, The structure, stratigraphy, tectonostratigraphy, and evolution of the southernmost part of the Appalachian orogen: U.S. Geological Survey Professional Paper 1475, 173 p.
- Horton, B.K., 1999, Erosional control on the geometry and kinematics of thrust belt development in the central Andes: *Tectonics*, v. 18, p. 1292-1304.
- Holland, S. M. and Patzkowsky, M. E., 1997, Distal orogenic effects of peripheral bulge sedimentation: Middle and Upper Ordovician of the Nashville dome: *Journal of Sedimentary Research*, v. 67, n. 2, p. 250-263.
- Hutchinson, R.B., Grow, J.A., and Klitgord, K.M., 1983, Crustal structure beneath the southern Appalachians: Nonuniqueness of gravity modeling: *Geology*, v. 11, p. 611-615.
- Ingersoll, R.V., Bullard, T.F., Ford, R.L., Grimm, J.P., Pickle, J.D., and Sares, S.W., 1984, The effect of grain size on detrital modes: A test of the Gazzi-Dickinson point-counting method: *Journal of Sedimentary Petrology*, v. 54, p. 103-116.
- Jamison, W.R., 1987, Geometric analysis of fold development in overthrust terranes: *Journal of Structural Geology*, v. 9, p. 207-219

- Jenkins, C.M., 1984, Depositional environments of the Middle Ordovician Greensport Formation and Colvin Mountain Sandstone in Calhoun, Etowah, and St. Clair Counties, Alabama (M.S. thesis): Tuscaloosa, Alabama, The University of Alabama, 156 p.
- Jones, B. and Desrochers, A., 1992, Shallow platform carbonates, *in* Walker, R. G., and James, N. P., Facies Models, Response to sea level change, Geological Association of Canada, p. 277-301.
- Jordan, T.E., 1981, Thrust loads and foreland basin evolution, Cretaceous, western United States: America of Association of Petroleum Geologists Bulletin, v. 65, p. 2506-2520.
- Kath, R., McClean, T., and Beriswill, J., 1994, Environmental impact studies, geology, hydrogeology, and foundation grouting of the Haig Mill dam Dalton, Georgia, *in* Watson, T. W., Environmental Geology and Hydrogeology: Georgia Geological Society Guidebooks, v. 14, n. 1, p. 104-128.
- Kellberg, J. M., and Grant, L. F., 1956, Coarse conglomerates of the Middle Ordovician in the southern Appalachian Valley: Geological Society of America Bulletin, v. 67, p. 697-716.
- Kent, D. V., 1988, Further paleomagnetic evidence for oroclinal rotation in the central folded Appalachians from the Bloomsburg and the Mauch Chunk Formations: Tectonics, v. 7, p. 749-759.
- Kesler, T.L., 1975, Rome and Coosa faults in northwest Georgia: Geological Society of America Bulletin, v. 86, p. 625-631.
- Kher, S., 1996, Patterns of meteoric diagenesis in the Middle and Late Ordovician carbonates of the southern Appalachians (Ph. D. dissertation): Tallahassee, Florida, The Florida State University, 181 p.
- Kidd, J. T., 1975, Pre-Mississippian subsurface stratigraphy of the Warrior basin in Alabama, *in* Paulson, O.L. Jr, ed., Transactions of the Gulf Coast Association of Geological Societies, v. 25, p. 20-39.
- Kolata, D.R., Huff, W.D., and Bergström, S.M., 1996, Ordovician K-bentonites of eastern North America: Geological Society of America Special Paper 313, 69 p.
- Kolata, D.R., Huff, W.D., and Bergström, S.M., 1998, Nature and regional significance of unconformities associated with the Middle Ordovician Hagan K-bentonite complex in the North America midcontinent: Geological Society of America Bulletin, v. 110, p. 723-739.

- Lee, A.M., 1983, Lithofacies and depositional environments of the Chickamauga Group in Jefferson county, north-central Alabama (M.S. thesis): Tuscaloosa, Alabama, University of Alabama, 198 p.
- Lehmann D., Brett, C.E., Cole, R., Baird, G., 1995, Distal sedimentation in a peripheral foreland basin: Ordovician black shales and associated flysch of the western Taconic foreland, New York State and Ontario: Geological Society of America, v. 107, p. 708-724
- Li, L., and Tull, J.F., 1998, Cover stratigraphy and structure of the southernmost external basement massifs in the Appalachians Blue Ridge: Evidence for the two-stage late Proterozoic rifting: American Journal of Science, v. 298, p. 829-867.
- Lorenzo, J. M., O'Brien, G.W., Stewart, J., and Tandon, K., 1998, Inelastic yielding and forebulge shape across a modern foreland basin: Northwest shelf of Australia, Timor Sea: Geophysical Research Letters, v. 25, p. 1455-1458.
- Macedo, J., and Marshak, S., 1999, Controls on the geometry of fold-thrust belt salients: Geological Society of America Bulletin, v. 111, p. 1808-1822.
- Mack, G.H., 1980, Stratigraphy and depositional environments of the Chilhowee Group (Cambrian) in Georgia and Alabama: American Journal of Science, v. 280, p. 497-517.
- Mack, G.H., 1985, Provenance of the Middle Ordovician Blount clastic wedge, Georgia and Tennessee: Geology, v.13, p. 299-302.
- Marrett, R., and Aranda-Garcia, M., 1999, Structure and kinematic development of the Sierra Madre Oriental fold-thrust belt, Mexico, *in* Marrett, R. Wilson, J.L., and Ward, W.C., eds., Stratigraphy and structure of the Jurassic and Cretaceous platform and basin systems of the Sierra Madre Oriental: South Texas Geological Society, a field book and related papers, p. 69-98.
- Marshak, S., and Mitra, G., 1988, Basic methods of structural geology: New Jersey, Prentice-Hall, 446 p.
- Marshak, S., Wilkerson, M. S, and Hsui A. T., 1992, Generation of curved fold-thrust belts: Insight from simple physical and analytical models, *in* McKlay, K., ed., Thrust Tectonics: London, Chapman and Hall, p. 83-92.
- Martin, A.J., 1991, Paleoenvironmental analysis of the Shellmound and Mannie Shale members, Sequatchie Formation (Upper Ordovician), Georgia and Tennessee (Ph.D. dissertation): Athens, Georgia, University of Georgia, 314 p.

- McBride, J., Hatcher, R.D., Jr., Stephenson, W.J., 2001, Toward a reconciliation of seismic reflection and field geologic mapping from the Pine Mountain belt; preliminary results: Geological Society of America Abstracts with Programs, v. 33, n. 2, p. 74
- Meyers, J.H., Suttner, L.J., Furer, L.C., May, M.T., and Soreghan, M.J., 1992, Intrabasinal tectonic control on fluvial sandstone bodies in the Cloverly Formation (Early Cretaceous) west-central Wyoming, USA: Basin Research, v. 4, p. 315-333.
- Milici, R.C., and Smith, J.W., 1969, Stratigraphy of the Chickamauga Supergroup in its type locality: Georgia Geological Survey Bulletin, v. 80, p. 5-35.
- Mitra, G., 1997, Evolution of salients in a fold-and-thrust belt: The effects of sedimentary basin geometry, strain distribution and critical taper, *in* Sengupta, S., ed., Evolution of geological structures in micro- to macro-scales: London, Chapman & Hall, p. 59-90.
- Moustafa, A.R., 2002, Controls on the geometry of transfer zones in the Suez rift and northwest Red Sea: Implications for the structural geometry of rift systems: American Association of Petroleum Geologists Bulletin, v. 86, p. 979-1002.
- Neathery, T.L., and Drahovzal, J.A., 1985, Lithostratigraphy of Upper Ordovician strata in Alabama: Geological Survey of Alabama Circular 124, 55 p.
- Nelson, K.D., and eight others, 1985, New COCORP profiling in the southeastern United States. Part I: Late Paleozoic suture and Mesozoic rift basin: Geology, v. 13, p. 714-718.
- Osborne, W.E., 1996, Geology of the Helena 7.5-minute quadrangle, Jefferson and Shelby counties, Alabama: Geological Survey of Alabama, Quadrangle Series Map 14, 21 p.
- Osborne, E.W., Szabo, M.W., Neathery, T.L., and Copeland, C.W., Jr, 1988, Geologic map of Alabama, northeast sheet: Geological Survey of Alabama, scale 1:250,000.
- Patton, T. L., and O'Connor, S. J., 1988, Cretaceous Flexural history of northern Oman Mountain foredeep, United Arab Emirates: American Association of Petroleum Geologists Bulletin, v. 72, p. 797-809.
- Paulsen, T., and Marshak, S., 1999, Origin of the Uinta recess, Sevier fold-thrust belt, Utah: Influence of basin architecture on fold-thrust belt geometry: Tectonophysics, v. 312, p. 203-216.
- Phillips, P.L., 1996, Carbonate petrology and strontium isotope stratigraphy of the Middle Ordovician Chickamauga Supergroup in its type area, Walker county, Georgia (M.S. thesis): Wilmington, North Carolina, University of North Carolina, 56 p.

- Phillips, P.L., and Hall, J.C., 1993, Conodont biostratigraphy of the Ordovician-Silurian boundary in the Central Appalachian Valley and Ridge province: Geological Society of America Abstracts with Programs, v. 25, n. 4, p. 61
- Pickering, S.M., Jr., and other 15 coauthors, 1976, Geologic map of Georgia: Georgia Geological Survey, scale 1:500,000.
- Pigram, C.J., Davies, P.J., Feary, D.A., and Symonds, P.A., 1989, Tectonic controls on carbonate platform evolution in southern Papua New Guinea: Passive margin to foreland basin: *Geology*, v. 17, p. 199-202.
- Powell, W.J., Copeland, C.W., and Drahovzal, J.A., 1970, Geologic and hydrologic research through space acquired data for Alabama: *The Journal of the Alabama Academy of Science*, v. 41, p. 145.
- Quinlan, G.M., and Beaumont, C., 1984, Appalachian thrusting, lithospheric flexure, and the Paleozoic stratigraphy of the eastern interior of North America: *Canadian Journal of Earth Sciences*, v. 21, p. 973-996.
- Rader, E. K., and Gathright, T. M., II, 1986, Stratigraphic and structural features of Fincastle Valley and Eagle Rock Gorge, Botetourt County, Virginia, *in* Neathery, T. L., ed., *Southeastern Section of the Geological Society of America: Geological Society of America, Centennial Field Guide*, v. 6, p. 105-108.
- Rankin, D.W., 1976, Appalachian salients and recesses; late Precambrian continental breakup and the opening of the Iapetus Ocean, *Journal of Geophysical Research*, v. 81, 5605-5619.
- Raymond, D.E., 1973, Upper Ordovician conodonts of Alabama (M.S. thesis): Tuscaloosa, Alabama, University of Alabama.
- Raymond, D.E., 1991, New subsurface information on Paleozoic stratigraphy of the Alabama fold and thrust belt and the Black Warrior basin: *Geological Survey of Alabama Bulletin* 143, 185 p.
- Raymond, D.E., 1993, The Knox Group of Alabama: An overview: *Geological Survey of Alabama Bulletin* 152, 160 p.
- Raymond, D.E., Osborne, W.E., Copeland, C.W., and Neathery, T.L., 1988, Alabama stratigraphy: *Alabama Geological Survey Bulletin* 143, 185 p.
- Renner, J. F., 1989, Clay mineralogy of the Rockmart slate (M.S. thesis): Athens, Georgia, University of Georgia, 120 p.

- Rindsberg, A.K., and Chowns, T.M., 1986, Ringgold Gap: Progradational sequences in the Ordovician and Silurian of northwest Georgia: Geological Society of America Centennial Filed Guide, v. 6, p. 159-162.
- Repetski, J. E., 1992, Knox Group and basal Stones River Group conodonts from near Graysville, Catoosa county, Georgia, *in* Chowns, T. M and O'Connor, B. J, eds., Cambro-Ordovician strata in Northwest Georgia and Southeast Tennessee; the Knox Group and the Sequatchie Formation, Georgia Geological Society Guidebook, v. 12, n. 1, p. 39-40.
- Roberson, K.E., 1988, The Post-Knox unconformity and its relationship to bounding stratigraphy, Alabama Appalachians (M.S. thesis): Tuscaloosa, Alabama, University of Alabama, 148 p.
- Roberson, K.E., 1994, Stratigraphy and depositional history of Middle Ordovician peritidal carbonate rocks overlying the post-Knox unconformity, East Tennessee (Ph. D. dissertation): Knoxville, Tennessee, University of Tennessee, 210 p.
- Rodgers, J., 1953, Geologic map of east Tennessee with explanatory text: Tennessee Department Conservatory Division Geology Bulletin 58, pt. 2, 168 p.
- Rosendahl, B.R., 1987, Architecture of continental rifts with special reference to east Africa: Annual Revision Earth Planetary Sciences, v. 15, p. 445-503.
- Ross, C.A. and Ross, J.R.P., 1995, North American Ordovician Depositional Sequences: *in* Cooper, J.D., Droser, M.I., and Finney, S.C., eds., Ordovician Odyssey: The Pacific Section Society for Sedimentary Geology, p. 309-313.
- Royden, L., Patacca, E., and Scandone, P., 1987, Segmentation and configuration of subducted lithosphere in Italy: An important control on thrust-belt and foredeep-basin evolution: Geology, v. 15, p. 714-717.
- Rowan, M.G., and Linares, R., 2000, Fold-evolution matrices and axial-surface analyses of fault-belt folds: Application to the Medina Anticline, Eastern Cordillera, Colombia: American Association of Petroleum Geologists Bulletin, v. 84, p. 741-764.
- Ruppel, S.C and Walker, K.R., 1984, Petrology and depositional history of a Middle Ordovician carbonate platform: Chickamauga Group, northeastern Tennessee: Geological Society of America Bulletin, v. 95, p. 568-583.
- Salisbury, J.W., 1961, Geology and mineral resources of the northwest quarter of the Cohutta Mountain quadrangle: Georgia Geological Survey Bulletin 71, 61 p.

- Schlager, W., 1981, The paradox of drowned reefs and carbonate platforms: Geological Society of America Bulletin, v. 92, p. 197-211.
- Sclater, J.G., and Christie, P.A.F., 1980, Continental stretching: an explanation of the post-mid-Cretaceous subsidence of the central North Sea Basin: Journal of Geophysical Research, v. 85, n. B7, p. 3711-3739.
- Shanmugam, G., and Lash, G.G., 1982, Analogous tectonic evolution of the Ordovician foredeeps, southern and central Appalachians: Geology, v. 10, p. 562-566.
- Shanmugam, G., and Lash, G.G., 1983, Analogous tectonic evolution of the Ordovician foredeeps, southern and central Appalachians, Reply to comment by R.N. Hiscott, G.M., Quinlan, and R.K., Stevens: Geology, v. 11, p. 732-733.
- Shanmugam, G., and Walker, K.R., 1978, Tectonic significance of distal turbidites in the Middle Ordovician Blockhouse and lower Sevier Formations in east Tennessee: American Journal of Science, v. 278, p. 551-578.
- Shanmugam, G., and Walker, K.R., 1980, Sedimentation, subsidence, and evolution of a foredeep basin in the Middle Ordovician, southern Appalachians: American Journal of Science, v. 280, p. 479-496.
- Shaw, T.H., Roberson, K.E., and Harris, A.G., 1990, Lithostratigraphy and conodont biostratigraphy across the Lower-Middle Ordovician disconformity (Early to Middle Whiterockian) at Pratt Ferry, Central Alabama: *in* Sando, W.J., ed., Shorter contributions to paleontology and stratigraphy, U.S. Geological Survey Bulletin 1895, p. C1-C13
- Sibley, D.M., 1983, The structural fabric of the Rockmart slate and its relation to the timing of orogenesis in the valley and ridge province of northwest Georgia (M.S. thesis): Auburn, Alabama, Auburn University, 121p.
- Sinclair, H.D., 1997, Tectonostratigraphic model for underfilled peripheral foreland basins: An Alpine perspective: Geological Society of America Bulletin, v. 109, p. 324-346.
- Sloss, L.L., 1963, Sequences in the cratonic interior of North America: Geological Society of America Bulletin, v. 74, p. 93-114.
- Spraggins, S.A., and Dunne, W.M., 2002, Deformation history of the Roanoke recess, Appalachians, USA, Journal of Structural Geology, v. 24, p. 411-433.
- Stamatakos, J., and Hirt, A. M., 1994, Paleomagnetic considerations of the development of the Pennsylvanian salient in the central Appalachians: Tectonophysics, v. 231, p. 237-255.

- Steinhauff D. M., and Walker, K. R., 1995, Recognizing exposure, drowning, and “missing beats”; platform-interior to platform-margin sequence stratigraphy of Middle Ordovician Limestones, East Tennessee: *Journal of Sedimentary Research*, v. B65, n. 2, p. 183-207.
- Steinhauff D.M., and Walker, K.R., 1996, Sequence stratigraphy of an apparently noncyclic carbonate succession: Recognizing subaerial exposure in a largely subtidal, Middle Ordovician stratigraphic sequence in eastern Tennessee, *in* Witzke, B.J., Ludvigson, G.A.M., and Day, J., eds., *Paleozoic sequence stratigraphy: Views from the North American craton*: Geological Society of America Special Paper 306, 87-115.
- Steltenpohl, M.G., and Tull, J.F., 2002, Structural and stratigraphic comparisons of outboard fragments of the Laurentian margin, southwesternmost Appalachians, Alabama and Georgia: *Geological Society of America Abstracts with Programs*, v. 34, n.2, p. 118.
- Stockmal, G.S., Beaumont, C., and Boutilier, R., 1986, Geodynamic models of convergent margin tectonics: Transition from rifted margin to overthrust belt and consequences for foreland-basin development: *American Association of Petroleum Geologists Bulletin*, v. 70, p. 181-190.
- Szabo, M.W., Osborne, E.W., and Copeland, C.W., Jr, 1988, Geologic map of Alabama, northwest sheet: Geological Survey of Alabama, scale 1:250,000.
- Tandon, K., Lorenzo, J. M., and O’Brien, G. W., 2000, Effective elastic thickness of the northern Australian continental lithosphere subducting beneath the Banda orogen (Indonesia): inelastic failure at the start of continental subduction: *Tectonophysics*, v. 329, p. 39-60.
- Taylor, S. R., and McLennan, S. M., 1985, *The continental crust: its composition and evolution*: Oxford, Blackwell Scientific publications, 312 p.
- Thelin, G.P., and Pike, R.J., 1991, *Landforms of the Conterminous United States - A Digital Shaded-Relief Portrayal*: USGS Geologic Investigations Series I-2206
- Thomas, W.A., 1977, Evolution of Appalachian-Ouachita salients and recesses from reentrants and promontories in the continental margin: *American Journal of Science*, v. 277, p. 1233-1278.
- Thomas, W.A., 1985, Northern Alabama sections, *in* Woodward, N. B., ed., *Valley and Ridge thrust belt: Balanced structural sections, Pennsylvania to Alabama (Appalachian Basin Industrial Associates)*: University of Tennessee Department of Geological Sciences Studies in Geology 12, p. 54-61.



- Thomas, W.A., 1986, A Paleozoic synsedimentary structure in the Appalachian fold-thrust belt in Alabama, *in* McDowell, R.C., and Glover, L., III, eds., The Lowry volume: Studies in Appalachian geology: Virginia Tech Department of Geological Sciences Memoir 3, p. 1-12.
- Thomas, W.A., 1988, The Black Warrior Basin, *in* Sloss, L.L., ed., Sedimentary cover – North American craton, U.S.: Geological Society of America, the Geology of North America, v. D-2, Plate 8.
- Thomas, W.A., 1990, Controls on locations of transverse zones in thrust belts: *Eclogae Geologicae Helveticae*, v. 83, p. 727-744.
- Thomas, W.A., 1991, The Appalachian-Ouachita rifted margin of southeastern North America: *Geological Society of America Bulletin*, v. 103, p. 415-431.
- Thomas, W.A., 1993, Low-angle detachment geometry of the late Precambrian-Cambrian Appalachian-Ouachita rifted margin of southeastern North America, *Geology*, v. 21, p. 921-924.
- Thomas, W.A., 1995, Comment on Nd isotopes link Ouachita turbidites to Appalachians sources, *Geology*, v. 23, p. 93-94.
- Thomas, W.A., 1997, Alternative interpretation to Nd isotopic constraints on sediment sources of the Ouachita-Marathon fold belt: *Geological Society American Bulletin*, v. 109, p. 779-787.
- Thomas, W.A., 2001, Mushwad: Ductile duplex in the Appalachian thrust belt in Alabama, *American Association of Petroleum Geologists Bulletin*, v. 85, p. 1847-1869.
- Thomas W.A., and Astini, R.A., 1999, Simple-shear conjugate rift margins of the Argentine Precordillera and the Ouachita embayment of Laurentia: *Geological Society of America Bulletin*, v. 111, p. 1069-1079.
- Thomas, W.A., and Bayona, G., 2001, Three-dimensional palinspastic restoration of the unmetamorphosed Appalachian thrust belt in Alabama and Georgia: *Geological Society of America Abstracts with Programs*, v. 33, n. 2, p. 5.
- Thomas, W. A., and Bayona, G., 2002, Palinspastic restoration of the Anniston Transverse Zone in the Appalachians thrust belt, Alabama: *Journal of Structural Geology*, v. 24, p. 797-826.
- Thomas, W.A., and Drahovzal, J.A., 1974, Geology of the Coosa deformed belt: Alabama Geological Society, Guidebook, 12th Annual Field Trip, p. 45-75.

- Thomas, W.A., Astini, R., and Bayona, G., 2002, Ordovician collision of the Argentine Precordillera with Gondwana, independent of Laurentian Taconic orogeny: *Tectonophysics*, v. 345, p. 131-152.
- Thomas, W.A., Astini, R.A., and Denison, R.E., 2001, Strontium isotopes, age, and tectonic setting of Cambrian Salinas along the rift and transform margins of the Argentine Precordillera and southern Laurentia: *Journal of Geology*, v. 109, p. 231-246.
- Thomas, W.A., Astini, R.A., Osborne, W.E., and Bayona, G., 2000, Tectonic framework of deposition of the Conasauga Formation, *in* The Conasauga Formation and equivalent units in the Appalachian thrust belt in Alabama edited by Osborne, W.E., Thomas, W.A., and Astini, R. A., Alabama Geological Society, Guidebook, 37th Annual Field Trip, p. 19-40.
- Tobin, K.J., and Walker, K.R., 1994, Meteoric diagenesis below a submerged platform: implication for  $\delta^{13}C$  compositions prior to pre-vascular plant evolution, Middle Ordovician, Alabama, U.S.A.: *Sedimentary Geology*, v. 90, p. 95-111.
- Tull, J.F., 1998, Analysis of a regional middle Paleozoic unconformity along the distal southeastern Laurentian margin, southernmost Appalachians: Implications for tectonic evolution: *Geological Society of America Bulletin*, v. 110, p.1149-1162.
- Tull, J.F., 2002, Southeastern margin of the middle Paleozoic shelf, southwesternmost Appalachians: Regional stability bracketed by Acadian and Alleghanian tectonism: *Geological Society of America Bulletin*, v. 114, p. 643-655.
- Turcotte D.L., and Schubert, G., 1982, *Geodynamics*: New York, John Wiley & Sons ed., 450 p.
- Ussami, N., Shiraiwa, S., and Landin-Dominguez, J.M., 1999, Basement reactivation in a sub-Andean foreland flexural bulge: The Pantanal wetland, SW Brazil: *Tectonics*, v. 18, p. 25-39.
- Van Wagoner, J.C., Mitchum, R.M., Campion, K.M., & Rahmanian, V.D. (1990) Siliciclastic sequence stratigraphy in well logs, cores, and outcrops: Concepts for high-resolution correlation of time and facies: *American Association of Petroleum Geologists Methods in Exploration Series*, 7, 55 p.
- Waldron, J.W.F., and van Staal, C.R., 2001, Taconian orogeny and the accretion of the Dashwoods block: A peri-Laurentian microcontinent in the Iapetus ocean: *Geology*, v. 29, p. 811-814.

- Walker, K. R., 1977, A brief introduction to the ecostratigraphy of the Middle Ordovician of Tennessee (southern Appalachians, USA), *in* Ruppel, S.C., and Walker, K.R., eds., The ecostratigraphy of the Middle Ordovician of the southern Appalachians (Kentucky, Tennessee, and Virginia), U.S.A.: A field excursion: Knoxville, University of Tennessee Department of Geological Sciences Studies in Geology 1, p. 12-17.
- Walker, K.R., Shanmugam, G., and Ruppel, S.C., 1983, A model for carbonate to terrigenous clastic sequences: Geological Society of America Bulletin, v. 94, p. 700-712.
- Walker, T.R., 1984, Diagenetic albitization of Potassium feldspar in arkosic sandstones: Journal of Sedimentary Petrology, v. 54, p. 3-16.
- Ward, W.I., 1983, Lithofacies and depositional environments of a portion of the Stones River Formation in Etowah and Delkalb counties, northeast Alabama (M.S. thesis): Tuscaloosa, Alabama, University of Alabama, 255 p.
- Waschbusch, P. J., and Royden, L. H., 1992, Spatial and temporal evolution of foredeep basins: lateral strength variations and inelastic yielding in continental lithosphere: Basin Research, v. 4, p. 179-196.
- Webby, B.D., 1998, Steps toward a global standard for Ordovician stratigraphy: Newsletter Stratigraphy, v. 36, n.1, p. 1-33
- Wheeler, R. L., 1980, Cross-strike structural discontinuities: Possible exploration tool for natural gas in Appalachian overthrust belt: American Association of Petroleum Geologists Bulletin, v. 64, p. 2166-2178.
- White, T., Furlong, K., and Arthur, M., 2002, Forebulge migration in the Cretaceous western interior basin of the central United States: Basin Research, v. 14, p. 43-54.
- Whiting, B.M., and Thomas, W.A., 1994, Three-dimensional controls on subsidence of a foreland basin associated with a thrust-belt recess: Black Warrior basin, Alabama and Mississippi: Geology, v. 22, p. 727-730.
- Wilson, C. W., 1949, Pre-Chattanooga Stratigraphy in central Tennessee, Tennessee Division of Geology Bulletin, v. 56, p. 1-407.
- Wiltschko, D., and Eastman, D., 1983, Role of basement warps and faults in localizing thrust fault ramps, *in* Hatcher, R.D., Jr., William, H., and Zietz, I., eds., Contributions to the tectonics and geophysics of mountain chains: Geological society of America Memoir 158, p. 177-190.

- Woodward, N. B., ed., Valley and Ridge thrust belt: Balanced structural sections, Pennsylvania to Alabama (Appalachian Basin Industrial Associates): University of Tennessee Department of Geological Sciences Studies in Geology 12, 64 p.
- Younes, A.I., and McClay, K., 2002, Development of accommodation zones in the Gulf of Suez – Red Sea rift, Egypt: American Association of Petroleum Geologists, v. 86, p. 1003-1026.
- Yu, H., and Chou, Y., 2001, Characteristics and development of the flexural forebulge and basal unconformity of western Taiwan foreland basin: Tectonophysics, v. 333, p. 277-291.
- Zeigler, E.L., 1988, Sedimentary petrology and depositional environments of the Upper Ordovician Sequatchie and Lower Silurian Red Mountain Formations, northwestern Georgia (M.S. thesis): Atlanta, Georgia, Emory University, 288 p.
- Zhang, G. and Bott, M.H.P., 2000, Modelling the evolution of asymmetrical basins bounded by high-angle reverse faults with application to foreland basins: Tectonophysics, v. 322, p. 203-218.

## VITA

### **Germán Bayona**

#### **Date and place of birth**

July 5<sup>th</sup>, 1969, Bogotá, Colombia

#### **Education**

1986 – 1992 Geology degree, Universidad Nacional de Colombia, Bogotá.

1996 – 1999 Master of Sciences degree, New Mexico State University, Las Cruces, NM.

#### **Professional experience**

1991 – 1993 Independent consultant geologist.

1993 – 1996 Research geologist and project manager, Corporación Geológica ARES

#### **Scholastic and professional honors**

- 2002 McFarlan fellowship, Department of Geological Sciences, University of Kentucky
- 2001 Commonwealth Research Award, University of Kentucky
- 2001 National grant of the Geological Society of America
- 2000 Commonwealth Research Award, University of Kentucky
- 2000 Dissertation Enhancement Award, University of Kentucky
- 2000 McFarlan fellowship, Department of Geological Sciences, University of Kentucky
- 2000 Geological Society of America Penrose scholarship
- 2000 Research grant, Southeastern Section Geological Society of America
- 1999-2002 Research assistantship, University of Kentucky
- 1998 University of New Mexico-Los Alamos National Laboratory scholarship
- 1998 New Mexico Geological Society grant
- 1997 Roswell Geological Society Scholarship
- 1997 LASPAU Trustees' Fund award
- 1996-1998 COLCIENCIAS, Fellowship
- 1996-1998 New Mexico State University Teaching Assistantship and Wemlinger scholarship

- 1989-1992 Universidad Nacional de Colombia; Assistantship and honor tuition

## **PUBLICATIONS**

- Bayona, G., and Lawton, T., 2003, Fault-proximal stratigraphic record of episodic extension and oblique inversion, Bisbee Basin, southwestern New Mexico, USA: *Basin Research*, v. 15, p. 1-20.
- Bayona, G., Thomas, W.A., and Van der Voo, R., 2003, Kinematics of thrust sheets within transverse zones: A structural and paleomagnetic investigation in the Appalachian thrust belt of Georgia and Alabama: *Journal of Structural Geology*, in press.
- Thomas, W.A., Astini, R., and Bayona, G., 2002, Ordovician collision of the Argentine Precordillera with Gondwana, independent of Laurentian Taconic orogeny: *Tectonophysics* 345, p. 131-152.
- Thomas, W.A., and Bayona, G., 2002, Three-dimensional palinspastic restoration of the Anniston transverse zone in the Appalachian thrust belt, Alabama: *Journal of Structural Geology*, v. 24, p. 797-826.
- Bayona, G., and Lawton, T., 2000, Aptian-Albian extensional faulting and subsequent Laramide inversion, central Peloncillo Mountains, southwestern New Mexico, *in* Lawton, T.F., McMillan, N., and McLemore, V.T., eds., *Southwest passage: a trip through the Phanerozoic: New Mexico Geologic Society, 51 Annual field conference*, p. 85-94.
- Thomas, W.A., Astini, R., Osborne, W.E., and Bayona, G., 2000, Tectonic framework of deposition of the Conasauga Formation, *in* Osborne W.E., Thomas, W.A., and Astini, R.A., eds, *The Conasauga Formation and equivalent units in the Appalachian thrust belt in Alabama: Alabama Geological Society, 37 Annual field conference*, p. 19-40.
- Jaramillo, C., and Bayona, G., 2000, Mangrove distribution during the Holocene in Tribugá Gulf, Colombia: *Biotropica*, v. 32, p. 14-22.
- Bayona, G., Garcia, D., Mora, G., 1994, La Formación Saldaña: Un ejemplo de acumulación en una cuenca de retro-arco, *in* Etayo, F., *Estudios Geológicos del Valle Superior del Magdalena, Publicación especial de la Universidad Nacional y Ecopetrol*, p. 11-121.

Bayona, G., Garcia, D., Mora, G., 1992, Estratigrafía detallada de la Formación Saldaña en su sección tipo, carretera Ataco-Planadas (Tolima). Unpublished thesis No.303, Departamento de Geociencias, Universidad Nacional, 64p, Bogotá.

Bayona, G., Mora, G., Ojeda, G., Peña, J., Roncancio, J., 1990, Anotaciones sobre límite Cretácico-Terciario en Colombia: Revista Facies, v.1 p 41-45.

### **EXTENDED ABSTRACTS**

Bayona, G., Van der Voo, R., and Thomas, W.A., 2002, Influencia de la configuración palinspástica de cuencas sedimentarias y estructura del basamento en la evolución de fajas de cabalgamiento que no involucran basamento. Memorias de la Segunda convencion técnica de la Asociación Colombiana de Geólogos y Geofísicos de el Petróleo. 5 p.

### **ABSTRACTS**

Bayona, G., and Thomas, W.A., 2002, Overprint of Basement-Fault Reactivation in Flexural Deformation and Deposition in the Blountian (Taconic) Peripheral Foreland Basin: Eos.Trans. AGU, 83 (47), Fall Meet. Suppl., Abstract S61A-1117.

Jaramillo, C., Bayona, G., Pardo, A., Mejia, V., Opdyke, N., and Sanchez, J., 2002, Constraining the Age of Synorogenic Continental Paleogene Strata in the Eastern Cordillera of Colombia, South America: A Combined Palynological and Paleomagnetic Approach: Eos.Trans. AGU, 83 (47), Fall Meet. Suppl., Abstract GP71A-0978.

Bayona, G., and Thomas, W.A., 2002, Location and composition of source areas for the Middle and Late Ordovician Blountian (Taconic) foreland basin, southeastern corner of Laurentia: Geological Society of America Abstracts with Programs, v. 34, n. 2, p. 118.

Bayona, G., Van der Voo, R., and Thomas, W.A., 2001, A Structural and Paleomagnetic Investigation in the Foreland Thrust Belt of Georgia and Alabama to Constrain Rotations in Lateral and Oblique Structures: Eos.Trans. AGU, 82 (47), Fall Meet. Suppl., Abstract GP11A-0180, p. 312.

Bayona, G., Thomas, W.A., Finney, S.C., and Repetski, J., 2001, Differentiating the effects of basement structures, elastic flexure, and eustasy In the evolution of the early Taconic (Blountian) foreland basin of southeastern Laurentia (North American Craton): Geological Society of America Abstracts with Programs, v. 33, n. 2, p. 18.

- Bayona, G., Thomas, W.A., Finney, S.C., and Repetski, J., 2001, Flexural Uplifting and Forebulge Migration as Reflection of Collisional Tectonism: An Example from the Alabama Promontory, Southeastern USA. Annual Meeting of the America Association of Petroleum Geologists, Official Program book, p. 14.
- Thomas, W.A., and Bayona, G., 2001, Three-dimensional palinspastic restoration of the unmetamorphosed Appalachian thrust belt in Alabama and Georgia. Geological Society of America Abstracts with Programs, v. 33, n. 2, p. 5.
- Bayona, G., and Thomas, W.A., 2001, Implication of a palinspastic map for the stratigraphic and tectonic framework of the Alabama-Georgia Appalachian thrust belt: Geological Society of America Abstracts with Programs, v. 33, n. 2, p. 18.
- Thomas, W.A., and Bayona, G., 1999, Three-dimensional palinspastic restoration of the Anniston transverse zone in the Appalachian thrust belt in Alabama: Geological Society of America Abstracts with Programs, v. 31, n. 7, p. 125.
- Jaramillo, C., and Bayona, G., 1999, Distribución del manglar durante el Holoceno en el golfo de Tribugá, Colombia. Libro de Resúmenes del Primer Congreso Colombiano de Botánica, Universidad Nacional de Colombia, p. 38.
- Bayona, G., and Lawton, T.F., 1998, Tectonic control on deposition of Cretaceous - Paleogene deposits, central Peloncillo Mountains, New Mexico: New Mexico Geology, v.20, p.51.
- Bayona, G., and Lawton, T.F., 1998, Normal faulting and inversion events recorded in Cretaceous-Paleogene deposits, Central Peloncillo Mountains, southwestern New Mexico: Geological Society of America, Abstracts with Programs, v.30, n. 6, p. 3.
- Bayona, G., and Jaramillo, C., 1998. Maastrichtian-Paleocene basin evolution of northwestern South America: the transition from a mature extensional basin to a foreland basin. 1998 AAPG Annual Meeting, Salt Lake City, Utah (in CD).
- Bayona, G., and Lawton, T.F., 1997, Analogous middle Mesozoic deposits of the Magdalena basin and Cordillera Oriental, Colombia, and southwest New Mexico and Southeast Arizona, USA. Geol. Soc. America Abs. with Programs, vol 29, n. 6.
- Bayona, G., and Lawton, T.F., 1997, Parallel Jurassic-Paleogene tectonic evolution of Magdalena basin and Cordillera Oriental, Colombia, and Borderland rift-Laramide basin systems, Southwest New Mexico and Southeast Arizona. New Mexico Geology, v.19, n.2, p. 53.



- Bayona,G., Cortes, M., 1996, Cambios faciales y caracterización estructural de la secuencia volcanoclástica de la Formación Saldaña en el sector norte del Valle Superior del Magdalena. Abstr. VII Congreso Colombiano de Geología, Bogotá, Colombia.
- Bayona,G., Cortes, M., 1995. Variación facial y petrogénesis de los depósitos de la Formación Saldaña en el sector norte del Valle Superior del Magdalena: *Geologia Colombiana*, v.21, p. 121.
- Cortes, M., Bayona,G., 1995. Comportamiento reológico y caracterización estructural de las rocas volcánicas de la Fm. Saldaña en el Valle Superior del Magdalena: *Geologia Colombiana*, v.21, p. 122
- Bayona, G., Mora G., 1994. The Saldaña Formation: a product of continental Stratovolcanoes activity in a Triassic - Jurassic Back-arc Basin, Colombia. *Geol. Soc. America Abs. with Programs*, v. 26, n. 7, p. 117-118